UCRL-16278

University of California

Ernest O. Lawrence Radiation Laboratory

DISPERSION OF OPTICAL ROTATION
AND BIREFRINGENCE OF BIOPOLYMERS:

I. THEORY OF FARADAY ROTATION IN POLYMERS
II. ELECTRICAL BIREFRINGENCE OF TOBACCO MOSAIC VIRUS
III. OPTICAL ROTATION OF DINUCLEOSIDE PHOSPHATES

TWO-WEEK LOAN COPY

This is a Library Circulating Copy which may be borrowed for two weeks. For a personal retention copy, call Tech. Info. Division, Ext. 5545

Berkeley, California

DISCLAIMER

This document was prepared as an account of work sponsored by the United States Government. While this document is believed to contain correct information, neither the United States Government nor any agency thereof, nor the Regents of the University of California, nor any of their employees, makes any warranty, express or implied, or assumes any legal responsibility for the accuracy, completeness, or usefulness of any information, apparatus, product, or process disclosed, or represents that its use would not infringe privately owned rights. Reference herein to any specific commercial product, process, or service by its trade name, trademark, manufacturer, or otherwise, does not necessarily constitute or imply its endorsement, recommendation, or favoring by the United States Government or any agency thereof, or the Regents of the University of California. The views and opinions of authors expressed herein do not necessarily state or reflect those of the United States Government or any agency thereof or the Regents of the University of California.

Research and Development

UCRL-16278

UNIVERSITY OF CALIFORNIA
Lawrence Radiation Laboratory
Berkeley, California

AEC Contract No. W-7405-eng-48

DISPERSION OF OPTICAL ROTATION AND BIREFRINGENCE OF BIOPOLYMERS:

I. THEORY OF FARADAY ROTATION IN POLYMERS

II. ELECTRICAL BIREFRINGENCE OF TOBACCO MOSAIC VIRUS

III. OPTICAL ROTATION OF DINUCLEOSIDE PHOSPHATES

C. Allen Bush
(Ph. D. Thesis)

July 1965

This thesis is dedicated to Amus, without whose constant assistance and stimulating companionship the present work would have been impossible.

TABLE OF CONTENTS

Foreward 1

I. Faraday Rotation in Polymers

Introduction 5

Qualitative Discussion 6

Quantitative Discussion 9

Comparison with Experiment 18

II. The Birefringence and Optical Rotatory Dispersion of Tobacco Mosaic Virus

Introduction 23

Preparation 23

Measurement of the Optical Rotation 25

Discussion of the ORD 26

Equipment for the Birefringence Measurement 30

Results and Discussion of the Birefringence 35

III. Calculation of the ORD of Dinucleoside Phosphates

Introduction 43

Qualitative Discussion of the Method 45

Quantitative Development of the Theory 46

The Model for Dinucleoside Phosphates 56

Computation of the ORD from the Rotational Strengths 71

Results of the Calculation 78

Discussion 86

Appendix A. Listings and Description of Computer Programs 95

Appendix B. Circular Dichroism Curves 102

SUMMARY

We discuss the use of optical properties of biological polymers in the ultraviolet and how interpretation of them can give information on the structure of biopolymers in solution. The general technique is to express theoretically the optical properties in terms of the polymer subunit properties and interaction between them. The interaction portion is sensitive to the conformation.

The theory of Faraday effect in organic molecules is developed and Faraday rotational strengths are defined. An exciton theory of the interaction of groups in a polymer is applied to Faraday rotation. This theory is used to predict how the Faraday effect changes with polymer conformation.

We describe experiments on the optical properties of tobacco mosaic virus (TMV) and TMV protein. The optical rotatory dispersion (ORD) of TMV, of TMV protein subunits, and of TMV protein in aggregated rods is reported and discussed in terms of absorbing groups. The electrical birefringence of TMV and TMV protein rods is determined as a function of wavelength of light in an attempt to determine the orientation of the absorbing groups.

We also carry out a calculation of the ORD of dinucleoside phosphates from an exciton model. The method assumes that the circular dichroism has the same dependence on wavelength as does the absorption. The ORD is obtained from a Kronig-Kramers transformation of the circular dichroism.

The results of the Faraday rotation theory are applied to the effect observed in ketones. The interpretation leads to the conclusion that the 280 mμ absorption is composed of two distinct electronic transitions. In polymers, the theory predicts a structure-dependent Faraday effect.

The ORD of TMV and its protein is interpreted as implying that the rods of aggregated protein resemble the native virus. The interpretation of the birefringence of TMV and the aggregated protein as a function of wavelength proved to be ambiguous. This ambiguity results partly from the small amount of RNA in the virus and partly from difficulties in separating the intrinsic birefringence from the form birefringence.

The calculation of the ORD of dinucleoside phosphates gives reasonably good agreement with experiment, indicating that the exciton interaction is the origin of the large Cotton effects observed in some dinucleosides. We also conclude that ApA and UpU are right handed helices and that, by implication, poly A at pH 7 also forms a right handed helix. The calculations suggest very strongly that all dinucleoside phosphates of the four RNA bases (A, U, G and C) are right handed in conformation, and that they have helical increment angles of 28 to 40°. The calculation also predicts that certain dinucleoside phosphates may have very large rotations at low temperature.

FOREWARD

The use of physical methods to investigate biological structures is a field of study which has recently come into great prominence. The ability of physical methods to give biological answers has given great impetus to the study of biological processes and has improved our knowledge of living things at an unprecedented rate.

Physical methods have certain advantages for studying biological systems. The methods are often capable of automation. Once they are worked out, the methods are not time consuming and many samples can be tested in a day. Also, the sample is not usually degraded by the measurement as it is by chemical analysis. The difficulty of physical methods is that they may be difficult to interpret.

Such is the case with optical methods; it is easy to measure the ultraviolet absorption spectrum in a scanning spectrophotometer, but it is difficult to extract all the information available. The interaction of photons with matter is basically a non-classical effect and therefore one must make theoretical treatments in quantum mechanics or at least in a hybrid, semi-classical language. This makes interpretation one step less reliable than for classical phenomena such as sedimentation or hydrodynamic experiments.

Ultraviolet absorption has been the most utilized technique in the past in biological studies, since the experiments are easy. However, it is limited in its information content. In the present study, we have undertaken some methods that are slightly more difficult experimentally and require more extensive interpretation. Such a method as Faraday effect or magneto-optical rotation can give a wealth of information, if it can be

understood. Experiments have been very few and attempts at interpretation are definitely needed (see Tinoco and Bush, 1964, for a review). In Chapter I we have presented a beginning attempt at a theoretical understanding of Faraday rotation of ultraviolet light in systems of biological interest.

In Chapter II we discuss the use of electrical birefringence in the study of tobacco mosaic virus. This is a method which has previously received some attention. However, in our case we attempt to understand the birefringence as a function of wavelength of light through an absorbing region. Unfortunately, we were unable to make any certain conclusions about the orientation of chromophores. We feel that the method might be useful in connection with other systems.

Our calculation of optical rotatory dispersion (ORD) of dinucleoside phosphates was, by comparison, rather successful (see Chapter III). In this case, we were able to understand what gives rise to the large optical rotation of these compounds and draw conclusions about their structure in solution. It appears that ORD will be a powerful tool in the determination of the chemical composition and sequence of oligonucleotides (Cantor and Tinoco, 1965).

We will see from the study of the three optical methods mentioned that one can have different degrees of success in using optical properties to investigate biological structure, but that where success is not found, it is clear in what direction the study should be extended to obtain the desired structural information. The possibilities of optical measurement with polarized light as a function of wavelength in electric and magnetic fields, and at different pH values and temperatures, are enormous. Use of all these variables extend the structural information greatly. If one could carry out sufficient experimental calibration and extend one's

theoretical understanding far enough, it might be possible to envision an automated machine capable of measuring such properties as ORD, Faraday effect, birefringence and dichroism over a range of pH, temperature and wavelength. Such a measurement could probably provide sufficient information to completely determine the structure of a long oligonucleotide. All this could be done without degrading the compound. This advantage could be quite significant for rare biological products which require rather extensive preparation and purification and are often obtained in very small quantity.

Perhaps such visionary concepts as a polynucleotide sequencing machine utilizing only physical methods are not justified at the present time, but recent studies on ORD of oligonucleotides have shown such promise that one ought not to dismiss the possibility too readily (Warshaw and Tinoco, 1965; Cantor and Tinoco, 1965). The use of analog to digital converters and subsequent computer analysis will greatly expedite the treatment of experimental data. Although the accomplishments of the following three chapters are a rather modest contribution, it is hoped that the reader will find sufficient encouragement to extend the investigation of optical properties of biological molecules, in order that they be allowed to yield up their rich store of structural information.

References

C. R. Cantor and I. Tinoco, Jr., (1965) J. Mol. Biol., in press.

I. Tinoco, Jr. and C. A. Bush (1964) Biopolymers Symposia 1, 235.

M. M. Warshaw and I. Tinoco, Jr. (1965) J. Mol. Biol., in press.

I. FARADAY ROTATION IN POLYMERS

Introduction

Michael Faraday (1845, 1846) found that plane polarized light was rotated on passing through matter in a magnetic field. He found that the effect was proportional to the magnetic field strength and that the light must propagate nearly parallel to the direction of the field. Furthermore, he found that the magnetic rotation was additive to natural optical rotation, but that the sign of magnetic rotation depended on the direction of propagation of the light relative to the magnetic field while natural rotation did not.

Shortly after its discovery the phenomenon of magnetic rotation aroused a great deal of interest. W. H. Perkin retired from dye manufacturing in 1874 to do fundamental research in this field. In 1884 Sir. G. G. Stokes made the following statement during the Burnett Lecture, "On Light."

> ".....the rotation of the plane of polarization produced by the action of magnetism.....is capable of laying hold of and revealing delicate differences of molecular grouping."

Unfortunately this statement has not yet been verified. However, work is progressing in various laboratories on the experimental difficulties which need to be overcome, and success at using Faraday rotation to investigate the properties of organic chemicals, especially ones of biological interest, may be near at hand. What we propose to do in this chapter is make an initial attempt at understanding what are the general effects we expect to find in organic molecules of low symmetry. In specific, we wish to find what, if any, are the special effects in polymers.

Qualitative Discussion

All matter in a magnetic field will rotate the plane of polarization of light. The effect is independent of whether the molecule has a point or plane of symmetry. If the molecule is naturally optically active, the Faraday rotation will simply add, and the Faraday rotation of the racemic mixture will be the same as that of either isomer. For all non-linear molecules without permanent magnetic moments, the wavelength dependence of the Faraday rotation can be represented by the same sort of terms as the natural rotation, i.e., a sum of Drude terms or damped Drude terms. Therefore, the same techniques can be used in analyzing the experimental Faraday rotatory dispersion as the natural rotatory dispersion (Schellman and Schellman, 1958; Moffit and Yang, 1956; Moscowitz, 1960). The analog to the natural rotational strength R for a transition from o to a is the magnetic field strength H parallel to the light times the Faraday rotational strength F (we shall omit the subscript oa in R_{oa} and F_{oa} unless it is necessary to distinguish one transition from another). The Faraday rotational strength depends on two molecular parameters: the electric dipole transition moment μ and another vector which we shall call S. More precisely

$$F = \mu S \cos \theta$$

where θ is the angle between μ and S. This form can be compared with the natural rotational strength ($R = \mu m \cos \theta$) where m is the magnetic dipole transition and θ is the angle between μ and m, and with the dipole strength ($D = \mu^2$) which characterizes the absorption. These equations indicate why the rotational strength may be more sensitive to molecular structure than the absorption. Absorption depends on only one molecular parameter while both natural and Faraday rotations depend on two parameters and the angle between them. One also can see that the Faraday rotational strength is not

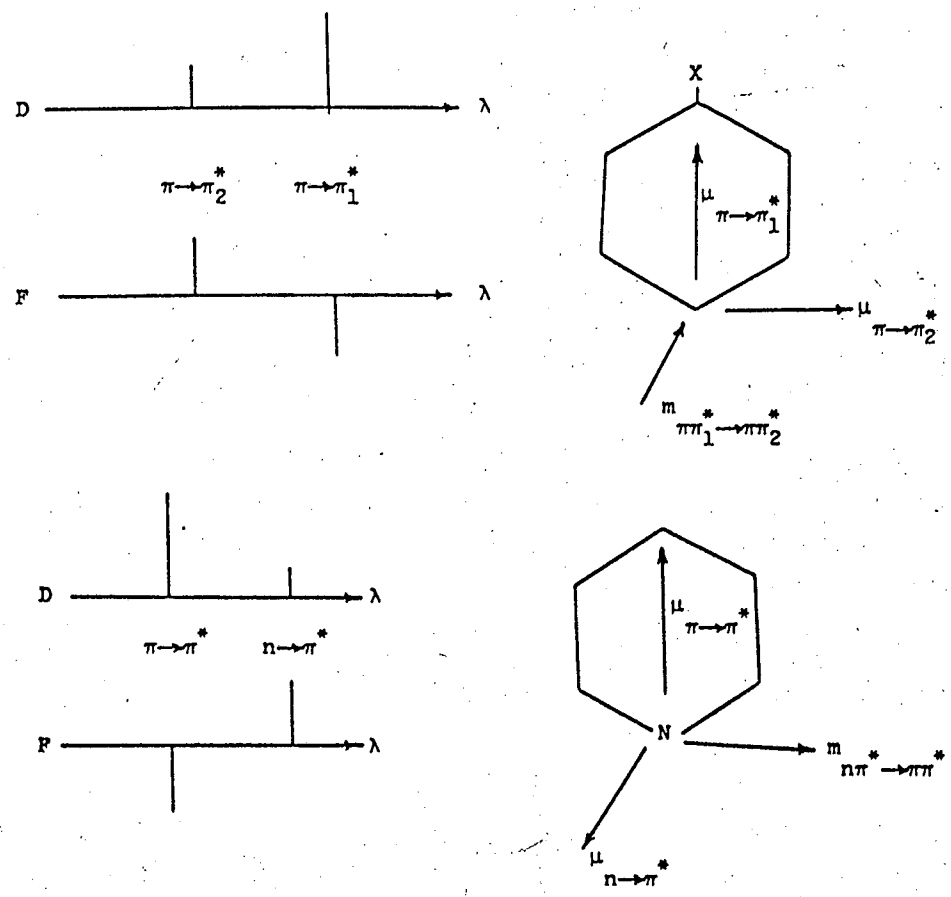

Figure I-1

Examples of molecular symmetries giving rise to large Faraday effects.

proportional to absorption. Weak transitions (μ small) may have large rotational strengths (S large) and vice versa.

To understand what types of transitions are needed to produce a significant Faraday rotation, we should know what is required for rotation of the plane of polarization of light. A dipole induced in the molecule at right angles to the plane of polarization of the incident light will radiate an electric field in this direction. When added to the incident light, this field will lead to rotation of the plane of polarization (Kauzmann, 1957). For a magnetic field to induce such a dipole, two conditions must be met: (a) two electric dipole transitions must exist in the molecule with components perpendicular to each other; and (b) two of the states of the transitions must be linked by a magnetic transition moment. The effect is largest when the two electric dipole transitions are very close in frequency. There are two types of terms: the large one is inversely proportional to the frequency difference between the two transitions; the other is inversely proportional to the frequency of one of the transitions. Figure I-1 illustrates two favorable cases in which there are either two perpendicular π-π^* transitions or an n-π^* transition perpendicular to a π-π^* transition. The two transitions will lead to nearly equal and opposite Faraday rotational strengths; the sign, magnitude and spearation of the rotational strengths will depend on the type and symmetry of substitution. In particular, the sign depends on the relative sign of the two electric dipole transition moments. Therefore, Faraday rotation in principle can give the sign of the transition moment, while absorption cannot. As the frequency difference of the two transitions increases from zero, the rotatory dispersion near these frequencies will change from (a) no dispersion to (b) a single minimum (or maximum) with one maximum (minimum) on each side to (c) two separate, opposite sign Cotton effects. If this type of

term is dominant, the Moffit-Yang (1956) equation may be useful for treating the results. Even if the two perpendicular electric dipole transitions are not close in frequency, there may still be a significant (though generally smaller) Faraday rotational strength. This latter term should lead to simple Cotton effects.

The units and magnitude of the Faraday rotational strength are related to natural optical rotation by

$$HF = (\mu H/h\nu)R$$

The magnetic field times the Faraday rotational strength has the same units as natural optical rotation. If one chooses a standard magnetic field strength (such as 10,000 gauss) (Shashoua, 1964) then HF can be conveniently reported in the same units as R. Either units of 10^{-38} cgs or reduced rotational strengths (Moscowitz, 1960) have been used. The experimental values to be expected in a 10,000 gauss field can be estimated from the value of $\mu H = 50$ cm^{-1} for a 1 Debye dipole moment. For the large term, ν represents the frequency difference of the two transitions (which should be a few hundred wave numbers or greater so that the equal and opposite Faraday rotational strengths do not completely cancel). For the small term ν is the transition frequency itself (which must be at least 10,000 cm^{-1} in the visible region). Therefore, we may expect values of HF to range from about 0.1 R to 0.005 R, where R is a fully allowed rotational strength. This may be compared with the steroids discussed by Djerassi (1960) which have rotational strengths of about .01 R. Thus, if we go to a 10,000 gauss field, we expect to see Faraday rotation in organic molecules which is the same order of magnitude as optical rotation.

When a rigid polymer is formed from the monomers (or random coil) we expect a similar change in the Faraday rotation as seen in the absorption. There will be a change in Faraday rotational strength for each monomer

transition which depends on the geometry, and there may be a shift or splitting of the transition frequencies. This does not mean of course that the change in rotation must mirror that of absorption. This will approximately occur if the vector S happens to be parallel to μ in each monomer. If S is perpendicular to μ, the monomer has zero Faraday rotational strength for that transition, but the polymer may have rotational strength. The Faraday rotational strengths of the polymer and their change in orientation can be used to determine the direction and magnitude of the vector S and therefore, might lead to the sign of electric dipole transition moments.

There have been few experimental studies published so far which measure rotatory dispersion through an absorption band in a magnetic field (Shashoua, 1964; Briat, 1964; Schooley, et al., 1965); no Faraday rotational strengths have been reported. However, reports from the various laboratories working on this phenomenon should soon be appearing.

Quantitative Discussion

In our quantitative discussion we will limit ourselves to first order perturbation theory. We know this procedure is correct for the magnetic field perturbation since the Faraday effect is linear in the magnetic field. Diatomic molecules have already been treated in Faraday effect (Tobias and Kauzmann, 1960). In addition, we feel that the electronic properties of triplet states and free radicals are not sufficiently well understood to include them in the present study. Therefore, we will exclude molecules with three fold or higher symmetry axies and molecules with unpaired electrons. This leaves us many ordinary organic molecules and in particular organic molecules of biological interest.

In order to obtain Faraday rotation, we will expand the molecular wave functions to first order in the magnetic field. When we come to the polymer effect, we will again expand the wave functions, this time in the electric field of the polymer. Therefore, we will develop the two expansions together in order to demonstrate the parallelism of the two procedures.

The energy of an isolated molecule in a static, uniform field is

$$E_n(E) = E_n - \underset{\sim}{\mu}_{nn} \cdot \underset{\sim}{E} + O(E^2) + \ldots \qquad \text{I-(1a)}$$

$$E_n(H) = E_n \qquad + O(H^2) + \ldots \qquad \text{I-(1b)}$$

where the subscript n refers to any state of the molecule and $\underset{\sim}{\mu}_{nn}$ is the permanent electric dipole moment in that state. The corresponding wave functions, neglecting terms of second and higher order, can be written

$$\psi_n(E) = \psi_n + \underset{\sim}{E} \cdot \sum_{m \neq n} \underset{\sim}{\mu}_{mn}\, \psi_m / h(\nu_m - \nu_n) \qquad \text{I-(2a)}$$

$$\psi_n(H) = \psi_n + \underset{\sim}{H} \cdot \sum_{m \neq n} \underset{\sim}{m}_{mn}\, \psi_m / h(\nu_m - \nu_n) \qquad \text{I-(2b)}$$

$$\underset{\sim}{\mu}_{mn} = \underset{\sim}{\mu}_{nm} = \int \psi_m^* \underset{\sim}{\mu}\, \psi_n d\tau = \text{electric dipole transition moment}$$

$$\underset{\sim}{m}_{mn} = \underset{\sim}{m}_{nm} = \int \psi_m^* \underset{\sim}{m}\, \psi_n d\tau = \text{magnetic dipole transition moment}$$

If we choose ψ_n real, $\psi_n(E)$ will also be real while $\psi_n(H)$ will be complex since m is imaginary.

These two equations allow us to understand all the first order electric and magnetic effects on the optical properties. The necessary parameters are the frequency, and the transition integral whose square characterizes the probability of transition of the molecule in the presence of light. These are

Frequency: (for transition from ground state to state a)

$$\nu_a(E) = \nu_a + \underset{\sim}{E} \cdot (\underset{\sim}{\mu}_{oo} - \underset{\sim}{\mu}_{aa})/h \qquad \text{I-(3a)}$$

$$\nu_a(H) = \nu_a \qquad \text{I-(3b)}$$

$$\nu_a (= (E_a - E_o)/h \qquad \text{I-(3c)}$$

Transition integral: (for transition from ground state to state a in presence of plane light wave travelling in direction z and polarized along x)

$$T_{xao}(E) = T_{xao} + \underset{\sim}{E} \cdot \sum_{b \neq a} \underset{\sim}{\mu}_{ba} \; T_{xbo}/h(\nu_b - \nu_a) + \underset{\sim}{E} \cdot \sum_{b \neq o} \underset{\sim}{\mu}_{bo} \; T_{xab}/h(h^{\nu}{}_{b} \qquad \text{I-(4a)}$$

$$T_{xao}(H) = T_{xao} + \underset{\sim}{H} \cdot \sum_{b \neq a} \underset{\sim}{m}_{ba} \; T_{xbo}/h(\nu_b - \nu_a) + \underset{\sim}{H} \cdot \sum_{b \neq a} \underset{\sim}{m}_{bo} \; T_{xab}/h^{\nu}{}_{b} \qquad \text{I-(4b)}$$

$$T_{xao} = \int \psi_a^{*} \, e^{i2\pi z/\lambda} \frac{\delta \psi_o d\tau}{\delta x} = \frac{i}{\hbar} \int \psi_a^{*} e^{i2\pi z/\lambda} \, p_x \, \psi_o d\tau$$

In practice one usually expands the exponential to obtain terms of the following type.

Momentum transition: (proportional to electric dipole transition)

$$\underset{\sim}{p}_{ao} = (2\pi i m/e)^{\nu}{}_{a} \underset{\sim}{\mu}_{ao} \qquad \text{I-(5)}$$

Magnetic dipole transition:

$$\underset{\sim}{m}_{ao} = (e/2mc)(\underset{\sim}{r} \times \underset{\sim}{p})_{ao} \qquad \text{I-(6)}$$

Electric quadrupole transition:

$$\underset{\sim}{Q}_{ao} = e(\underset{\sim}{r}\underset{\sim}{r})_{ao} \qquad \text{I-(7)}$$

Equation (5) comes from the first term of the expansion, while Eqs. (6) and (7) come from the second. Any one of these can replace T_{xao} in Eq. I-(4).

For electrically allowed transitions one customarily approximates the transition integral by the square of the electric dipole transition moment as given in I-(5) above. Thus one may define the oscillator strength f_a which is proportional to both μ_{ao}^2 and to the integral of the absorbance over the absorption band.

$$\int \epsilon_a d\nu = \left(\frac{\pi e^2 N_o}{2303mc} \right) f_a \qquad \text{I-(8)}$$

$$f_a = (8\pi^2 m/3he^2)\nu_a \, \mathrm{Re} \; \underset{\sim}{\mu}_{oa} \cdot \underset{\sim}{\mu}_{oa}^{*}$$

However, in the static field the relative directions of the light and the field are important so we must consider the oscillator strength tensor. For light incident polarized along unit vector $\underset{\sim}{i}$ the absorption in the static electric field is

$$\int \varepsilon_a d\nu(E) = \int \varepsilon_a d\nu + (8\pi^3 N_o/2303hc)$$

$$\underset{\sim}{E} \cdot \left\{ 2\nu_a \left[\sum_{b\neq o} (\underset{\sim}{\mu}_{ob}\, \underset{\sim}{i} \cdot \underset{\sim}{\mu}_{ab} \underset{\sim}{\mu}_{oa} \cdot \underset{\sim}{i})/h\nu_b + \sum_{b\neq a} (\underset{\sim}{\mu}_{ab}\, \underset{\sim}{i} \cdot \underset{\sim}{\mu}_{ob} \underset{\sim}{\mu}_{oa} \cdot \underset{\sim}{i})/h(\nu_b - \nu_a) \right] \right. \qquad \text{I-(9a)}$$

$$\left. + (\underset{\sim}{\mu}_{oo} - \underset{\sim}{\mu}_{aa})\, \underset{\sim}{i} \cdot \underset{\sim}{\mu}_{oa} \underset{\sim}{\mu}_{oa} \cdot \underset{\sim}{i} \right\}$$

If the static field is space fixed and the molecule is randomly oriented, we average the above expression (Brown, 1962) over all equally probable orientations of the molecule and obtain

$$\left\langle \int \varepsilon_a d\nu(E) \right\rangle = \left\langle \int \varepsilon_a d\nu \right\rangle \qquad \text{I-(10a)}$$

As the magnetic field adds terms which are purely imaginary, there is no effect for either fixed or randomly oriented molecules.

$$\int \varepsilon_a d\nu(H) = \int \varepsilon_a d\nu \qquad \text{I-(9b)}$$

$$\left\langle \int \varepsilon_a d\nu(H) \right\rangle = \left\langle \int \varepsilon_a d\nu \right\rangle \qquad \text{I-(10b)}$$

The rotation of polarized light has been described in terms of the transition integrals (Kirkwood, 1937; Stephan, 1958). As in absorption, however, it is usually sufficient to keep only the first two terms in the expansion of the exponential. The rotation in radians/cm for light incident along the $\underset{\sim}{k}$ (z) direction is

$$\theta_z = (8\pi^2 N_o \nu^2/hc)\ \mathrm{Im} \sum_{a\neq o} (\nu_a^2 - \nu^2)^{-1} \left\{ \underset{\sim}{i} \cdot \underset{\sim}{\mu}_{oa} \underset{\sim}{\mu}_{oa} \cdot \underset{\sim}{i} \right.$$

$$\left. + (e/mc) \left[\underset{\sim}{i} \cdot \underset{\sim}{\mu}_{oa}\, \underset{\sim}{k} \cdot (\underset{\sim}{r}\underset{\sim}{p})_{ao} \cdot \underset{\sim}{i} - \underset{\sim}{i} \cdot \underset{\sim}{\mu}_{oa}\, \underset{\sim}{k} \cdot (\underset{\sim}{r}\underset{\sim}{p})_{ao} \cdot \underset{\sim}{i} \right] \right\} \qquad \text{I-(11)}$$

The Only the imaginary terms in Eq. 1-(11) contribute [illegible] to the rotation. [illegible] The second term characterizes the natural optical rotation which can be influenced by a static electric field, but not a magnetic field. Using Eq. I-(4a) to introduce the magnetic field perturbation, one finds that the first term leads to Faraday rotation, which has no electric field analog. Rotatory power, however, can be induced in a molecule by a static electric field. The effect is not characterized by the first term, but requires the action of a static electric field gradient on a quadrupole transition moment (Shellman and Oriel, 1962).

Natural optical rotation, including the effect of an internal static electric field, (Tinoco, 1960; 1961;1962), has been thoroughly discussed. Substitution of the wave functions of Eq. I-(2) into the second term of Eq. I-(11) shows the effect produced by the electric field. Again, if the molecule is randomly oriented relative to the static field, there is no effect of the field on the optical rotation.

The rotation of polarized light by any molecule in a magnetic field is obtained with the wave functions in Eq. I-(2) and the first term of Eq. I-(11). The result is

$$\theta_z(H) = (8\pi^2 N_o \nu^2/hc)\,\mathrm{Im}\, H \cdot \Sigma\, (\nu_2^2-\nu^2)^{-1} \qquad \text{I-(12)}$$

$$\left[\Sigma_{b\neq a}\, \underset{\sim}{m}_{ab}\, (\underset{\sim}{\mu}_{oa} \times \underset{\sim}{\mu}_{ob})/h(\nu_b-\nu_a) - \Sigma_{b\neq o}\, \underset{\sim}{m}_{ob}\, (\underset{\sim}{\mu}_{oa} \times \underset{\sim}{\mu}_{ab})/h\nu_b\right] \cdot k$$

where $\underset{\sim}{k}$ is a unit vector in the direction of propagation of the light. It is clear that changing the sign of the magnetic field $\underset{\sim}{H}$ or the direction of propagation of light $\underset{\sim}{k}$ will change the sign of rotation. One also sees that only the components of the magnetic transition moments parallel to $\underset{\sim}{H}$

contribute, while the components of the electric dipole transition moments must be perpendicular to k. If the molecule is randomly oriented, one finds

$$\theta_z(H) = (8\pi^2 N_o \nu^2/3hc)\, H_z \sum_{a\neq o} \frac{F_{oa}}{\nu_a^2-\nu^2}$$

$$F_{oa} = \mathrm{Im}\left[\sum_{b\neq a} \underset{\sim}{m}_{ab} \cdot \frac{(\underset{\sim}{\mu}_{oa} \times \underset{\sim}{\mu}_{ob})}{h(\nu_b-\nu_a)} - \sum_{b\neq o} \frac{\underset{\sim}{m}_{ob} \cdot (\underset{\sim}{\mu}_{oa} \times \underset{\sim}{\mu}_{ab})}{h\nu_b}\right] \qquad \text{I-(13)}$$

$$= \mathrm{Im}\, \underset{\sim}{\mu}_{oa} \cdot \left[\sum_{b\neq a} \frac{\underset{\sim}{\mu}_{ob} \times \underset{\sim}{m}_{ab}}{h(\nu_b-\nu_a)} - \sum_{b\neq o} \frac{\underset{\sim}{\mu}_{ab} \times \underset{\sim}{m}_{ob}}{h\nu_b}\right]$$

This equation agrees with the corresponding terms in Groenewege (1962), but differs from the V_c term in Tobias and Kauzmann (1961) which agrees with Serber (1932). Our Eq. I-(13) includes the b = o term in the first summation and the b = a term in the second. These terms are zero for non-polar molecules. There is some question as to whether such terms should appear. They arise from use of substitution 1-5 and subsequent expansion of μ in a perturbing field. Hameka and Goodman (1965) have pointed out that in a truncated expansion, such as ours, it is unclear whether the terms actually contribute or whether they would be cancelled if the expansion were complete. They have pointed out that the terms involving the permanent dipole moments seem to give correct results in certain situations where it is not formally correct to include $\underset{\sim}{\mu}_{aa}$ and $\underset{\sim}{\mu}_{oo}$ terms. We include them here solely to point out the problem. There is a possibility that molecules with large permanent dipole moments might show a larger Faraday rotation than similar non-polar ones. We note that on inversion of the molecule ($\underset{\sim}{\mu} = -\underset{\sim}{\mu}$, $\underset{\sim}{m} = \underset{\sim}{m}$) F_{oa}, unlike R_{oa}, does not change sign.

Before making approximations to this equation for practical use, one should determine what sum rule the F_{oa}'s obey and one should be convinced that each F_{oa} is independent of choice of origin for the molecular wave function.

It is seen that the F_{oa} sum rule is

$$\sum_a F_{oa} = 0 \qquad \text{I-(14)}$$

The $(\nu_b-\nu_a)$ terms in the sum cancel in pairs while the ν_b terms lead to $(\underset{\sim}{\mu} \times \underset{\sim}{\mu})_{ob} \cdot \underset{\sim}{m}_{ob}/h\nu_b = 0$. To show origin independence, one chooses two different origins, and calculates F_{oa} for each. That is, onw can choose

$$\underset{\sim}{\mu} = \sum_i \underset{\sim}{r}_i \text{ and } \underset{\sim}{R} + \sum_i \underset{\sim}{r}_i$$
$$\underset{\sim}{m} = (e/2mc)\sum_i \underset{\sim}{r}_i \times \underset{\sim}{p}_i \text{ and } (e/2mc)(\underset{\sim}{R} \times \sum_i \underset{\sim}{p}_i + \sum_i \underset{\sim}{r}_i \times \underset{\sim}{p}_i) \qquad \text{I-(15)}$$

where R is a constant vector from one origin to the other, and find that F_{oa} does not depend on R.

The calculation and interpretation of F_{oa} will be easiest when one of the terms in the first sum of Eq. I-(13) is dominant. That is, $(\nu_b-\nu_a)$ is small and $\underset{\sim}{\mu}_{oa}$ is perpendicular to $\underset{\sim}{\mu}_{ob}$. If no such term exists, a Taylor series approximation to F_{oa} seems obvious. Expanding the sums in Eq. I-(13) around ν_F, one obtains for the first two terms

$$F_{oa} \cong \mathrm{Im}(\underset{\sim}{\mu}_{oa}/h) \cdot \Big\{ (2/\nu_F)(\underset{\sim}{m} \times \underset{\sim}{\mu} - \underset{\sim}{\mu} \times \underset{\sim}{m})_{oa} - (1/\nu_F^2) \Big[(e/2\pi im)(\underset{\sim}{p} \times \underset{\sim}{m} + \underset{\sim}{m} \times \underset{\sim}{p})_{oa} + \nu_a(\underset{\sim}{m} \times \underset{\sim}{\mu} + \underset{\sim}{\mu} \times \underset{\sim}{m})_{oa} \Big] \Big\} \qquad \text{I-(16)}$$

which can be simplified to (Condon and Shortley, 1935)

$$F_{oa} \cong -\mathrm{Im}(4\underset{\sim}{\mu}_{oa}/h) \cdot \Big[(1/\nu_F)(\underset{\sim}{\mu} \times \underset{\sim}{m})_{oa} + (ih\, e\, \underset{\sim}{\mu}_{oa}/2mc)(\nu_a \nu_F^{-2} - \nu_F^{-1}) \Big] \qquad \text{I-(17)}$$

However, Eq. I-(17) does not obey the sum rule and it is not independent of choice of origin. Similar difficulties with approximations to the magnetic susceptibility have been discussed by Hameka (1962).

To obtain an explicit expression for the Faraday rotation of a polymer, one can in principle simply substitute previously derived polymer wave

functions (Tinoco, 1962) into Eq. I-(12) or I-(13). However, because in Faraday rotation a transition moment between two excited states is required, the polymer wave function must include doubly excited polymer states. These states do not contribute to the absorption and natural rotation in first order and have not been previously included. Furthermore, if the contribution to the polymer wave functions of the static field of the rest of the polymer is included, the resultant Faraday rotation expression is origin dependent. To avoid this difficulty introduced by the approximate wave functions, we will here set equal to zero all terms involving static internal electric fields. This is equivalent to putting the static field effects of the polymer into the unperturbed monomer wave functions (Tinoco, 1962). We also set all permanent dipoles equal to zero. The wave functions we will use are then

$$\psi_o^1 = \psi_o^o - \sum_i \sum_{j>i} \sum_{a,b\neq o,} \frac{V_{ioa;job}\,\psi^o_{ia,jb}}{h(\nu_a + \nu_b)}$$

$$\psi_{AK}^1 = \sum_{i=1}^{N} C_{iaK} \left\{ \psi^o_{ia} - \sum_{j\neq i} \sum_{b\neq a,o} \frac{V_{ioa;job}\,\psi^o_{jb}}{h(\nu_b - \nu_a)} \right. \qquad \text{I-(20)}$$

$$\left. - \sum_{j\neq i} \sum_{c,b\neq o} \frac{V_{iab;joc}\,\psi^o_{ib,jc}}{h(\nu_b + \nu_c - \nu_a)} \right\}$$

In zero-order, the Faraday rotation for a transition to the K exciton level in an N-mer is thus

$$F_{OAK} = NF_{ioa} + \mathrm{Im} \sum_{i=1}^{N} \sum_{j\neq i}^{N} C_{iaK}\, C^*_{jaK}\, \underset{\sim}{\mu}_{ioa} \cdot \left[\sum_{b\neq a} \underset{\sim}{\mu}_{job}\, \underset{\sim}{m}_{jab}/h(\nu_b - \nu_a) \right.$$

$$\left. - \sum_{b\neq o} \underset{\sim}{\mu}_{jab}\, \underset{\sim}{m}_{job}/h\nu_b \right] \qquad \text{I-(21)}$$

If we sum Eq. I-(21) over K, the second term disappears and we have

$\sum_K F_{OAK} = NF_{ioa}$ as it should be. Eq. I-(21) is analogous to the corresponding equation for the dipole strength of an exciton level.

$$D_{OAK} = ND_{ioa} + \mathrm{Re} \sum_{i=1}^{N} \sum_{j\neq i}^{N} C_{iaK} C^{*}_{jaK} \underset{\sim}{\mu}_{ioa} \cdot \underset{\sim}{\mu}_{joa}$$

$$F_{OAK} = NF_{ioa} + \mathrm{Im} \sum_{i=1}^{N} \sum_{j\neq i}^{N} C_{iaK} C_{jaK} \underset{\sim}{\mu}_{ioa} \cdot \underset{\sim}{S}_{joa} \qquad \text{I-(22)}$$

where S_{joa} represents the term in brackets in Eq. I-(21). Both the dipole strength and Faraday rotational strengths differ in form from the natural optical rotation of a polymer of optically inactive groups. The natural rotation has an additional term which depends on the distance between groups.

$$R_{OAK} = \mathrm{Im} \sum_{i=1}^{N} \sum_{j\neq i}^{N} C_{iaK} C^{*}_{jaK} \underset{\sim}{\mu}_{ioa} \cdot \underset{\sim}{m}_{joa}$$

$$+ (\pi\nu_a/c) \sum_{i=1}^{N} \sum_{j\neq i}^{N} C_{iaK} C_{jaK} \underset{\sim}{R}_{ij} \cdot (\underset{\sim}{\mu}_{ioa} \times \underset{\sim}{\mu}_{joa}) \qquad \text{I-(23)}$$

In Chapter III we will use an equation like I-(23) to compute optical activity of dimers. The effect is seen in the ORD of dinucleoside phosphates in the region of ultraviolet absorption. In that case the effect is large and demonstrates where we might see a Faraday rotation in polymers which would result from degenerate interaction of the polymer groups; that is, the region of the absorption. Far from the absorption band, the sum rule tells us that this effect of degenerate interaction should be small.

In first order each rotational strength of the exciton band will be modified. However, as often only the properties of the entire band are measured, we will give the first order equations for the rotational strengths summed over K

$$F_{OA} = NF_{ioa} - 2\,\mathrm{Im} \sum_{i} \sum_{j\neq i} \sum_{c\neq a,o} \left[\frac{\nu_c \mu_{joc}}{h^2(\nu_c^2 - \nu_a^2)} \right]$$

$$\left\{ \sum_{b\neq a} \frac{V_{ioa;joc}(\mu_{iob} \times m_{iab}) - V_{iob;joc}(\mu_{ioa} \times m_{iab})}{\nu_b - \nu_a} \right.$$

$$\left. \sum_{b\neq o} \frac{V_{iab;joc}(\mu_{ioa} \times m_{iob}) - V_{ioa;joc}(\mu_{iab} \times m_{iob})}{\nu_b} \right\} \qquad \text{I-(24)}$$

Far from the absorption band, we expect Eq. I-(24) to give us the differences between the Faraday rotation of the monomers and that of the polymer. Of course, it is easier to measure Faraday rotation far from the absorption where the effect is theoretically complicated by interactions of many bands. The interpretation of Faraday rotation of a polymer is simpler in the region of absorption where one can concentrate one's attention on a few electronic transitions (see Eq. 1-23), but alas, there the experiment is more difficult.

Comparison with Experiment

We would surely like to be able to compare the formulas we have derived with some experiments to see what effects are important in both monomers and in polymers. Unfortunately, we have no published polymer data as yet, and the data on small molecules are sparse. We do not really have enough to make generalizations about Faraday effect, even for small organic molecules. Faraday rotation is generally a somewhat smaller effect than natural rotation, but the major experimental problem is that in Faraday effect, unlike natural optical activity, the solvent also shows rotation. Thus the sample under investigation in dilute solution may have a rotation very small compared to the solvent.

Some measurements on ketones have been published by Briat (1964) using a permanent magnet in a system described by Briat, Billardon and Badoz (1963)

in which they used weakly absorbing pure liquids at short path length. In Fig. I-(2) we show their results for methylethyl ketone, which are typical of their curves for several ketones. This curve will be recognized as the type arising from two Faraday rotational strengths which are similar in magnitude but opposite in sign at frequencies separated by an amount smaller than the half width of the absorption. This tells us immediately that there must be two transitions contributing to the rotation near 280 mμ, and that probably the first term of Eq. 1-(13) dominates the rotational strength.

There is no simple way to compute the rotational strength from a curve such as Fig. I-(2). The proper way is to do a Kronig-Kramers transform to the magnetic circular dichroism and then integrate the resulting curve. This technique will be discussed in connection with natural optical activity in Chapter III, where we will use the transform from circular dichroism to rotation. The problem in going from rotation to circular dichroism is that one does not yet know how to approximate the long tails of the rotation curve which make a significant contribution to the rotational strength. In order to get a crude estimate of the rotational strength, we will assume a Drude equation and take a value for rotation outside the absorbing region.

The rotation due to a single electronic transition, but away from the absorption is given by a single term in the sum over transitions a, in Eq. I-(13). We write that single term in the notation used by Briat,

$$[\Lambda] = \frac{(360)8\pi^2 \nu^2 N_0}{3hc\ (2\pi)} \frac{F_{oa}}{\nu_a^2-\nu^2} \qquad \text{I-(25)}$$

where $[\Lambda]$ is in degrees/ cm-gauss-mol. If we pick a frequency outside the absorption band centered at 280 mμ, we may compute the rotational strength from

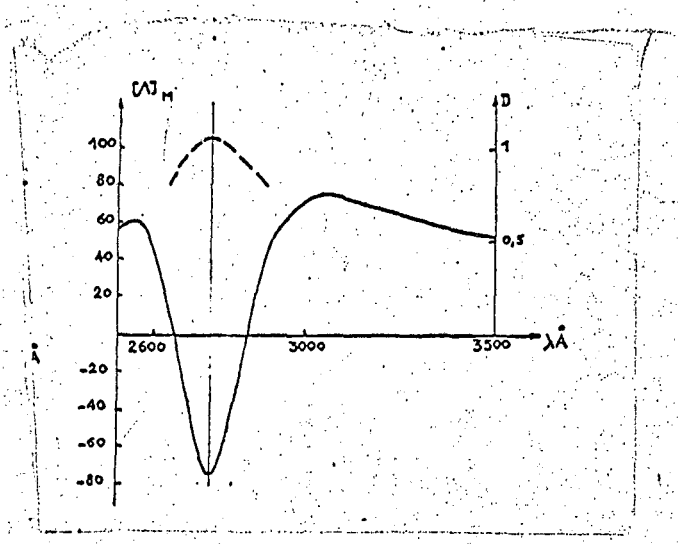

Fig. I-2

---- O.D. of methyl-ethyl ketone. Pure liquid, 5×10^{-2} mm. path length

—— Faraday rotation in degrees, $\times 10^{-3}$/ cm-mol-gauss

(Briat, 1964)

$$F_{oa} = 2.18 \times 10^{-43} [\Lambda] \frac{\nu_a^2 - \nu^2}{\nu^2} \qquad \text{I-(26)}$$

Taking the values $\nu_a^2 = (1/280 \times 10^7)^2 = (31{,}650\ cm^{-1})^2 = 1001 \times 10^6$ and $\nu^2 = (1/316 \times 10^7)^2$, where $[\Lambda] = 64 \times 10^{-3}$, we obtain

$$F_{oa} = (2.18 \times 10^{-43})(64 \times 10^{-3})(\frac{240}{1001}) = 3.34 \times 10^{-45} \text{ cgs.}$$

This should be considered as correct only to order of magnitude since we cannot assess the influence of the other rotational strength at slightly higher energy and the influence of bands farther into the uv. The latter influence is probably small, as the curve is fairly symmetric and there are no strong absorptions near 280 mμ. If anything, the estimate will be low for $F_0 \rightarrow 280$.

We may also compute the value of the first term of Eq. I-(13) for this case. From the absorption, which is very weak, we may estimate a dipole strength of 0.12 Debye units from the single gaussian method of Moscowitz (1960). We also assume a second absorption band at 300 cm^{-1} higher in frequency. This second absorption band cannot be any more intense, so assume it to have the same dipole strength. Since we do not know the symmetry properties of this second hypothetical absorption near 280 mμ, we assume the two states are connected by a magnetic transition moment of $1/2 \times 10^{-20}$ cgs, or one half that of the fully magnetically allowed value of one Bohr magneton. Lastly, we assume these three moments are mutually perpendicular so that no trigonometric factors enter the tripole product. Our results for this choice of parameters is

$$F_{o-280} = \frac{(1.2)(1.2)(.5) \times 10^{-58}}{(300)(6.62 \times 10^{-27})} = 3.8 \times 10^{-45} \text{ cgs.}$$

This value is consistent with the number we derived from the experimental

curve, showing that our assumptions are at least possible. The only assumption which is difficult to accept is the most basic one, that there is a second absorption band near the one at 280 mμ. If, however, we are willing to accept the measured curve as correct, we are forced to admit two transitions near one another connected by a strong magnetic transition moment.

These results are a bit hard to reconcile with current thinking on the 280 mμ absorption in ketones, which is assumed to be a single n-π* transition. We will have to wait until data on Faraday rotation of other types of compounds are available to assess these results in proper proportion.

References

B. Briat (1964) C. R. Acad. Sci. 258, 2788.

B. Briat, M. Billardon and J. Badoz (1963) C. R. Acad. Sci. 256, 3440.

L. S. Brown (1962) I.B.M. J. Res. Dev. 6, 338.

E. U. Condon and G. H. Shortley (1935) The Theory of Atomic Spectra, Cambridge Univ. Press, Cambridge. p. 44.

C. Djerassi (1960) Optical Rotatory Dispersion, McGraw-Hill Co., New York.

M. Faraday (1845) Diary, Sept. 13, 1845.

M. Faraday (1846) Phil. Trans. 136, 1.

M. P. Groenewege (1962) Mol. Phys. 5, 541.

H. F. Hameka (1962) Rev. Mod. Phys. 34, 87.

H. F. Hameka and L. Goodman (1965) J. Chem. Phys. 42, 2305.

W. Kauzmann (1957) Quantum Chemistry, Academic Press Inc., New York, p. 616.

J. A. Kirkwood (1937) J. Chem. Phys. 5, 479.

W. Moffit and J. T. Yang (1956) Proc. Nat. Acad. Sci. U.S. 42, 596.

A. Moscowitz (1960) Chap. 12 in Optical Rotatory Dispersion by C. Djerassi, McGraw-Hill Book Co., New York.

C. Schellman and J. A. Schellman (1958) Compt. Rend. Trav. Lab. Carlsberg, Ser. Chim. 30, 463.

D. A. Schooley, E. Bunnenberg and C. Djerassi (1965) Proc. Nat. Acad. Sci. U.S. 53, 579.

R. Serber (1932) Phys. Rev. 41, 489.

V. E. Shashoua (1964) J. Am. Chem. Soc. 86, 2109.

M. J. Stephan (1958) Proc. Camb. Phil. Soc. 54, 81.

G. G. Stokes (1892) On Light, Macmillan and Co., London, p. 168.

I. Tinoco, Jr. (1960) J. Chem. Phys. 33, 1332.

I. Tinoco, Jr. (1961) J. Chem. Phys. 34, 1067.

I. Tinoco, Jr. (1962) Adv. Chem. Phys. 4, 113.

I. Tobias and W. Kauzmann (1961) J. Chem. Phys. 35, 538.

II. THE BIREFRINGENCE AND OPTICAL ROTATORY DISPERSION OF TOBACCO MOSAIC VIRUS

Introduction

Our second example of the use of optical methods to assist in the study of a biological structure will be experiments on a well characterized virus (Gierer, 1960). The electric birefringence of tobacco mosaic virus (TMV) has been studied with visible light (O'Konski and Haltner, 1957); we wish to extend these measurements over a range of wavelengths extending into the ultraviolet. This technique has the ability to give us information about the orientation of chromophores in the virus. We will also measure the ORD in order to compare it with the measurements of Simmons and Blout (1960). We anticipate that the improved instrumentation of the Cary model 60 scanning spectropolarimeter will give us added detail in the ORD curve, and we should also be able to extend the measurements to shorter wavelengths.

Preparation

The TMV used in these optical experiments was the common strain, and was prepared by Dr. Stanley Mandeles of the Space Sciences Laboratory of the University of California at Richmond, Calif. The method of preparation was that of Boedtker and Simmons (1958) with certain modifications suggested by Steere (1963). Versene at pH 7.5 was used in place of phosphate buffers in the purification to reduce aggregation by the bivalent matal ions present in the leaf juice. Concentrations of the virus were determined from the extinction coefficient for 265 mμ light of 30.6 in units of 100 ml/g (Boedtker and Simmons, 1958). A Beckman DU was used in the above reference, but we have checked the Cary 15 against the DU in our laboratory and the readings at 265 mμ are the same, indicating that the two instruments record

approximately the same amount of scattered light. Thus the Cary 15, which was used for all the uv absorption spectrum measurements in this study, may also be used to determine concentration of virus.

As further purification, we centrifuged the 1% stock solution we received from Dr. Mandeles at 9000 rpm in the Spinco model L (rotor #30) for 20 minutes with refrigeration. The supernatant was then centrifuged for 180 minutes at 18,500 rpm and the pellet suspended in .002 M Versene at pH 7.5. This solution was then diluted 100 fold with 10^{-4} M Versene at pH 7.4. The ultraviolet absorption spectrum measured on the Cary 15 is shown in Fig. II-(1). The concentration of virus is 0.0908 mg/ml. This solution was used for all of the electric birefringence and ORD measurements. The TMV solution was stored at 4°C for the course of these experiments, approximately 6 months. O'Konski and Haltner (1957) have reported that TMV stored under refrigeration remains stable for as much as two years. The pH of our preparation remained at 6.8-6.9 as measured on a Beckman pH meter, and showed no signs of deterioration, such as precipitation of large aggregates.

The TMV protein for these experiments was prepared by a method of Fraenkel-Conrat (1957). 10 ml of the 1% stock solution mentioned above was added to 20 ml of glacial acetic acid (Brothers Chemical Co., Reagent A.C.S.) in a cold room at 5°C, and allowed to stand 35 minutes. The precipitate, composed primarily of RNA, which appears was removed by centrifugation in a clinical centrifuge also in the cold room. The supernatant was then dialyzed against distilled water for 24 hours. As the dialysis proceeds, the pH rises above 4 and the protein aggregates. A few drops of pH 5.0 sodium acetate buffer were then added to stabilize the pH at a value below 6, where the protein is aggregated into large rod-like particles. (Schramm and Zillig, 1955; Fraenkel-Conrat, 1957). The solution was centrifuged at 19,000 rpm

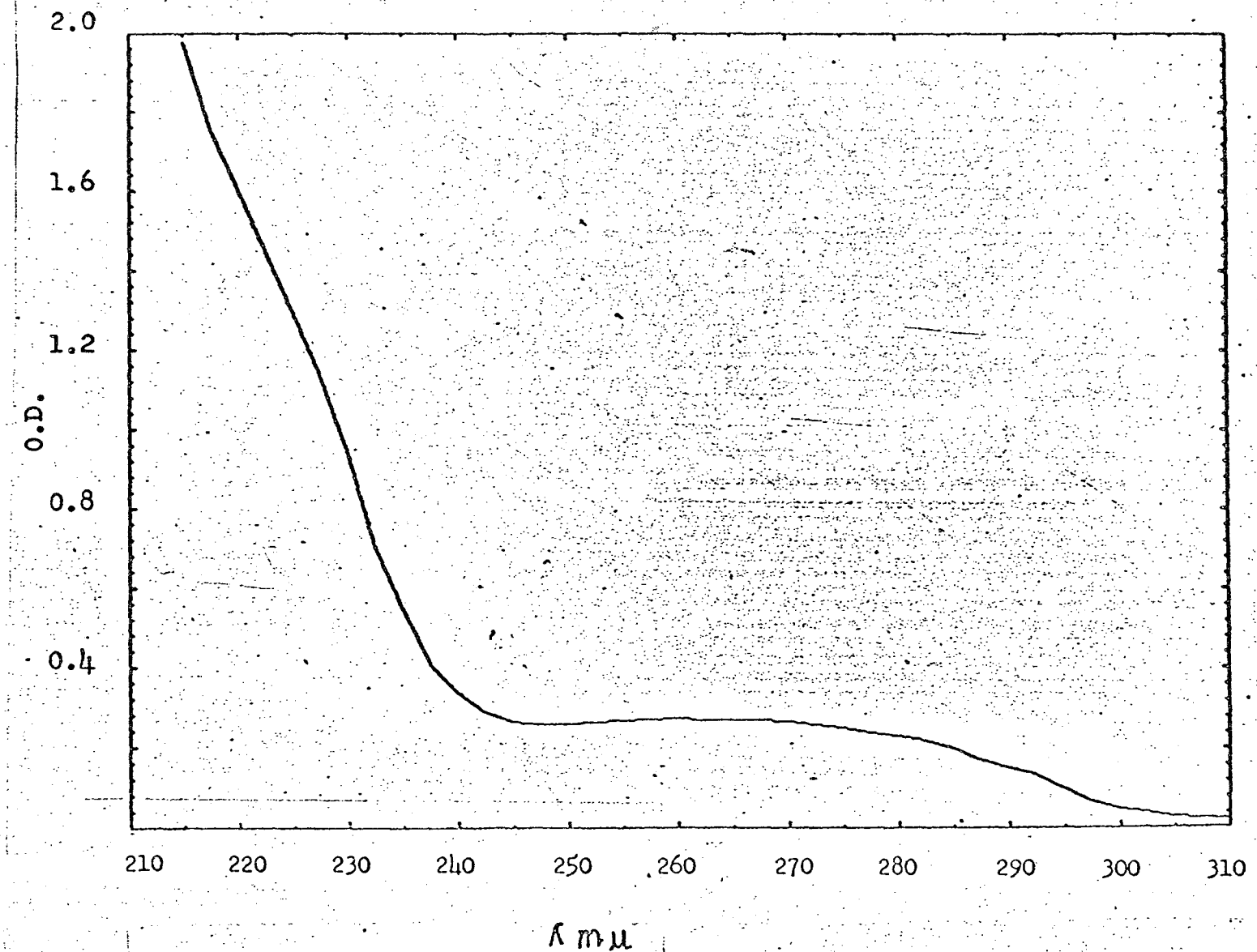

Figure II-1 U.V. ABSORPTION OF TMV AT .0908 MG/ML

for 180 minutes and the pellet of aggregated protein taken up in 3×10^{-3} M potassium phosphate buffer at pH 7.5. At this pH, the protein gives non-turbid solutions of the small protein subunits. This solution was then centrifuged at 19,000 rpm for 180 minutes to precipitate any undegraded virus. The ultraviolet absorption spectrum is shown in Fig. II-(2). It agrees well with the spectrum of Fraenkel-Conrat and Williams (1955), with a ratio of optical densities at the maximum to that at the minimum of 2.3, which compares to their quoted value of 2.4. We also notice the long wavelength shoulder at 290 mμ and a second shoulder to the short wavelength side of the peak at 277 mμ in agreement with Fraenkel-Conrat and Williams (1955).

The solution was then dialyzed against 10^{-3} M sodium acetate at pH 4.8 in order to give aggregated protein rods of dimensions similar to native TMV (Schramm and Zillig, 1955; Franklin, 1956). The absorption spectrum of the aggregated protein rods is shown in Fig. II-(3).

In order to determine the concentration of the protein solutions, we first determine the concentration of the pH 7.5 solution of unaggregated subunits from the extinction coefficient at 282 mμ given in Fraenkel-Conrat and Williams (1955). This solution is then dialyzed to pH 4.8 and the spectrum again taken. Since the salt concentration is small before and after dialysis, we assume the protein concentration has not changed appreciably during dialysis. The optical density is higher since the protein rods scatter light strongly. The concentration of any solution of protein rods can now be determined by comparison to the solution of known concentration.

Measurement of the Optical Rotation

Now having the sample, we proceed to measure the ORD with the Cary model 60. The temperature was 25°C and all the measurements were repeated with at least three scans through the wavelength range. The precision is

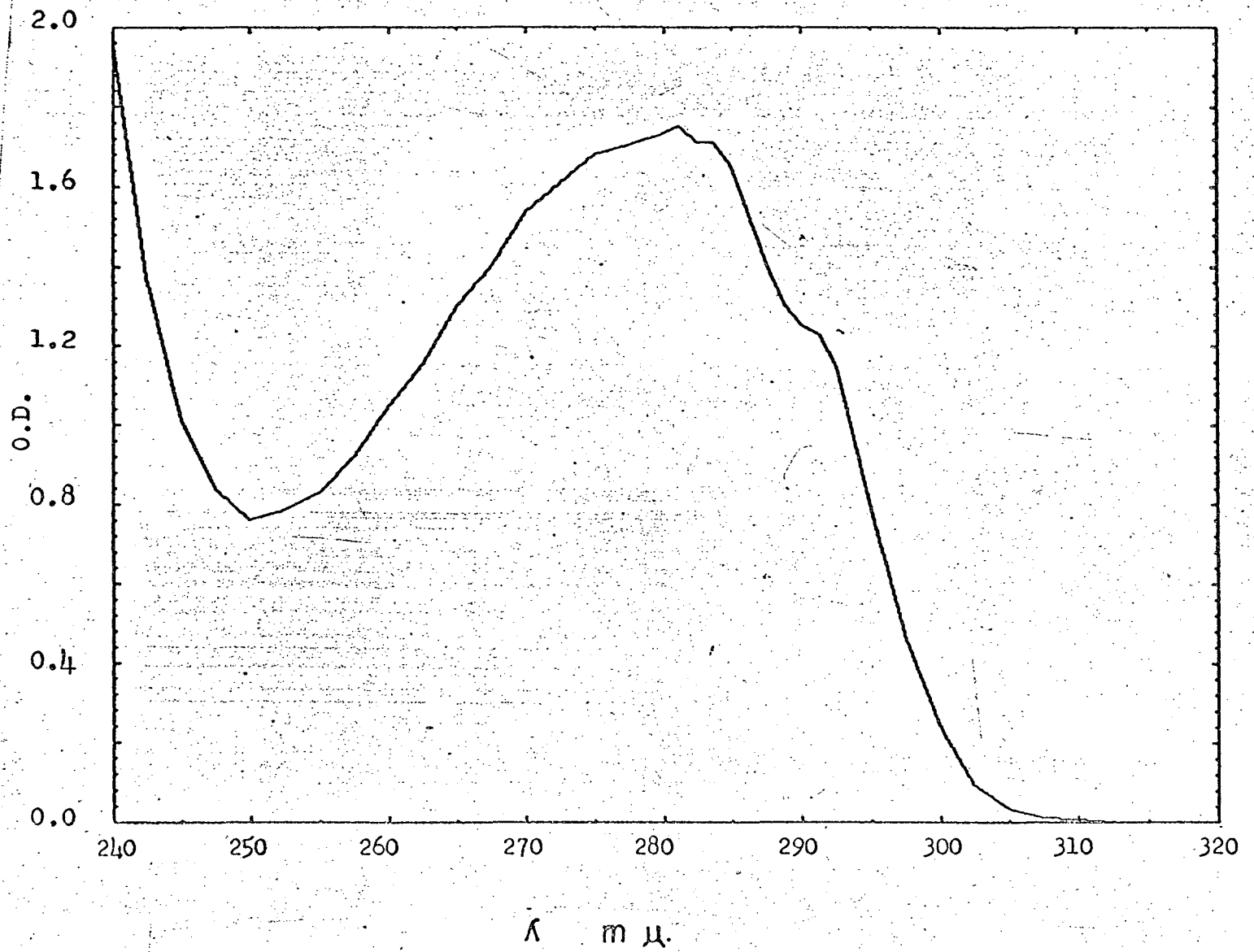

Figure II-2 U.V. ABSORPTION OF TMV PROTEIN PH 7.5 (UNAGGREGATED)

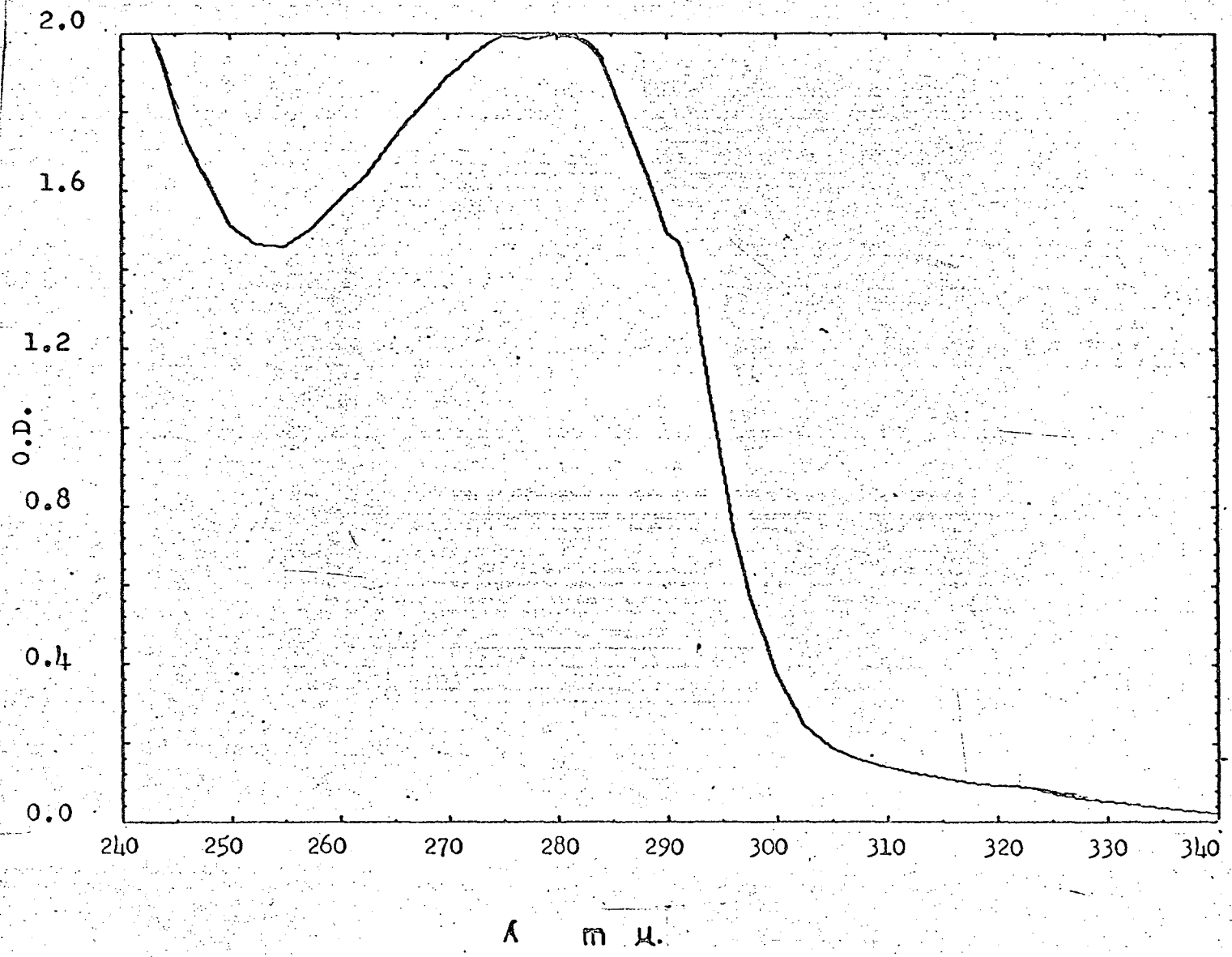

Figure II-3 U.V. ABSORPTION OF TMV PROTEIN PH 4.8 (AGGREGATED)

[illegible] The solution of TMV mentioned above (.0908 mg/ml) was measured and the results appear in Fig. II-(4) and are tabulated in Table II-(1). The specific rotation, $[\alpha]$, is in the customary units defined by: $[\alpha] = 100 \cdot \alpha / L \cdot c$ where α is the rotation in degrees, L is the path length in decimeters and c is the concentration in grams per 100 ml of solution. In Fig. II-(5) we show the ORD of unaggregated protein subunits at pH 7.5 with the values appearing in Table II-(2). The ORD of the aggregated protein rod is shown in Fig. II-(6), and in Table II-(3).

Discussion of the ORD

Our results compare favorably with those of Simmons and Blout (1960) shown in Fig. II-(7). We did extend the range of the measurement to shorter wavelengths to show the trough which is characteristic of protein rotation. In native TMV, this trough occurs at 236 mμ. The improved detail also shows us a small but reproducible anomaly in TMV at 290 mμ. This may be due to the aromatic rings of tyrosine and tryptophan in the asymmetric field of the protein, since it is also seen in the unaggregated protein. The second anomaly we see in TMV (Fig. II-4) is at 258 mμ and is also reproducible. This is probably due to the nucleic acid absorption at that wavelength, since it is absent in the ORD of the protein. This anomaly is small due to the low proportion (5%) of nucleic acid in TMV.

In the protein, both aggregated and unaggregated, we see the anomaly near 290 mμ, but the overall shape of the two curves is rather different, in agreement with Simmons and Blout (1960). The 231 mμ trough of the unaggregated protein undergoes a shift to 235 mμ in the aggregate and decreases to approximately half the magnitude. Smaller changes could be the result

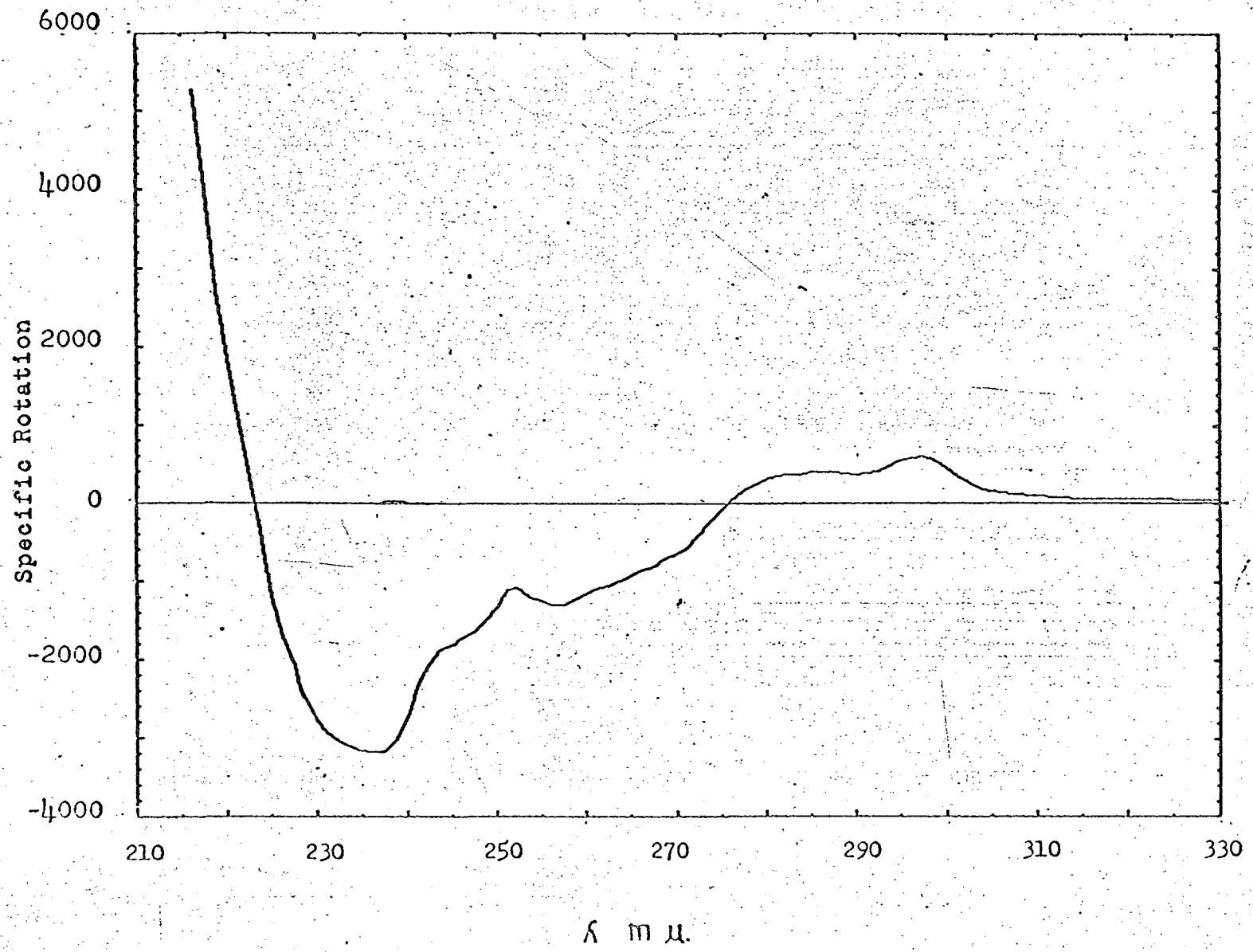

ORD OF TMV AT .0908 MG/ML IN VERSENE PH 6.9

Figure II-4

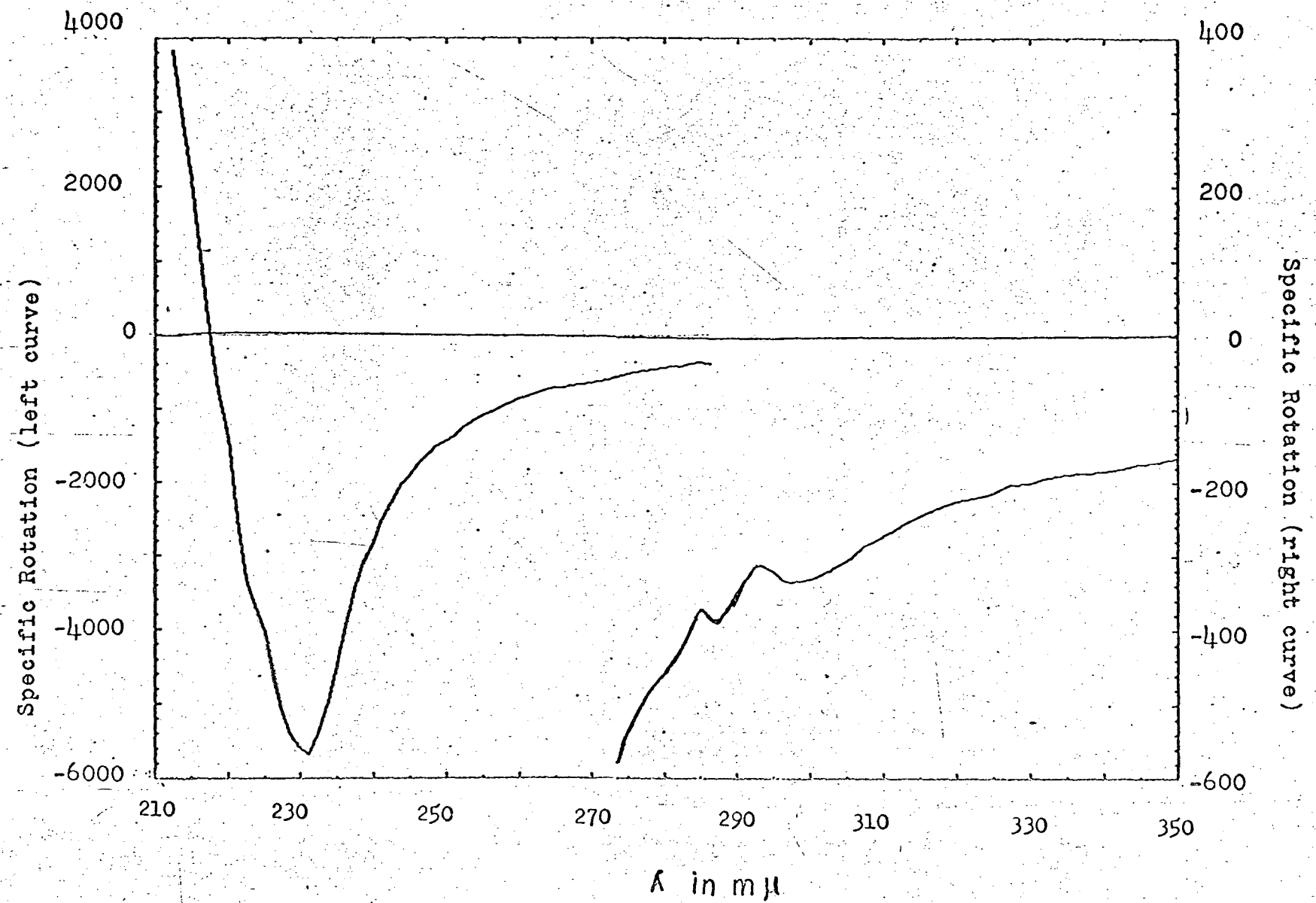

Figure II-5 ORD OF TMV PROTEIN (UNAGGREGATED) PH 7.5

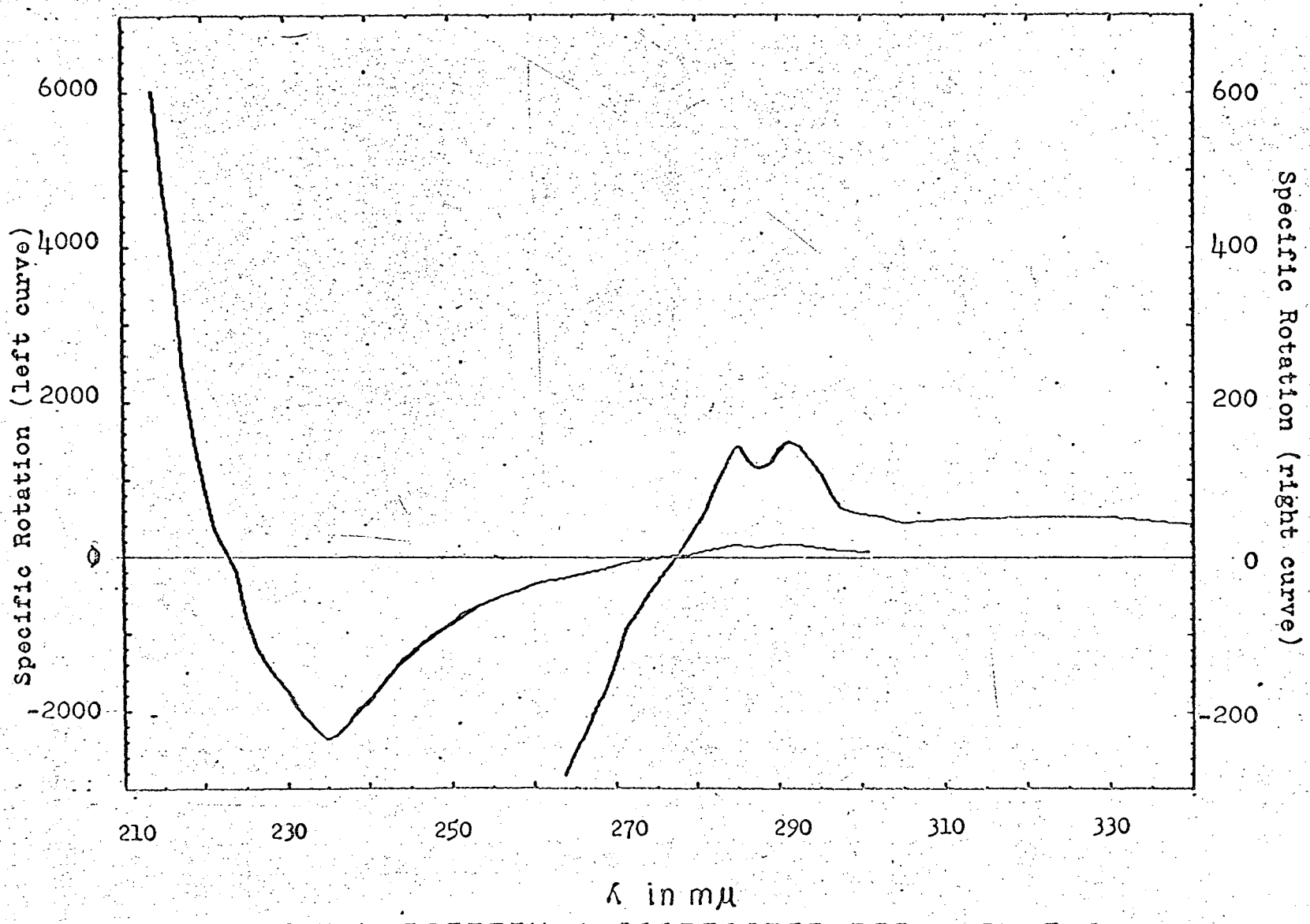

Figure II-6 ORD OF TMV PROTEIN (AGGREGATED RODS) PH 5.3

Figure II-7

Results of Simmons and Blout (1960)

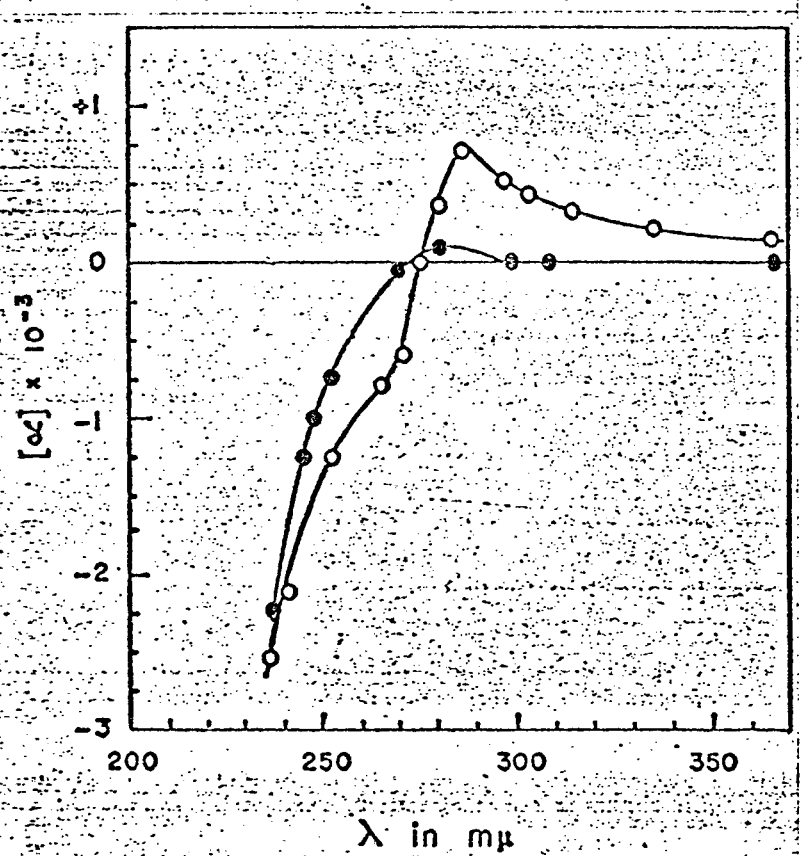

—o——o— ORD of TMV in distilled water

—•—•— ORD of TMV protein (aggregated) in .01m NaH_2PO_4

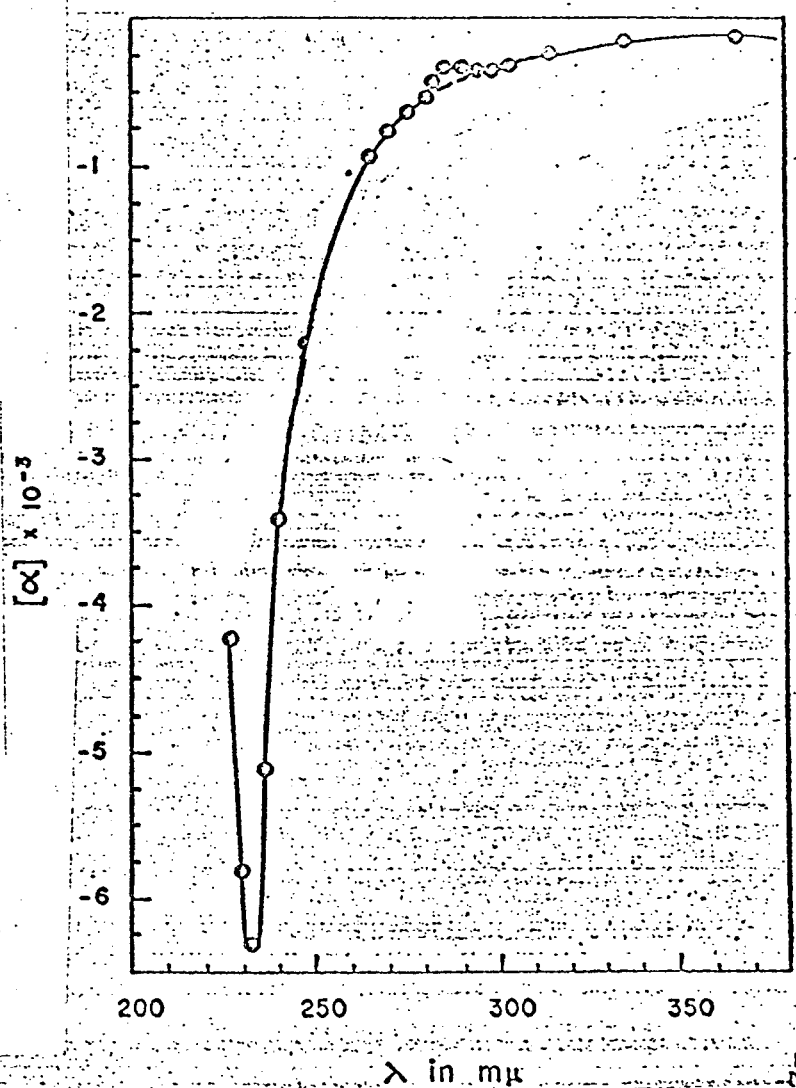

ORD of TMV protein (unaggregated) in distilled water

Table II-(1)

ORD of TMV at .0908 mg/ml in Versene pH 6.9

λ in mμ	[α]	λ in mμ	[α]
		continued	
330.0	44	262.5	-1059
320.0	66	261.2	-1100
315.0	77	260.0	-1147
312.5	88	258.7	-1232
310.0	110	257.5	-1300
307.5	121	256.2	-1290
307.5	121	255.0	-1232
307.5	121	253.7	-1190
305.0	165	252.5	-1069
303.7	209	251.2	-1100
302.5	287	250.0	-1321
301.2	363	248.7	-1488
300.0	474	247.5	-1653
298.7	573	246.2	-1708
297.5	605	245.0	-1805
296.2	595	243.7	-1871
295.0	540	242.5	-2060
293.7	495	241.2	-2290
292.5	419	240.0	-2730
291.2	397	238.7	-3030
290.0	374	237.5	-3170
288.7	396	236.2	-3180
287.5	419	235.0	-3150
286.2	419	233.7	-3095
285.0	408	232.5	-3040
283.7	374	231.2	-2910
282.5	363	230.0	-2755
281.2	341	228.7	-2665
280.0	308	227.5	-2060
278.7	231	226.2	-1674
277.5	154	225.0	-1169
276.2	44	223.7	-330
275.0	-88	222.5	440
273.7	-242	221.2	1157
272.5	-419	220.0	1871
271.2	-561	218.7	2750
270.0	-650	217.5	4185
268.7	-715	216.2	5290
267.5	-805		
266.2	-859		
265.0	-936		
263.7	-1000		

Table II-(2)

ORD of TMV Protein (unaggregated) pH 7.5

λ in mμ	[α]	λ in mμ continued	[α]
350.0	-168	270.0	-647
347.5	-174	268.7	-661
345.0	-175	267.5	-687
342.5	-181	266.2	-705
340.0	-186	265.0	-716
337.5	-188	263.7	-749
335.0	-190	262.5	-786
332.5	-194	261.2	-823
330.0	-201	260.0	-876
327.5	-204	258.7	-931
325.0	-216	257.5	-986
322.5	-221	256.2	-1041
320.0	-226	255.0	-1097
317.5	-236	253.7	-1170
315.0	-246	252.5	-1241
312.5	-260	251.2	-1370
310.0	-274	250.0	-1443
308.7	-282	248.7	-1518
307.5	-285	247.5	-1627
306.2	-298	246.2	-1755
305.0	-307	245.0	-1920
303.7	-314	243.7	-2045
302.5	-322	242.5	-2283
301.2	-327	241.2	-2485
300.0	-332	240.0	-2815
298.7	-334	238.7	-3088
297.5	-336	237.5	-3455
296.2	-331	236.2	-3930
295.0	-320	235.0	-4480
293.7	-311	233.7	-5025
292.5	-314	232.5	-5390
291.2	-332	231.2	-5670
290.0	-352	230.0	-5570
288.7	-371	228.7	-5390
287.5	-391	227.5	-5025
286.2	-384	226.2	-4570
285.0	-368	225.0	-4020
283.7	-398	223.7	-3650
282.5	-424	222.5	-3290
281.2	-439	221.2	-2470
280.0	-459	220.0	-1370
278.7	-473	218.7	-730
277.5	-490	217.5	90
276.2	-512	216.2	1098
275.0	-534	215.0	2100
273.7	-577	213.7	3015
272.5	-603	212.5	3840
271.2	-623	211.2	4750

Table II-(3)

ORD of TMV Protein (aggregated rods) pH 5.3

λ in mμ	[α]	λ in mμ continued	[α]
340.0	42	256.2	-520
330.0	53	255.0	-571
320.0	53	253.7	-625
310.0	49	252.5	-681
305.0	45	251.2	-738
303.7	49	250.0	-890
302.5	53	248.7	-946
301.2	55	247.5	-1040
300.0	57	246.2	-1135
298.7	61	245.0	-1249
297.5	64	243.7	-1361
296.2	83	242.5	-1532
295.0	110	241.2	-1684
293.7	129	240.0	-1890
292.5	144	238.7	-1970
291.2	151	237.5	-2155
290.0	140	236.2	-2290
288.7	121	235.0	-2365
287.5	114	233.7	-2235
286.2	125	232.5	-2100
285.0	149	231.2	-1930
283.7	125	230.0	-1720
282.5	98	228.7	-1555
281.2	64	227.5	-1400
280.0	36	226.2	-1170
278.7	10	225.0	-756
277.5	0	223.7	-189
276.2	-17	222.5	94
275.0	-34	221.2	378
273.7	-53	220.0	945
272.5	-76	218.7	1515
271.2	-95	217.5	2360
270.0	-134	216.2	3780
268.7	-174	215.0	4920
267.5	-197	213.7	6050
266.2	-231	212.5	7280
265.0	-252		
263.7	-284		
262.5	-307		
261.2	-334		
260.0	-367		
258.7	-424		
257.5	-476		

of simple coulombic fields of the subunits on each other in the aggregate, but the changes we observe are large enough to suggest that the subunits may undergo actual conformational changes on aggregation. The aggregated protein ORD resembles the native TMV much more than the unaggregated subunit spectrum, indicating that the aggregate may have the same structure as the native virus, the only difference being that the RNA is missing.

Equipment for the Birefringence Measurements

In order to measure the birefringence spectrum we used an electric birefringence apparatus built by Dr. K. Yamaoka (1964). The light source was a high pressure mercury xenon arc enclosed in a quartz envelope (Hanovia, 1000 watt, type 528 B). A Bausch and Lomb 500 mm grating monochromator (Bausch and Lomb Optical Co., Rochester, N. Y.) was used to select mercury lines from the arc. The intensities and wavelengths of these lines at high pressure, given by the manufacturer (Hanovia Lamp Division, Newark, N. J.) were used to calibrate the monochromator. In order to ensure spectral purity, a filter, Corning C. S. 7-54, which transmits wavelengths between 260 mμ and 365 mμ was used for measurements in that range. At wavelengths shorter than 260 mμ, the second order dispersion of the grating is unimportant and no filter was used. For polarizing and analyzing the light, a Rudolph 80 Q polarimeter was used. It could be read to a millidegree. The polarized light passed through the sample cell in a water jacket kept at a constant temperature by a Blue M Magni-Whirl Utility water bath at 25°C. The cells used were quartz cuvettes of 1 cm. path length, with a Teflon electrode holder inserted. The platinum electrodes slide into the cuvette so that they are vertical and the light passes through the sample solution which is between them. Thus the sample is in a horizontal uniform electric field when the voltage is applied to the electrode plates. The spacing of the plates in the cell used in these experiments was measured with a Gaert-

ner Comparator and found to be 1.28 cm ± .02 cm. The light is polarized at 45° from the vertical so that the birefringent solution induces ellipticity in the emerging light. Fig. II-(8) shows a cutaway diagram of the cell and water jacket (Yamaoka, 1964).

A Fresnel rhomb constructed by Tinsley Laboratories (Berkeley, Calif.) of optical quartz is used to retard one of the components of light emerging from the birefringent solution. A retardation of 90 degrees is accomplished by four reflections at 74.3° from the surfaces. The retardation will be constant to ± 1.5° over the wide range of wavelengths used (Yamaoka, 1964). This retardation by the rhomb converts elliptically polarized light into plane polarized light rotated by an amount equal to half the retardation. This phenomenon will be described below. The method gives improved instrumental sensitivity over measuring the induced elliptical component directly and also gives the sign of the retardation. The light then passes through the analyzer of the polarimeter and is detected by a photomultiplier enclosed in a quartz envelope (Dumont type 7664) which is in a light tight box. The photomultiplier power supply was a regulated model, adjustable from 1000 to 1500 volts.

In order to generate the electric field on the sample cell plates, a square wave generator giving pulses of 10 microseconds to several milliseconds in length and from a few hundred to 10,000 volts in amplitude was employed. Tektronix pulse generators model 161 and model 163 generated pulses of appropriate length at approximately 25 volts. A pulse amplifier utilizing a type 5D21 tube amplified the voltage for application to the plates of the birefringence cell. The wiring diagram is shown in Fig. II-(9). Our wiring is similar to that of Yamaoka (1964) except that larger coupling capacitors are used between the stages because of the longer pulses used in our study. The high voltage for the pulse amplifier was

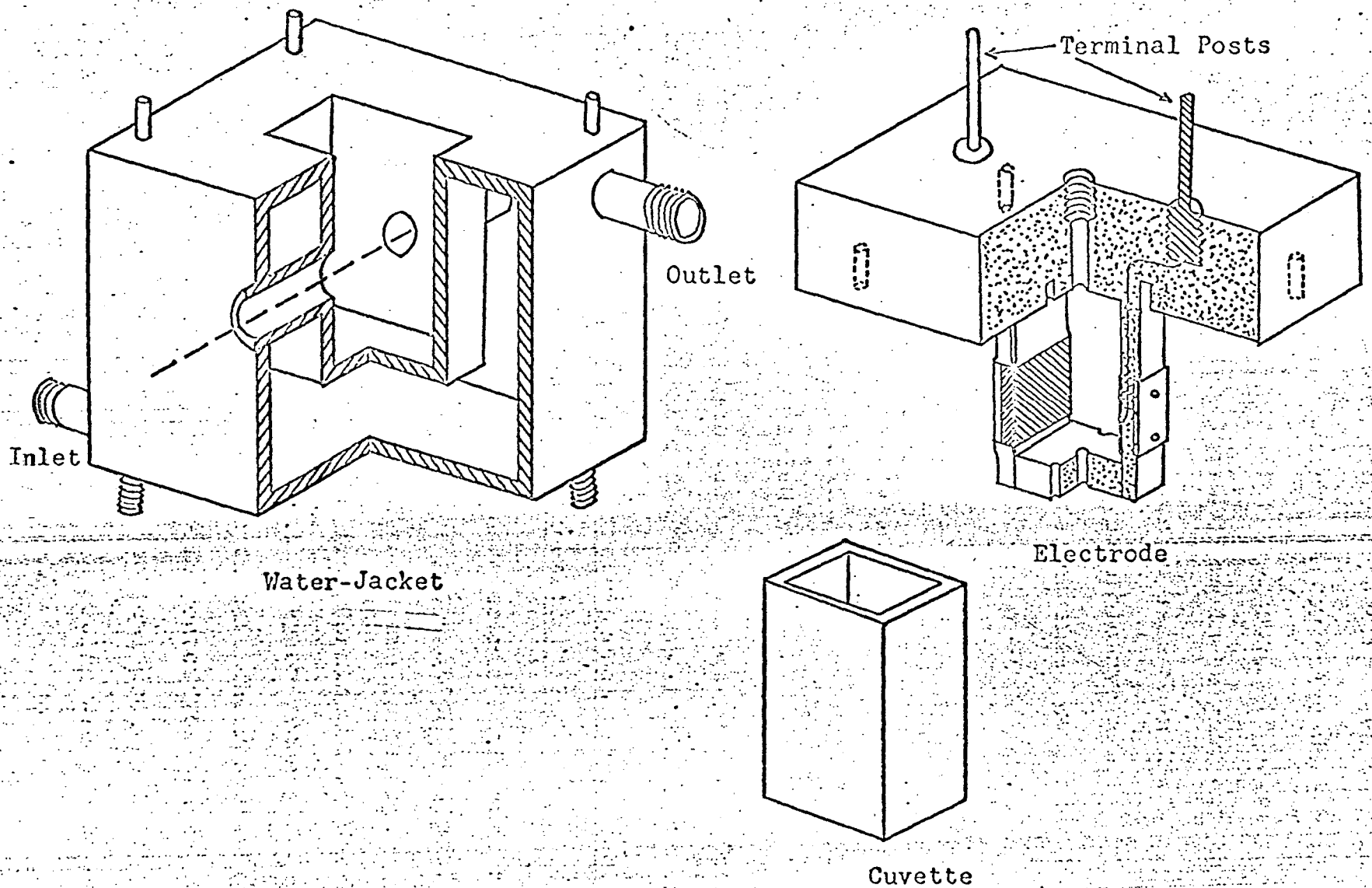

Figure II-8 Diagram of cell, electrodes and water-jacket

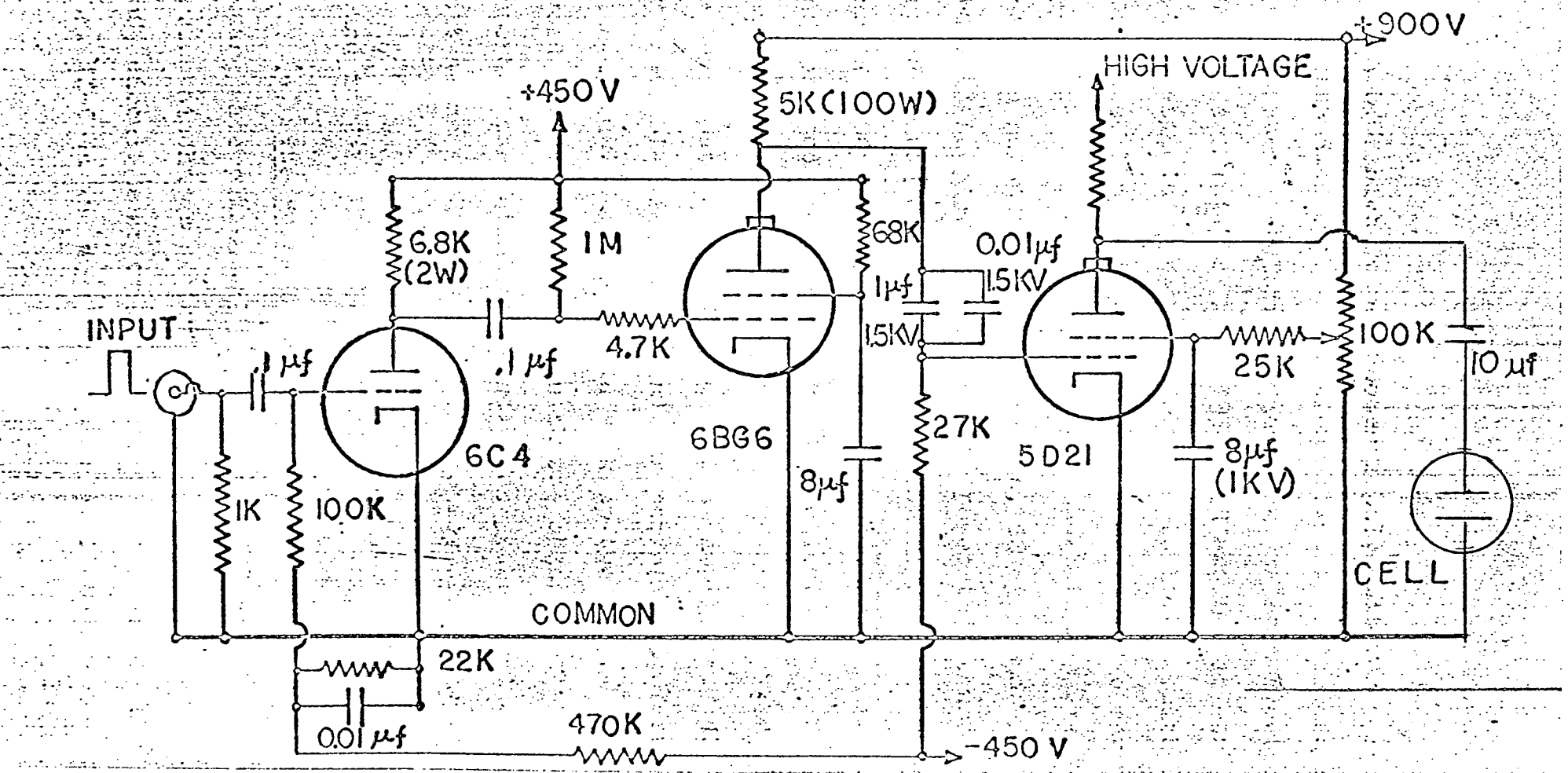

Figure II-9
Wiring diagram of high Voltage pulse amplifyer
and birefringence cell

supplied by a Beta Electric power supply model 1030-10 R5D.

For simultaneous observation of the square wave pulse applied to the cell and the photomultiplier output, a Hewlet-Packard 152-B dual trace oscilloscope was used. On one channel, we observe the voltage drop across the cell, appropriately attenuated by a Tektronix model P 6015 high voltage probe, and on the other channel we observe the voltage drop of the photomultiplier tube across a resistor of a few thousand ohms. This resistance is chosen such that the relaxation time of the photomultiplier circuit is short compared to the molecular relaxation time. The oscilloscope traces are recorded on a Pentax model H-2, 35 mm camera for subsequent measurement. In order to synchronize the camera shutter properly with the pulse and the oscilloscope trace, the flash synchronizer on the camera triggered a Tektronix model 162 waveform generator. The pulse output from the waveform generator triggered the scope sweep and the rising sawtooth wave could be adjusted to trigger the pulse generator at an appropriate time later so that the square pulse would appear near the middle of the screen. We used the model 161 to generate the millisecond length pulses used in the present TMV study; for shorter pulse durations, the model 163 could be used. In Fig. II-(10) we show a schematic block diagram of the wiring of the pulse circuit. A typical photograph is shown in Fig. II-(11) demonstrating the square pulse and the output from the photomultiplier which reflects the birefringence of the sample (TMV in this case) in a manner to be treated below. The time scale for Fig. II-(11) is one millisecond per cm (one line on the ruled scale). The pulse voltage is 2000 V per cm of screen deflection and the photomultiplier circuit sensitivity is 10 V per cm.

The difference between the refractive index for light polarized parallel and that for light polarized perpendicular to the direction of the orienting

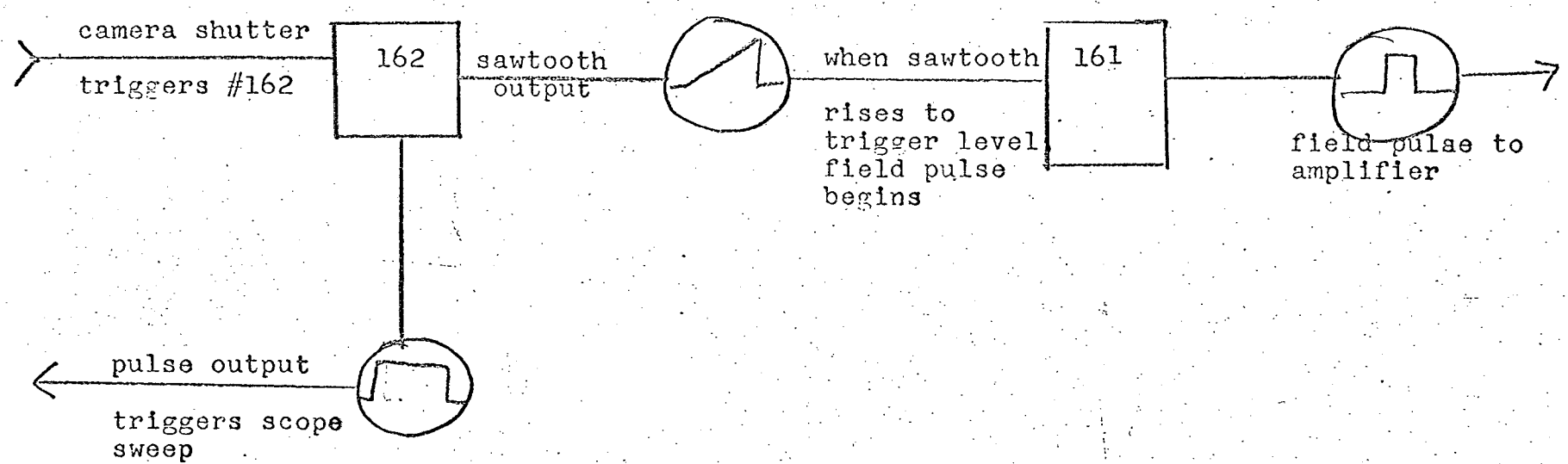

Figure II-10 Block diagram of the pulse circuit

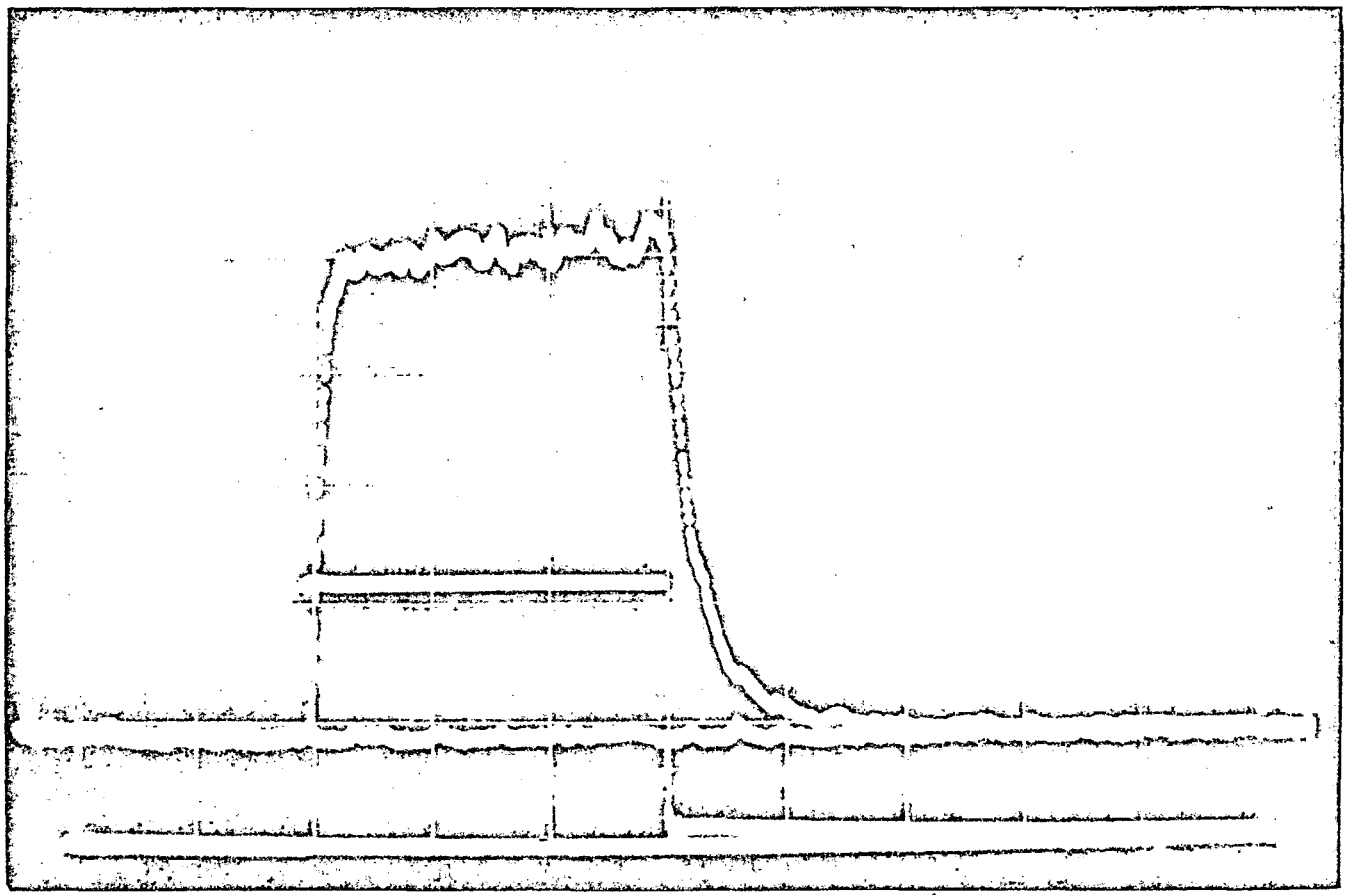

Figure II-11 Photograph of a typical oscilloscope trace.

electric field is known as the electric birefringence. It is closely related to the retardation, δ, defined as: $\delta = (2\pi L/\lambda)(n_{\parallel} - n_{\perp})$, where L is the path length and λ is the wavelength of the light expressed in the same units.

A thorough discussion of the optical system used here has been given by Haschemeyer (1961). We will give a brief summary of that derivation in order to illustrate the essentials of the method. Fig. II-(12) shows a schematic diagram of the cell with the light polarized in the Y direction 45° away from the $\underset{\sim}{e}$ direction, the direction of the uniform electric field. The light path is along Z. The plane polarized light emerging from the polarizer and having amplitude A is: $\underset{\sim}{A} = \underset{\sim}{j}\, A \sin \omega t$, where $\underset{\sim}{j}$ is the unit vector along Y and ω is the angular frequency of the light. Its components along the static field directions $\underset{\sim}{o}$ and $\underset{\sim}{e}$ are:

$$\underset{\sim}{A}_o = \underset{\sim}{o}\,(A/\sqrt{2}) \sin \omega t \text{ and } \underset{\sim}{A}_e = \underset{\sim}{e}\,(A/\sqrt{2}) \sin \omega t \qquad \text{II-(1)}$$

The light emerges from the birefringent sample with the $\underset{\sim}{e}$ component retarded by δ with respect to $\underset{\sim}{o}$, $\underset{\sim}{A}_e = \underset{\sim}{e}\,(A/\sqrt{2}) \sin (\omega t - \delta)$. The Fresnel rhomb is oriented so as to retard the X component of the light by 90° with respect to the Y component. We write the light emerging from the rhomb as the sum of two components:

$$\underset{\sim}{A}_x = \underset{\sim}{A}_{ex} + \underset{\sim}{A}_{ox} = \underset{\sim}{i}\; 1/2\, A\, [\sin (\omega t - \delta - \pi/2) - \sin (\omega t - \pi/2)]$$
$$\underset{\sim}{A}_y = \underset{\sim}{A}_{ey} + \underset{\sim}{A}_{oy} = \underset{\sim}{j}\; 1/2\, A\, [\sin (\omega t - \delta) + \sin \omega t] \qquad \text{II-(2)}$$

Using a little trigonometry, we may rewrite the equations as:

$$\underset{\sim}{A}_x = -\underset{\sim}{i}\, A \sin (\delta/2) \sin (\omega t - \delta/2)$$
$$\underset{\sim}{A}_y = \underset{\sim}{j}\, A \cos (\delta/2) \sin (\omega t - \delta/2) \qquad \text{II-(3)}$$

If the analyser is set at an angle θ with respect to the X axis, which axis

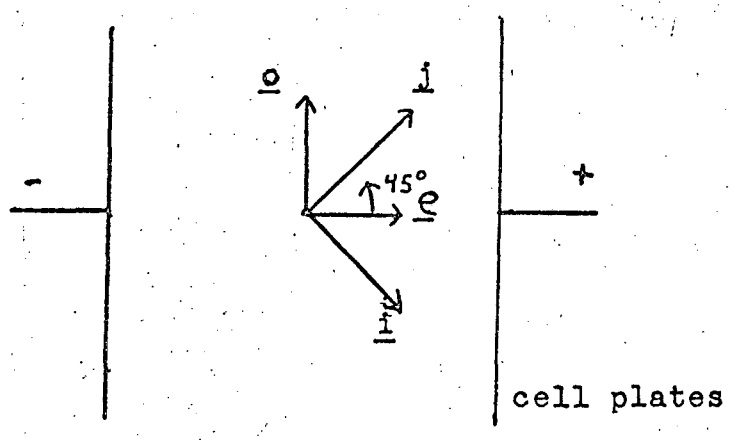

Figure II-12

Diagram of the cell showing the direction of the static electric field (e), and the plane of polarization of the light (plane of vector j and k, the light direction which is out of the page)

is perpendicular to the original axis of polarization, Y, the amplitude of the light surviving the analyzer is given by:

$$A(\theta, \delta) = A \sin(\theta + \delta/2) \sin(\omega t - \delta/2) \qquad \text{II-(4)}$$

If the static field is off, there is no orientation of the sample and hence $\delta = 0$. In this case,

$$A(\theta, 0) = A \sin(\theta) \sin(\omega t), \qquad \text{II-(5)}$$

which gives the well-known Malus law for analysis of polarized light. Since the voltage of the photomultiplier is proportional to the intensity, I, of the light, we give the value of the difference of the squares of the amplitudes with the field on and with the field off.

$$\Delta I = I_{on} - I_{off} = A^2(\theta,\delta) - A^2(\theta,0) = I_o [\sin^2(\theta + \delta/2) - \sin^2\theta] \qquad \text{II-(6)}$$

where I_o is the original intensity, A^2. The photomultiplier voltage, V, which is the quantity observed on the oscilloscope, is proportional to I, so we may rewrite II-(6) as:

$$\frac{\Delta V}{V_o} = 1/2 [\cos(2\theta) - \cos(2\theta - \delta)] \qquad \text{II-(7)}$$

In order to determine the retardation, we need two numbers, V_o and ΔV. The ΔV are simply read from the photographs of the oscilloscope trace, such as Fig. II-(11), using the calibration lines of the oscilloscope as a scale. The 35 mm negatives were measured directly using a Gaertner comparator (Wm. Gaertner Co., Chicago, Ill.) V_o, the photomultiplier voltage with the polarizer and analyzer parallel, may be large and beyond the linear range of the photomultiplier, so it is measured by setting the analyzer at some angle away from the crossed position which gives an easily measured photomultiplier voltage, and then using the $\sin^2\theta$ relation to get

the voltage at full transmission. These voltages depend on the light output from the mercury-xenon lamp and should, therefore, be measured as soon as possible before each photograph of a pulse is made in order to account for fluctuations in the lamp intensity. The measurement can be quickly accomplished directly on the oscilloscope screen using the same analyzer setting as is used for the ΔV-measuring photograph. The voltage, $V_o \sin^2\theta$, can be read as oscilloscope trace deflection caused by opening a shutter in the light path or by using a calibrated voltage divider to return the trace to the dark photomultiplier position. In these experiments a helipot voltage divider was used with a battery of calibrated voltage. The battery was calibrated to 0.5% with the aid of an ordinary potiontometer and the helipot was linear to 0.5%. The horizontal sweep was set to give a trace with the light path blocked by the shutter. The shutter was opened, and the trace returned to its original vertical deflection with the calibrated helipot voltage divider which gives V_o. A picture is then taken to record the ΔV.

Results and Discussion of the Birefringence

The photograph, Fig. II-(11), shows the DC square wave pulse voltage across the cell plates and also the output from the photomultiplier. The photomultiplier output shows the rise of the birefringence, the static equilibrium value with the field on, and its decay. This decay is a measure of the rotational diffusion coefficient, and has been treated elsewhere (Tinoco, 1955). Very long decay times, corresponding to small rotational diffusion coefficients, would indicate aggregates of the TMV. This effect was studied by O'Konski and Haltner (1957) who report a rotational diffusion coefficient for unaggregated TMV of $\theta = 333\ \text{sec}^{-1}$. In our experiments, plots of the logarithm of the birefringence decay are linear with time, in-

dicating a monodisperse system and giving rotational diffusion coefficients of about 300 sec^{-1}, indicating very little aggregation.

Fig. II-(13) shows a plot of the steady state birefringence of TMV for wavelength 312 mμ and virus concentration .0908 mg/ml in 10^{-4} M Versene at pH 7 as a function of the square of the applied field. The plot is linear for low voltages, as dictated by Kerr's law. Above 1000 volts/cm, saturation sets in, and for fields of 3-4000 volts/cm the virus is completely oriented. It will be these values of saturation birefringence which we will discuss as a function of wavelength of incident light.

The causes of birefringence in solutions of oriented particles have been assumed to come from two sources. First, the particle may have indices of refraction different in the direction parallel and perpendicular to the orienting field. This is known as intrinsic birefrincence because it depends on the anisotropy of the polarizability of the particle, according to the famous theoretical treatment of Peterlin and Stuart (1943). The textural or form birefringence depends only on the difference in indices of refraction of the particle and of the solvent. Since the birefringence of TMV, at least for visible light, can be eliminated by adjusting the index of refraction of the medium (Lauffer, 1938). Lauffer proposed that it arose from the form birefringence described by Wiener (1926). Wiener's formula, however, assumes long rods closely spaced, and predicts a birefringence 100 times greater than is actually observed for TMV, for which the index of refraction is 1.57 (Lauffer, 1938). Peterlin and Stuart's (1943) model is more plausible in that it considers single particles and makes no reference to close or regular spacing. Their formula, reduced to the simplified case of completely oriented rods having an axial ratio greater than about 20 and no intrinsic birefringence (O'Konski, Yoshioka and Orttung, 1959) is:

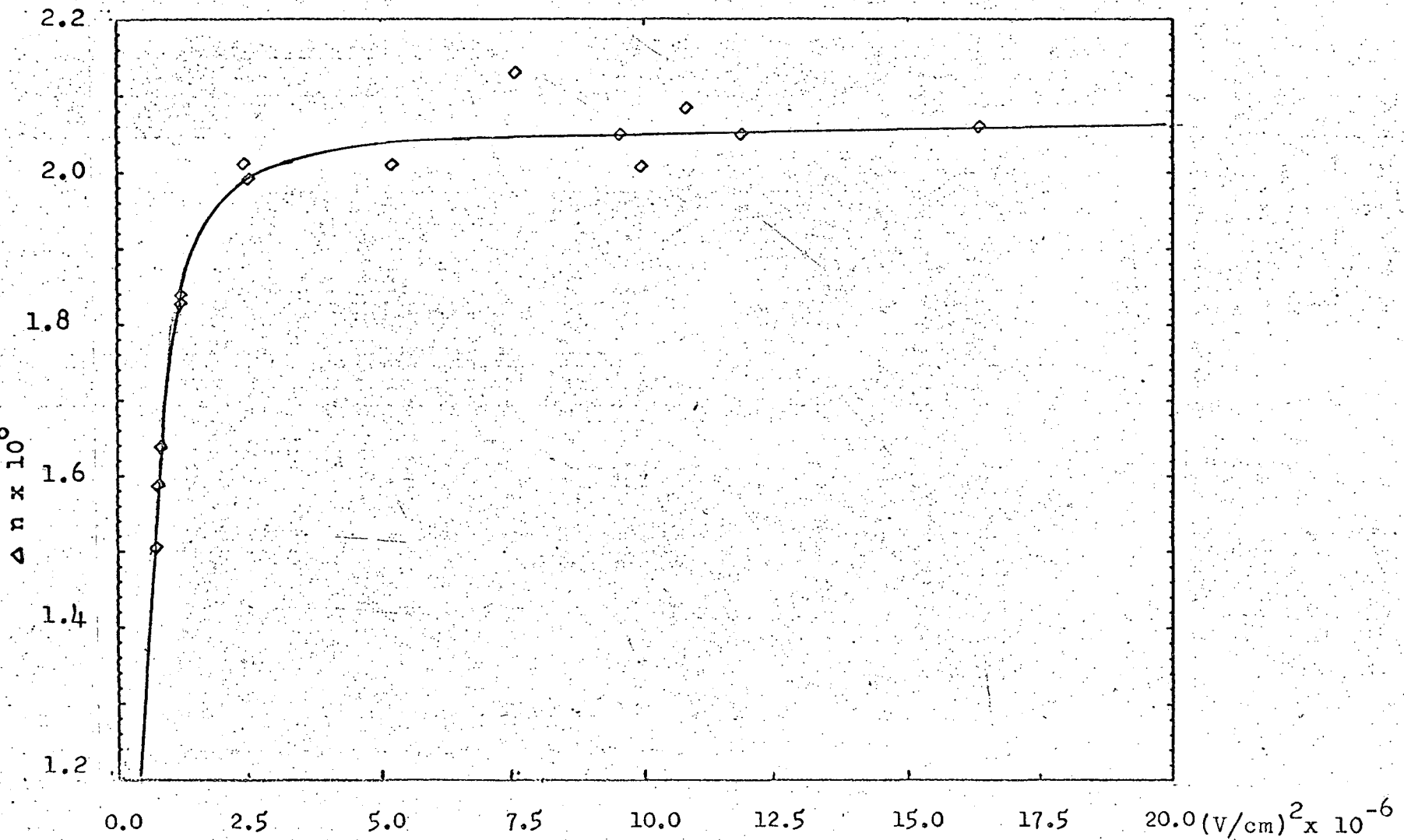

Figure II-13 BIREFRINGENCE OF TMV VERSUS E^2, 312 Mμ., CONC.=.0908 MG/ML

$$\Delta n_{sat.} = C_v \frac{(n_1^2-n_2^2)^2}{2(n_1^2+n_2^2)} \qquad \text{II-(8)}$$

in which C_v is the volume fraction of particles, n_1 is the refractive index of the solvent and n_2 that of the particle. Taking $n_1 = 1.33$ and $n_2 = 1.57$ (Lauffer, 1938) we calculate a birefringence of about 5×10^{-6} for our 0.0908 mg/ml solution while the value we measure at $\lambda = 467$ mμ is 1.50×10^{-6}. We compare this value to the value obtained by O'Konski, et al.(1959) reduced to our concentration ($\Delta n = 1.91 \times 10^{-6}$). Other workers have also found deviation from what one would expect to find according to the Peterlin and Stuart formulas (Taylor, 1965). The primary inadequacy in applying it to protein and virus solutions is that the theory is based on thinking about fields induced within a macroscopic particle of dielectric suspended in a uniform medium. For TMV the length of the rod is about 300 mμ, a dimension exactly comparable with the wavelengths of light used in this study. Therefore, although we shall discuss our results in the traditional terms of intrinsic and form birefringence, we must recognize that our theoretical grounds are a bit marshy. It may not be rigorously possible to separate birefringence into a part depending on the anisotropy of the particle polarizability and a part depending only on the difference between the solute and solvent indices of refraction.

Our results for the birefringence of 0.0908 mg/ml TMV in 10^{-4} M Versene at pH 7 appears in Fig. II-(14) and in Table II-(4). It represents an average of measurements over the complete wavelength range on five separate days. We see that the birefringence increases smoothly with wavelength with the exception of two small anamalies in the region of absorption. At the outset of our study, it was hoped that the anomaly at 260 mμ might be large and give sensitive indication of the orientation of the bases in

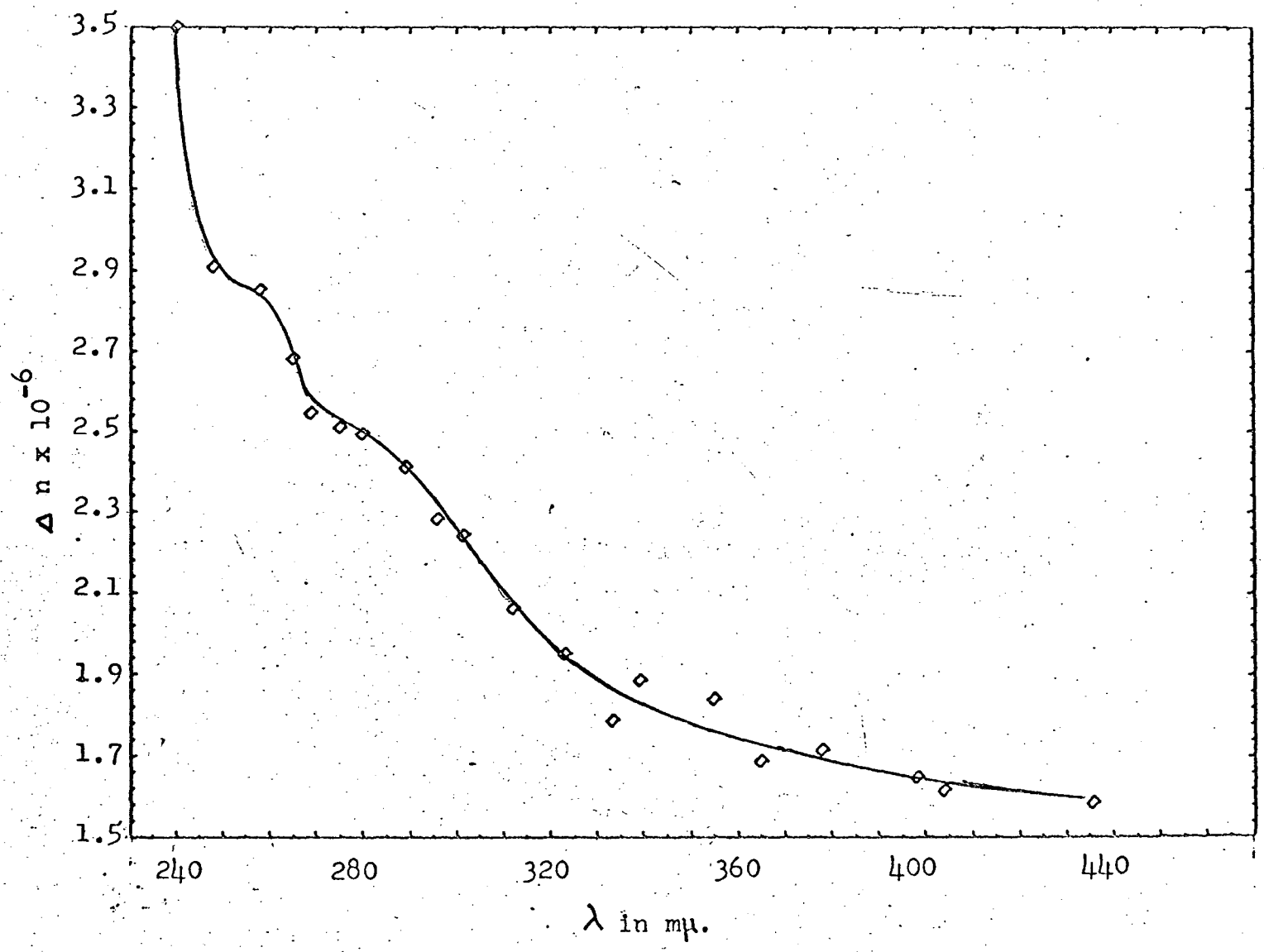

Figure II-14 BIREFRINGENCE OF TMV .0908 MG/ML PH7 VERSENE

Table II-(4)

Birefringence of TMV versus wavelength

λ in mμ	$\Delta n \times 10^{-6}$
240.0	3.500
248.0	2.914
258.0	2.859
265.0	2.687
269.0	2.550
275.0	2.515
280.0	2.496
289.0	2.414
296.0	2.285
301.5	2.244
312.0	2.064
323.0	1.953
333.3	1.790
339.2	1.891
355.0	1.842
365.0	1.690
378.0	1.718
398.0	1.648
404.0	1.619
435.5	1.584
467.0	1.498

the RNA of the virus. The fact that the anomaly is little greater than the experimental error coupled with our lack of a rigorous separation of this intrinsic birefringence from the large positive form biregringence prevents us from making a quantitative calculation of the angle of the base planes with respect to the axis of the virus. We shall restrict ourselves to a qualitative explanation of the effect.

The small anomaly at 290 mμ is apparently part of the form birefringence and caused by the small anomaly one would expect in the index of refraction of TMV due to absorption at this wavelength. The anomaly is, as it must be for rod form birefringence, positive in sign; that is, it shows positive deviation at long wavelength. This is because the index of refraction must show a positive deviation on the long wavelength side of an absorption. Therefore, the rod form birefringence must have the same positive anomaly (see Eq. II-(8). We interpret the anomaly at 260 mμ as an intrinsic effect due to the absorption of the RNA; it could have either sign depending on the orientation of the absorbing chromophore at that wavelength relative to the axis of the rod. The fact that the anomaly is positive would indicate that nucleic acid base planes, which absorb at 260 mμ are oriented predominantly parallel to the axis of the rod. Previous studies of the dichroism of TMV have tentitatively reached the same conclusion, but they too are hampered by lack of a proper theoretical understanding of birefringence and dichroism in particles whose size is comparable to that of the wavelength of light (Seeds and Wilkins, 1950).

Our results for the birefringence of rods of aggregated TMV protein as a function of wavelength are shown in Fig. II-(15), and tabulated in Table II-(5). The concentration of protein is 0.151 mg/ml in 3×10^{-4} M potassium phosphate at pH 5.3. The data are an average over three separate determinations throughout the wavelength range. The experimental uncertainties

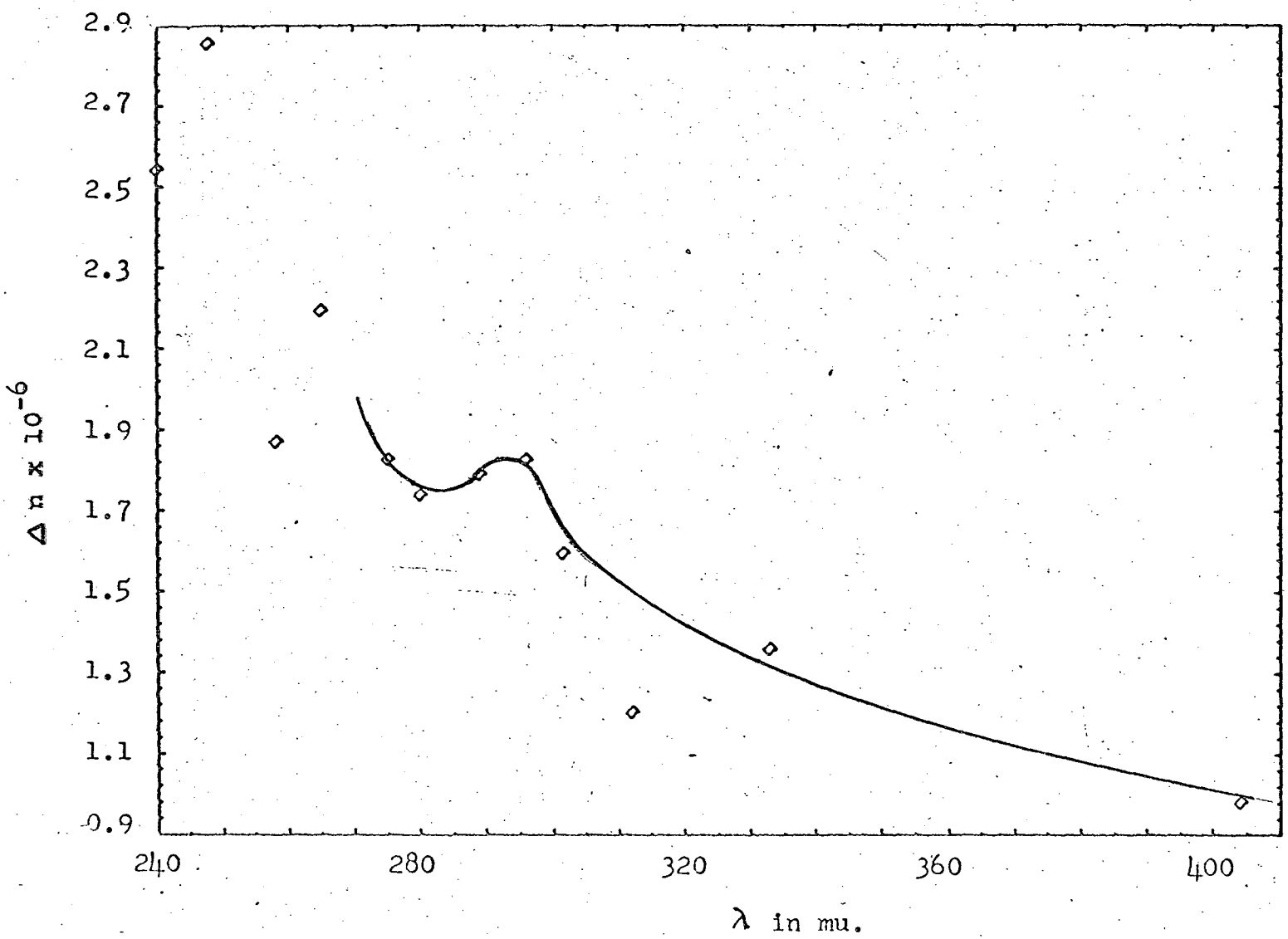

Figure II-15 BIREFRINGENCE OF TMV PROTEIN (AGGREGATED RODS) PH 5.3

Table II-(5)

Birefringence of aggregated TMV protein rods

λ in mμ	$\Delta n \times 10^{-6}$
240.0	2.544
248.0	2.859
258.0	1.873
265.0	2.198
275.0	1.831
280.0	1.741
289.0	1.795
296.0	1.829
301.5	1.597
312.0	1.204
333.0	1.361
365.0	0.854
404.0	0.980

here are greater than in native TMV, probably because of the influence of aggregates of some type other than TMV-like rods 300 mμ long. Our results for the rotatory diffusion coefficient are dependent on the preparation of the protein aggregate and range in value from $\theta = 40$ to 70 sec^{-1}, indicating that the aggregates were larger than native TMV. The anomaly at 290 mμ seems to be present and somewhat larger than in the case of TMV. We would expect a somewhat sharper anomaly in the index of refraction of the protein aggregate due to the sharper absorption peak (Fig. II-3). The data at shorter wavelengths are probably not reliable and are quoted only to give a general idea of the effect. We do not feel that any anomalous dispersion can be inferred from the data.

lated structure might be possible (Luzzati et al., 1965), the circumstantial evidence for a single stranded, stacked structure with the bases perpendicular to the axis is very strong. We will call this a single stranded helix, even though there is porbably only short range order. Over expanses greater than a few bases, the structure is probably more like a random coil.

A study of the kinetics of endonuclease attack showed that TMV RNA in solution is a single strand (Gierer, 1957). Until recently, no pure endonuclease attacking poly A was known and thus a kinetic experiment analogous to the one for RNA has not been done to verify the single stranded nature of poly A at pH 7. Although the structure of RNA in solution is not as regular as poly A at pH 7, it may have conformational similarities.

A simple starting point for investigation of single stranded poly A seems to be a polymer of length two, such as adenosyl (3'-5') adenosine ApA. (The structure of a related compound, adenosyl (3'-5') uridine is shown in Fig. III-(1). Its ORD (Warshaw, et al., 1965) and its circular dichroism (VanHolde, et al., 1965) are similar to that of neutral poly A, and the temperature dependence of its optical rotation at 260 mμ is like that of poly A (Warshaw and Tinoco, 1965). As a simple model, we may assume that only nearest neighbor interactions affect the ORD of polymers, and that the structure of ApA is that of the beginning of the single strand poly A. Under these assumptions, the ORD of poly A, having twice as many nearest neighbor interactions as ApA, ought to be twice that of the dinucleoside. This is approximately correct; the experimental ratio of polymer to dimer rotation is 2.5 (Holcomb and Tinoco, 1965). This reasoning can also be extended to dinucleosides of other bases, uracil (U), guanine (G), and cytosine (C). The mixed dimers provide a similar model for co-polymers.

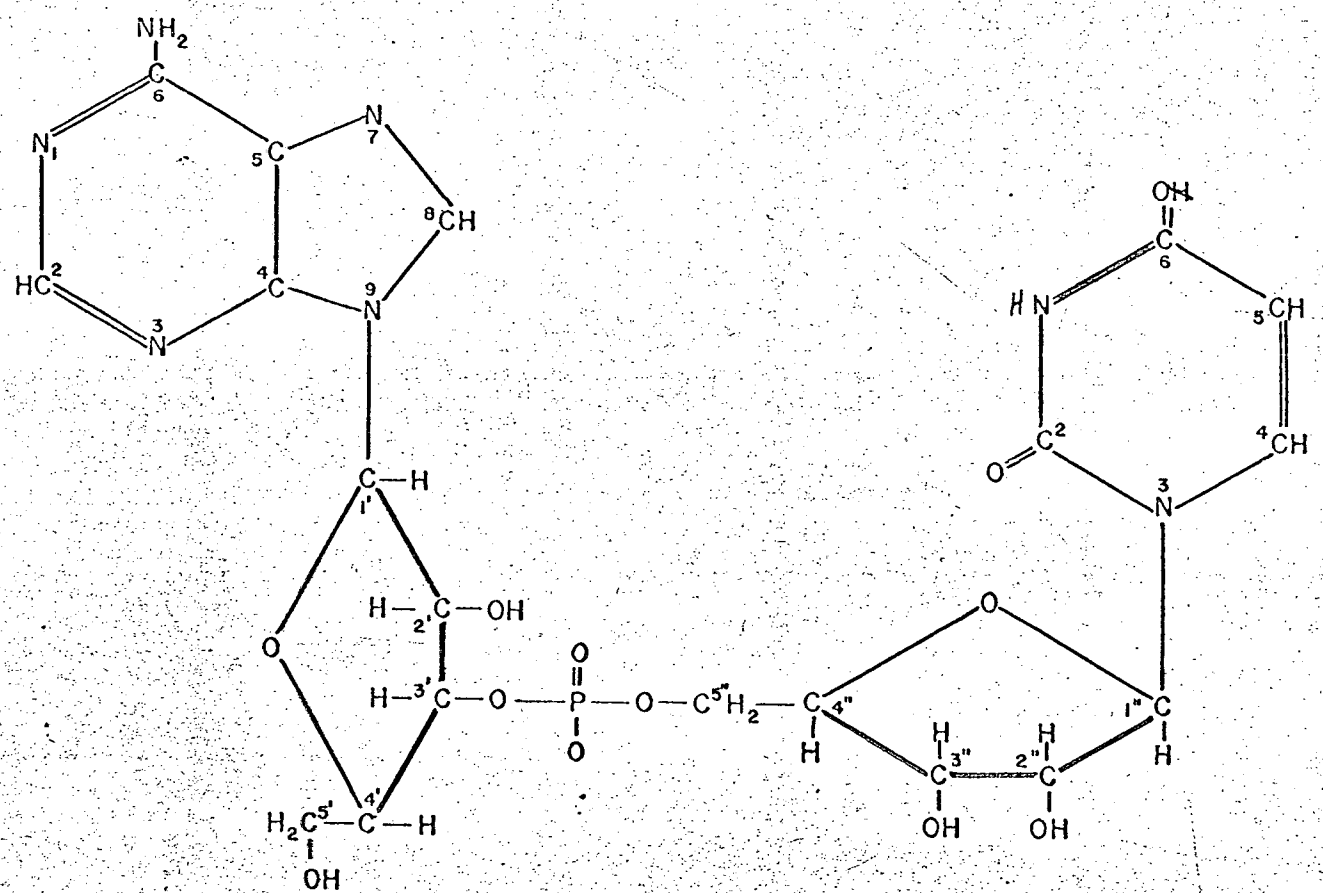

Figure III-1 Adenosyl (3'-5') uridine

Qualitative Discussion of the Method

The optical rotation of polymers composed of identical subunits has been thoroughly discussed by Tinoco, Woody and Bradley (1963) and related predictions for dimers (dinucleoside phosphates in our case) are presented by Tinoco (1963). Our calculation will serve as a check on the theory of the interaction which gives rise to the optical rotation of polymers as proposed in the above references.

Optical rotation may be described by a molecular parameter known as the rotational strength for the optical transition o to a, $R_{oa} = \mathrm{Im}\,(\underset{\sim}{\mu}_{oa} \cdot \underset{\sim}{m}_{ao})$. In this expression, Im indicates the imaginary part; $\underset{\sim}{\mu}_{oa}$ is the electric dipole transition moment, and $\underset{\sim}{m}_{ao}$ is the magnetic dipole transition moment (Rosenfeld, 1928). R_{oa} must be zero in molecules with a point or plane of symmetry as, in these molecules, $\underset{\sim}{m}_{ao}$ can have no non-zero component along $\underset{\sim}{\mu}_{oa}$. In molecules with an asymmetric carbon atom, such as steroids etc. treated by Djerassi (1960), a small rotational strength (of the order of 10^{-40} cgs) is usually seen. In rigid polymers such as helical polypeptides and nucleic acid polymers, a rotational strength per monomer which is greater by a factor of ten may be found. One can explain this effect as the interaction between the electric dipole transition moments of polymer subunits.

The magnetic transition moment, $\underset{\sim}{m}_{ao}$, is derived from the angular momentum of the electrons. Therefore, if we sit on one subunit and watch the motion of the electrons on an adjacent subunit, there will be an apparent magnetic moment whenever there is a net motion of electrons on the adjacent subunit. This occurs when the adjacent monomer undergoes an electric dipole transition. Therefore we can write the transition magnetic moment for the polymer as $\underset{\sim}{M}_{ao} = \underset{\sim}{m}_{ao} + e/2mc\,(\underset{\sim}{r} \times \underset{\sim}{p}_{ao})$ where $\underset{\sim}{m}_{ao}$ is the

inherent monomer magnetic transition moment, $\underset{\sim}{p}_{ao}$ is the linear momentum operator for the transition o to a, $\underset{\sim}{r}$ is the distance and e, m, and c are well known universal constants representing the charge of the electron, its mass and the speed of light.

According to an argument of Moffitt (1956), the second term of $\underset{\sim}{M}_{ao}$ is expected to dominate since the distance, $\underset{\sim}{r}$, between the subunits is large compared to the dimensions of the subunits. This may be approximately true for polypeptides but for polynucleotides, the extent of the base may be 5 Å while the spacing of the base planes is 3.4 Å. We feel the first term makes a small contribution for reasons of the symmetry of the polymer resulting from the parallel base places of the polymer. This will be explained in connection with the quantitative development below.

However, it is certainly clear from experiment that the dimer, ApA, has a much larger rotation than the two monomers. This is shown in Fig. III-(2) (Warshaw et al., 1965). What we propose to do in this study is to make a quantitative calculation of the ORD of dinucleoside phosphates using the second term of $\underset{\sim}{M}_{ao}$. The calculation proves to give good experimental agreement and also points out difficulties in the interpretation of the ORD of polynucleotides.

Quantitative Development of the Theory

In order to develop the theory for dimers of identical subunits, we will employ simple degenerate perturbation theory. We designate ϕ_{1o} and ϕ_{1a} as the unperturbed wave functions of the ground and excited states of monomer i. The difference of their energies is E_{oa}. We combine monomers 1 and 2 to form the dimer ground state wave function: $\psi_o = \phi_{1o}\phi_{2o}$. For the excited state, we take the symmetric (+) and the antisymmetric (-) combinations:

$$\psi_{A\pm} = (1/\sqrt{2})(\phi_{1a}\phi_{2o} \pm \phi_{1o}\phi_{2a}) \qquad \text{III-(1)}$$

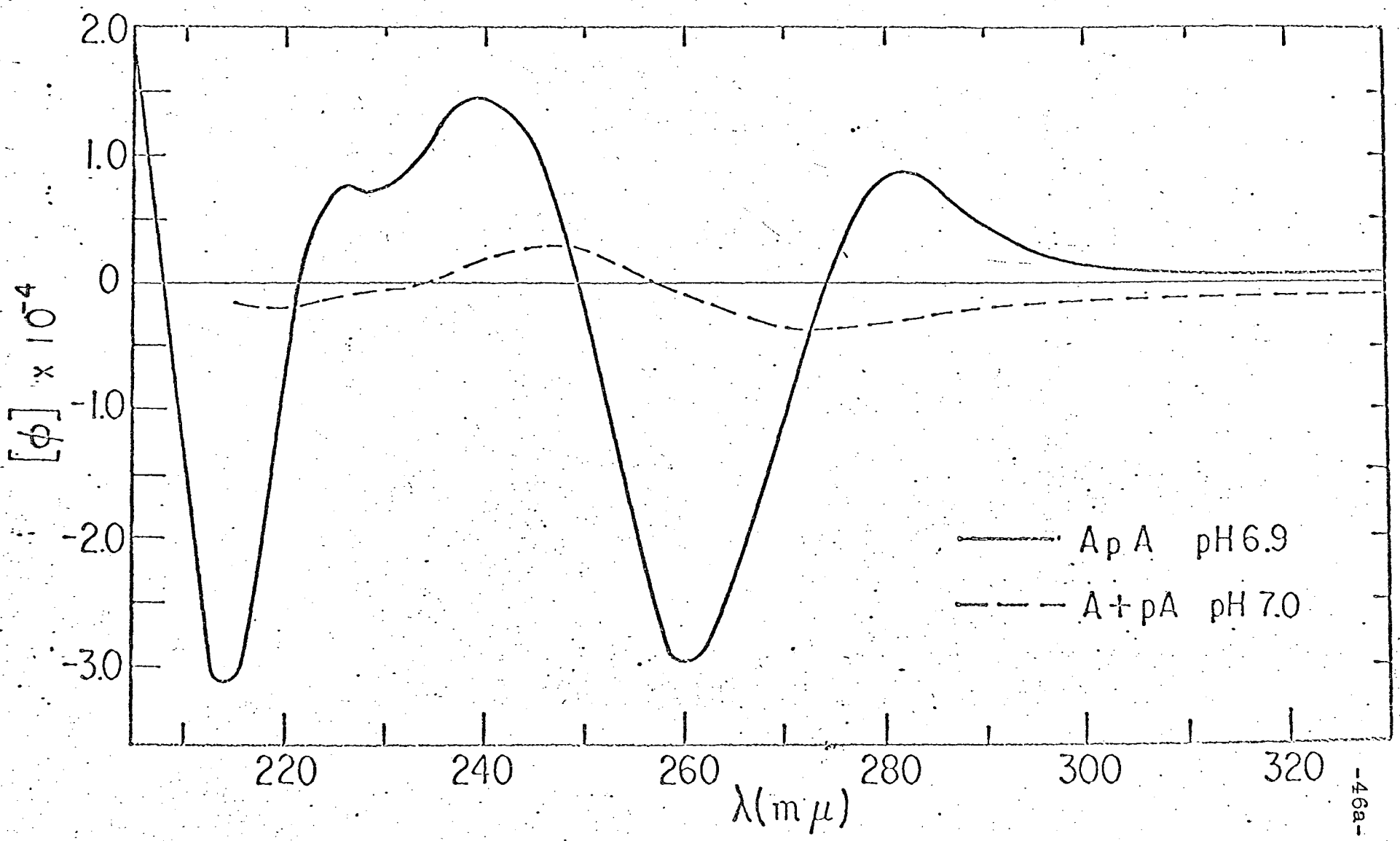

Figure III-2 ORD of ApA and ORD of adenosine + adenylic acid

The two states + and - have different energies due to the coulomb interaction of the electrons on one monomer with the other. This perturbation potential is simply $V_{12} = \sum e^2/r_{ij}$, where r_{ij} is the distance between the electrons. The index i ranges over the electrons of monomer one, while j ranges over the electrons of monomer two.

Even though the absorption spectra of nucleosides show broad bands, we will speak of the states as having a single frequency. This amounts to ignoring vibronic interactions and lumping the broad absorptions into single transitions to the excited states. With the understanding that we will have to introduce some way of constructing broad absorption bands from sharp absorption lines, we give the energies of the split states, $E_{\pm} = E_a \pm V_{1a;2a}$. $V_{1a;2a}$ is the perturbation potential evaluated between the two unperturbed upper states,, $V_{1a;2a} = \langle \phi_{1a}\phi_{2o} | V_{12} | \phi_{1o}\phi_{2a} \rangle$. (Here and following, we use the usual Dirac bracket notation). This splitting energy may be evaluated directly from the definition by expressing the ϕ_1 as molecular orbitals. When the MO's are taken as linear combinations of atomic orbitals, the potential is evaluated between each of the atomic orbitals on monomer 1 interacting with each of the atomic orbitals of monomer 2. The method is called Pariser-Parr by Nesbet (1964), but it is also known as the monopole-monopole interaction method. If one uses Pariser-Parr MO's, the methods are identical, because one sums up the energy of coulomb interaction between the transition charge density of each atom on monomer 1 with that of each atom on monomer 2.

A different way to calculate $V_{1a;2a}$ is to consider the assembly of transition charges (monopoles) on one monomer, and then to do a multiple expansion keeping the first term (dipole term) only. The dipole involved is simply the dipole transition moment, so the interaction becomes:

$$V_{1a;2a} = \frac{1}{R^3}\left[\underset{\sim}{\mu}_{1oa} \cdot \underset{\sim}{\mu}_{2oa} - \frac{3(\underset{\sim}{R}_{12} \cdot \underset{\sim}{\mu}_{1oa})(\underset{\sim}{R}_{12} \cdot \underset{\sim}{\mu}_{2oa})}{R^2}\right] \qquad \text{III-(2)}$$

according to ordinary dipole-dipole interaction. $\underset{\sim}{R}_{12}$ is the vector distance between the two point dipoles; $\underset{\sim}{R}_{12} = (\underset{\sim}{R}_2 - \underset{\sim}{R}_1)$ and R is its magnitude.

We now proceed to the rotational strengths of the bands. For the dimer electric dipole transition moment

$$\underset{\sim}{\mu}_{oa\pm} = \left\langle \phi_{1o}\phi_{2o} \mid \underset{\sim}{\mu}_1 + \underset{\sim}{\mu}_2 \mid \frac{1}{\sqrt{2}}(\phi_{1a}\phi_{2o} \pm \phi_{1o}\phi_{2a}) \right\rangle \qquad \text{III-(3)}$$

which may be evaluated as

$$\underset{\sim}{\mu}_{oa\pm} = (1/\sqrt{2})(\underset{\sim}{\mu}_{1oa} \pm \underset{\sim}{\mu}_{2oa}) \qquad \text{III-(4)}$$

We also need the magnetic transition moment whose form is a bit different. For the magnetic moment of the dimer, we take the sum of the magnetic moments of the monomers, and in addition, we take the magnetic moment arising from the linear momentum of the electrons relative to an arbitrary origin.

$$\underset{\sim}{M} = \underset{\sim}{m}_1 + \underset{\sim}{m}_2 + (e/2mc)(\underset{\sim}{R}_1 x \underset{\sim}{p}_1 + \underset{\sim}{R}_2 x \underset{\sim}{p}_2)$$

We now evaluate the magnetic transition moment for the transition O to $A\pm$ in the same way as for the electric moment.

$$\underset{\sim}{M}_{AO\pm} = (1/\sqrt{2}) \left\langle (\phi_{1a}\phi_{2o} \pm \phi_{1o}\phi_{2a}) \middle| \underset{\sim}{m}_1 + \underset{\sim}{m}_2 + e/2mc\,(\underset{\sim}{R}_1 x \underset{\sim}{p}_1 + \underset{\sim}{R}_2 x \underset{\sim}{p}_2) \middle| \phi_{1o}\phi_{2o} \right\rangle \qquad \text{III-(5)}$$

$$\underset{\sim}{M}_{AO\pm} = (1/\sqrt{2})[\underset{\sim}{m}_{1ao} \pm \underset{\sim}{m}_{2ao} + (e/2mc)(\underset{\sim}{R}_1 x \underset{\sim}{p}_{1ao} \pm \underset{\sim}{R}_2 x \underset{\sim}{p}_{2ao})] \qquad \text{III-(6)}$$

We now recall a well known substitution which may be easily derived from the Schrödinger equation (Eyring, Walter and Kimball, 1944)

$$\underset{\sim}{p}_{ao} = -\underset{\sim}{p}_{oa} = \frac{2\pi i m}{e}\, \nu_{oa}\, \underset{\sim}{\mu}_{oa} \qquad \text{III-(7)}$$

where

$$\nu_{oa} = \frac{E_a - E_o}{h} \quad . \qquad \text{III-(8)}$$

We may now substitute for the momentum operator, p_{ao}, to obtain the magnetic transition moment in terms of the monomer magnetic transition moment and monomer electric transition moment only.

$$\underset{\sim}{M}_{AO\pm} = (1/\sqrt{2})[\underset{\sim}{m}_{1ao} \pm \underset{\sim}{m}_{2ao} + \frac{\pi i \nu_{oa}}{c} (\underset{\sim}{R}_1 \times \underset{\sim}{\mu}_{1oa} \pm \underset{\sim}{R}_2 \times \underset{\sim}{\mu}_{2oa})] \qquad \text{III-(9)}$$

We now have the necessary matrix elements for writing the rotational strengths of the two dimer transitions.

$$\begin{aligned} R_{OA\pm} = \mathrm{Im}(\underset{\sim}{\mu}_{OA} \cdot \underset{\sim}{m}_{AO}) = \mathrm{Im}\Big\{ & (1/2)(\underset{\sim}{\mu}_{1oa} \cdot \underset{\sim}{m}_{1ao} + \underset{\sim}{\mu}_{2oa} \cdot \underset{\sim}{m}_{2ao} \\ & \pm \underset{\sim}{\mu}_{1oa} \cdot \underset{\sim}{m}_{2ao} \pm \underset{\sim}{\mu}_{2oa} \cdot \underset{\sim}{m}_{1ao} \\ & + \frac{\pi i}{2c} \nu_{oa} [\underset{\sim}{\mu}_{1oa} \cdot (\underset{\sim}{R}_1 x \underset{\sim}{\mu}_{1oa} \pm \underset{\sim}{R}_2 x \underset{\sim}{\mu}_{2oa}) \\ & \pm \underset{\sim}{\mu}_{2oa} \cdot (\underset{\sim}{R}_1 x \underset{\sim}{\mu}_{1oa} \pm \underset{\sim}{R}_2 x \underset{\sim}{\mu}_{2oa})] \Big\} \end{aligned} \qquad \text{III-(10)}$$

At this point we will assume that $\underset{\sim}{m}_{ao} = 0$ so that the monomer has no optical activity itself before formation of the dimer. In this way we lose the first four terms. The assumption that the $\underset{\sim}{R} x \underset{\sim}{\mu}$ terms are much more important than the $\underset{\sim}{m}$ terms seems to be valid for certain dinucleosides. For example, the monomer, A, shows little optical activity (see Fig. III-2) but the dimer, ApA, gives large rotation. The reason for the small monomer activity is probably not that m is small compared to $\underset{\sim}{R} x \underset{\sim}{p}$ but that $\underset{\sim}{m}$ is nearly perpendicular to $\underset{\sim}{\mu}$. For the base alone, which has a plane of symmetry, we know that the magnetic transition moments for π-π^* transitions must be perpendicular to the base plane and to the electric transition moments which are in this plane. The addition of the asymmetric sugar perturbs

this situation slightly, giving rise to the small monomer rotational strength. For dimers in which the base planes are parallel, the rotational strength arising from $\underset{\sim}{m}_1 \cdot \underset{\sim}{\mu}_2$ must be small for the same reason, hence the $\underset{\sim}{R} \times \underset{\sim}{p}$ dominates the dimer rotation. For polymers, such as double stranded poly A (Rich, et al., 1961) where the base planes are tilted, this will not be the case. Our assumption that the $\underset{\sim}{R} \times \underset{\sim}{p}$ terms dominate the dimer rotational strength is valid only for polynucleotides of a single strand or for double stranded ones in which the base planes are all parallel.

For the reasons outlined above we will drop the contribution of $\underset{\sim}{m}$ to the polymer magnetic moment $\underset{\sim}{M}$. We will then compare our calculated curves with the experimental curves for the dimers with the monomer rotation subtracted. This will at least partially correct for the contribution of $\underset{\sim}{m}$.

If we take real wave functions to represent the operators that survive, the resulting expression is purely imaginary. Taking the imaginary part:

$$R_{OA\pm} = \frac{\pi\nu_{oa}}{2c} \Big[\underset{\sim}{R}_1 \times \underset{\sim}{\mu}_{1oa} \cdot \underset{\sim}{\mu}_{1oa} + \underset{\sim}{R}_2 \times \underset{\sim}{\mu}_{2oa} \cdot \underset{\sim}{\mu}_{2oa} \pm \underset{\sim}{R}_2 \times \underset{\sim}{\mu}_{2oa} \cdot \underset{\sim}{\mu}_{1oa} \pm \underset{\sim}{R}_1 \times \underset{\sim}{\mu}_{1oa} \cdot \underset{\sim}{\mu}_{2oa} \Big] \cdot \qquad \text{III-(11)}$$

The first two terms of this expression are zero simply because two of the vectors in the triple product are identical. The second two can be combined to give a particularly pleasing and simple result.

$$R_{OA\pm} = \pm \frac{\pi\nu_{oa}}{2c} \Big[(\underset{\sim}{R}_2 - \underset{\sim}{R}_1) \times \underset{\sim}{\mu}_{1oa} \cdot \underset{\sim}{\mu}_{2oa} \Big] \qquad \text{III-(12)}$$

This equation is the same as that given by Tinoco (1963) except that the signs in his Eq. 6 are reversed, apparently due to a misprint since his examples are correct.

We see from Eq. III-(12) that the rotational strengths depend only on the distance between the monomers and not on any choice of origin for $\underset{\sim}{R}$. If it at first appears troublesome that the rotational strength goes to infinity for infinite distance, $\underset{\sim}{R}$, one should remember that the physically observable quantity, the optical rotation, also depends on the separation in energy between the two states (+) and (-). This splitting goes to zero very fast with increasing $\underset{\sim}{R}$, for example, like $1/\underset{\sim}{R}^3$ in the dipole approximation. An any case, the splitting will disappear much faster than the rotational strength grows with distance and the rotational strengths will cancel completely at large $\underset{\sim}{R}$, since they are equal in magnitude and opposite in sign. This will become quite apparent when we construct the circular dichroism curves whose amplitudes are determined by the rotational strength.

In the wavelength range 210 to 300 mμ, A and U each have a single absorption band at pH 7 (see Figs. III-3 and III-4). For dimers of identical groups having a single isolated absorption band (i.e., ApA and UpU), Equ. III-(12) will be adequate. However, we would also like to be able to treat dimers of two different nucleotides. Furthermore, we can see from the absorption spectra of guanosine and cytidine at pH 7 (Figs. III-5 and III-6) that there are two distinct electronic absorption bands near each other in the range of the ultraviolet in which we are interested. Therefore we will develop a formula for the rotational strengths when there is non-resonance interaction as well as the resonant or degenerate effect described above. The non-degenerate terms will be expected to contribute to the rotation when two bands are near in frequency.

We now consider a dimer made up of subunits having a ground state and two excited states, a and b. The ground state now has first order perturbations included,

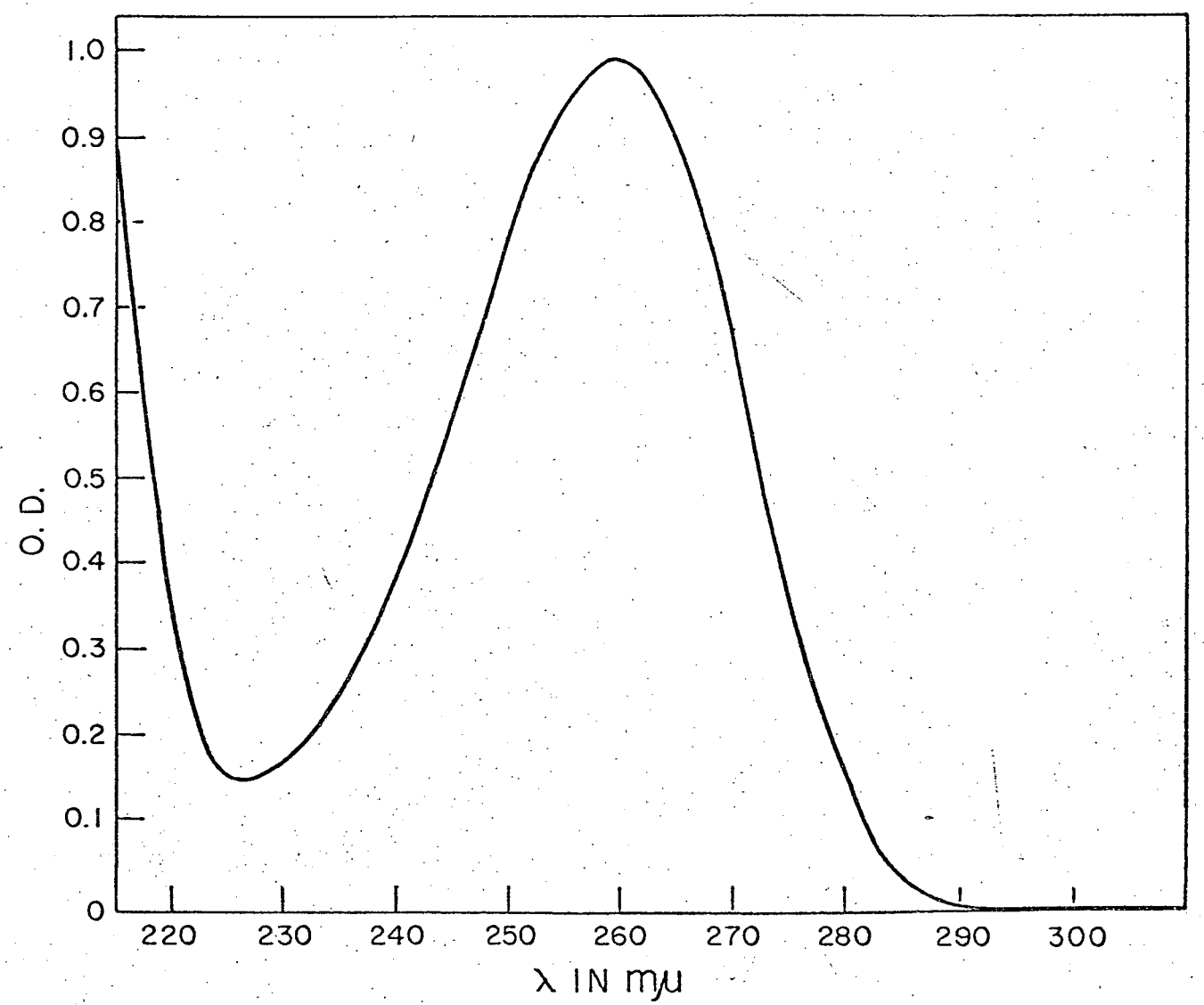

Figure III-3 Optical density of adenosine. conc=.648 x 10^{-4}M

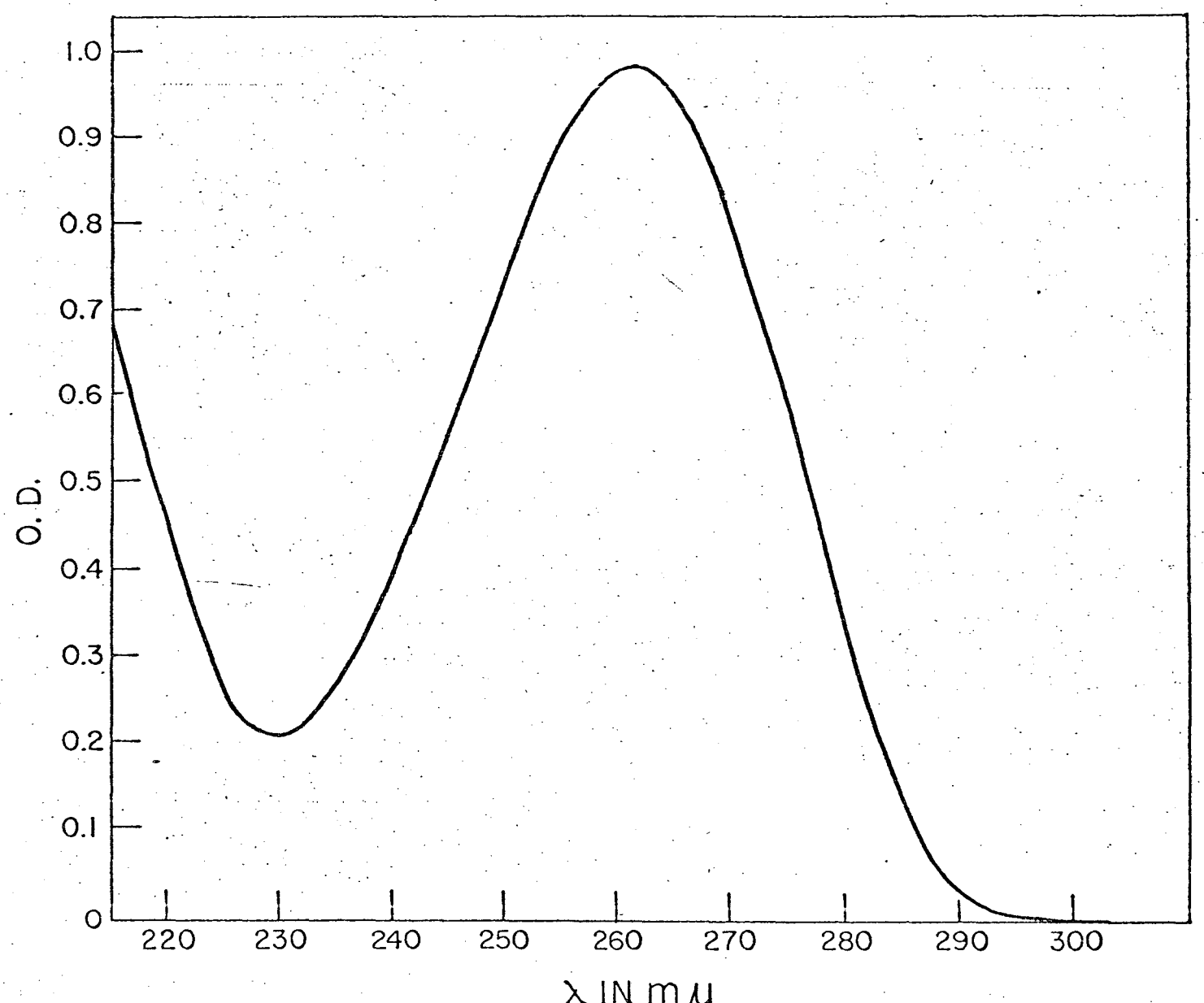

Figure III-4 Optical density of uridine. conc =1.009 x 10^{-4}M

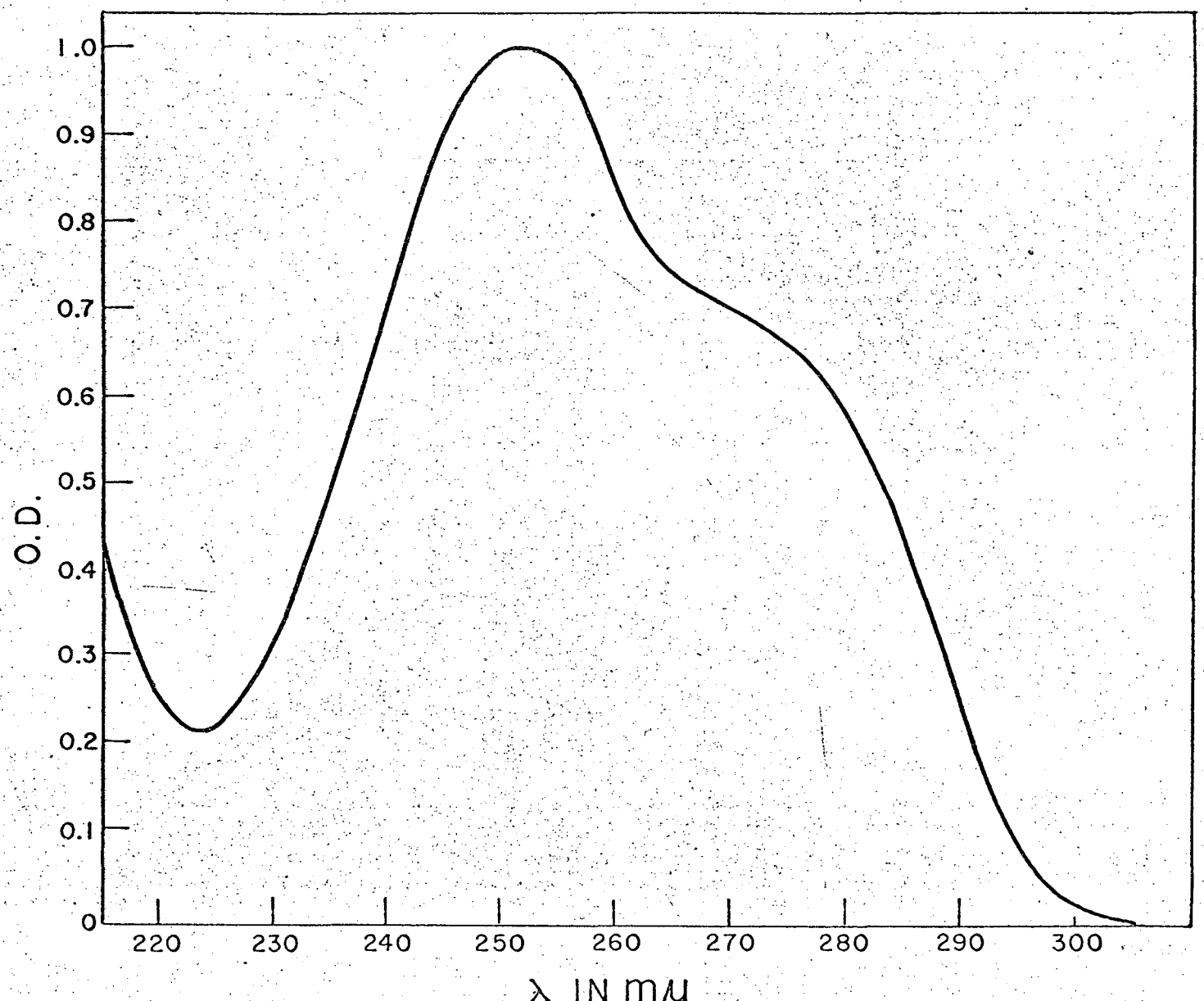

Figure III-5 Optical density of guanosine. conc= .761 x 10^{-4}M

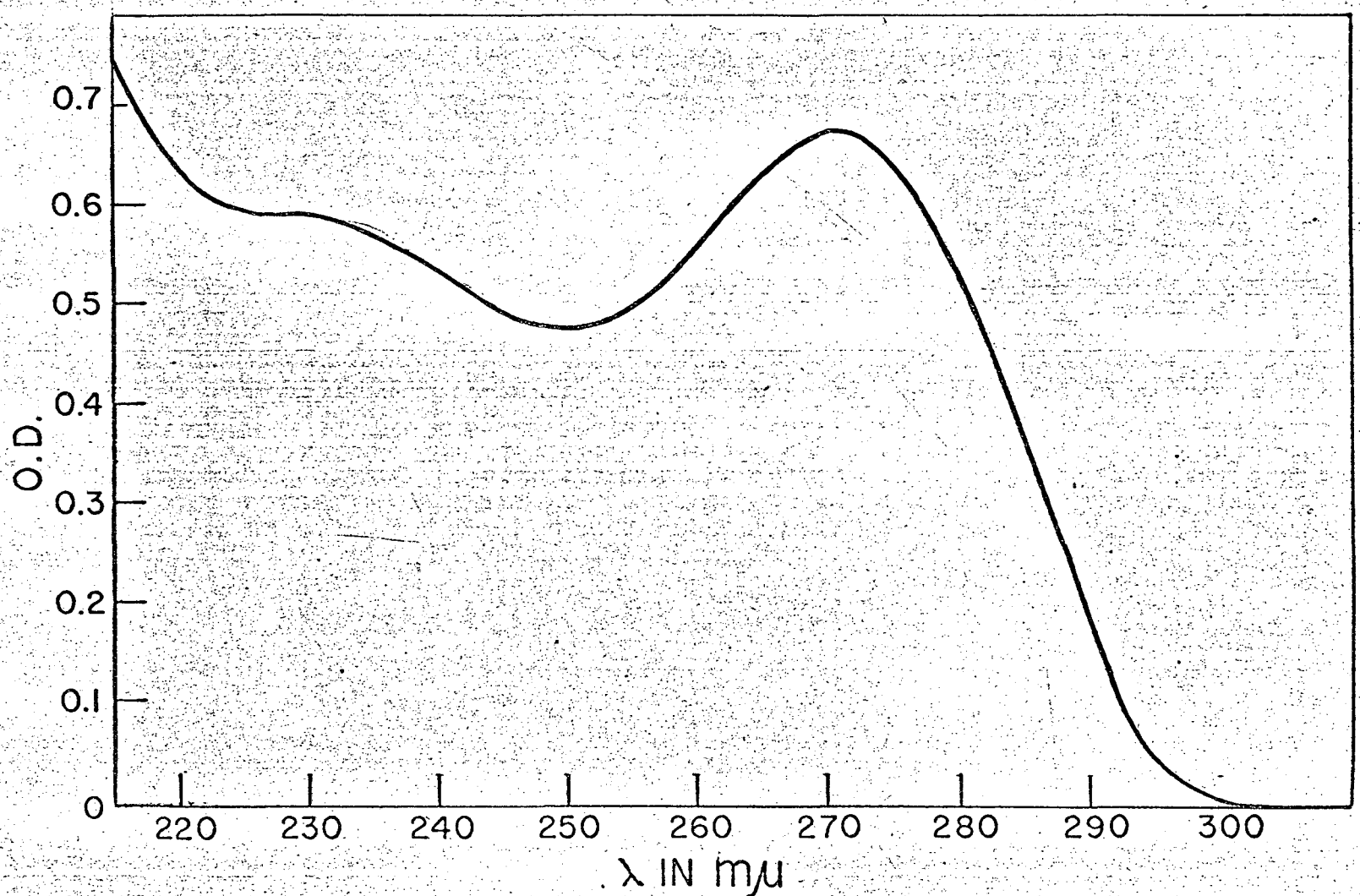

Figure III-6 Optical density of Cytidine. conc= $.7695 \times 10^{-4}$M

$$\psi_o^1 = \phi_{1o}\phi_{2o} - \frac{V_{1a;2b}\ \phi_{1a}\phi_{2b}}{h(\nu_a + \nu_b)} - \frac{V_{1b;2a}\ \phi_{1b}\phi_{2a}}{h(\nu_a + \nu_b)} \qquad \text{III-(13)}$$

Here $V_{1a;2b}$ is not equal to $V_{1b;2a}$. This may be seen from the geometry of the model (shown in Fig. III-7) we will use in the computation. The definition of the interaction is similar to that of $V_{1a;2a}$ above,

$$V_{1a;2b} = \left\langle \phi_{1o}\phi_{2o} \middle| V_{12} \middle| \phi_{1a}\phi_{2b} \right\rangle = \left\langle \phi_{1o}\phi_{2b} \middle| V_{12} \middle| \phi_{1a}\phi_{2o} \right\rangle \qquad \text{III-(14)}$$

We have left out of Eq. III-(13) the states of the kind $\phi_{1a}\phi_{2a}$ because they give rise to terms which cancel when one forms the rotational strength product. We also leave out terms arising from static electric field perturbations. These give rise to energy shifts and they may also make magnetically allowed n-π^* transitions electrically allowed and give contributions to the rotation (Tinoco, 1962). In polynucleotides, n-π^* transitions probably exist in the wavelength ragne of interest, but they are masked by the very strong electrically allowed π-π^* transitions, and their contribution to the rotation is unknown but apparently not large.

To the same level of approximation, we give the first order excited state wave functions for the dimer:

$$\psi^1_{A\pm} = 1/\sqrt{2}\left[(\phi_{1a}\phi_{2o} \pm \phi_{1o}\phi_{2a}) - \frac{V_{1a;2b}\ \phi_{1o}\phi_{2b}}{h(\nu_b - \nu_a)} \pm \frac{V_{1b;2a}\ \phi_{1b}\phi_{2o}}{h(\nu_b - \nu_a)}\right] \qquad \text{III-(15)}$$

To get the transition moments to these two perturbed excited states, we form the usual integrals exactly as in Eqs. III-(3) and III-(5) above. We also combine the first order terms having denominators $h(\nu_b - \nu_a)$ and $h(\nu_b + \nu_a)$ to get the resulting electric dipole transition moment,

$$\underset{\sim}{\mu}^1_{OA\pm} = (1/\sqrt{2})\left[(\underset{\sim}{\mu}_{1oa} \pm \underset{\sim}{\mu}_{2oa}) - \frac{2\nu_b\ V_{1a;2b}\ \underset{\sim}{\mu}_{2ob}}{h(\nu_b^2 - \nu_a^2)} \mp \frac{2\nu_b\ V_{1b;2a}\ \underset{\sim}{\mu}_{1ob}}{h(\nu_b^2 - \nu_a^2)}\right] \qquad \text{III-(16)}$$

In writing the dimer magnetic moment, we will drop $\underset{\sim}{m}_{ao}$, the monomer magnetic moment for the reasons we have mentioned in connection with the previous, degenerate case.

$$\underset{\sim}{M}^{1}_{AO\pm} = (1/\sqrt{2})(e/2mc)\left[(\underset{\sim}{R}_1 \times \underset{\sim}{p}_{1ao}) \pm (\underset{\sim}{R}_2 \times \underset{\sim}{p}_{2ao}) - \frac{V_{1a;2b}\,\underset{\sim}{R}_2 \times \underset{\sim}{p}_{2bo}}{h(\nu_b - \nu_a)}\right.$$

$$\left. \mp \frac{V_{1b;2a}\,\underset{\sim}{R}_1 \times \underset{\sim}{p}_{1bo}}{h(\nu_b - \nu_a)} - \frac{V_{1a;2b}\,\underset{\sim}{R}_2 \times \underset{\sim}{p}_{2ob}}{h(\nu_b + \nu_a)} \mp \frac{V_{1b;2a}\,\underset{\sim}{R}_1 \times \underset{\sim}{p}_{1ob}}{h(\nu_b + \nu_a)}\right] \qquad \text{III-(17)}$$

In this case, since $\underset{\sim}{p}_{ob} = \underset{\sim}{p}_{bo}$, the relative signs of the terms with denominators $h(\nu_b - \nu_a)$ and $h(\nu_b + \nu_a)$ are reversed and we get a ν_a in the numerator instead of ν_b as we did in combining them in the electric dipole moment.

$$\underset{\sim}{M}_{AO\pm} = (1/\sqrt{2})(e/2mc)\left[\underset{\sim}{R}_1 \times \underset{\sim}{p}_{1ao} \pm \underset{\sim}{R}_2 \times \underset{\sim}{p}_{2ao} - \frac{2\nu_a V_{1a;2b}\,\underset{\sim}{R}_2 \times \underset{\sim}{p}_{2bo}}{h(\nu_b^2 - \nu_a^2)}\right.$$

$$\left. \mp \frac{2\nu_a V_{1b;2a}\,\underset{\sim}{R}_1 \times \underset{\sim}{p}_{1bo}}{h(\nu_b^2 - \nu_a^2)}\right] \qquad \text{III-(18)}$$

At this point, one may again use Eq. III-(7) to substitute for the momentum operators and obtain $\underset{\sim}{M}^{1}_{AO\pm}$ in terms of the electric dipole moment operators and polymer geometry only,

$$\underset{\sim}{M}^{1}_{AO} = \pm \frac{\pi_1}{\sqrt{2}c}\left[\nu_a (\underset{\sim}{R}_1 \times \underset{\sim}{\mu}_{1oa} \pm \underset{\sim}{R}_2 \times \underset{\sim}{\mu}_{2oa}) - \frac{2\nu_a\nu_b V_{1a;2b}\,\underset{\sim}{R}_2 \times \underset{\sim}{\mu}_{2ob}}{h(\nu_b^2 - \nu_a^2)}\right.$$

$$\left. \mp \frac{2\nu_a\nu_b V_{1b;2a}\,\underset{\sim}{R}_1 \times \underset{\sim}{\mu}_{1ob}}{h(\nu_b^2 - \nu_a^2)}\right] \qquad \text{III-(19)}$$

We now have the operators necessary for writing the rotational strength, including only terms which are linear in the potential, V_{12}. We give $R_{OA\pm}$ written as the triple products divided into three groups

depending on whether they are zero order, or contain $V_{1a;2b}$ or $V_{1b;2a}$.

$$R^1_{OA\pm} = \frac{\pi}{2c}\Bigg[\mp \nu_a(\underset{\sim}{R}_2 - \underset{\sim}{R}_1) \times \underset{\sim}{\mu}_{1oa} \cdot \underset{\sim}{\mu}_{2oa}$$

$$\mp \frac{2\nu_a\nu_b V_{1b;2a}}{h(\nu_b^2 - \nu_a^2)} \left(\underset{\sim}{R}_1 \times \underset{\sim}{\mu}_{1ob} \cdot \underset{\sim}{\mu}_{1oa} \pm \underset{\sim}{R}_1 \times \underset{\sim}{\mu}_{1ob} \cdot \underset{\sim}{\mu}_{2oa} + \underset{\sim}{R}_1 \times \underset{\sim}{\mu}_{1oa} \cdot \underset{\sim}{\mu}_{1ob} \pm \underset{\sim}{R}_2 \times \underset{\sim}{\mu}_{2oa} \cdot \underset{\sim}{\mu}_{1ob}\right) \qquad \text{III-(20)}$$

$$- \frac{2\nu_a\nu_b V_{1a;2b}}{h(\nu_b^2 - \nu_a^2)} \left(\underset{\sim}{R}_1 \times \underset{\sim}{\mu}_{1oa} \cdot \underset{\sim}{\mu}_{2ob} \pm \underset{\sim}{R}_2 \times \underset{\sim}{\mu}_{2oa} \cdot \underset{\sim}{\mu}_{2ob} + \underset{\sim}{R}_2 \times \underset{\sim}{\mu}_{2ob} \cdot \underset{\sim}{\mu}_{1oa} \pm \underset{\sim}{R}_2 \times \underset{\sim}{\mu}_{2ob} \cdot \underset{\sim}{\mu}_{2oa}\right)\Bigg]$$

Among the three groups of terms in Eq. III-(20), the first refers to the same degenerate interaction between identical monomers discussed previously. In the second group, containing $V_{1b;2a}$, the first and third products cancel as do the second and forth triple products of the third group, the one with $V_{1a;2b}$. Therefore we may combine terms so the answer depends only on the distance between the groups and the three terms can be easily understood:

$$R^1_{OA\pm} = \frac{\pi}{2c}\Bigg[\mp \nu_a(\underset{\sim}{R}_2 - \underset{\sim}{R}_1) \cdot \underset{\sim}{\mu}_{1oa} \times \underset{\sim}{\mu}_{2oa} \qquad \text{III-(21a)}$$

$$+ \frac{2\nu_a\nu_b V_{1a;2b}}{h(\nu_b^2 - \nu_a^2)} (\underset{\sim}{R}_2 - \underset{\sim}{R}_1) \cdot \underset{\sim}{\mu}_{1oa} \times \underset{\sim}{\mu}_{2ob} \qquad \text{III-(21b)}$$

$$+ \frac{2\nu_a\nu_b V_{1b;2a}}{h(\nu_b^2 - \nu_a^2)} (\underset{\sim}{R}_2 - \underset{\sim}{R}_1) \cdot \underset{\sim}{\mu}_{1ob} \times \underset{\sim}{\mu}_{2oa}\Bigg] \qquad \text{III-(21c)}$$

Eq. III-(21) contains the rotational strength of the dimer of identical monomers (III-21a). In addition, the rotational strength arising from a dimer in which monomer one has an absorption frequency ν_a and monomer two absorbs at ν_b is given by III-(21b), while III-(21c) gives the rotational strength for the dimer in which monomer one absorbs at ν_b and monomer two

absorbs at ν_a. In the calculations, we may picture III-(21b) and III-(21c) as the rotational strengths of two sequence isomers where monomer 1 is 3' linked and monomer 2 is 5' linked. III-(21b) will be different from III-(21c) so we expect to see some sequence dependence to the ORD in the calculated curves.

In the range of wavelength we are considering, 210 to 300 mμ, C and G show two overlapping bands (see Figs. III-5 and III-6). Therefore, all three terms will contribute as we shall see for CpG and CpC. We also notice that by replacing one by two and a by b, that the rotational strength R_{OB}, arising from band a interacting with band b is equal in amplitude and opposite in sign from the rotational strength of band b interacting with band a. This means that the rotational strengths will sum to zero if all the bands being considered are included in the sum.

The reader may notice that in III-(21b) and III-(21c) we actually intend a summation over b. That is, we should include non-degenerate interactions with all other excited states. In practice, we have found that the ORD of dinucleoside phosphates can be explained in terms of the transitions in the range of the ORD measurement. Therefore we will consider only transitions in the range 300 - 210 mμ and we will not extend the sum over b to include higher energy excited states. However, in the cases such as ApG, when we compute the rotational strength at the A absorption frequency, we include interactions with two absorption bands in G so we are actually summing over b, even if the index only runs from one to two. One might argue, therefore, that we should have written the summation over b in Eq. III-(21); we have left the summation sign out solely for clarity in the derivation since it adds nothing in the more illustrative case of ApU.

The Model for Dinucleoside Phosphates

In order to apply the theory we have developed, we must choose an explicit model for calculations. In Fig. III-(7) we show the helical geometry used in these calculations with two pyrimidines and a purine. If we think of the upper two subunits, we have a model for a pyrimidine 3'-5' purine dinucleoside (UpA) while the lower pair represents a purine 3'-5' pyrimidine (ApU). We will compute the interaction energy, $V_{1a;2b}$ from a monopole interaction method due to Dr. H. DeVoe of National Institutes of Health. We assume the bases to be in the positions they would have if they were successive residues of a single strand of DNA (Langridge, et al., 1960). This means that the bases are in parallel planes spaced 3.4 Å apart. The coordinates of Langridge, et al. (1960) for their model 3 are diagrammed in Figs. III-(8) to III-(11). The polar coordinate system is specified by the helix axis and the dyad axis, the line in the base plane across which base pairing occurs in DNA.

It may seem a bit arbitrary to assume this DNA-type geometry, but it is impossible to say a priori exactly what the favored conformation of dimers in solution will be and we know that this one is at least sterically possible for 10 residues per turn. Moreover, we know that single strand poly A at pH 7 has 3.4 Å spacing, indicating that the bases are perpendicular to the helix axis. What we do not know is the increment of helix angle per nucleotide. This is the angle γ of Fig. III-(7). We shall leave this as a parameter and do all our computations over a range of these angles that seems reasonable. By comparing the calculated results to experimental dinucleoside ORD, perhaps we can make some prediction about the true geometry. We notice that in Fig. III-(7), which is drawn with a positive angle, γ, we must make a right handed screw transformation

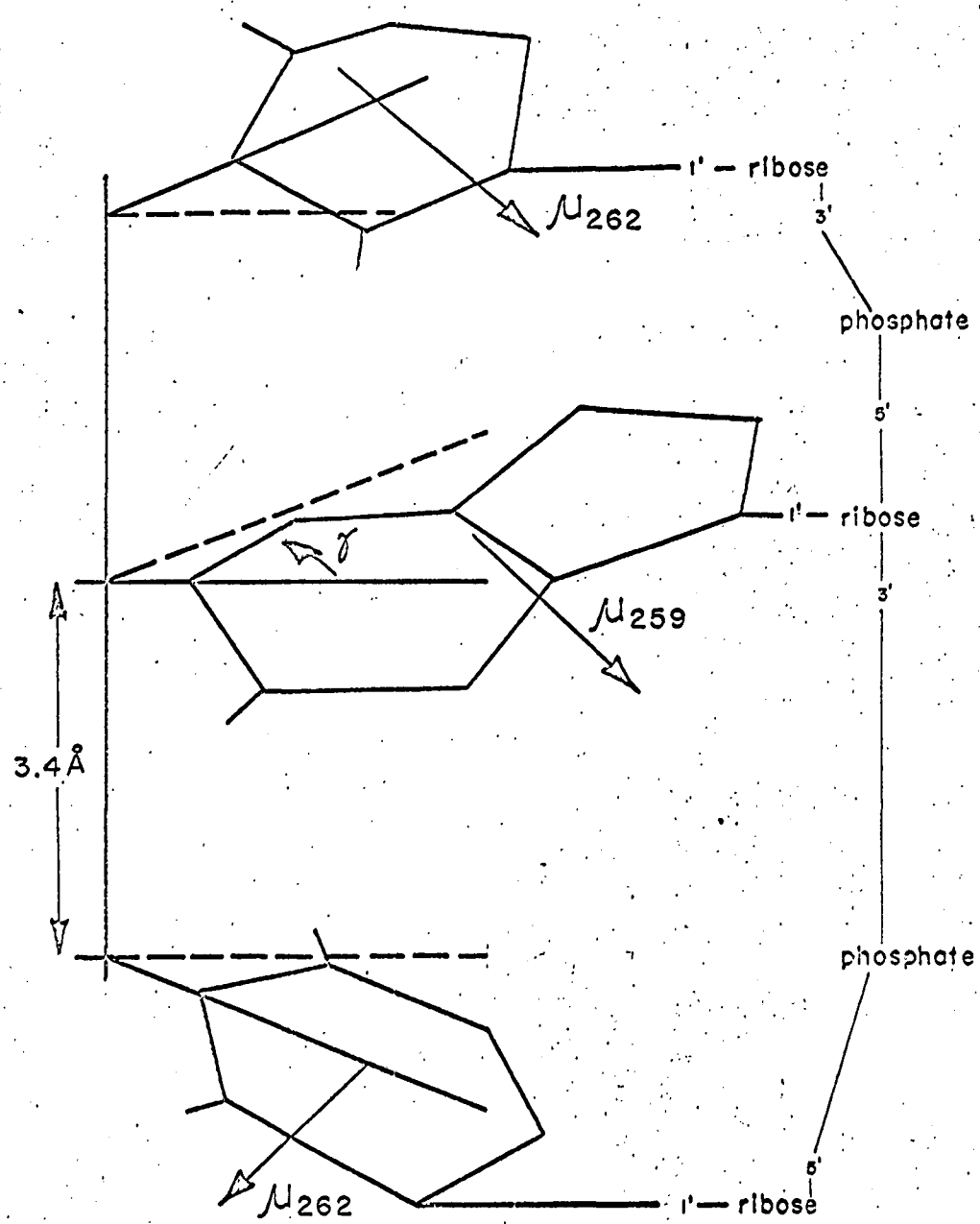

Figure III-7
Geometry of the model

to get from one subunit to the next. Thus it represents a right handed helix, while a negative value of γ would represent a left handed helix.

The concept of monopole interactions as used to compute V_{12} was introduced on p.47 above. The monopole interactions are computed by summing all the coulomb interactions of each atom on monomer one, with each atom on monomer two according to $\rho_i \rho_j / r_{ij}$. ρ_i is the transition monopole on the ith atom of monomer one, ρ_j is the transition monopole on the jth atom of monomer two and r_{ij} is the distance between them. The transition monopoles come from molecular orbitals and are simply $\rho_{ioa} = \left\langle \phi_o \middle| P_i \middle| \phi_a \right\rangle$, where P_i projects out the part of the function that is centered on atom i. For molecular orbitals which are linear combinations of atomic orbitals, the projection operator P_i simply tells us to use the atomic orbitals centered on atom i.

In Table III-(1) we give a summary of the transitions of the four nucleosides, one each for adenosine and uridine and two each for guanosine and cytidine. To obtain the experimental dipole strengths, we have used the absorption data of Pabst Laboratories (1956) as shown in Figs. III-(3) to III-(6). The absorptions are approximated as sums of gaussian curves of fixed position and half width. The heights of the gaussians are fitted to the experimental curve by a least square solution of linear equations by the IBM 7094 (see Appendix A). The curves may then be easily integrated. We had to separate the observed absorption into distinct bands for the computation, and this decomposition is shown in Table III-(2). Since we have no information on the vibratomonic nature of the transitions, it is impossible to know exactly how to decompose the absorption into distinct bands. Therefore, in making Table III-(2), we have taken the bands to be roughly symmetrical. The exact shape of the curves will not affect the ORD too much. The transitions are summarized in Table III-(1) with the experi-

Table III-(1)

Electronic transitions in the bases

Base	λ in mμ	$\lvert\mu\rvert$ exp. (debye)	β calc. (degrees)
Adenine	259	4.07	22.9
Uracil (Thymine)	262	3.53	34.4
Guanine band 1	276	2.75	65.4
band 2	252	3.71	-47.5
Cytosine band 1	271	3.03	22.3
band 2	230	3.66	-7.1

Table III-(2)

Absorption Spectra

Adenosine (concentration = 0.648×10^{-4} molar)

Guanosine (concentration = 0.761×10^{-4} molar)

λ in mμ	O.D. Adenosine	O.D. Guanosine total	O.D. Guanosine band 1	O.D. Guanosine band 2
305	.000	.003	.003	.000
302.5	.000	.010	.010	.000
300	.000	.025	.025	.000
297.5	.000	.051	.051	.000
295	.002	.097	.097	.000
292.5	.004	.159	.159	.000
290	.008	.253	.253	.000
287.5	.018	.353	.353	.000
285	.039	.449	.449	.000
282.5	.084	.534	.534	.000
280	.162	.594	.594	.000
277.5	.260	.641	.641	.000
275	.377	.678	.678	.000
272.5	.522	.705	.641	.064
270	.688	.728	.594	.134
267.5	.820	.749	.534	.205
265	.911	.777	.449	.328
262.5	.974	.818	.353	.465
260	.998	.888	.253	.635
257.5	.987	.974	.159	.815
255	.941	1.029	.070	.959
252.5	.864	1.044	.010	1.034
250	.809	1.038	.000	1.038
247.5	.680	1.005	.000	1.005
245	.573	.933	.000	.933
242.5	.477	.832	.000	.832
240	.389	.724	.000	.724
237.5	.313	.611	.000	.611
235	.251	.497	.000	.497
232.5	.202	.398	.000	.398
230	.158	.321	.000	.321
227.5	.110	.268	.000	.205
225	.062	.244	.000	.134
222.5	.020	.242	.000	.064
220	.008	.270	.000	.020
217.5	.003	.354	.000	.000
215	.000	.476	.000	.000

Table III-(2) (con't)

Absorption Spectra

Uridine (concentration = 1.009×10^{-4} molar)

Cytidine (concentration = 0.7695×10^{-4} molar)

λ in mμ	O.D. Uridine	O.D. Cytidine total	O.D. Cytidine band 1	O.D. Cytidine band 2
305	.000	.000	.000	.000
302.5	.004	.003	.003	.000
300	.005	.010	.010	.000
297.5	.006	.028	.028	.000
295	.007	.057	.057	.000
292.5	.014	.110	.110	.000
290	.038	.192	.192	.000
287.5	.072	.298	.298	.000
285	.138	.398	.398	.000
282.5	.243	.483	.483	.000
280	.343	.562	.562	.000
277.5	.472	.628	.628	.000
275	.592	.677	.677	.000
272.5	.719	.699	.699	.000
270	.822	.697	.697	.000
267.5	.900	.680	.680	.000
265	.963	.648	.638	.010
262.5	.991	.610	.562	.048
260	.992	.568	.483	.085
257.5	.961	.528	.398	.130
255	.908	.501	.298	.203
252.5	.834	.483	.192	.291
250	.744	.476	.110	.366
247.5	.655	.478	.057	.421
245	.562	.491	.028	.463
242.5	.474	.511	.010	.501
240	.394	.538	.003	.535
237.5	.324	.560	.000	.560
235	.269	.580	.000	.580
232.5	.220	.598	.000	.598
230	.172	.610	.000	.610
227.5	.126	.618	.000	.598
225	.078	.621	.000	.580
222.5	.040	.634	.000	.560
220	.015	.664	.000	.535
217.5	.005	.720	.000	.501
215	.000	.780	.000	.463
212.5	.000			.421
210	.000			.366
207.5	.000			.291
205	.000			.203
202.5	.000			.130
200	.000			.085
197.5	.000			.048
195	.000			.010

mental dipole moment magnitudes and the calculated transition moment angles, (see Fig. III-8 to III-11). Thymine and uracil are assumed to be identical electronically as the methyl group does not affect the MO calculations and the optical properties are nearly identical. The directions for the transition dipole moments are also shown in Figs. III-(8) to III-(11). These are the calculated directions which are consistent with the known directions from polarized absorption of crystals of adenine and thymine (Stewart and Davidson, 1964, for thymine; Stewart and Jensen, 1964, for adenine). Our calculated direction for the transition in uracil is 34° while the experimental value is 23° in our coordinate system. For adenine the value we use is the same as that of Stewart and Jensen (1964), within experimental error. For G and C we do not have such polarized crystal spectra, so we must guess at the correct transition moment directions. For guanine we assume the lower energy transition is in roughly the same direction as it is in adenine while the second transition is roughly perpendicular, as would be expected from experiments on polarized fluorescence (Callis, et al., 1964). For cytosine, we take the lower energy transition to be close in direction to that in uracil or thymine. We take the second one to be about 30° from the first transition, as suggested by polarized fluorescence of cytosine (Callis, 1965).

The monopoles for the transitions were obtained by a SCF-LCAO-CI calculation done by Dr. H. DeVoe of National Institutes of Health. His method was that of Viellard and Pullman (1963) extended to the excited states. The resulting monopoles are shown in Table III-(3). The states in Table III-(3) are not just the lowest energy transitions as they come from the calculation. They are chosen so that the transition moment directions agree with known experimental directions, or what we infer to be the most likely directions from incomplete data. This procedure amounts

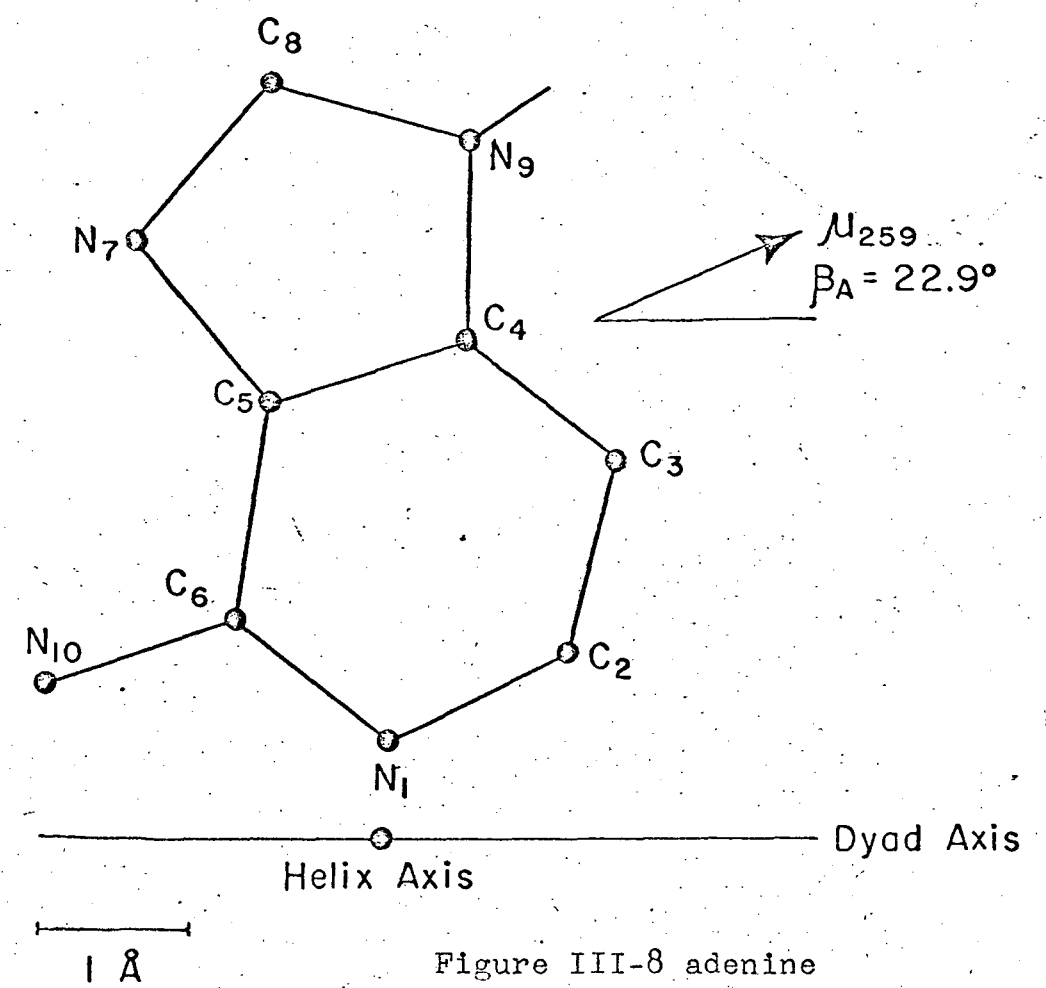

Figure III-8 adenine

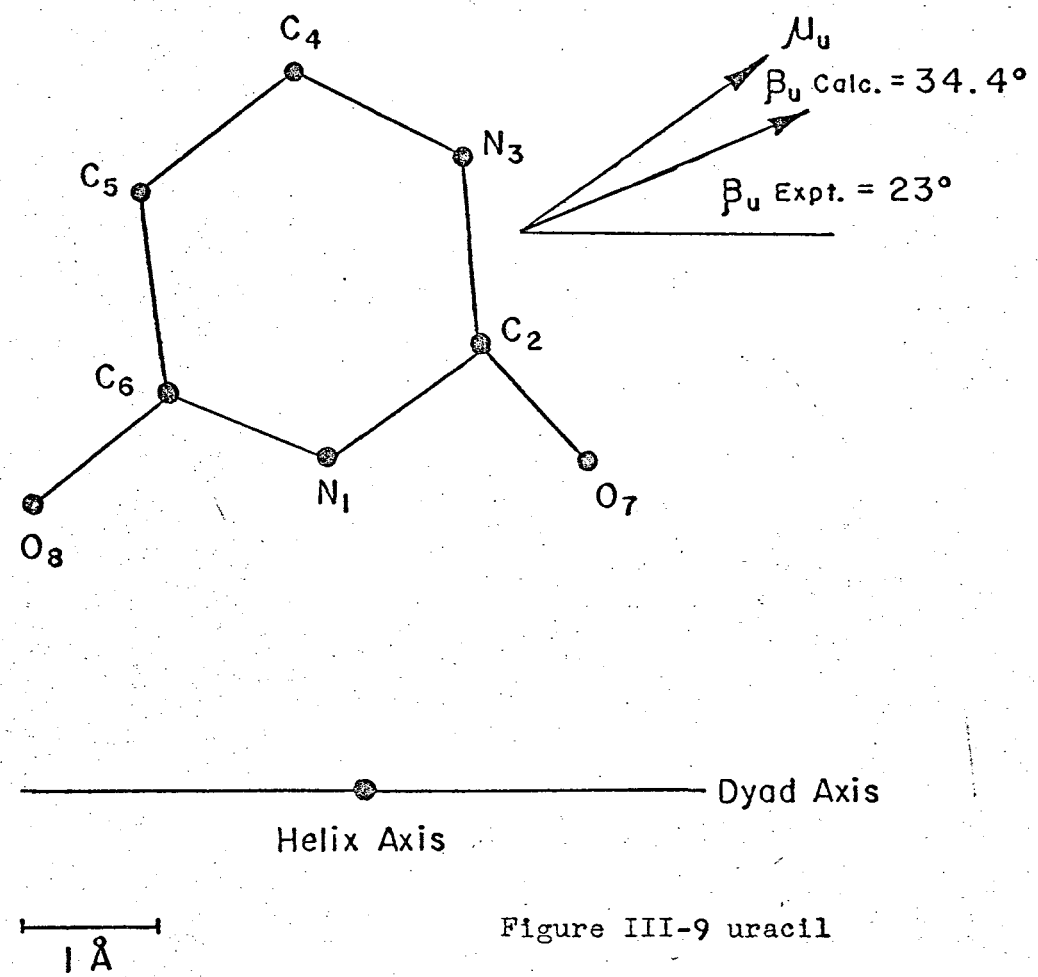

Figure III-9 uracil

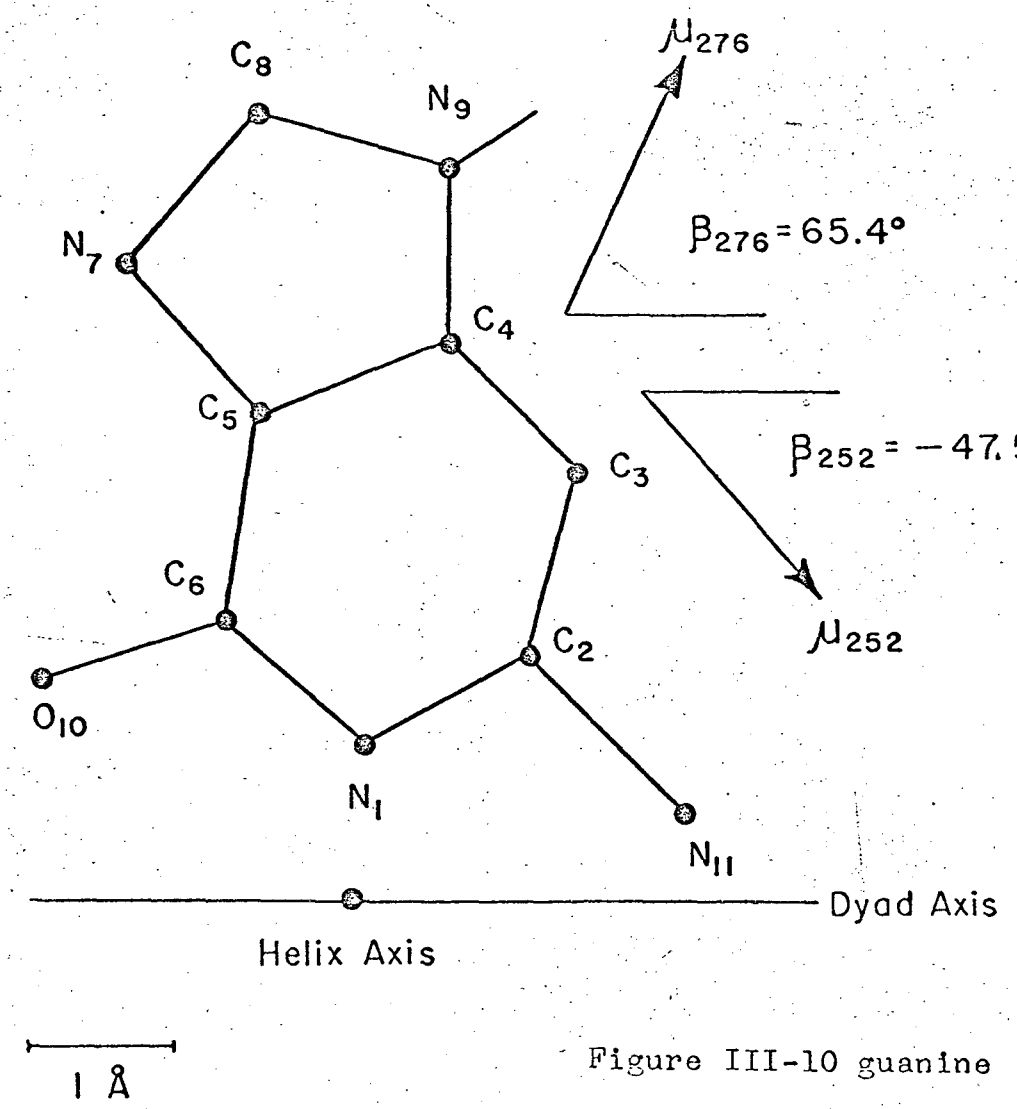

Figure III-10 guanine

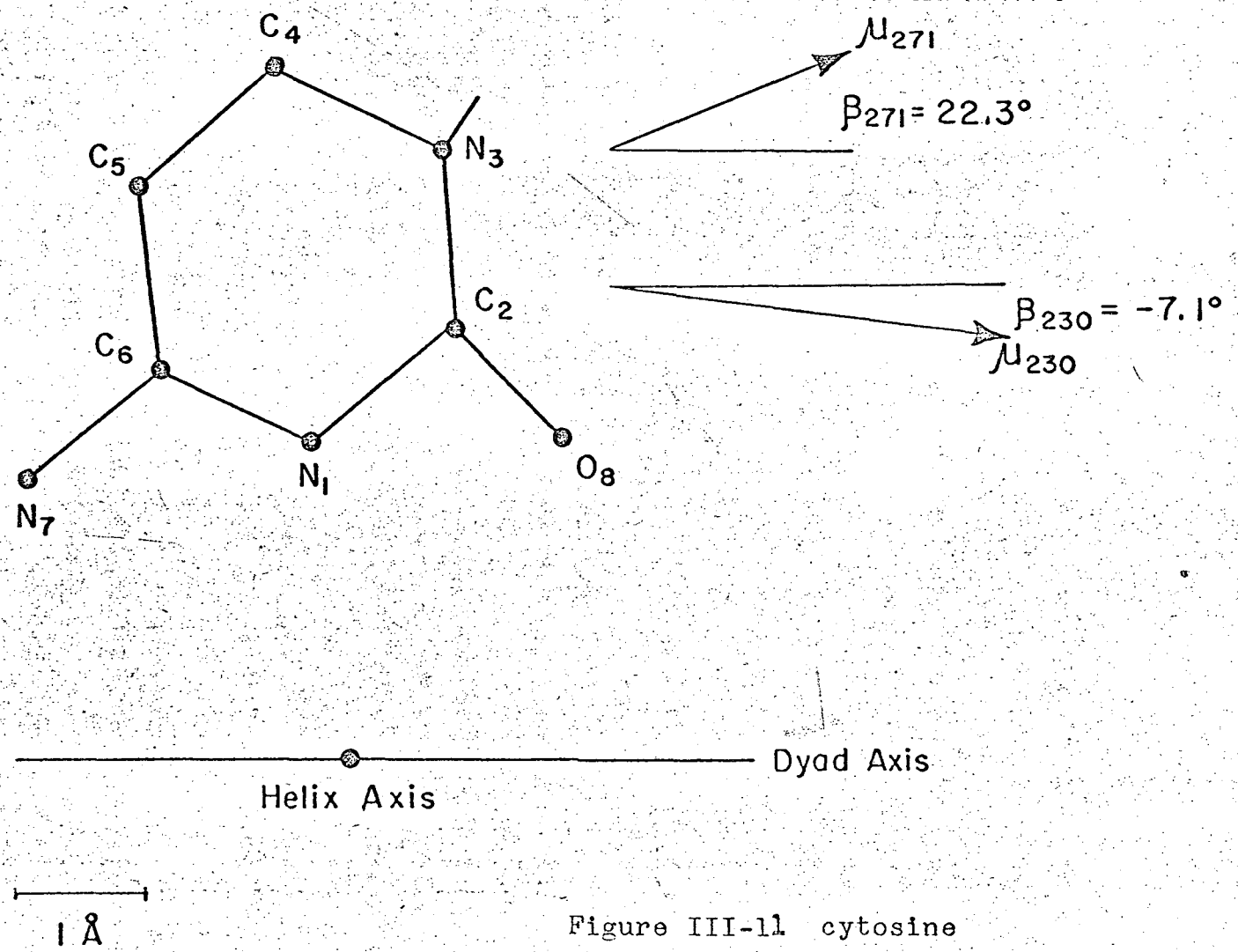

Figure III-11 cytosine

Table III-(3)

Transition monopoles used in the calculation

atom	Adenine	atom	Uracil (Thymine)
N_1	-.0206	N_1	-.0097
C_2	-.0255	C_2	-.0053
N_3	-.0743	N_3	-.1431
C_4	-.2011	C_4	-.3721
C_5	.0869	C_5	.4151
C_6	.1601	C_6	-.0127
N_7	.0377	O_7	-.0077
C_8	-.0731	O_8	.1355
N_9	.0774	$\mu_{calc.}$ =	1.09 eÅ 5.2 debye
$(NH_2)_{10}$	.0323		
$\mu_{calc.}$ =	.56 eÅ 2.7 debye		

Table III-(3) (con't)

Transition monopoles used in the calculation

Guanine			Cytosine		
atom	band 1	band 2	atom	band 1	band 2
N_1	-.0221	-.0658	N_1	-.1857	-.0875
C_2	.0208	-.2453	C_2	.0073	.0249
N_3	-.0345	.1115	N_3	-.1340	-.0151
C_4	-.0726	-.2249	C_4	-.0435	-.1576
C_5	-.0234	.2455	C_5	.0605	.3524
C_6	.0245	.0040	C_6	.0963	.0795
N_7	.0301	-.0630	$(NH_2)_7$	.2141	.0278
C_8	-.2025	.1891	O_8	-.0150	-.2244
N_9	.1733	.0414	$\mu_{calc.}$ =	.87 4.2	1.11 eÅ 5.3 debye
O_{10}	.1154	.0806			
$(NH_2)_{11}$	-.0053	-.0732			
$\mu_{calc.}$ =	.33 1.6	1.20 eÅ 5.8 debye			

to the assumption that although the MO calculation gives states that are correct, the order of the excited states in energy may be incorrect. We also investigated MO's from a paper by Nesbet (1964). However, we could not make so simple a correspondence with the experimental directions as we could with DeVoe's states, so the Nesbet MO's were not used in later calculations.

In order to further utilize experimental data, we have multiplied the transition monopoles by a factor μ_{exp}/μ_{calc} (see Tables III-1 and III-3) so that the dipole moments we compute will also agree in magnitude with experiment. Surely this kind of mutilation of a molecular orbital calculation cannot be justified on theoretical grounds, but it does ensure that the V_{12} we calculate will not be too far off. Of course, there remains the possibility that the MO's may give an incorrect charge distribution which happens to add up in such a way as to give the correct transition direction. Also, it might be argued that we should just use the experimental dipole moments and compute the V_{12} directly from Eq. III-(2). Actually, the monopole method scaled in this way will be more accurate in that it is sensitive to the shape of the bases. In other words, the dipole approximation is not very good when the charges are spread out over a plane roughly 5 Å wide and separated from the next plane by only 3.4 Å. The resulting interactions are tabulated in Table III-(4). In the cases of non-degenerate interactions, there are two values, corresponding to the two different sequences. Our convention is that the head of the column is the first (3'linked) and that the row indicates the second (5' linked) nucleoside). The angle of helix increment is taken to be 34.4°, per nucleotide. This is in the range we feel to be particularly illustrative for reasons we shall come to later. For interaction between degenerate groups, the V_{12} refers to the splitting of the degenerate bands

Table III-(4)

$V_{1a;2b}$ in cm^{-1} for helix increment (γ) = 34.4°

	A	U	G band 1	G band 2	C band 1	C band 2
A	736	310	71	555	193	566
U	354	77	-148	428	77	484
G band 1	904	668	212	249	494	572
G band 2	-123	-127	-137	541	-144	41
C band 1	499	198	-86	530	178	568
C band 2	69	-268	-169	611	-138	275

* Sequence dependence: base at hear of column is 3' linked.

into the (+) and (-) levels, while for non-degenerate interactions, the V_{12} is included explicitly in the rotational strength, as can be seen from Eq. III-(21). Since the splitting in degenerate groups is small compared to the half width of the absorption, the role played by the V_{12} in the degenerate case is not too different from that of the non-degenerate case in computation of the observed rotation. In the degenerate case, a large splitting causes the positive and negative branches of the rotation to separate and become more prominent in the optical rotatory dispersion. This point will become clearer as we proceed to computation of the actual rotation.

We next proceed to calculation of the rotational strengths from Eq. III-(21). For this we will need the scalar triple product $\underset{\sim}{R}_{12} \cdot \underset{\sim}{\mu}_{1oa} \times \underset{\sim}{\mu}_{2oa}$ in the degenerate case, or $\underset{\sim}{R}_{12} \cdot \underset{\sim}{\mu}_{1oa} \times \underset{\sim}{\mu}_{2ob}$ in the non-degenerate case. If we take the cross product between the transition moments first, we see that the result is particularly simple. $\underset{\sim}{\mu}_{1oa} \times \underset{\sim}{\mu}_{2ob} = |\underset{\sim}{\mu}_{1oa}|\,|\underset{\sim}{\mu}_{2ob}| \sin(\beta_2 - \beta_1 + \gamma)\underset{\sim}{e}$, with $\underset{\sim}{e}$ parallel to the helix axis since the bases are in parallel planes which are perpendicular to this axis. Referring to Fig. III-(7), we see that if the bases are identical, the angle of the transition moment of the first base, β_1, must be equal to the angle of the transition moment of the second base, β_2. Here the angle, $\beta = (\beta_2 - \beta_1 + \gamma)$ whose sine we take, is simply γ, the angle of helix increment. So for a degenerate dimer, no matter what β_1, the angle of the transition moment is, we get a positive sign for the triple product since the cross product of the $\underset{\sim}{\mu}$'s is nearly parallel to $\underset{\sim}{R}_{12}$ for helix increment angles between 0 and about 70°. For left handed helixes with γ between 0 and -70°, the triple product is negative. This tells us that in ApA and UpU, where we have only the degenerate term to consider, a positive γ will give us a positive rotational strength for the long wavelength transition. Fig. III-(2) shows

that this is true for ApA and that we have a strong case for a right handed helical sense for ApA. We present also in Fig. III-(12) the rotation of UpU with the rotation of the monomers subtracted. This figure is from the unpublished data of Mr. Myron Warshaw. UpU also shows a positive rotation at the long wavelength side of the transition, thus indicating a right handed conformation.

For non-degenerate interactions there will also be a tendency for right handed helixes to have positive rotation at long wavelength. From Eq. III-(21) we see that $\underset{\sim}{R}_{OA}$ for a single non-degenerate term, as in UpA or ApU, will be positive for the longer wavelength transition if $\beta_1 - \beta_2$ is not greater than γ, and $V_{1a;2b}$ is positive. That the latter is true for helix increments between $\pm$ ~70 degrees can be seen from the dipole approximation, Eq. III-(2), or by considering that V_{12} for small angles must surely be positive (i.e. repulsive) since the atoms of one monomer are directly above like atoms in the second. Table III-(1) shows that the β's for A and U transitions are only 11° apart, so we expect the same general kind of rotation for ApU and UpA as for ApA and UpU if γ is greater than 11°. Figs. III-(13) and III-(14) show Warshaw's experimental ORD (with monomers subtracted) for ApU and UpA. They do, in fact, show the expected behavior: positive rotation at the long wavelength side of the transition. In contrast to A and U, the angles of the transition moments of G and C are very different, and in some cases they will make angles in the dimer that are larger than 70-90°, giving a negative V_{12}. Others make angles less than zero giving rise to negative triple products; thus we may expect to find some cases of negative rotational strengths at long wavelength.

Later we will put these predictions on more firm numerical ground, but let us say for now that the dinucleosides which have been measured up

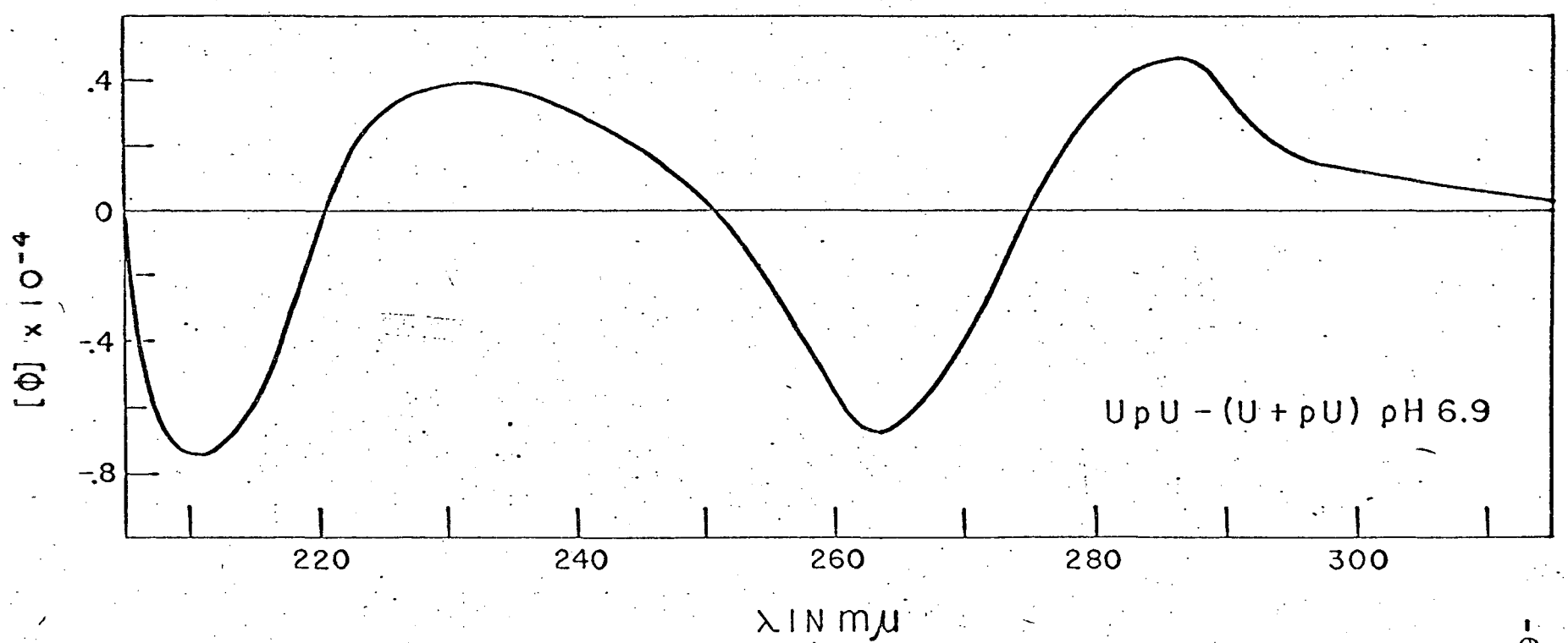

Figure III-12 Experimental ORD of UpU

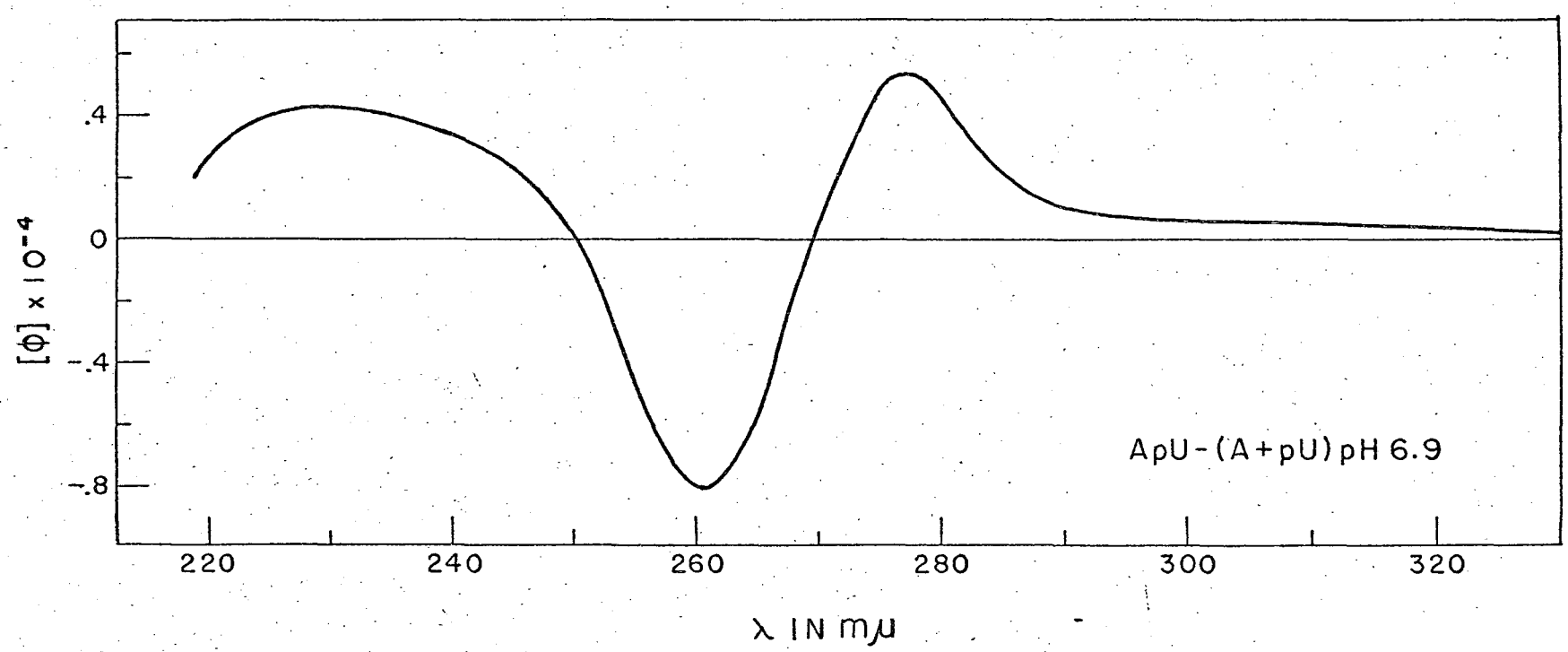

Figure III-13 Experimental ORD of ApU

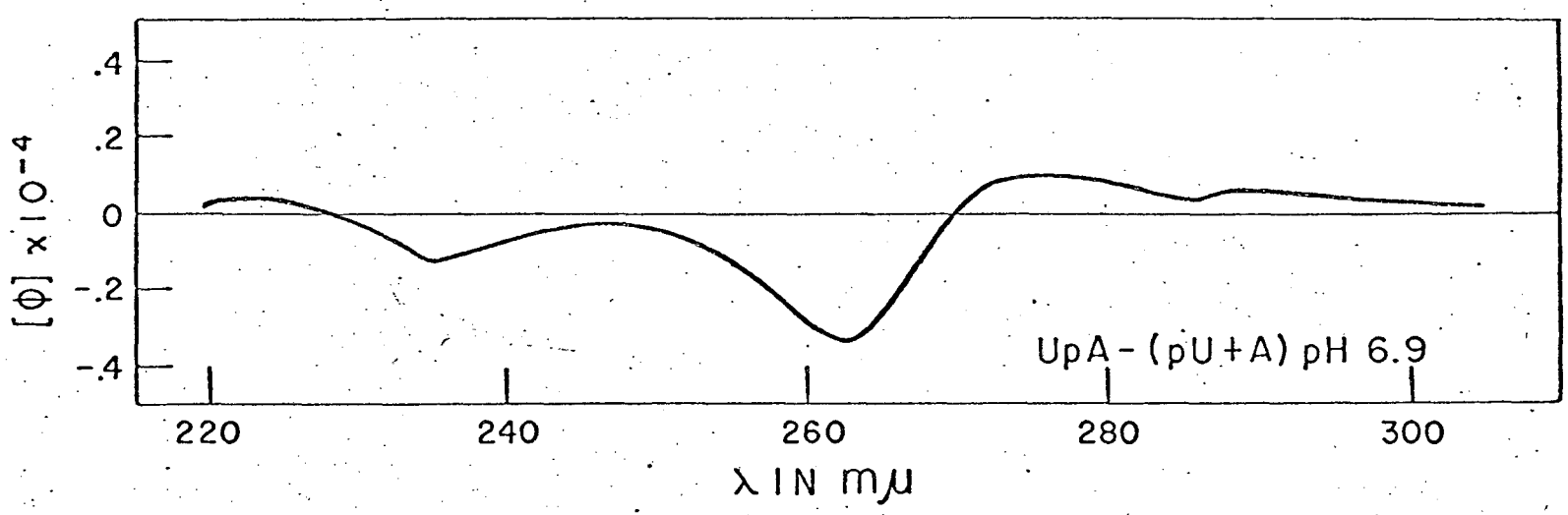

Figure III-14 Experimental ORD of UpA

Table III-(5)

Rotational strengths for $\gamma = 34.4°$

	frequency in cm^{-1}	rotational strength $\times 10^{40}$ cgs
ApA	37874	200
	39346	-200
UpU	38173	144
	38327	-144
ApU	38250	229
	38610	-229
UpA	38250	371
	38610	-371
ApG	36232	170
	38610	-128
	39682	-43
GpA	36232	-2
	38610	324
	39682	-322
ApC	36900	82
	38610	-81
	43478	-1
CpA	36900	33
	38610	38
	43478	-70
UpG	36232	117
	38250	-57
	39682	-60
GpU	36232	-2
	38250	148
	39682	-147
UpC	36900	24
	38250	-20
	43478	-4
CpU	36900	18
	38250	33
	43478	-51
GpC	36232	-35
	36900	-33
	39682	37
	43478	31

Table III-(5) (con't)

Rotational strengths for $\gamma = 34.4°$

	frequency in cm^{-1}	rotational strength $\times 10^{40}$ cgs
CpG	36232	15
	36900	-59
	39682	15
	43478	29
GpG	36020	46
	36444	-123
	39141	203
	40223	-126
CpC	36722	96
	37078	-108
	43203	185
	43753	-173

to now generally show positive rotation at long wavelength and that we feel this is convincing evidence for their right handedness. We will not ignore left handed helices entirely, but we will concentrate our efforts on right handed models.

In order to investigate the steric possibilities of the model in Fig. III-(7) with adjustable helix increment angle γ, we used Courtauld molecular models. Since known van der Waals radii and bond lengths are used to set the dimensions of these models, they give one a fairly realistic picture of steric effects. For right handed dimers with our geometry, γ's of 28° to 40° are sterically possible, and if one is willing to abandon the location of the helix axis relative to the base (as shown in Figs. III-8 to III-11), one could extend γ to 25° or 55°. For angles of zero degrees, the ribose sugars are too crowded to allow stacking of the bases at 3.4 Å. In order to construct left handed helices, one must turn the sugars so that they are not in the same relative conformation. That is, they are not related to each other by the same transformation that related the bases in their helical geometry. This means that although the bases can be in a helical geometry with $\gamma<0$, the sugars are not relates by the same z increment and helix increment angle that relates the bases. Therefore, one could not form a polymer longer than the dinucleoside. Nevertheless, for dimers, we may have the bases in a left handed helical geometry with γ's between -15 and -50° and still maintain the same position of the helix axis relative to the bases. By moving the helix axis relative to the bases, we could extend the range to -65°.

We have not considered the possibility of rotation of the bases about the glycoside bond. Extensive investigation of the X-ray scattering of many nucleosides and derivatives by Haschemeyer and Rich (1965) have led them to conclude that the main conformation occurring naturally is that

which is found in DNA. That is the conformation which we have used by taking the coordinates given by Langridge, et al. (1960).

Computation of the ORD from Rotational Strengths

We now have the rotational strengths and locations of the various bands in the dinucleosides, and it remains to calculate the optical rotatory dispersion from this information. The molecular rotation per nucleoside is

$$[\phi] = \alpha \frac{18\ M}{\pi\ C\ N} \qquad \text{III-(22)}$$

where α is the rotation in radians/cm, M is the molecular weight, C is the concentration in grams per cc, and N is the number of nucleosides, in our case two. The use of molecular rotation per residue allows direct comparison of oligomer and polymer rotations. We could write the ORD simply as damped Drude equations:

$$[\phi] = \frac{48\ N_o\ \nu^2}{2nc} \sum_k \frac{R_k\ (\nu_k^2 - \nu^2)}{(\nu_k^2 - \nu^2)^2 + \nu^2 \Gamma^2} \qquad \text{III-(23)}$$

(Tinoco, Woody and Bradley, 1963). This method makes an assumption about the curve shape which we may avoid by using absorption data to construct the ORD curve. In this way we hope to predict details in the ORD curve which will be detected in experiments.

The method we have in mind is to construct the circular dichroism curve by making the assumption that the circular dichroism for any band has the same curve shape as the absorption. This is probably a reasonable assumption for the allowed absorptions which we consider in nucleotides ((Moffit and Moscowitz, 1959). We then derive the ORD by using a Kronig-Kramers dispersion relation, the details of which will follow below.

To construct the circular dichroism having the same curve shape as the absorption and the rotational strength computed from Eq. III-(21), we recall that we already have the absorption in a particularly convenient form. To get the dipole strehgths, we expressed the absorption of Table III-(2) as a sums of gaussians:

$$\epsilon\ (\nu) = \sum \epsilon_i\ e^{-\left(\frac{\nu_i - \nu}{\Delta_i}\right)^2} \qquad \text{III-(24)}$$

We will construct the CD curve having the same form as the absorption in Eq. III-(24). The units of circular dichroism will be molecular ellipticity (Moscowitz, 1960),

$$[\theta] = 2.303\ \frac{(4500)}{\pi}\ (\epsilon_L - \epsilon_R) \qquad \text{III-(25)}$$

where ϵ_L and ϵ_R are the extinction coefficients for left and right handed circularly polarized light. This molecular ellipticity will then be expressed as a sum of gaussians:

$$[\theta] = \sum_i c_i\ e^{-\left(\frac{\nu_i - \nu}{\Delta_i}\right)^2} \qquad \text{III-(26)}$$

for which we must determine the c_i. They will be related to the ϵ_i by a single factor which we can easily derive by writing down the formulas for dipole strength and rotational strength of gaussian bands (Moscowitz, 1960). For the dipole strength of a gaussian band,

$$D_{oa} = \frac{3hc}{8\pi^3 N_1} \int_0^\infty \frac{\epsilon(\nu)d\nu}{\nu}\ , \qquad \text{III-(27a)}$$

where N_1 is the number of absorbing molecules per cc. For the case of an absorption band expressed as a sum of gaussians,

$$D_{oa} = .92 \times 10^{-38} \sqrt{\pi} \sum_i \frac{\epsilon_i \Delta_i}{\nu_i} \quad . \qquad \text{III-(27b)}$$

For the rotational strength of a gaussian band,

$$R_{oa} = \frac{3hc}{8\pi^3 N_1} \int [\theta(\nu)] \frac{d\nu}{\nu} \quad , \qquad \text{III-(28a)}$$

and for the rotational strength of a band expressed as a sum of gaussian circular dichroisms,

$$R_{oa} = 0.696 \times 10^{-42} \sqrt{\pi} \sum_i \frac{C_i \Delta_i}{\nu_i} \quad . \qquad \text{III-(28b)}$$

We now simply take the quotient R_{oa}/D_{oa} by dividing Eq. III-(28b) by III-(27b), and pick one value of i from the sums, to give the ratio of c_i to ϵ_i.

$$\frac{R}{D} = \frac{1}{1.325 \times 10^4} \frac{c_i}{\epsilon_i} \quad , \text{ or } \quad c_i = \frac{R}{D} \epsilon_i \times 1.325 \times 10^4 \qquad \text{III-(29)}$$

We may obtain circular dichroism curves from III-(26). Although we are primarily interested in ORD, we will also quote some of our results for circular dichroism (see Appendix B), since some measurements have already been given (Van Holde, et al., 1965) and others will probably be forthcoming.

Now we will develop the transformation to the ORD by means of the Kronig-Kramers relation, which relates the molar rotation to the molar ellipticity,

$$[\phi(\nu)] = \frac{2}{\pi} \int [\theta(\nu')] \frac{\nu^2}{\nu'} \left(\frac{1}{\nu'^2 - \nu^2} \right) d\nu' \qquad \text{III-(30)}$$

(Moffitt and Moscowitx, 1959; Moscowitz, 1957). For the case of gaussian circular dichroism, Eq. III-(30) can be integrated according to a method

due to Moscowitz (1957). We begin by breaking the integral up into the sum of three fractions.

$$[\phi(\nu)] = 2/\pi \int \sum_i c_i e^{-\frac{(\nu' - \nu_i)^2}{\Delta_i}} \nu^2 \, d\nu' \left[\frac{-1}{\nu^2 \nu'} + \frac{1}{2\nu^2(\nu' - \nu)} + \frac{1}{2\nu^2(\nu' + \nu)} \right] \qquad \text{III-(31)}$$

We now make the substitution: $x = (\nu' - \nu_i)/\Delta_i$.

$$[\phi(\nu)] = 2/\pi \sum_i c_i \int \frac{-e^{-x^2}}{x + \frac{\nu_i}{\Delta_i}} + \frac{e^{-x^2}}{2\left(x + \frac{\nu_i - \nu}{\Delta_i}\right)} + \frac{e^{-x^2} dx}{2\left(x + \frac{\nu_i + \nu}{\Delta_i}\right)} \qquad \text{III-(32)}$$

We now quote a relation derived by Moscowitz (1957) which will allow us to numerically evaluate the above integrals.

$$\int \frac{e^{-x^2}}{x+C} dx = 2\sqrt{\pi} \, e^{-C^2} \int_0^C e^{-x^2} dx \qquad \text{III-(33)}$$

Eq. III-(33) has a very simple asymptotic form, $= \sqrt{\pi}/C$, for values of C very different from zero. In Eq. III-(32), ν_i, the frequency of the gaussian, is always much greater than the gaussian half width Δ_i. Therefore, the asymptotic form will be adequate to represent the first and third integrals of III-(32). In the second integral, the asymptotic form is valid only far from the absorption band where ν is very different from ν_i. Hence we write the equation in the following form which was the one used in our calculations,

$$[\phi(\nu)] = 2/\pi \sum_i C_i \left[\frac{-\Delta_i \sqrt{\pi}}{\nu_i} + \frac{\Delta_i \sqrt{\pi}}{\nu + \nu_i} + \int_0^C 2\sqrt{\pi} e^{-c^2} e^{-x^2} dx \right] \qquad \text{III-(34)}$$

where $C = \frac{(\nu_i - \nu)}{\Delta_i}$. The values of the integral were taken from a table of 400 values from C=0 to C=$\pm$4 (Lohmander and Rittsten, 1958). For values of C greater than 4 or less than -4, the asymptotic expression was used.

The above formulas were evaluated on an IBM 7094 computer at the Lawrence Radiation Laboratory, Berkeley. The basis for the computation of the interaction energies, V_{12}, was formed by a program of H. DeVoe. The monopoles of Table III-(3) were scaled by μ_{exp}/μ_{calc} and V_{12} was computed by the method described above (see p. 57; also Appendix A). To compute the rotational strengths, we simply need the triple products of Eq. III-(21). These were computed as a function of the helix increment angle, γ, for intervals of .1 radian over the range -1.5 to +1.5 rad for ApA and from 0 to .8 radians for the other dimers. The method used on the IBM 7094 was to compute $\underset{\sim}{\mu}_1 \times \underset{\sim}{\mu}_2 = \mu_1\mu_2 \sin(\beta_1 - \beta_2 + \gamma)$, which is a vector parallel to the helix axis. The dot product of this vector with the line joining the bases $(\underset{\sim}{R}_{12}) = (\underset{\sim}{R}_2 - \underset{\sim}{R}_1)$ was computed from the geometry of Fig. III-(7). (See p. 26 above and Appendix A).

The fitting of the absorption curves to sums of gaussians was done by fixing the positions in frequency and the half widths of the gaussians, and then solving a set of linear equations to fit the amplitudes of the gaussians to the experimental absorption curves. We chose half widths $\Delta_i = 700\ cm^{-1}$ and spaced gaussians every $500\ cm^{-1}$ through the absorption. This yielded positive gaussian amplitudes for the center of the band (see Table III-(6). The linear equations were solved by an IBM Share routine on the 7094. The fitting to the sums of gaussians is not a very exact procedure. The fit is very good at the experimental absorption points, but in some cases anomalous excursions and wiggles were discovered in the fitted curves. This shows up when the gaussian curves are added to construct circular dichroism curves. In the curves to be shown below, these

Table III-(6)

Amplitudes of absorption gaussians, $\Delta_i = 700\ cm^{-1}$

Adenine		Guanine band 1		Guanine band 2	
ν_i cm^{-1}	ε_i	ν_i cm^{-1}	ε_i	ν_i cm^{-1}	ε_i
45110	-74.5	39600	-101.2	45600	89.4
44610	209.8	39100	59.1	45100	-223.44
44110	1158.0	38600	1758.2	44600	1294.3
43610	839.1	38100	1028.9	44100	-17.1
43110	775.9	37600	3582.1	43600	2285.2
42610	1649.4	37100	2297.0	43100	1733.2
42110	1784.5	36600	4237.8	42600	2441.5
41610	2324.7	36100	3590.0	42100	3387.6
41110	3301.7	35600	2892.2	41600	3842.3
40610	3511.5	35100	2897.3	41100	4580.8
39610	5224.1	34600	1320.6	40600	5436.3
39110	6344.8	34100	570.3	40100	5477.0
38610	6252.9	33600	102.5	39600	5762.2
38110	6175.3	33100	21.0	39100	5466.5
37610	5784.5	32600	-25.0	38600	3513.8
37110	4646.6			38100	2392.9
36610	1905.2			37600	1419.2
36110	2885.1			37100	247.0
35610	-540.2			36600	961.9
35110	977.0			36100	-1172.1
34610	-491.4			35600	-
34110	330.5				
33610	-155.2				

Table III-(6) (con't)

Amplitudes of absorption gaussians, Δ_1 = 700 cm^{-1}

Uracil		Cytosine band 1		Cytosine band 2	
45600	-34.4	41700	1.3	51500	-48.1
45100	82.8	41200	2.6	51000	214.4
44600	52.2	40700	174.1	50500	-254.7
44100	178.3	40200	263.8	50000	1920.7
43600	393.6	39700	744.6	49500	-2050.7
43100	470.1	39200	1516.6	49000	4347.0
42600	882.8	38700	2630.3	48500	-2487.3
42100	1066.2	38200	2317.1	48000	5133.2
41600	1693.0	37700	4044.2	47500	-645.9
41100	1792.4	37200	3359.3	47000	4098.8
40600	2522.3	36700	3942.8	46500	1286.5
40100	2728.7	36200	3615.3	46000	3246.3
39600	3610.2	35700	2901.9	45500	2517.2
39100	3447.1	35200	2352.2	45000	3031.8
38600	4430.6	34700	1662.1	44500	3063.0
38100	3774.5	34200	-88.4	44000	2973.4
37600	4356.7	33700	399.0	43500	3494.5
37100	3224.2	33200	-236.5	43000	2965.6
36600	2961.8	32700	102.7	42500	3142.3
36100	2192.4			42000	2834.3
35600	1107.0			41500	2877.2
35100	484.1			41000	2413.3
34600	0.0			40500	2371.7
34100	3.8			40000	1954.4
33600	-3.8			39500	1598.4
				39000	1544.5
				38500	335.3
				38000	612.1
				37500	-844.7
				37000	690.1

rough spots have been removed.

The Kronig-Kramers transform was also computed on the 7094, and values of [ϕ] were obtained over the range of 200 to 300 mμ. Listings and descriptions of all the programs used appear in Appendix A.

Results of the Calculation

All these calculations assume a rigidly fixed conformation of the bases as shown in Fig. III-(7). This is a low temperature approximation which is not valid at room temperature, as may be seen from the temperature dependence of the rotation (Warshaw and Tinoco, 1965). The optical rotation increases with decreasing temperature, indicating that the proportion of the stacked or rigid model conformation is increasing. In no case has any leveling-off of the curve with temperature been found. If one could go below 0°C, presumably the stacked form would eventually predominate and the experiments would be strictly comparable with the present calculation. Since such low temperature experiments have not yet been done, we will have to scale our calculated curve by a factor, roughly representing the amount of the dimer in the stacked form, in order to compare our curves with experiments at room temperature.

We have done this for ApA where the factor necessary for fitting the curve (calculated for $\gamma = 34°$) at the minimum near 261 mμ is .39. In Fig. III-(15) we have plotted both the scaled calculation and the experimental ORD curves with the monomer rotation subtracted (Warshaw, et al., 1965). The agreement is good; the calculation gives approximately correct points and the peak near 284 mμ. Since we have not included the influence of the 206 mμ absorption of adenine, the trough at 216 mμ is not reproduced in the calculated curve.

We do not have very much experimental or theoretical information pertaining to the nature of this shorter wavelength absorption band. If

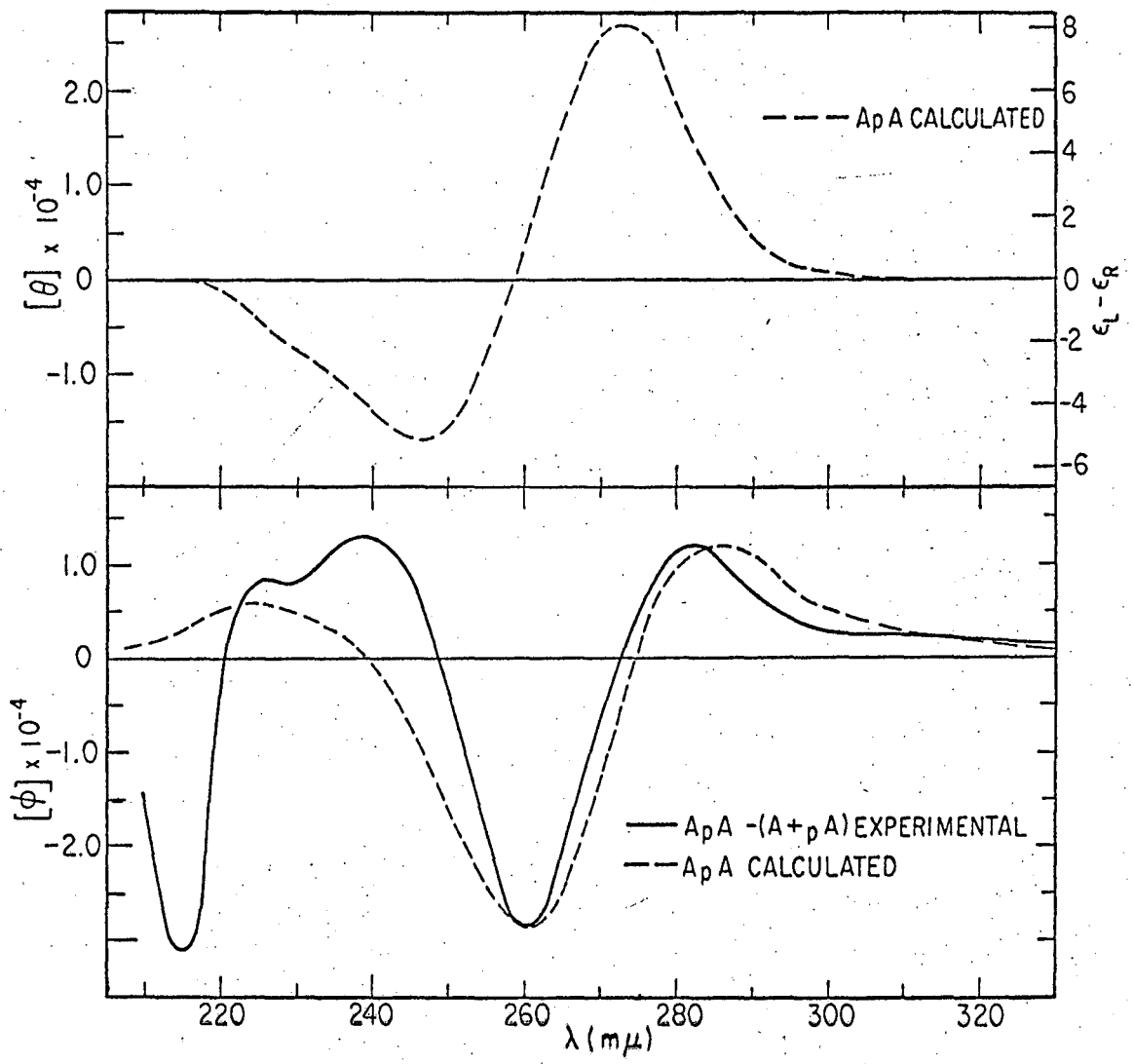

Figure III-15
CD and ORD of ApA

we assume that it is a π-π^* type transition, we know it will be polarized in the base plane. The interaction $V_{1a;2a}$ will be positive since it represents the interaction of two identical transitions at a small angle (34°) from each other. Since we have a right handed helix, the rotational strength of the long wavelength exciton component is positive, so the general shape of the ORD resulting from this 206 mμ absorption must be the same as that from the 260 mμ band. We would therefore expect to see the trough at 206 mμ while it in fact occurs at 216 mμ. This shift could be due to interaction of the 206 mμ band with higher bands or with static fields.

We also show in Fig. III-(15) the circular dichroism curve calculated for ApA. This is scaled by the same factor as is the ORD. Comparison with the C.D. curve for ApA given in Van Holde, et al. (1965) shows that the agreement is also very good here. Their curve shows a slightly sharper peak and trough than the calculated one. This is probably because we have assumed that the monomer absorption curve is not changed in shape in the dimer. If one considers the interaction between the two monomers in terms of each of the vibronic components making up the broad absorption curve, there will be changes in the transition probability to the different vibronic components of the band on dimerization (Young, 1965). Inclusion of these effects would give a narrowing of the band, and might improve the agreement with experiment (Young, 1965).

In Fig. III-(16) we have plotted the optical rotation at 261 mμ as a function of the helix increment angle, γ, for ApA. For all the angles studied, the curve has a turning point at this wavelength; it has a minimum for γ greater than zero and a maximum for γ less than zero. This plot is an explicit demonstration of the property that we have already mentioned, that right handed dimers of identical bases show a double cotton effect

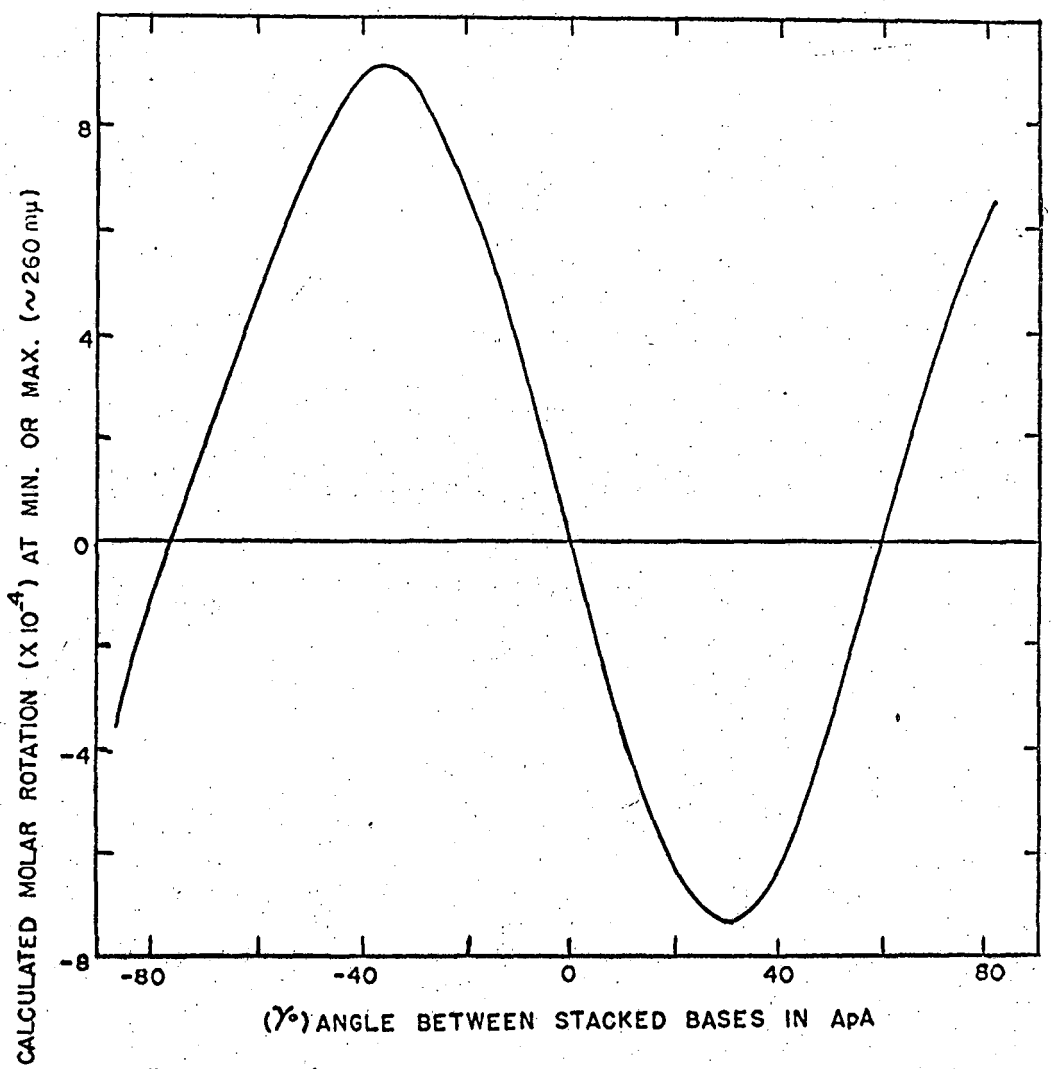

Figure III-16 ORD of ApA as a function of helix increment angle

with the long wavelength rotational band positive. For left handed helices, the curve is reversed with two minima and a maximum near the monomer absorption peak.

The calculated ORD for UpU is shown in Fig. III-(17) for the same angle of helix increment, $\gamma = 34.4°$. It is similar in shape to that for ApA but is broader due to the broader absorption band of the monomer. The magnitude is reduced, primarily because the V_{12} is an order of magnitude smaller (see Table III-4). For this dimer, the angle, γ, at which the largest rotation is found, is lower than in ApA; the base itself is smaller and gives a large V_{12} only at small angles. Thus for $\gamma = 17°$, we find a rotation similar in shape to the one in Fig. III-(17) but showing $[\phi] = -1.8 \times 10^4$ at the minimum. Looking at Warshaw's experimental curve in Fig. III-(12), we see that our calculation agrees generally with the shape and position of the minimum. The magnitudes are not strictly comparable, because the experiment is at room temperature.

When we calculate the ORD of dimers with different bases, additional parameters become important. In calculating the triple product of Eq. III-(21b) and III-(21c), we need the angle between the transition moments, $\beta = (\gamma + \beta_1 - \beta_2)$. This requires knowledge of the direction of the transition moments (β_1 and β_2) relative to the base coordinate system as seen in Fig. III-(8) to III-(11). We show the calculated ORD for ApU at $\gamma = 34.4°$ in Fig. III-(18) and for UpA in Fig. III-(19). These curves show qualitative agreement with the experimental curves of Figs III-(13) and III-(14) but the positions of the minima are wrong. This is not improved if we choose other values of γ. This is probably due to changes in the monomer absorption upon dimerization, and could be predicted only with a study of the vibronic interaction mentioned in connection with the ApA circular dichroism. The sequence dependence of the ORD in the case of

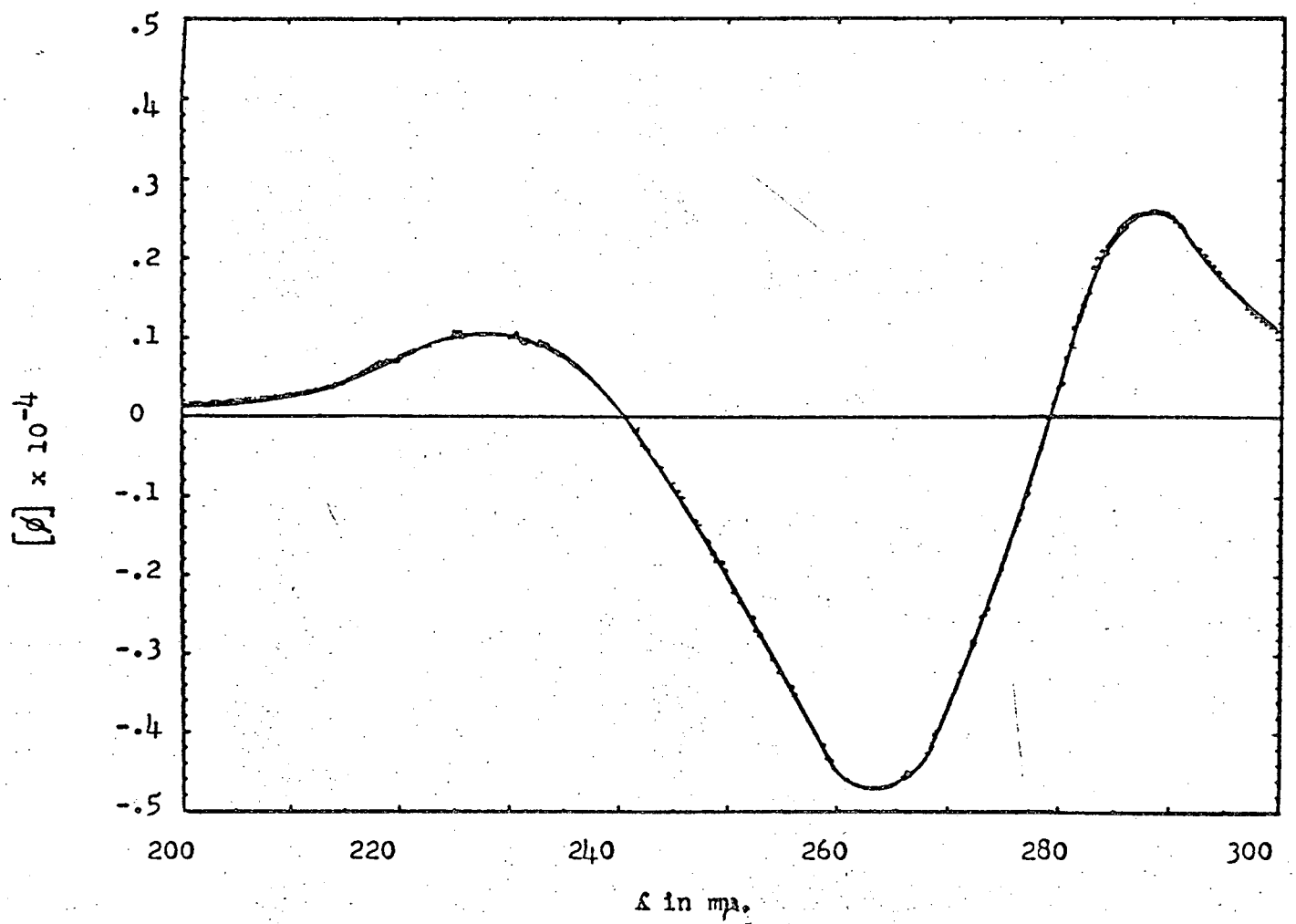

Figure III-17 UPU ROTATION VS. WAVELENGTH

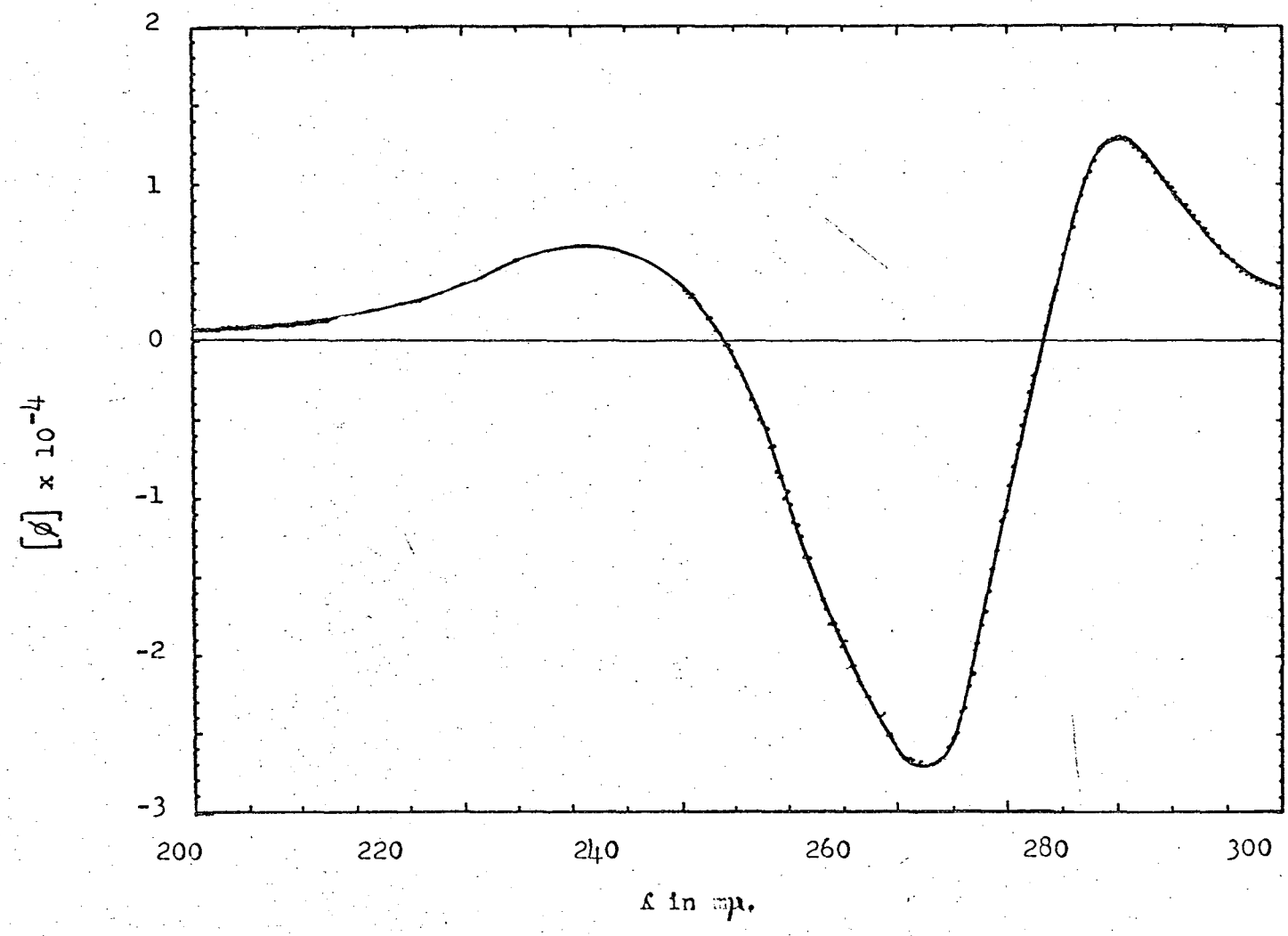

Figure III-18 APU ROTATION VS. WAVELENGTH

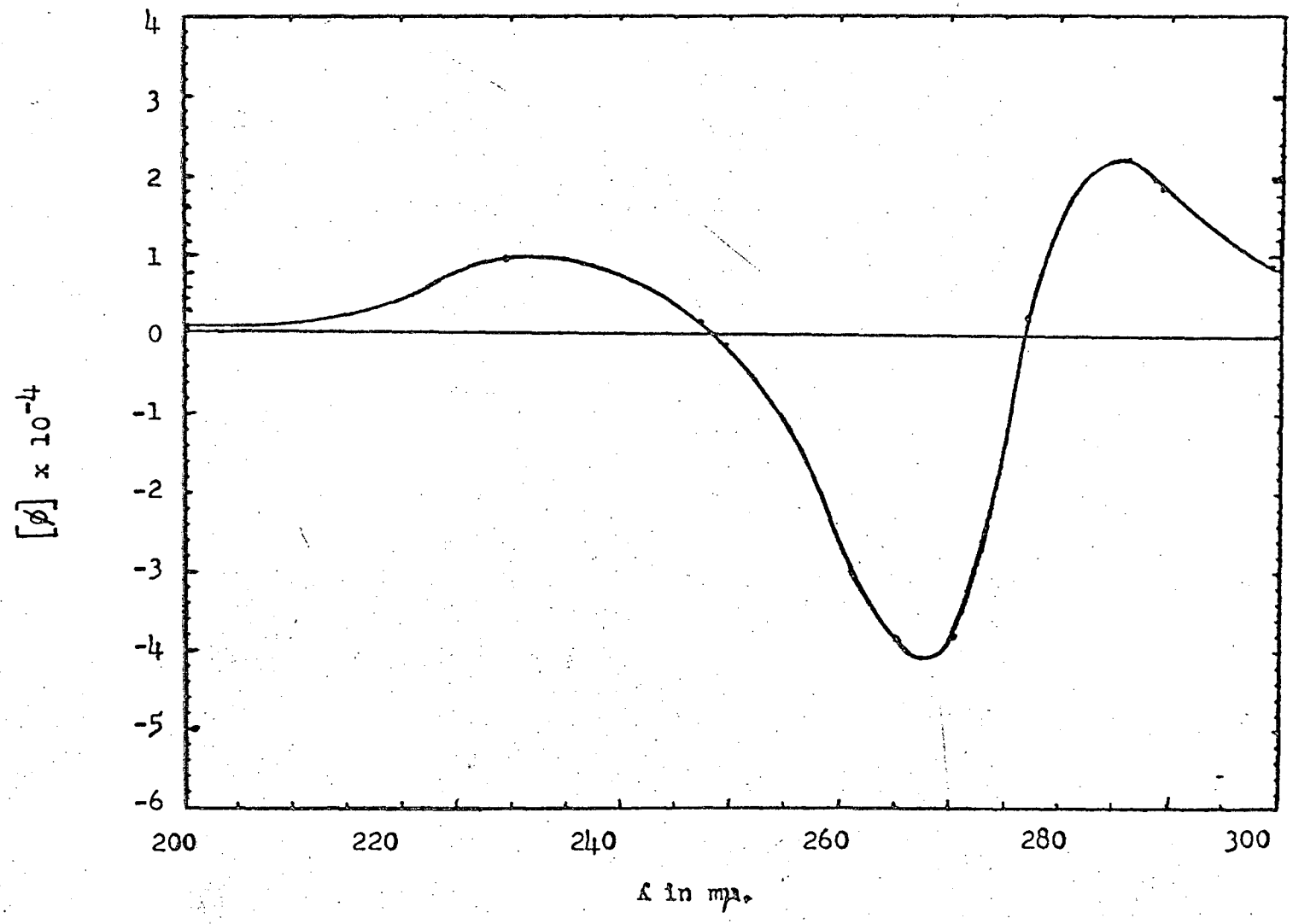

Figure III-19 UPA ROTATION VS. WAVELENGTH

these two sequence isomers is very small, as the angles of the transition moments in these two bases are very similar (see Figs. III-8 and III-9). We expect a strong sequence dependence in cases where the angles of transition moments are very different. The dependence of the rotation at the turning point near 267 mμ as a function of helix increment angle γ, is similar to that for ApA shown in Fig. III-(16) except that the angle of zero rotation occurs at $\gamma = 11°$ for ApU and at $\gamma = -11°$ for UpA. These are γ's at which the transition moments in the two bases are parallel, giving a zero triple product in the non-degenerate terms of Eq. III-(21).

The next group of dimers we wish to consider is the large group of dimers of different bases containing either a guanosine (G) or a cytidine (C) linked to an adenosine or a uridine. These dimers are more complicated than ApU and UpA because C and G both have two absorption bands in the wavelength range 210 to 300 mμ (see Figs. III-5 and III-6). Thus we compute rotational strengths for three separate bands. This involves two different V_{12}'s and two triple products. The sum of these three rotational strengths is, of course, zero. However, the two interactions may have different dependence on angle γ, due to the differences in the nature of the two electronic transitions in the base (G or C) having two bands. Therefore, the dependence of the rotation on the helix increment angle, γ, is rather complicated. For a given rotation curve, the general shape does not change greatly with changing γ, and only the amplitude of the maxima and minima change. However, at values of γ where two transition moments become parallel, we do find qualitative changes in the ORD curve shape. It would be confusing to present the hundreds of plots necessary to illustrate this point, so we will quote ORD curves for a fixed value of γ.

Because of our study of the simpler dimers, we believe that the conformation of all the dimers is right handed, and this assumption of right handedness gives us reasonable results for the remaining dinucleosides. Moreover, we have mentioned that steric considerations limit us to values of γ between 28 and 40°. Therefore, we will choose $\gamma = 34°$ as a geometry which seems likely and will illustrate the kind of results we can obtain.

In Fig. III-(20) and III-(21) we show our calculated results for ApG and GpA. We may compare these with the experimental curves for ApG and GpA of Figs. III-(22) and III-(23) which were again provided by Mr. Myron Warshaw. Surely the agreement in curve shape is not so good as in the simpler cases we have quoted previously. Also, the calculated magnitudes of the rotation are very large; in fact, this pair of sequence isomers has the largest rotation of any dinucleoside we have calculated. This may indicate that the room temperature rotation curves are measuring a rather small proportion of the stacked conformation and that on going to lower temperature, ApG and GpA might show exceptionally large rotations. In spite of these discrepancies, we notice that we do calculate a sequence dependence, indicating that our calculation is capable of predicting this feature which is very important to the use of ORD as a means of analyzing oligonucleotides. Moreover, the positions of the first maxima and the minima are rather well predicted. The positions of the second maxima, around 230 to 240 mμ are not reproduced, and the ratio of maxima to minima are not correct. Inclusion of the higher frequency absorptions of A and G might improve this situation. We also expect that inclusion of the vibronic interaction would improve the agreement of the curve shape.

We next compare our calculated curve for ApC (Fig. III-24) and CpA Fig. III-25) with Warshaw's unpublished experimental curves for these two

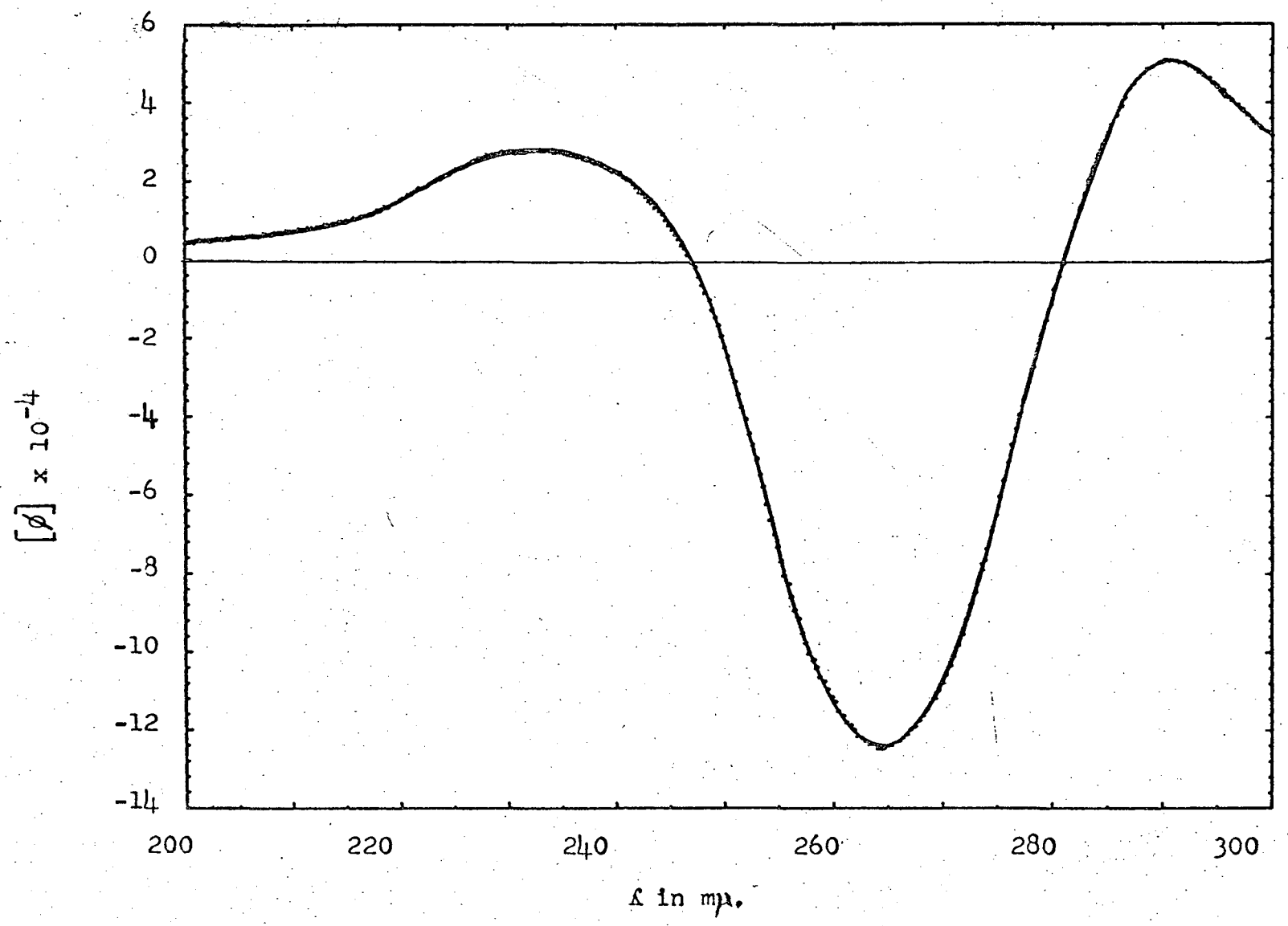

Figure III-20 APG ROTATION VS. WAVELENGTH

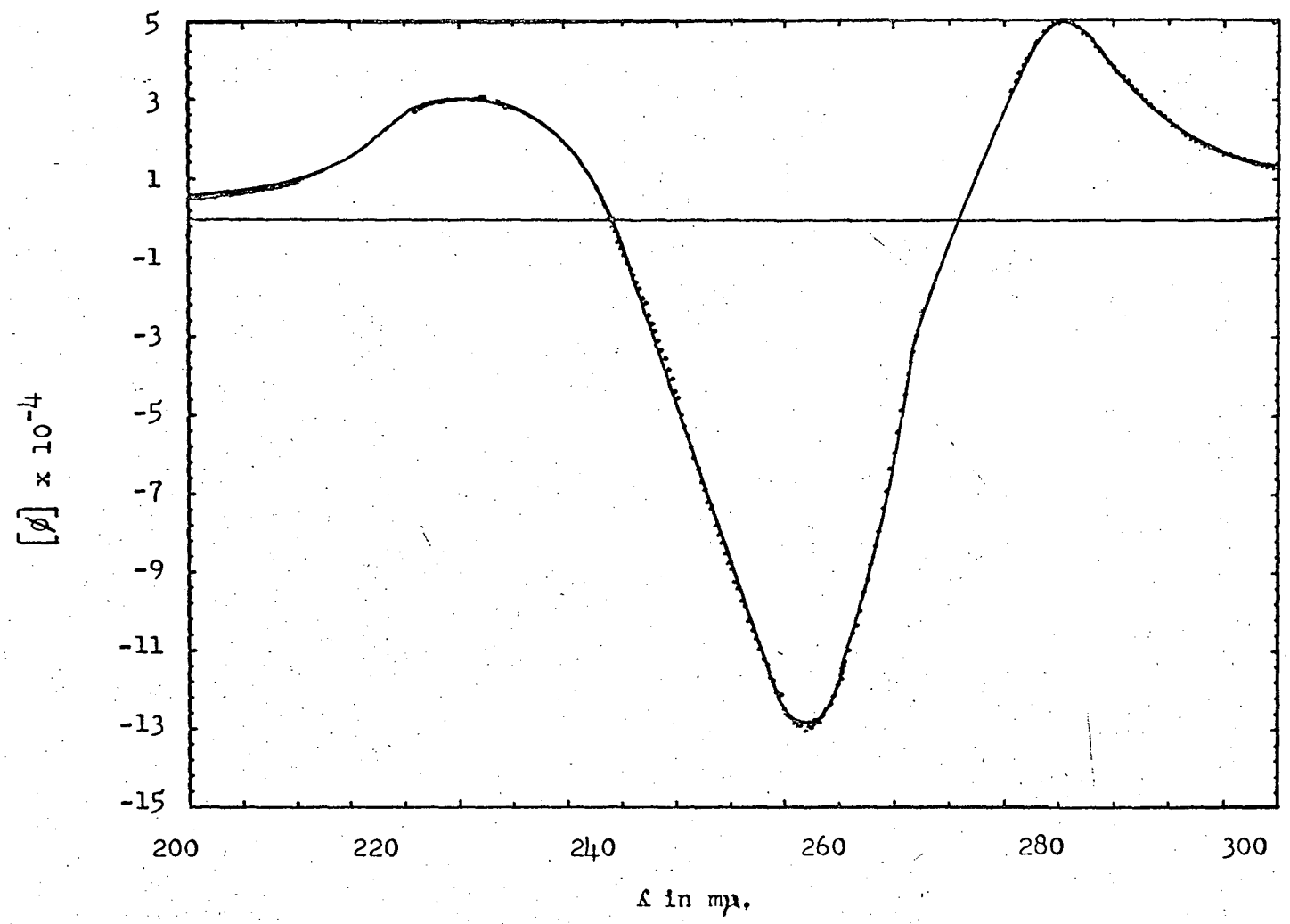

Figure III-21 GPA ROTATION VS. WAVELENGTH

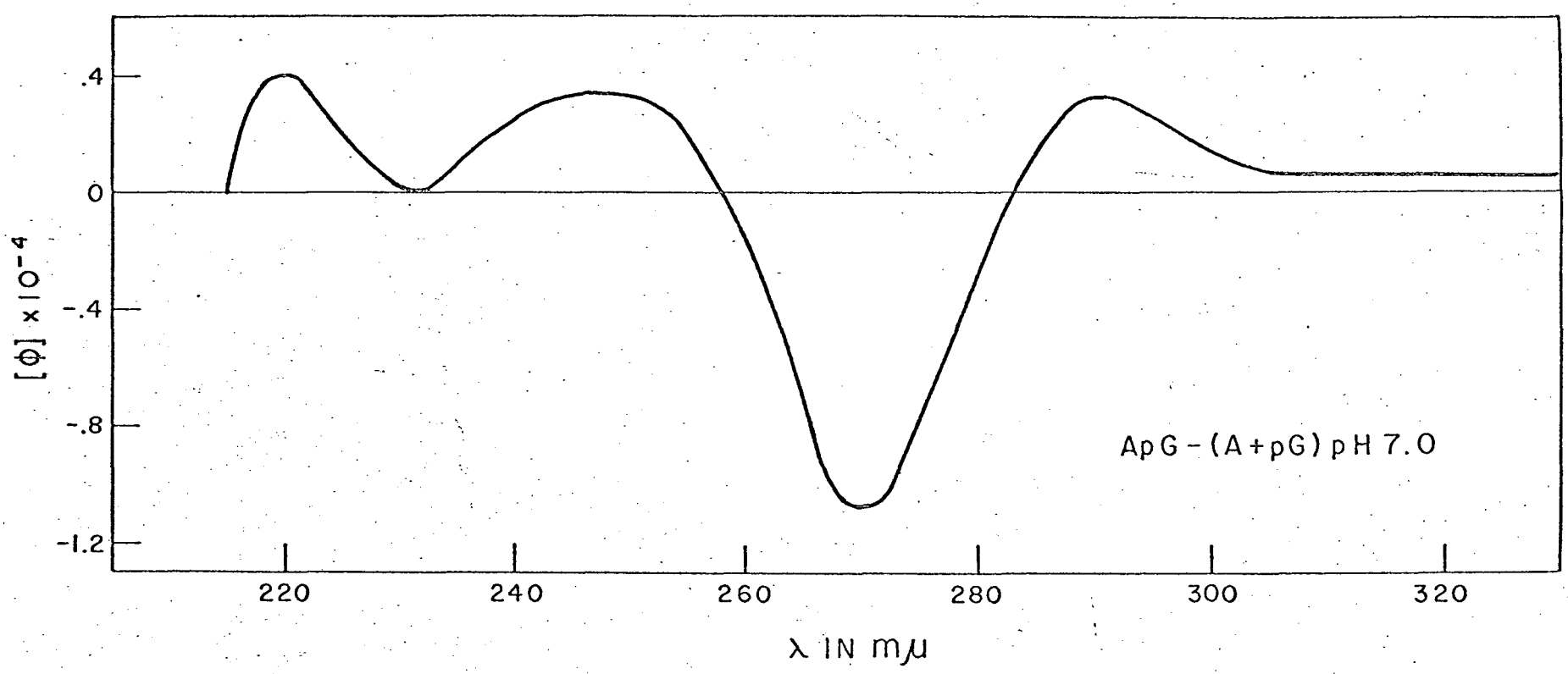

Figure III-22 Experimental ORD of ApG

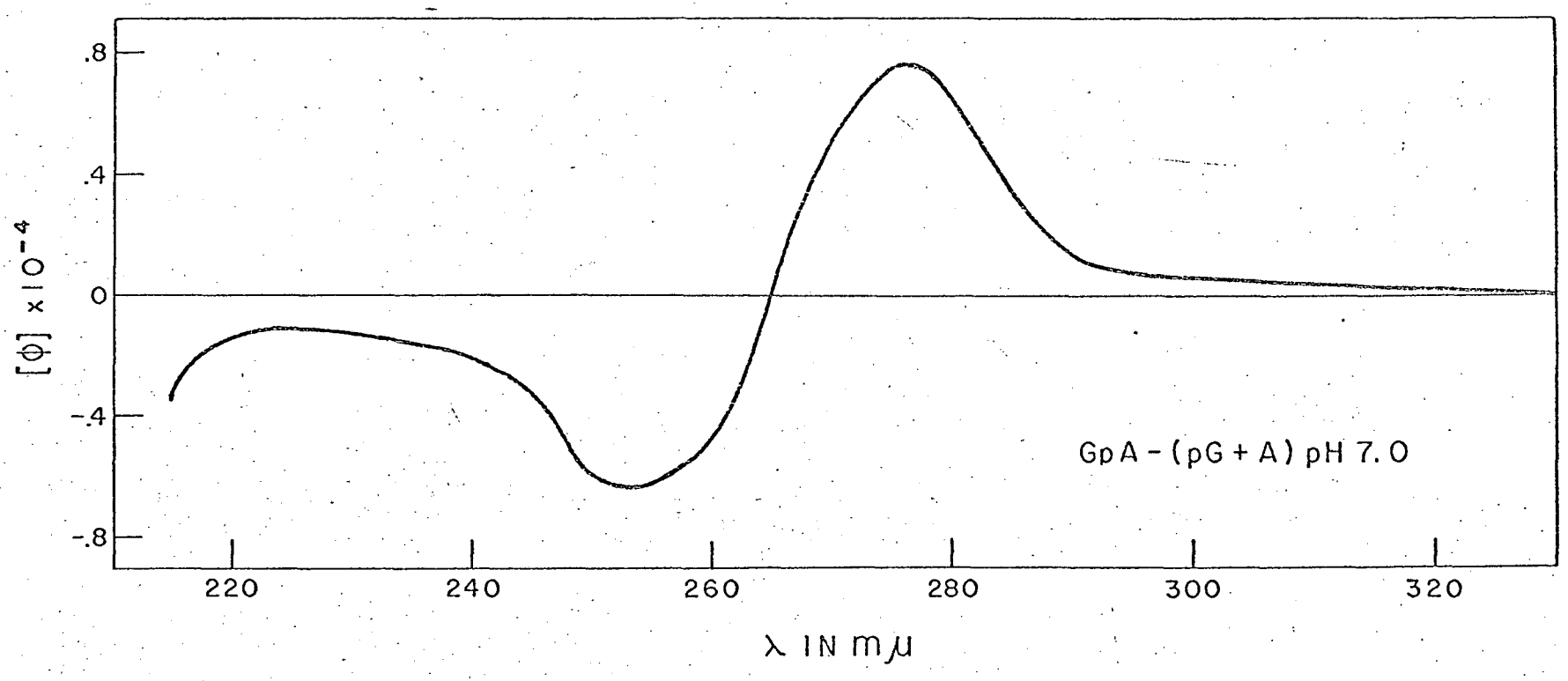

Figure III-23 Experimental ORD of GpA

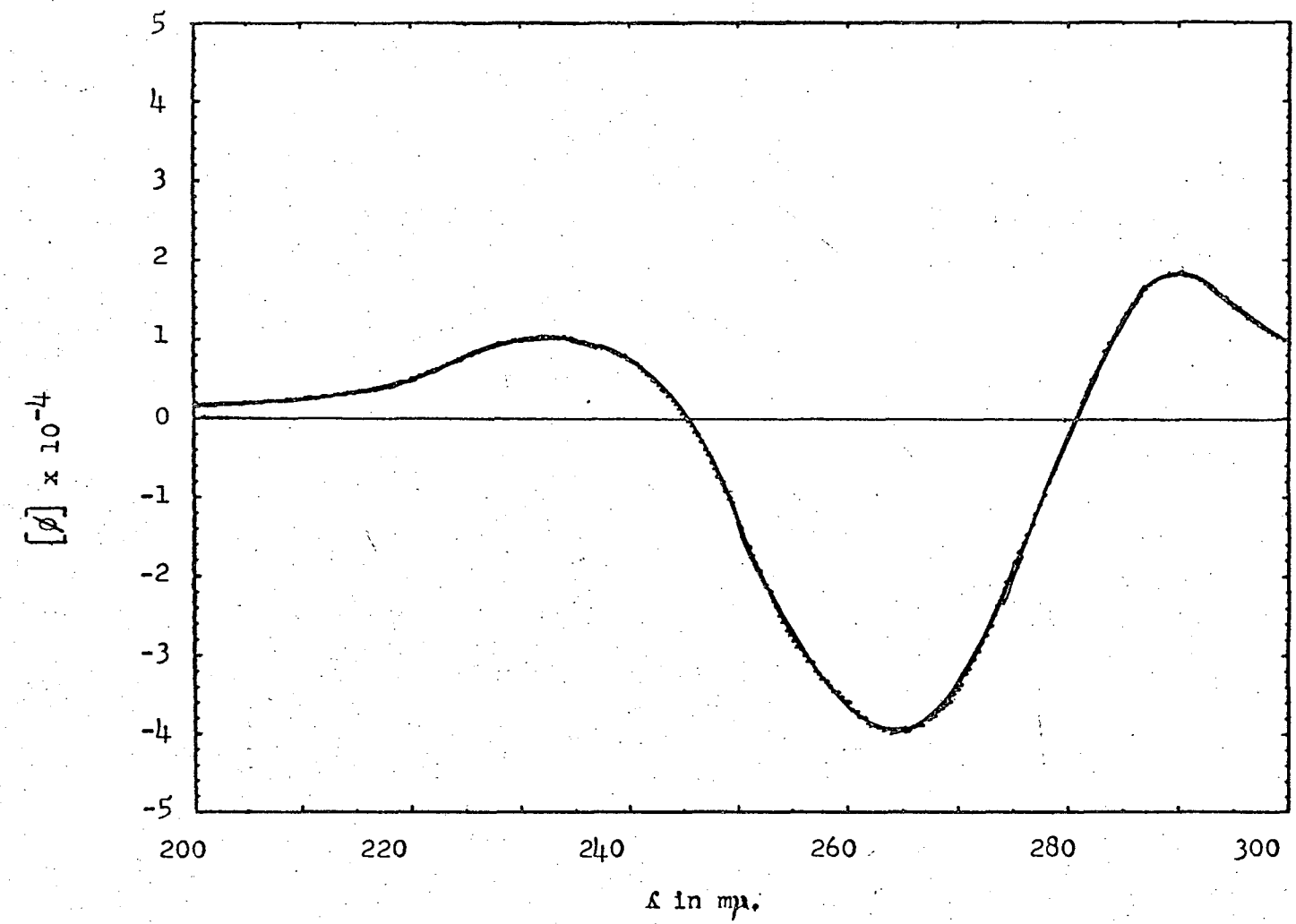

Figure III-24 APC ROTATION VS. WAVELENGTH

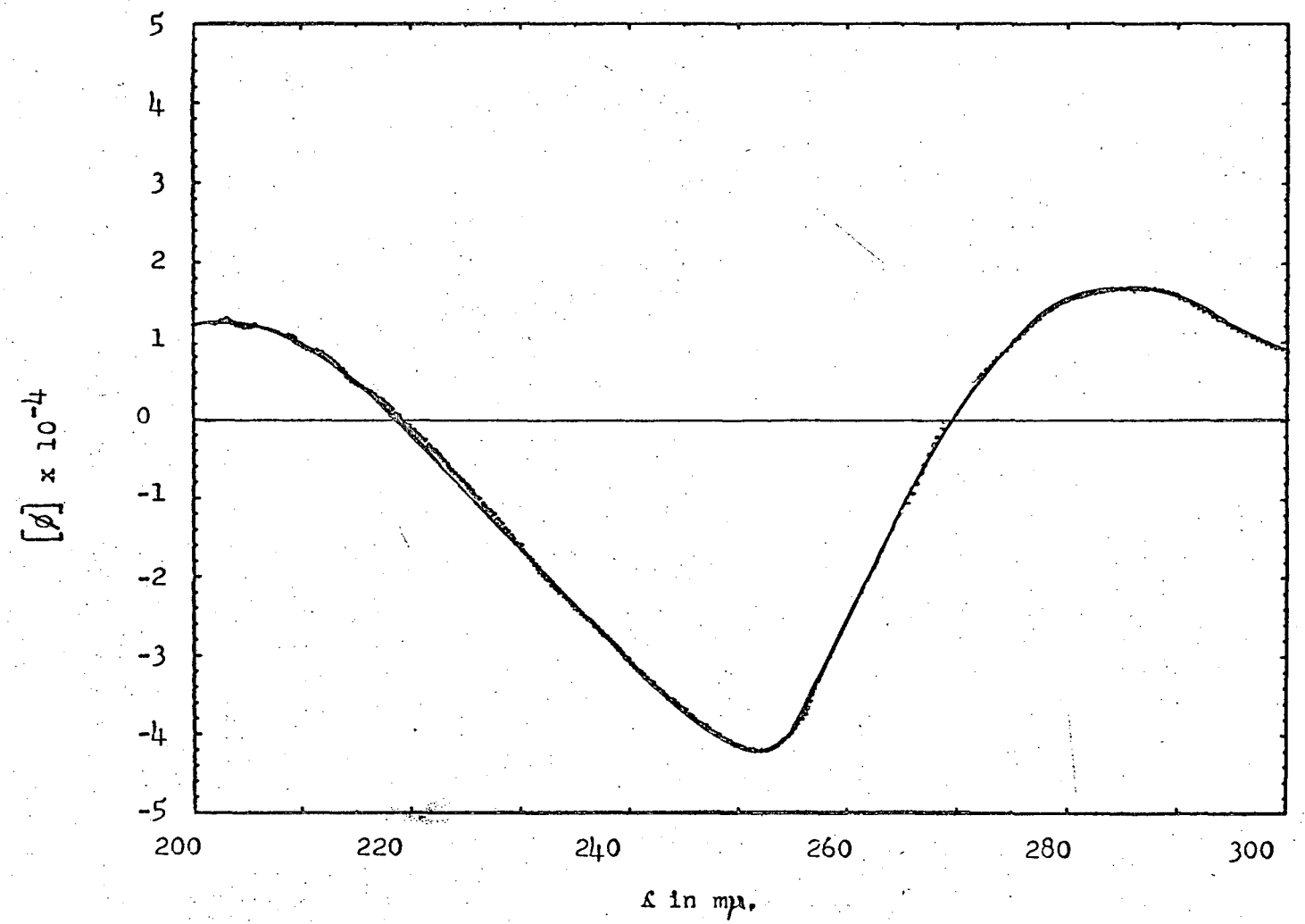

Figure III-25 CPA ROTATION VS. WAVELENGTH

dinucleosides (Figs. III-26 and III-27). In this case we have computed a greater dependence on sequence than is actually observed; the experimental curves for ApC and CpA are rather similar. The agreement of the calculation with experiment is not improved by assuming other values of γ in the range of 20 to 40°. Our inability to predict the experimental curve for this case is probably due to bad assumptions about the direction of the transition moments for C. We actually have very little information about the transitions in C, but we can hope that an experimental determination of the correct direction of the transition moments might tell us how to calculate better values of V_{12}'s and the triple products.

Moving on to the calculated curves for UpG and GpU, in Figs. III-(28) and III-(29), we see that the magnitudes of the rotations are large while the experimental curves (Figs. III-30 and III-31) show rather small rotation. Our failure to obtain good agreement here may be due to a low proportion of stacked conformation in the dimer at room temperature. The rotation of pyrimidine monomers is larger than that of purine monomers (Warshaw and Tinoco, 1965). Therefore, the contribution of the interaction of the electric dipole transition moment of one base with the magnetic transition moment of the other may be large (see Eq. III-10). We have no way of knowing what the nature of this contribution is except that it may be significant in a case such as this, where the monomer rotation is large. Of course, there is also the possibility that our agreement in the cases of ApG and GpA is fortuitous and that we really have the wrong directions for the transition moments in G. Either of these two effects could be the source of the error and it is difficult to decide where improvement should be sought. It would be helpful to have the experimental ORD of GpG which has not been measured, as a result of difficulties in obtaining and working with that compound.

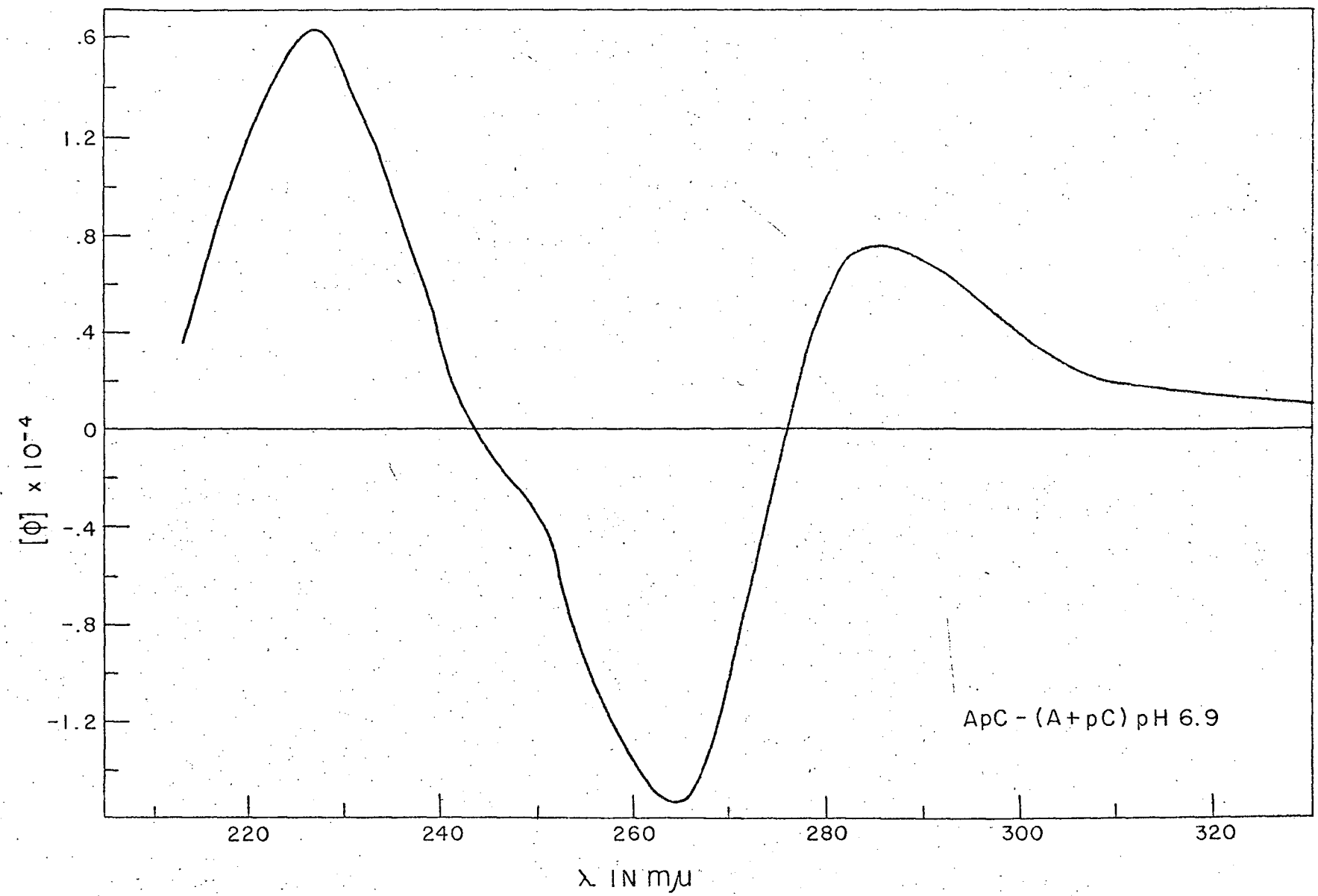

Figure III-26 Experimental ORD of ApC

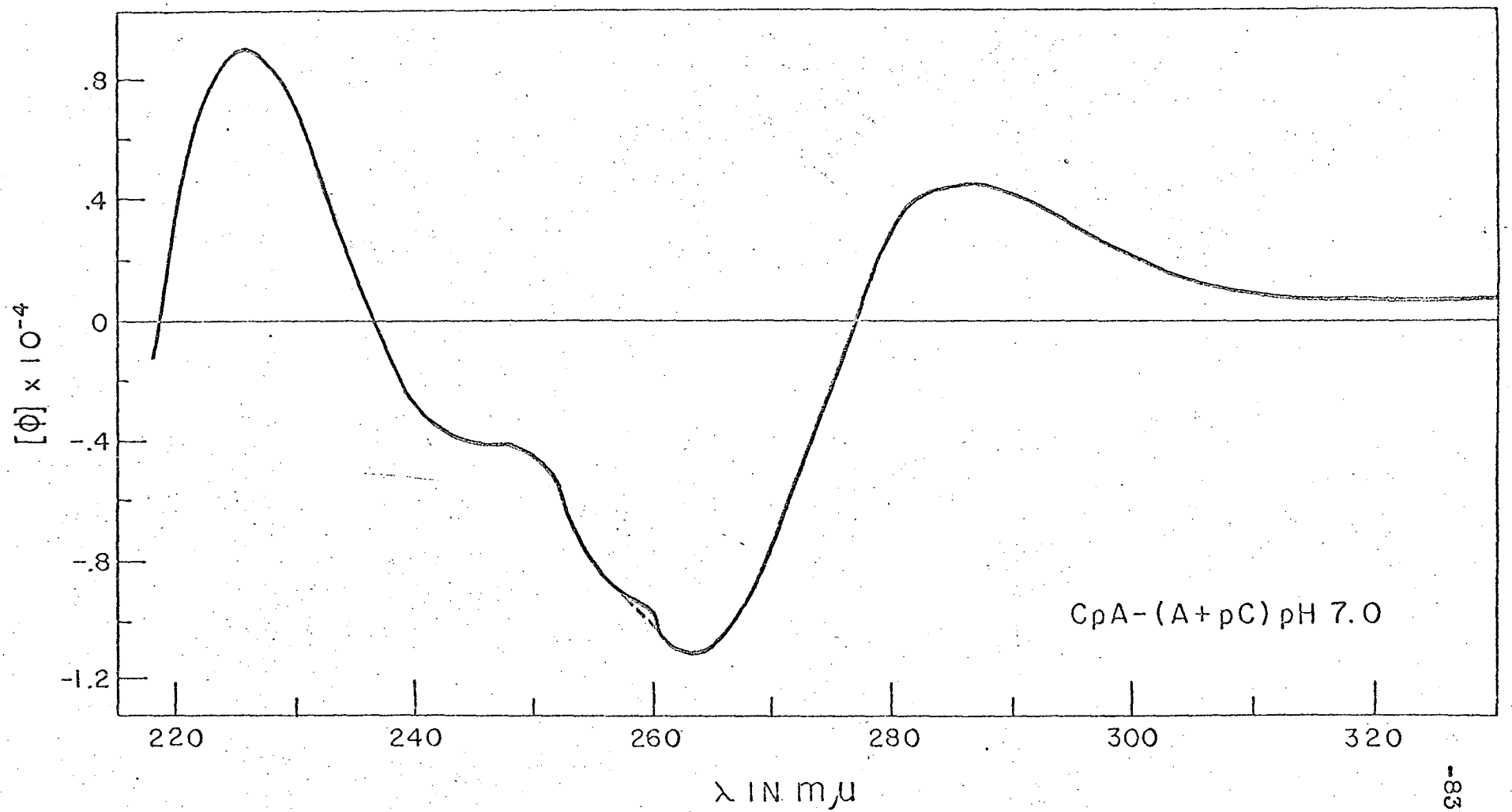

Figure III-27 Experimental ORD of CpA

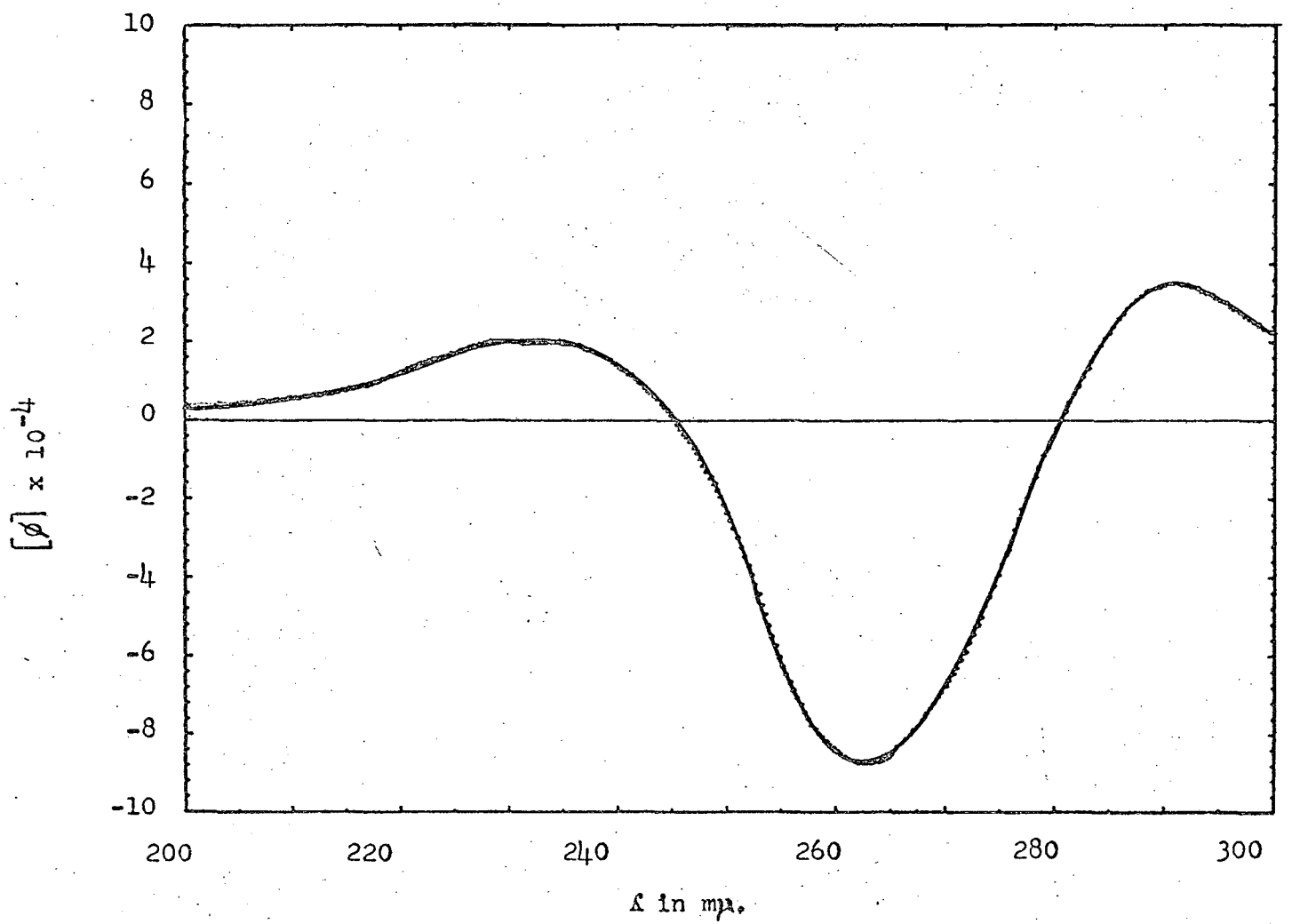

Figure III-28 UPG ROTATION VS. WAVELENGTH

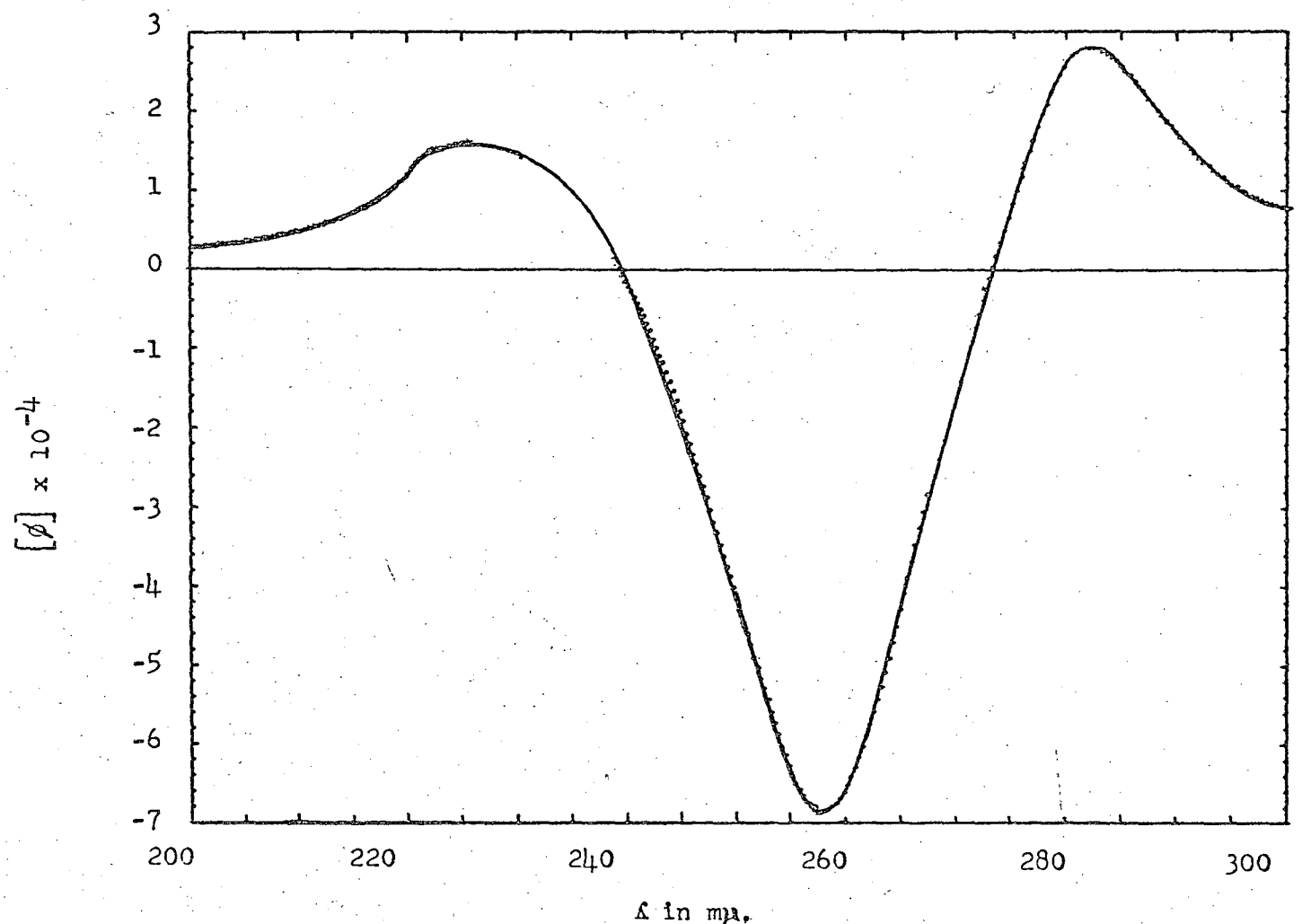

Figure III-29 GPU ROTATION VS. WAVELENGTH

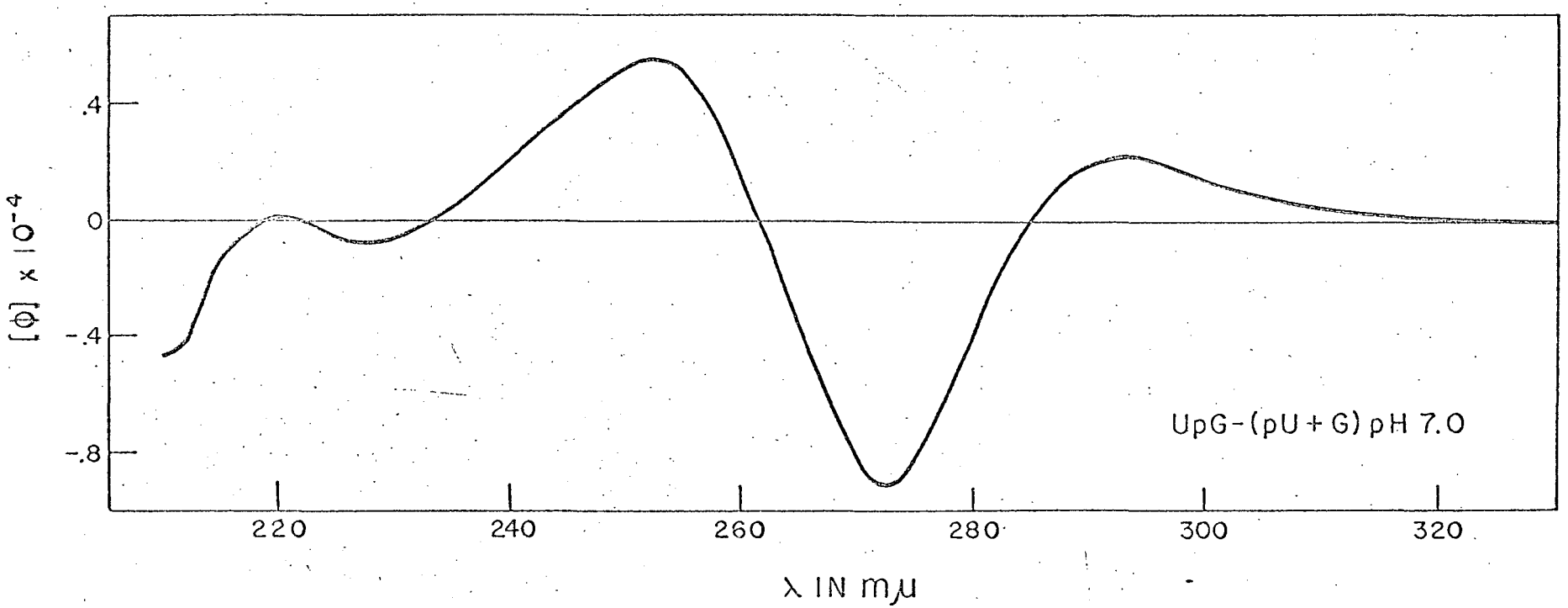

Figure III-30 Experimental ORD of UpG

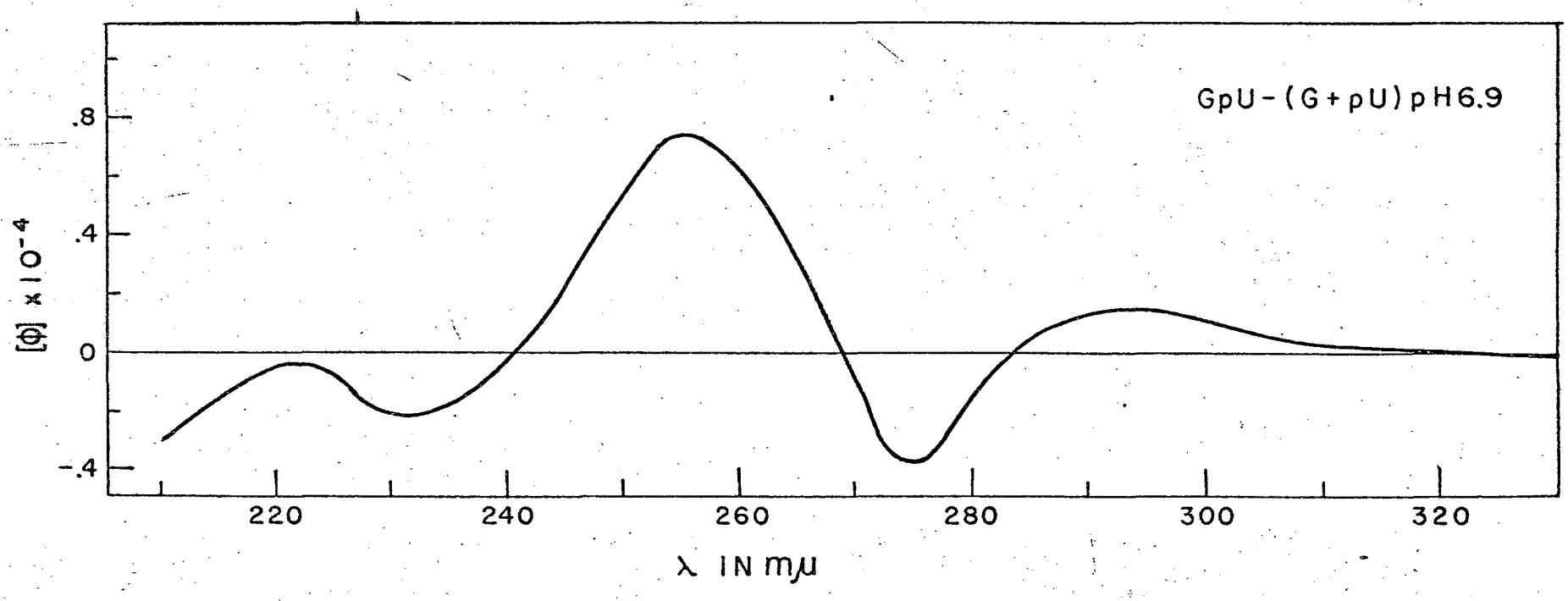

Figure III-31 Experimental ORD of GpU

In the case of UpC and CpU we have two pyrimidines with large monomer rotations. Therefore we expect that the electric dipole-magnetic dipole interaction may make a large contribution to the rotations of the dimer. The agreement of the calculated curves (Figs. III-32 and III-33) with Warshaw's experimental curves (Figs. III-34 and III-35) is not very good. On the other hand, our lack of knowledge of the transition moments in C is a likely source of the discrepancy. Our computed results for CpC do not show good agreement with experiment.

For the sequence isomers GpC and CpG, we have four absorption bands interacting and four separate terms with V_{12}'s and triple products to calculate. This means that we need to know four transition moment directions to calculate the rotations shown in Figs. III-(36) and III-(37). None of these four transition moment directions is known from experimental polarized spectra, so we are unsure of the validity of the computation. The experimental curve for GpC at pH 7 is shown in Fig. III-(38); CpG is not available for experiment. The experimental rotation is extremely small indicating that probably the proportion of stacked conformation at room temperature is extremely small. There is no real comparison of the experimental with the theoretical curve. If, however, we look at the curve for the experimental ORD of GpC at pH 1 from Warshaw's unpublished data (see Fig. III-38) we do see similarity to the computed ORD curve for GpC. We see a minimum near 289 mμ in both curves and a maximum at 260 mμ in the calculation, and at 265 mμ in the experimental curve. This is not simple to interpret since we would expect to find the bases protonated at this low pH and that the stacked conformation would not be favored. Also, the electronic properties might not be the same at pH 1 as at pH 7, the pH for which all our calculations have been made. Obviously there are chemical subtleties involved, and we need further experimental studies to understand

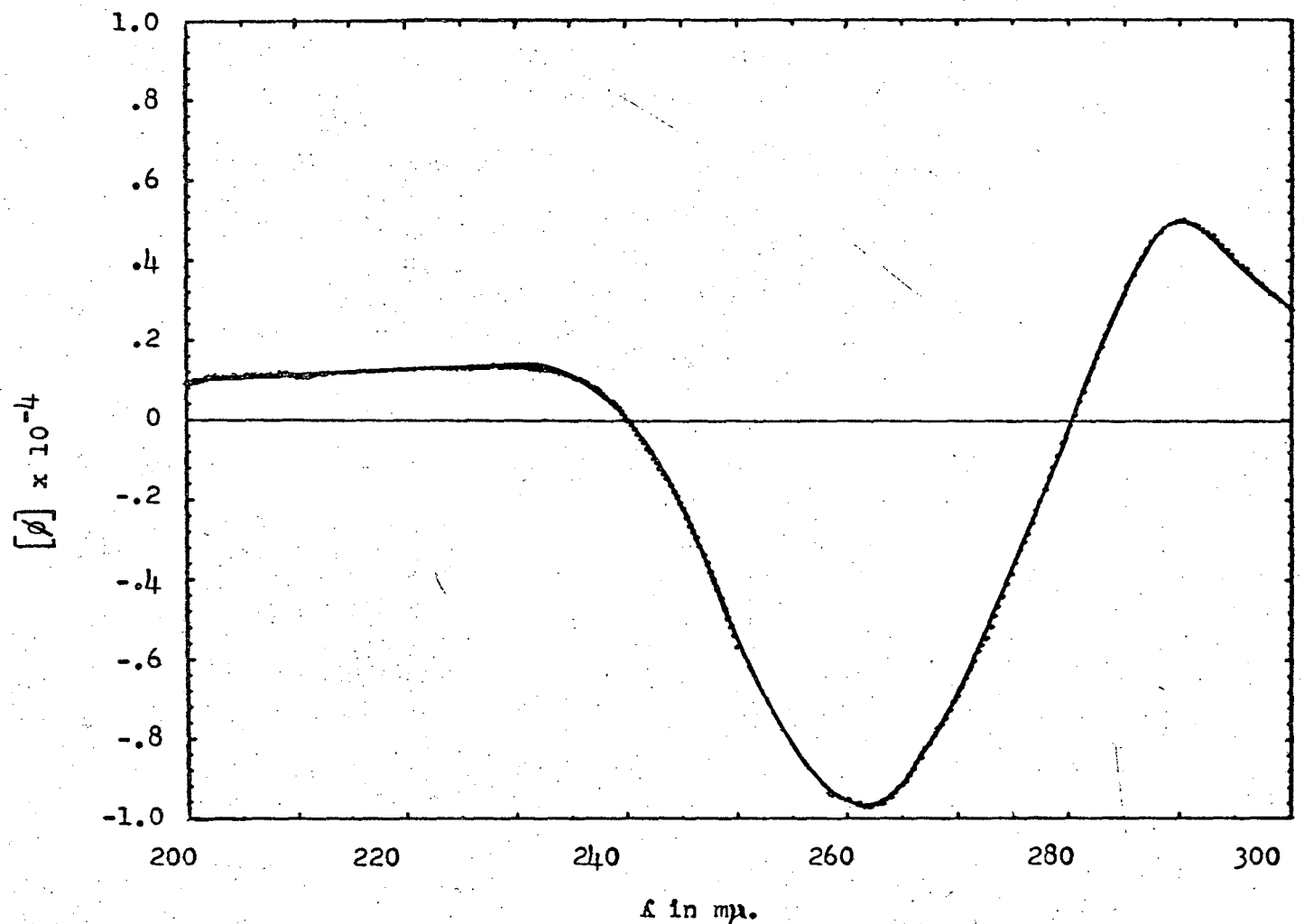

Figure III-32 UPC ROTATION VS. WAVELENGTH

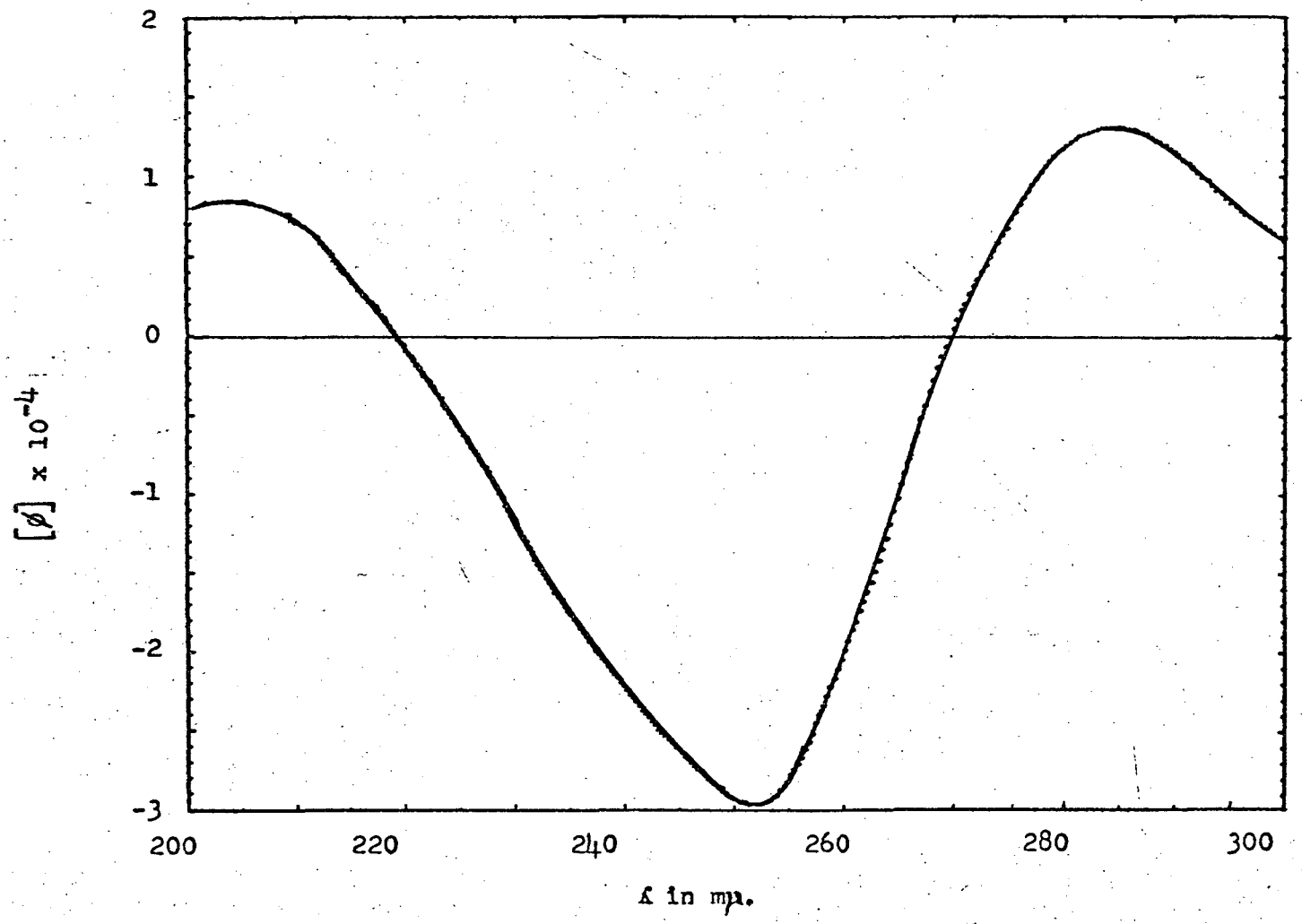

Figure III-33 CPU ROTATION VS. WAVELENGTH

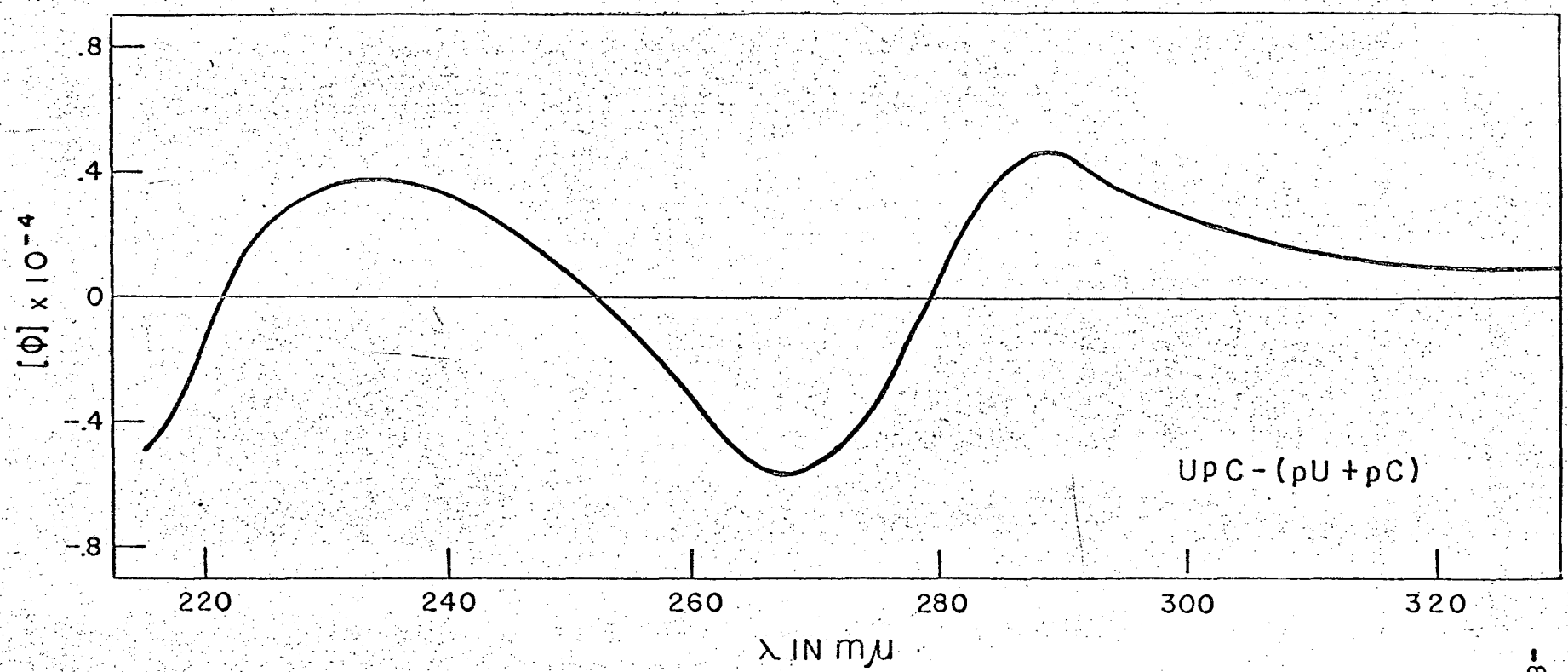

Figure III-34 Experimental ORD of UpC

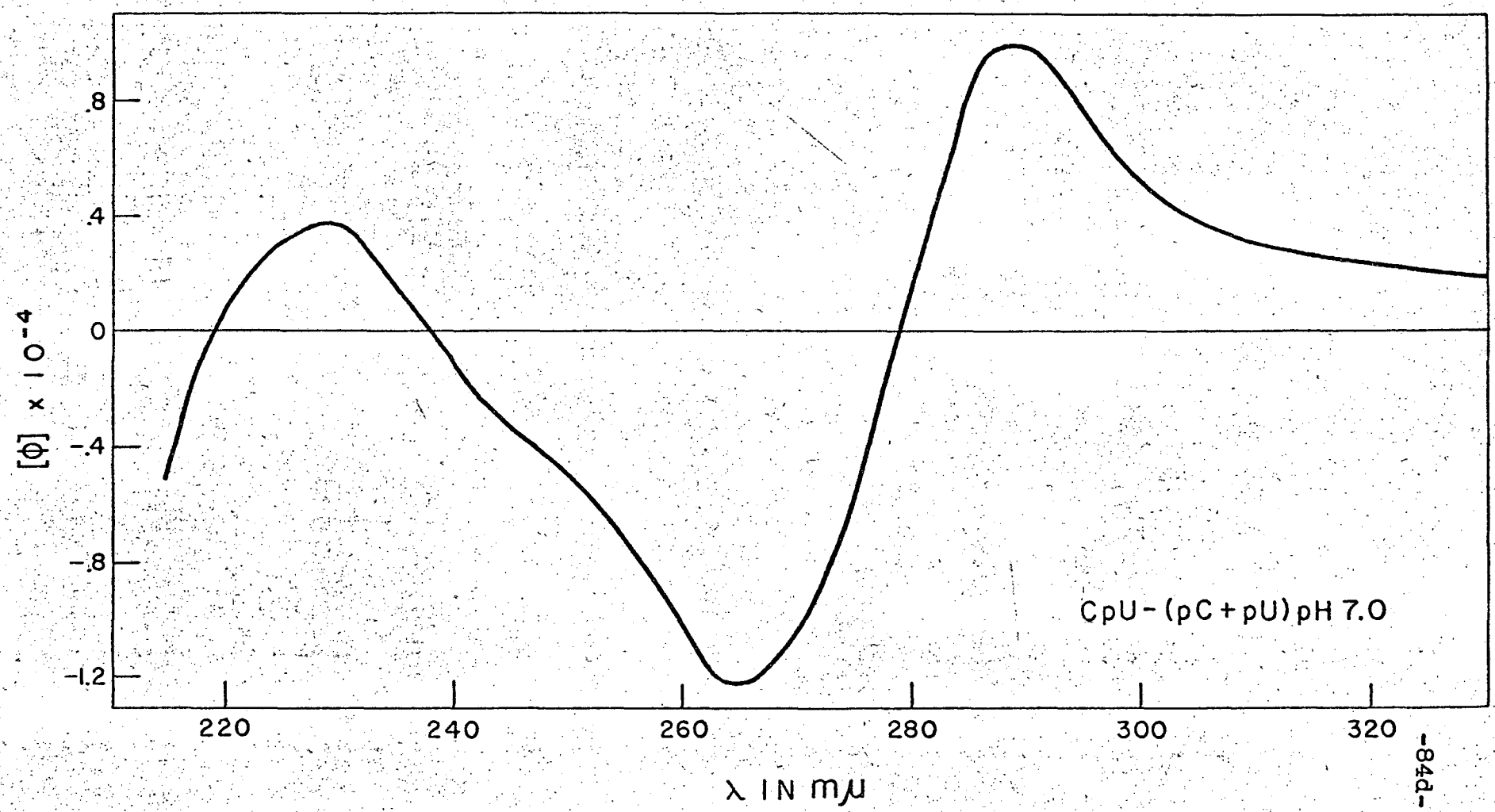

Figure III-35 Experimental ORD of CpU

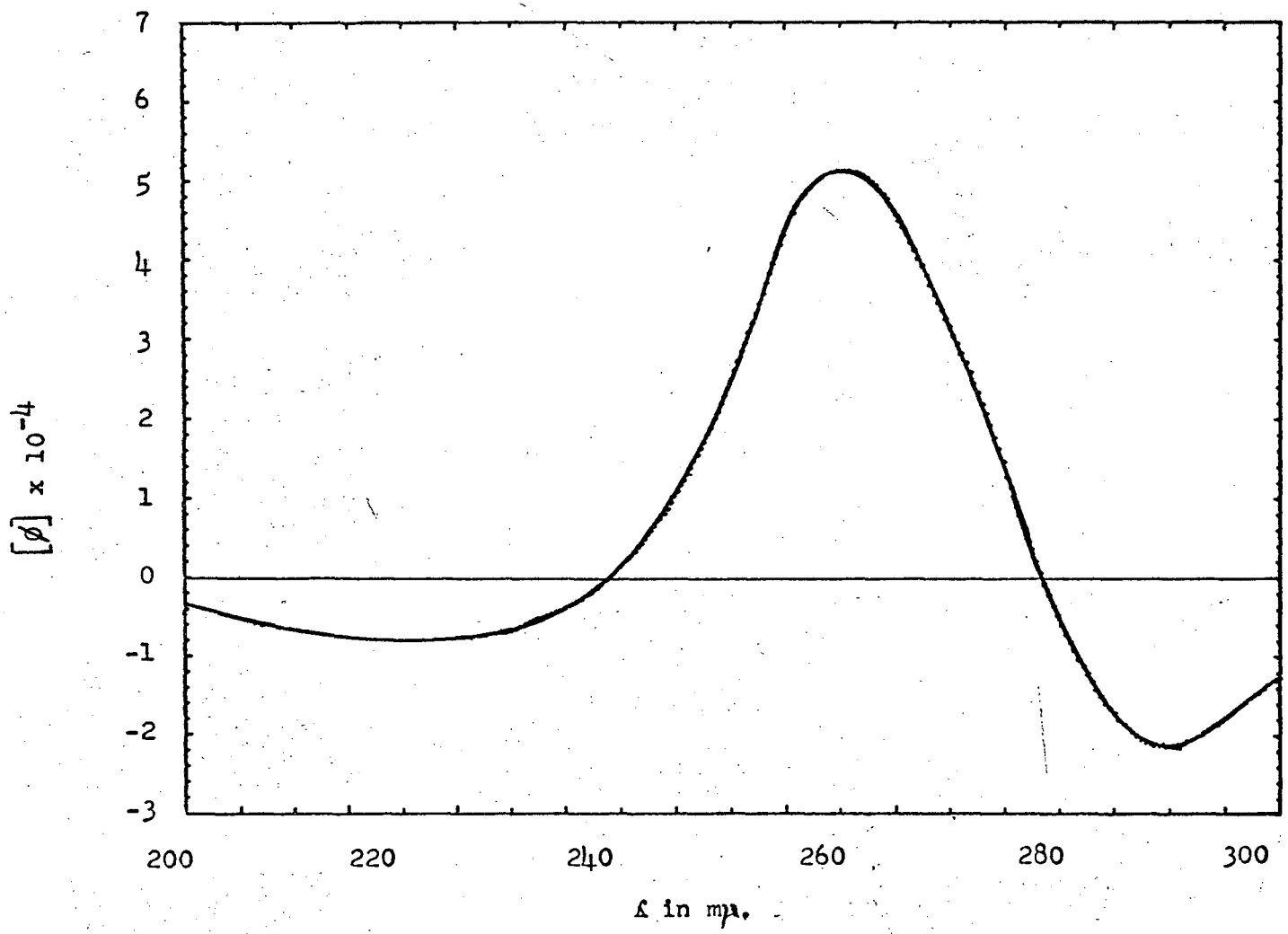

Figure III-36 GPC ROTATION VS. WAVELENGTH

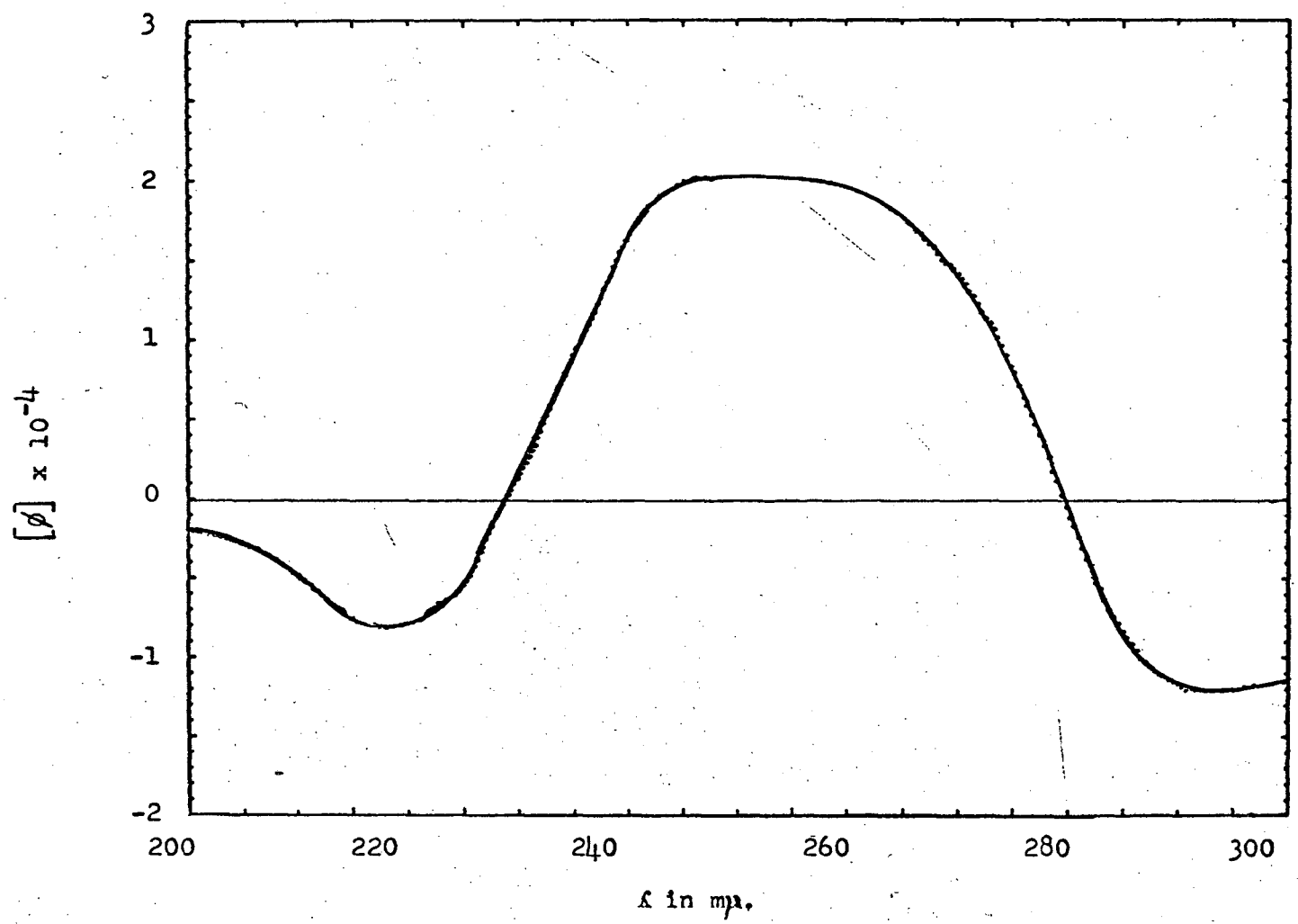

Figure III-37 CPG ROTATION VS. WAVELENGTH

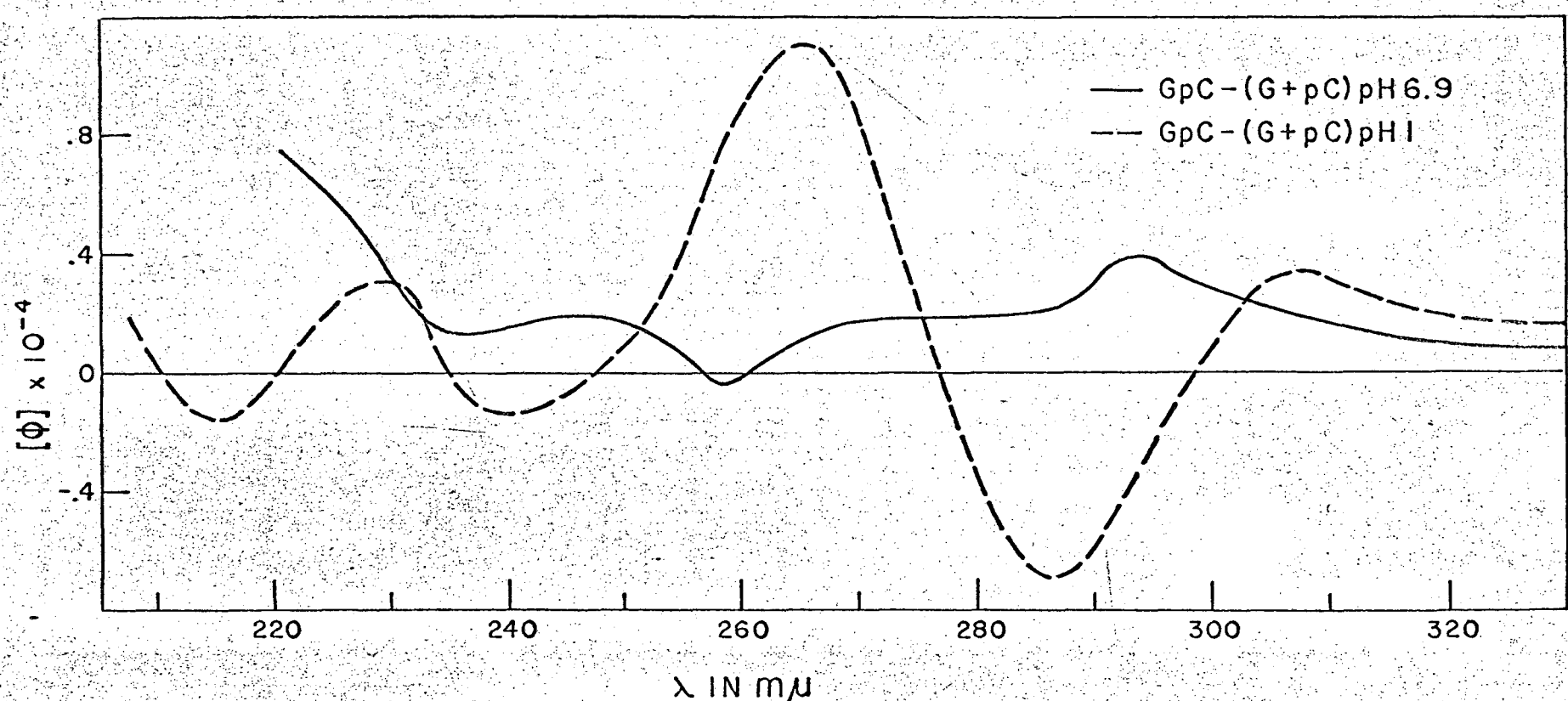

Figure III-38 Experimental ORD of GpC

the conformation of GpC at pH 1 and pH 7.

The agreement between the calculated curve and the experimental ORD at pH 1 leads us to suggest that perhaps there is some reason why the dimer is not stacked at pH 7, but that it is at pH 1. It may be that the bases have a charge at pH 7 and do not at pH 1. This would require a rather large shift of pK of the bases on dimerization, but remains a possibility. In order to properly compute ORD curves at pH's other than neutral, one should use the spectra at that pH as a starting point. The electronic properties at pH 1 might be quite different since the spectra differ considerably from the pH 7 spectra. It would be interesting to see the experimental curves for CpG at pH 7 and pH 1 to see whether similar effects arise in that case.

The remaining two dicnucleosides are homodimers; however, they are not so simple as are ApA and UpU. GpG and CpC contain contributions from both the degenerate and the non-degenerate terms of Eq. III-(21). For GpG (see Fig. III-39) we see that the non-degenerate part dominates the curve; it is not simply a sum of two curves of the ApA type. The fact that the curve is one with two minima and a central maximum indicates that the lowest wavelength rotational strength is negative. Because of the greatly different angles of the transition moments, the triple products for the non-degenerate terms are negative, giving rise to this ORD curve which looks like one for a left handed geometry, but which is in fact right handed with respect to the bases. The relative orientation of the two transition moments which give rise to the strong rotation is, of course, left handed in spite of the right handedness of the helix.

The calculated curve for CpC is shown in Fig. III-(40), and the experimental curve is shown in Fig. III-(41). In this calculated curve, we see contributions from both the non-degenerate and degenerate terms of Eq. III-

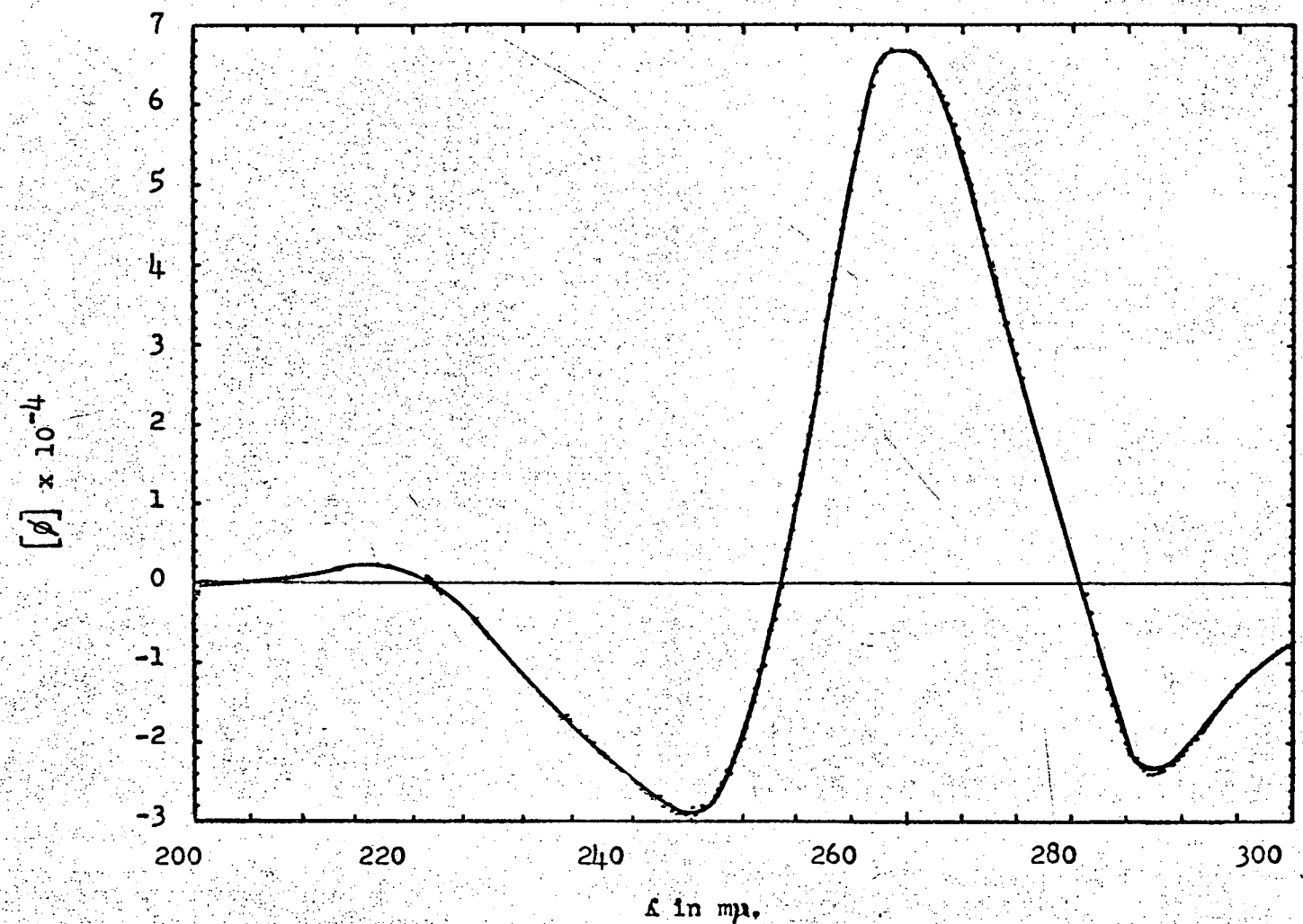

Figure III-39 GPG ROTATION VS. WAVELENGTH

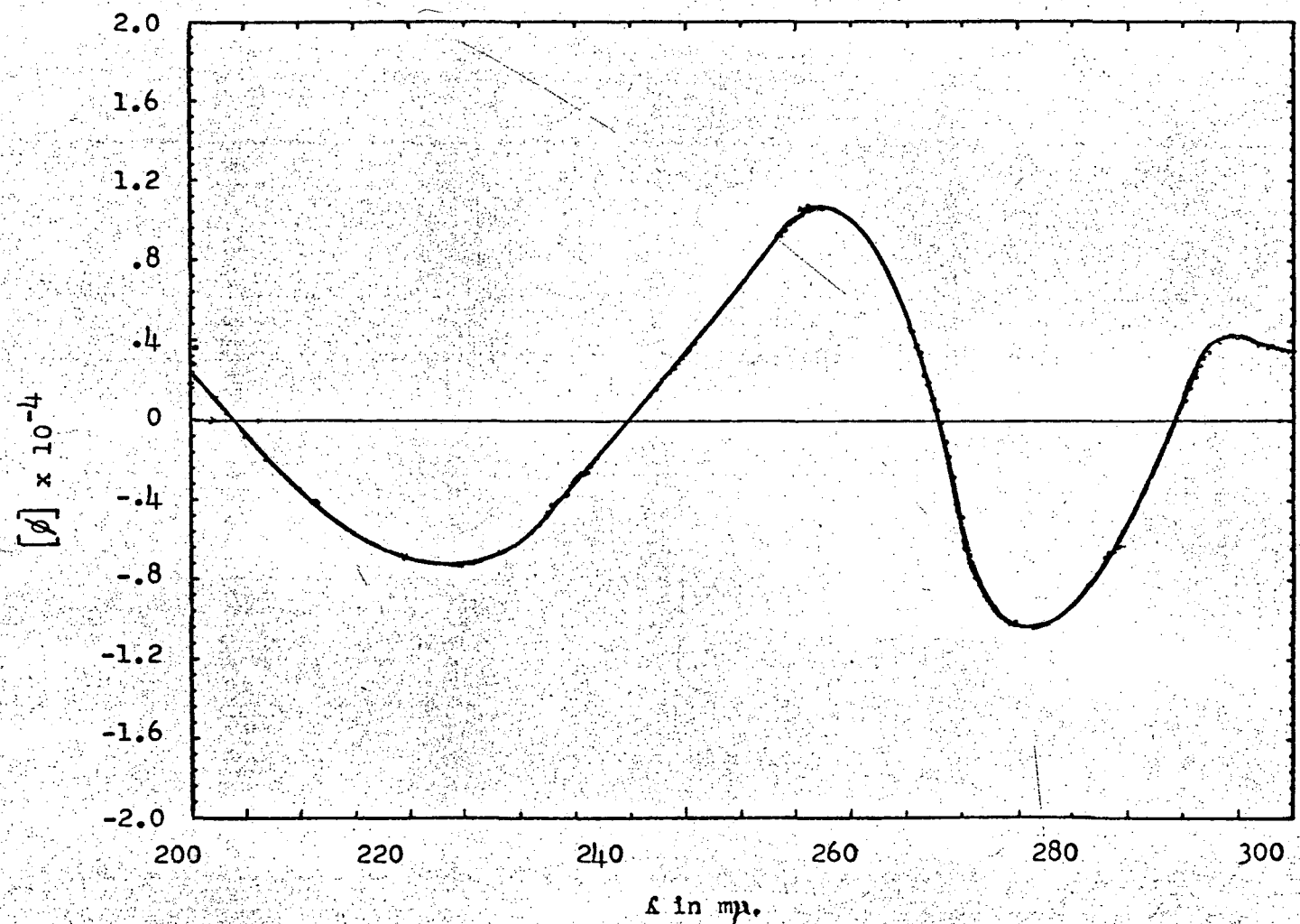

Figure III-40 CPC ROTATION VS. WAVELENGTH

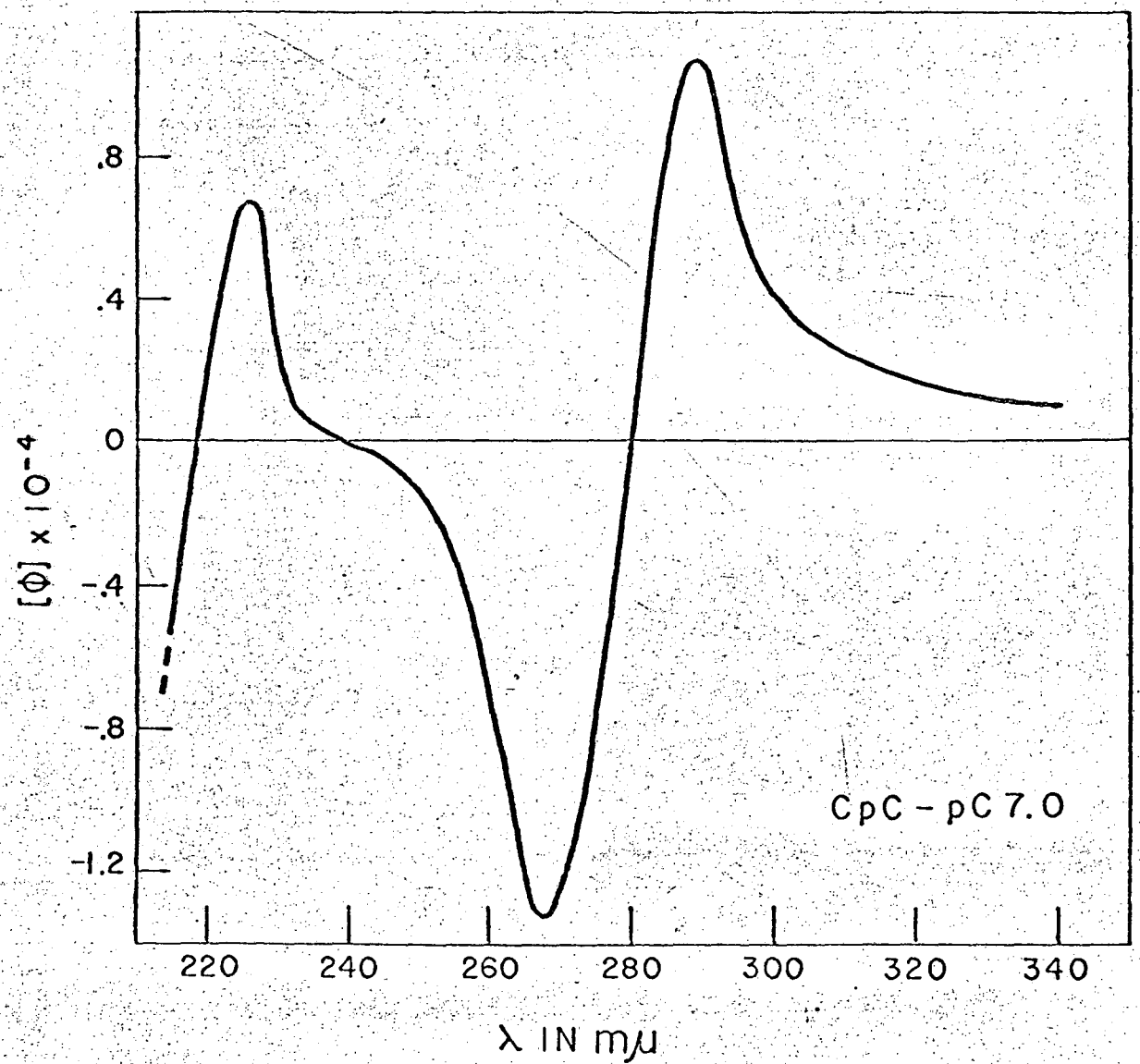

Figure III-41 Experimental ORD of CpC

(21), while the experimental curve looks actually simpler. The failure to get good agreement here is most likely due to wrong assumptions for the directions for the transition moments in the base, C. Rather small changes in the transitions (see Fig. III-11 and Table III-3) could increase the peak at 290 mμ and shift the minimum of the calculated curve from 275 mμ to 268 mμ. Unfortunately, we do not have any way of knowing what changes to make owing to our lack of knowledge of the transition moment directions.

Discussion

In Table III-(7) we give a summary of the experimental (pH 7) and calculated ($\gamma = 34.4°$) peaks, troughs and crossovers of the axis for the ORD curves. We can see that agreement of the calculated curves with experimental ones is best in the case of ApA (see Fig. III-15). In that case the stacked conformation seems to be present in good proportion at room temperature, the monomer rotation is small, we have good experimental information on the direction of the trnasition moment, and there is only one absorption band contributing to the rotation near 260 mμ. It is fortunate that this dinucleoside phosphate was the first available for experiment, since it illustrates the effect most vividly.

For UpU, the effect is calculated to be smaller, and hypochromism measurements indicate that the stacked conformation is probably less favored at room temperature (Tinoco and Warshaw, 1965). In addition, the monomer rotation is large. However, we do see reasonable agreement with experiment. This is encouraging; the monomer rotation does not seem to interfere too greatly, even though it is large.

For the simplest non-degenerate cases (ApU and UpA), we still have good experimental knowledge of the transition moment directions, and thus

Table III-(7)

Comparison of calculated and experimental peaks, troughs and crossings.

	Peak				Trough				Crossing	
	Calc. λ in mμ	Calc. $[\phi]x10^4$	Expt., pH 7 λ in mμ	Expt., pH 7 $[\phi]x10^4$	Calc. λ in mμ	Calc. $[\phi]x10^4$	Expt., pH 7 λ in mμ	Expt., pH 7 $[\phi]x10^4$	$\lambda_{calc.}$	$\lambda_{expt.}$
ApA	286	3.2	283	1.2	261	-7.2	261	-2.8	274	272
UpU	287	.27	286	.45	264	- .47	264	- .68	279	275
ApU	284	1.3	278	.54	267	-2.7	261	- .80	278	270
UpA	284	2.3	277	.11	267	-4.2	263	- .32	279	270
ApG	291	5.2	291	.32	264	-12.4	270	-1.3	281	283
GpA	281	4.9	277	.76	257	-12.8	253	- .62	271	265
ApC	290	1.8	285	.75	264	-4.0	265	-1.5	281	276
CpA	286	1.7	286	.44	252	-4.2	263	-1.64	269	277
UpG	291	3.6	293	.23	262	-8.6	273	- .9	281	285
GpU	282	2.8	293	.16	258	-6.8	275	- .38	273	283
UpC	290	.5	288	.45	262	- .98	267	- .66	280	280
CpU	284	1.3	288	1.0	252	-3.0	260	-2.05	270	277
GpC	260	5.2	294	.38	290	-2.1	259	- .05	278	261
CpG	264	2.0	-	-	292	-1.1	-	-	280	-
GpG	264	6.7	-	-	287	-2.3	-	-	281	-
CpC	294	.4	285	1.07	276	-1.04	264	-1.3	289	280

we get reasonable agreement with experiment. It is when we come to dimers with C or G in them that our lack of experimental polarized spectra becomes apparent. In some cases we do well, but there is enough uncertainty so we would be unable to assign sequence isomers solely on the basis of calculated rotation curves.

If experimental information on the polarized spectra of crystals of C and G or on electric dichroism were available, we could make a better choice of transitions for the calculation. If we had this information, it would be nice to recompute the molecular orbitals with adjustable parameters, such as core and resonance integrals, which are often chosen empirically. In this way, we could fit the experimental magnitude and direction of the transition moments and obtain MO's that would be excellent for computation of V_{12}'s.

It might be possible to use the ORD to fix the directions of the transition moments. To do this one would need to test various assumptions about the dipole moment direction by making rough calculations using the dipole approximation (Eq. III-2). In this way, one could find a consistent set of transition dipole moments that gave agreement with the experimental ORD curves.

A further way to improve our predictions of the shapes of the circular dichroism and consequently the ORD curves would be to take into account the vibronic interaction. This would lift the assumption that the monomer absorption band shape does not change in the dimer and would presumably improve the details of the curve shape.

An additional source of discrepancy with experiment which we have mentioned is the dropping of $\underset{\sim}{m}_{ao}$ in Eq. III-(10). Subtracting the rotation of the monomers accounts for part of this, but it does not correct for the terms $\underset{\sim}{m}_{1ao} \cdot \underset{\sim}{\mu}_{2oa}$ and $\underset{\sim}{m}_{2ao} \cdot \underset{\sim}{\mu}_{1oa}$. Estimates of these terms are

difficult to make since $\underset{\sim}{m}_{ao}$ is not directly accessible to experiment as is $\underset{\sim}{\mu}_{oa}$. The fact that the monomer rotation curves show the crossing-over of the cotton effect near the absorption peak (Yolles, 1964) indicates that the allowed $\pi-\pi^*$ transition is giving rise to the monomer cotton effect. Since we know $\underset{\sim}{\mu}_{oa}$, the monomer rotation allows us to estimate $\underset{\sim}{m}_{ao}$ in order of magnitude, but not in direction. A possible way of getting directions for magnetic transitions is the Faraday effect (see Chapter I). Hopefully, magnetic rotation experiments will be carried out on the bases, giving us a better understanding of the subtleties of the magnetic transitions to excited states in the ultraviolet.

Also necessary to a full understanding of the experimental spectra is a determination of just what proportion of the stacked form is present at room temperature. This will require extensive studies of the ORD at different temperatures and in solvents other than water at low ionic strength, in order to go to temperatures below 0°C. Also, studies at different pH may be able to explain certain mysteries such as GpC, where the rotation is small at pH 7 and large at pH 1, the reverse of what would be expected from the pK's. We hope that the present calculations may be of some assistance in understanding the ORD of the dinucleosides under various experimental conditions.

One thinks of various ways of extending the present calculation to other systems. Calculations for the trimer would be especially easy. The model of Fig. III-(7) implies directly that one need only extend the geometry to compute the triple products and the V_{12}'s in order to calculate the rotational strength arising from the interaction of the next nearest neighbors. This would provide a small correction to the nearest neighbor calculation of the trimer ORD.

Also, we have included only the commonly occurring RNA bases in this calculation. In some RNA's, especially s-RNA, there are several other bases found. These include pseudo-uracil, di-hydro uracil, hypoxanthine, N,N-dimethyl guanine, and N-methyl adenine. In order to include these and other "strange" bases, one would need to do MO calculations in order to determine transition moment directions. In addition, there is a well known dinucleotide, nicotinamide-adenine dinucleotide (NAD) whose ORD has not been reported in the absorption region. One could surely extend the calculation to this compound.

One might also notice that the model of Fig. III-(7) could also serve as the computational basis for the ORD of intercalated structures. Such a structure was recently proposed by Ohnishi and McConnel (1965) for chlorpromazine in DNA. If the same intercalation occurred in RNA or poly A at pH 7, we could calculate the ORD from a model like Fig. III-(7). The fact that adjacent rings are not connected by ribose phosphates would not affect the calculation.

RNA in solution is probably composed partly of single stacks of the type found in poly A at neutral pH and partly of "hairpin loops" in which the strand is folded back on itself and stabilized by hydrogen bonds (Spirin, 1964). We have computed the ORD for the first conformation but not for the hydrogen bonded one. One could extend the calculation to include hydrogen bonded forms by taking one base plane to be actually a hydrogen bonded base pair. As a simple model to test computations of the double stranded or hydrogen bonded conformation, one could choose poly A plus poly U, which forms a hydrogen bonded double strand under appropriate conditions.

One can see that calculations of the type we have carried out here can lead to a better understanding of the ORD of polynucleotides in solution. Moreover, ORD is a powerful analytical tool if it can be interpreted. ORD is sensitive to the amount and type of three dimensional structure of polynucleotides and it can be used in solution, rather than necessitating the use of crystals or fibers.

References

P. Callis, E. J. Rosa and W. T. Simpson (1964) J. Am. Chem. Soc. 86, 2292.

P. Callis (1965) private communication.

C. Djerassi (1960) Optical Rotatory Dispersion, McGraw-Hill Co., New York.

H. Eyring, J. Walter and G. E. Kimball (1944) Quantum Chemistry, John Wiley and Co., New York., p. 111.

J. R. Fresco and E. Klemperer (1959) Ann. N. Y. Acad. Sci. 81, 730.

J. R. Fresco (1959) J. Mol. Biol. 1, 106.

A. Gierier (1957) Nature 179, 297.

A. E. V. Haschemeyer and A. Rich (1965) to be published.

D. N. Holcomb and I. Tinoco, Jr., (1965) Biopolymers 3, 121.

R. Langridge, D. A. Marvin, W. E. Seeds, H. R. Wilson, C. W. Hooper, M. H. F. Wilkins, and L. D. Hamilton (1960) J. Mol. Biol. 2, 38.

B. Lohmander and S. Rittsten (1958) Kungl. Fys. Sallsk i Lund., Forh. 28, 45.

V. Luzatti, A. Mathis, and F. Masson (1965) J. Mol. Biol., In press.

W. Moffitt (1956) J. Chem. Phys. 25, 467.

W. Moffitt and A. Moscowitz (1959) J. Chem. Phys. 30, 648.

A. Moscowitz (1957) Thesis. Harvard University.

A. Moscowitz (1960) Chapt. 12 in Optical Rotatory Dispersion by C. Djerassi, McGraw-Hill Co., New York.

R. K. Nesbet (1964) Biopolymers Symposia 1, 129.

S. Ohnishi and N. M. McConnell (1965) J. Am. Chem. Soc. 87, 2293.

Pabst Laboratories (1956) Circular OR-10. Pabst Laboratories, 1037 West McKinley Ave., Milwaukee, Wisconsin.

L. Rosenfeld (1928) Zeits. Physik 52, 161.

A. Rich, D. R. Davies, F. H. C. Crick and J. D. Watson (1961) J. Mol. Biol. 3, 71.

A. S. Spirin (1964) Macromolecular Structure of Ribonucleic Acids, translated by J. A. Stekol, Reinhold Publ. Co., New York.

J. A. Schellman and P. Oriel (1962) J. Chem. Phys. 37, 114.

R. F. Stewart and L. H. Jensen (1964) J. Chem. Phys. 40, 2071.

R. F. Stewart and N. Davidson (1964) Biopolymers Symposia 1, 465.

I. Tinoco, Jr., R. W. Woody and D. F. Bradley (1963) J. Chem. Phys. 38, 1317.

I. Tinoco, Jr. (1963) Radiation Research 20, 133.

I. Tinoco, Jr. (1962) Adv. Chem. Phys. 4, 113.

P. O. Ts'o, G. K. Helmkamp and C. Sander (1962) Proc. Nat. Acad. Sci. U. S. 48, 686.

K. E. VanHolde, J. Brahms and A. M. Michelson (1965) J. Mol. Biol., In press.

A. Viellard and B. Pullman (1963) J. Theoret. Biol. 4, 37.

M. M. Warshaw, C. A. Bush and I. Tinoco, Jr. (1965) Biochem. Biophys. Res. Comm. 18, 633.

M. M. Warshaw and I. Tinoco, Jr. (1965) J. Mol. Biol., In press.

R. S. Yolles (1964) private communication.

ACKNOWLEDGMENTS

We are deeply indebted to Professor Ignacio Tinoco, Jr., who directed this research. More than a research director, he has been a fine teacher and excellent friend. We would also like to thank Mr. Myron Warshaw, Mr. Charles Cantor, and Dr. Marcos Maestre for helpful discussions in interpreting the present work.

We also express our gratitude to Dr. Howard DeVoe of NIH for making available to us the transition monopoles used in the calculations of Chapter III. We are especially indebted to Mr. Myron Warshaw for providing us with his unpublished experimental ORD curves of dinucleoside phosphates, which we quoted in Chapter III.

APPENDIX A

Listing of Programs

There are three programs used to compute the rotations. The first is called MONOPOL, which computes $V_{1a;2b}$ as a function of γ from the monopoles. On the print-out, one sees all the interactions, in units of electronic charge and Å, grouped by angle. The subroutine, SORT, groups them by interaction and punches V_{12} in units of cm^{-1}.

One gets punched-card output, which is used in the DIMEROT program. ROTCUR fits the experimental absorption curves to gaussians and computes the magnitude of the transition dipole moment. This punches cards which are used as input to DIMEROT. The last program, DIMEROT, computes rotational strengths for each value of helix increment angle, γ, then constructs the CD curve from the gaussian absorptions and does the Kronig-Kramers transform to the ORD. The printed output contains one ORD point every ten (i.e., every 500 cm^{-1} in our present study), while the binary output has every point. The binary output tape is rewound and the turning points of the ORD curves are found. The binary tape is again rewound and selected ORD curves are plotted versus wavelength.

We also mention the subroutine IOSET, which is used in many of the routines to set the input and output units. This subroutine simply assigns values in the labeled common block, IOPOOL. Therefore, it is called before any input or output can be accomplished. In MONOPOL, for example, the unit NI (=2) is the card reader, NO (=3) is the printed output, NK (=11) is used for output to the sorting routine, SORT. NP is not used in the present form. The unit numbers specified in parentheses are appropriate for the IBM 7094 at LRL, Berkeley, as may be seen from the user's manual at the LRL computer center.

The input cards for MONOPOL specify the monopoles (in units of electronic charge) and the monopole cylindrical coordinates (see Figs. III-7 to III-11). A group is taken to be a transition in a base, so that one computes interactions (V_{12}'s) between groups. The input cards are as follows:

1. Title of the problem (one card).
2. GMINCR, ZINCR, NL, NG, NGI, NGJ (one card).

   GMINCR is the smallest value of helix increment angle in radians (=01 in this study)(floating pt., 8 cols.).

   ZINCR is the helix distance increment in Å (3.4 Å used in this study)(floating pt., 8 cols.).

   NL is the number of levels. Use 1 for nearest neighbor, 2 for next nearest neighbor, etc. (=1 in this study)(fixed pt., 4 cols.).

   NG is the number of groups (=6) in the present study)(fixed pt., 4 cols.).

   NGI is the last group used for I (=6) in the present study) (fixed pt., 4 cols.).

   NGJ is the first group used for J (=1 in the present study) (fixed pt., 4 cols.).
3. N,F (one card).

   N is the number of monopoles (fixed pt., 2 cols.).

   F is the factor for scaling the monopoles ($=\mu_{exp}/\mu_{calc}$)(floating pt., 5 cols.).
4. and following cards containing the monopole cylindrical coordinates and transition monopoles, 2 per card.

   A, radius in Å (floating pt., 8 cols.).

   Gamma, angle in degrees (floating pt., 8 cols.).

Z in Å (floating pt., 8 cols.).

RHO the transition monopoles, unscaled (floating pt., 12 cols.).

Repeat 3 and 4 for all groups. One blank card at end terminates the program.

The program computes all interactions of groups for the I,J interactions specified by NGI and NGJ and then increments the angle GMINCR by .1 radian and recomputes all interactions until GMINCR = .7 rad or 40.1°. Then SORT is called. This explicitly uses unit 11 (NK in MONOPOL) as input. It sorts the interactions (V_{12}'s) by interaction and putputs on unit 14. The output from unit 14 must be punched into BCD cards, and is then sorted for input to the rotation program, DIMEROT. (Unit 14 is the normal punched output unit at LRL). The way one uses these cards depends on the model one is calculating. In the present study, 6 groups were used, one each for the transitions of A and U and two each for the transitions of G and C. For dimers, we need only the ±1 interactions so we set NL=1. If we number the groups 1 through 6 in the order they are given in Table III-(4), it may be seen that the I=1, J=1 interaction is the one for ApA. The +1 and -1 levels are identical because there is no sequence dependence. The I=1, J=2 interaction is for A and U. The +1 level gives the interaction for the upper pair of bases in Fig. III-(7) (UpA) and the -1 level gives the interaction of the lower pair of bases in Fig. III-(7) (ApU). In this way we are able to construct Table III-(4).

For the curve fitting to the sum of gaussians, the program ROTCUR is used. We are indebted to Dr. I. Tinoco, Jr., who wrote this program. This program calls MATINV to solve the linear equations, and this subroutine is also listed. The input cards for ROTCUR are as follows:

1 1. N, START, STOP, DELTA, FACT, SPACE, WIDTH, CMOLS

N is N is an integer greater than zero (fixed pt., 5 cols.).

START is the smallest wavelength used for absorption data in mμ (floating pt., 10 cols.).

STOP is the largest wavelength used for absorption data (floating pt., 10 cols)

DELTA is the spacing between the experimental absorption points in mμ (floating pt., 10 cols.)

FACT should be set equal to .1 for internal setup of the gaussians. If it is desired to use gaussians of irregular spacing and width, this should be set =0, and the gaussian position and width put in explicitly on cards.

SPACE is the spacing in cm^{-1} between gaussians (=500 in this study)(floating pt., 10 cols.)

WIDTH is the half width of the gaussians (=700 cm^{-1} in this study)(floating pt., 10 cols.)

CMOLS is the molarity of the solution whose OD is to be fitted. This is necessary in finding the dipole strength (floating pt., 10 cols.)

2. and following cards containing the absorptions from the lowest wavelength (START) to the highest (STOP), every DELTA mμ (floating pt., 10 cols.)and 7 values per card).

The last program, OIMEROT, used the V_{12}'s to compute rotational strengths and the gaussian curves to compute CD and ORD. The control program MAIN first calls ROTS. NI (=2) is again used for the card reader and NO (=3) is the printed output. NK (=35) is the binary output which contains all the rotations and circular dichroisms. NP is first used for a

BCD scratch (=11) to record rotational strengths and is then reassigned (as 15) by MAIN as an output from SELECT, which will be described.

The input cards for this program fall into groups according to which routine reads them. They will be discussed in such groups, and are to be loaded in the order described. The first group of cards is read by ROTS, and are the ones necessary to the rotational strengths.

1. Title for the dimer (one card).
2. Z, RAD1, RAD2, GMINCD, NCASE (one card).

   Z is the helix distance increment in Å (=3.4 in this study) (floating pt., 5 cols.)

   RAD1, RAD2 are the distances in Å from the helix axis to the center of the base (see Figs. III-8 to III-11) for monomer one and monomer two. 1 is 3' linked, and 2 is 5' linked (floating pt., 5 cols. each)

   GMINCD is the first value of helix increment angle in degrees (floating pt., 5 cols.)

   NCASE is a fixed pt. number (2 cols.) which tells which kinds of interaction are to be calculated.

   =1 for degenerate term only (ApA and UpU)

   =2 for non-degenerate term, one band each monomer (ApU, UpA)

   =3 for non-degenerate terms, one band for one monomer and two bands in the other (ApG, GpA, ApC, CpA, UpG, GpU, UpC, CpU)

   =4 for non-degenerate terms, two bands each monomer (GpC, CpG)

   =5 for both degenerate and non-degenerate terms (GpG, CpC)
3. and following cards describing the transitions FNU, DMU, GAM, V12

   FMU is transition frequency in cm^{-1} (floating pt., 10 cols.)

   DMU is the transition moment in Debye units (floating pt., 10 cols.)

GAM is the angle of the transition moment in degrees (see Table III-1) (floating pt., 10 cols.)

V12 in cm^{-1} for the first helix angle (floating pt., 10 cols.)

4. Output cards from MONOPOL containing V12 and helix increment angles. Repeat from title (card 1) for each dimer.

Two blank cards signal the end of this rotational strength calculation. Transfer goes to ROTEM which computes the CD and ORD curves from the rotational strengths and the gaussian curves of the absorption. The routine XFIL loads the table of values of the Dawson integral needed for Eq. III-(34) taken from Romander and Rittsten (1958). The data cards for ROTEM are:

1. N, START, STOP, DELTA, NB (one card).

N = positive number (fixed point, 5 cols.)

START is the lowest frequency used to compute the K-K transform in cm^{-1} (floating pt., 10 cols.)(=33, 333 in this study).

STOP is the highest frequency (floating pt., 10 cols.) (=50,000 in this study).

DELTA is the interval in cm^{-1}. The rotation and CD will be computed every DELTA cm^{-1} between START and STOP. (floating pt., 10 cols.)(=50 cm^{-1} in this study).

NB is the number of bands in the dimer (fixed pt., 5 cols.)

2. There follows one card for each dimer band containing NG, CMOLS, PEEK.

NG is the number of gaussian making up the band (fixed pt., 5 cols.)

CMOLS is the concentration in mols/liter of the solution whose absorption band was fitted (floating pt., 10 cols.)

PEEK is the peak frequency of the band in cm^{-1} (floating pt., 10 cols.)

3. After these cards come the gaussians for the bands, 2 per card. These are punched in correct format by ROTCUR. FNU, E, THETA.

   FNU is frequency in cm^{-1}

   E is amplitude of gaussian

   THETA is the half width in cm^{-1} (all floating pt., 10 cols.)

Repeat from card 1 for each dimer. The printout contains one point for the transform in every ten. All the points are on the binary tape (NK). A card like the first, with 0 for the value of N, stops the program and transfers to CHOOSE which examines the curves and finds maxima and mimina. This routine reads no cards but calls the cal comp plot routine, PLODO, which reads one card per plot as a title. So, for each dimer, put in three title cards, for the rotation at the first, seocnd and third turning point as a function of the helix angle, γ.

The last routine SELEK is called to plot rotation versus wavelength for selected values of helix increment angle, γ. It reads cards to select which curves to plot.

1. JMAX, KPUO

   JMAX is the number of dimers computed (fixed pt., 5 cols.)

   KPUO =1 for BCD output of selected curves ORD and CD on NP

   =0 for no output.

2. One card for each dimer, specifying which curves to plot (fixed pt., 2 cols.) For example:

   010518 would specify plotting for curve 1, curve 5, and curve 18. All others would be ignored.

3. After all specification cards, one title card for each graph to be plotted in the order selected.

This completes the data check.

```
MONPOL MONPOL                                                          04/
          EXTERNAL FORMULA NUMBER  -  SOURCE STATEMENT  -  INTERNAL

C  THIS WAS USED TO COMPUTE V12 FOR THE DEC 64 ROTATION CALCNS
C  NK IS USED FOR SECOND OUTPUT AND NP IS USED FOR SCRATCH
CMONPOL COMPUTE MONOPOLE-MONOPOLE INTERACTIONS                          MC
C       DEVOE, 1228IA.  PROGRAM FOR MONOPOLE-MONOPOLE INTERACTION.      MC
        DIMENSION TITLE(12), NC(24),
     1            ZMU(24), GAMMU(24), XYMU(24), VALMU(24)
        COMMON /IOPOOL/NI,NO,NK,NP
        COMMON /POLES/ A(24,12),GAMMA(24,12),Z(24,12),RHO(24,12),NPOLE(24)
        CALL IOSET
   91   READ(NI,101)TITLE,GMINCR,ZINCR, NL, NG, NGI, NGJ

        IF (GMINCR) 27,99,27
   27   CONTINUE
        WRITE(NO,103) TITLE
        DO 50 I = 1, NG                                                 MO
        READ(NI,102) N,F,(A(I,K),GAMMA(I,K),Z(I,K),RHO(I,K),K=1,N)

        NPOLE(I)=N
C       INSERT FOR CONVERTING PHI TO RADIANS FROM DEGREES AND SCALING RHO
        DO 26 K=1,N
        RHO(I,K)=RHO(I,K)*F
   26   GAMMA(I,K)=GAMMA(I,K)/57.2958
C       END INSERT
        NC(I) = N                                                       MO
C       COMPUTE COMPONENTS ETC. OF DIPOLES AT ZERO LEVEL.               MO
        XMU = 0.0                                                       MO
        YMU = 0.0                                                       MO
        ZMU(I) = 0.0                                                    MO
        DO 25 K = 1, N                                                  MO
        XMU = XMU-A(I,K)*RHO(I,K)*COS(GAMMA(I,K))                       MO
        YMU = YMU-A(I,K)*RHO(I,K)*SIN(GAMMA(I,K))                       MO
   25   ZMU(I) = ZMU(I)-Z(I,K)*RHO(I,K)                                 MO
        GAMMU(I) = ATAN(YMU/XMU)                                        MO
        IF (XMU) 30, 35, 40                                             MO
   30   GAMMU(I) = GAMMU(I) + 3.1415927                                 MO
        GO TO 40                                                        MO
   35   IF (YMU) 36, 38, 38                                             MO
   36   GAMMU(I) = -1.5707963                                           MO
        GO TO 40                                                        MO
   38   GAMMU(I) = 1.5707963                                            MO
        GO TO 40                                                        MO
   40   XYMU(I) = SQRT(XMU**2 + YMU**2)                                 MO
        VALMU(I) = SQRT(XMU**2 + YMU**2 + ZMU(I)**2)                    MO
   50   WRITE(NO,104)I,VALMU(I),GAMMU(I), ZMU(I), XYMU(I)               MO
C       COMPUTE INTERACTION ENERGIES AND DIPOLE DOT PRODUCTS.           MO
   80   GMINCR=GMINCR+.1
        GMINCD=GMINCR*57.2958
        WRITE(NO,111) GMINCD
  111   FORMAT (17H1GAMMA INCREMENT=,F6.1,7HDEGREES)
        N21 = 2*NL+1                                                    MO
        DO 100 I = 1, NGI                                               MO
        MAX = MAX0(I,NGJ)                                               MO
        DO 100 J = MAX,NG                                               MO
        VALMUP= VALMU(I)*VALMU(J)                                       MO
        WRITE(NO,105)I,J,VALMUP
```

```
MONPOL MONPOL                                                          04/2
      EXTERNAL FORMULA NUMBER   -   SOURCE STATEMENT   -   INTERNAL F

      NCI = NC(I)                                                       MON
      NCJ = NC(J)                                                       MON
      TOTV = 0.0                                                        MON
      TOTVDP = 0.0                                                      MON
      RTN=0.                                                            M/N
      DO 75 L = 1, N21                                                  MON
      EL = L-NL-1                                                       MON
      LE = EL                                                           MON
      DELGAM = EL*GMINCR                                                MON
      DELZ = EL*ZINCR                                                   MON
      V = 0.0                                                           MON
      IF (LE) 92,75,92
   92 CONTINUE
      DO 60 K = 1, NCI                                                  MON
      DO 60 M = 1, NCJ                                                  MON
   60 V = V + RHO(I,K)*RHO(J,M) / SQRT(A(I,K)**2+A(J,M)**2-2.0*A(I,K)*  MON
     1A(J,M)*COS(GAMMA(J,M)+DELGAM-GAMMA(I,K))+(Z(I,K)-Z(J,M)+DELZ)**2)
      DPMU = XYMU(I)*XYMU(J)*COS(GAMMU(J)+DELGAM-GAMMU(I))+ZMU(I)*      MON
     1ZMU(J)                                                            MON
      VDPMU = V*DPMU                                                    MON
      IF (LE) 65, 75, 65                                                MON
   65 TOTV = TOTV + V                                                   MON
      TOTVDP = TOTVDP + VDPMU                                           MON
      LEABS=ABS(LE)
      IF(LEABS) 75,74,75
   74 VCM=V*116000.
      GD1=GMINCR*57.2958
      WRITE (NK,112)VCM,LE,I,J,GD1
  112 FORMAT (F10.2,I10,10X,I2,1H,,I2,F20.4)
   75 WRITE(NO,106)LE,V,DPMU,VDPMU
  100 WRITE (NO,107) TOTV,TOTVDP
      IF (GMINCR- .6) 80,80,81
   81 CONTINUE
      WRITE(NO,108)GMINCR,ZINCR,NL,NG,NGI,NGJ                           MON
      DO 41 I=1,NG                                                      MON
   41 WRITE(NO,109)(A(I,K),GAMMA(I,K),Z(I,K),RHO(I,K),K=1,11)

  101 FORMAT (12A6/2F8.5, 4I4)                                          MON
  102 FORMAT(I2,F5.0/  2(F8.2,F8.3,F8.2,F12.6))
  103 FORMAT (1H1,24X,12A6/1H0/1H ,38X,10HABS. VALUE,18X,7HZ COMP.,6X,13MON
     1HPROJECTION OF/1H ,28X,5HGROUP,8X,5HOF MU,8X,5HGAMMA,8X,5HOF MU,7XMON
     2,14HMU IN XY PLANE)                                               MON
  104 FORMAT (1H ,30X,I2,F15.5,F13.4,F14.5,F15.4)                       MON
  105 FORMAT (1H0/1H ,29X,14HGROUPS I, J = ,I2,2H, ,I2,18H.  MU(I) X MU(MON
     1J) =,F9.5/1H ,29X,8HLEVEL OF/1H ,30X,7HGROUP J,8X,6HV(I,J),7X,15HMMON
     2U(I) DOT MU(J),3X,15HV X DOT PRODUCT)                             MON
  106 FORMAT (1H ,33X,I3,1X,3E18.6)                                     MON
  107 FORMAT (1H ,29X,45HTOTALS EXCLUDING ZERO LEVEL OF GROUP J -  V =, MON
     1E14.6/1H ,57X,17HV X DOT PRODUCT =,E14.6)                         MON
  108 FORMAT(1H1,20X,4HDATA/2F10.3,4I10)
  109 FORMAT(5X,1HA,7X,5HGAMMA,7X,1HZ,10X,3HRHO/20(3F10.4,F10.6/))
  110 FORMAT(48H 6*PI*Z/HC* MUSQUARE * SUM OF J*VJ* SIN 2PI J/P=,1PE12.6
     1)
      GO TO 91
   99 CONTINUE
      REWIND NK
```

```
MONPOL MCNPOL                                                    04/27
      EXTERNAL FORMULA NUMBER  -  SOURCE STATEMENT  -  INTERNAL FO

      CALL SORT
      STOP
      END                                                          MONP
```

```
$IBFTC SORTS   DECK
      SUBROUTINE SORT
      DIMENSION V12(1260),GAMMA(1260),V(42,30),G(42,30)
      REWIND 11
C     INPUT IS ON 11, OUTPUT ON 14(PUNCH)
      NGAMS=8
      NVS= NGAMS*42
      READ(11,12) (V12(I),GAMMA(I),I=1,NVS)
   12 FORMAT (F10.0,25X,F20.0)
       DO 9 J=1,42
      K=0
      DO 9 I=J,NVS ,42
      K=K+1
      V(J,K)=V12(I)
    9 G(J,K)=GAMMA(I)
      DO 10 J=1,42
   10 WRITE(14,13)(V(J,K),G(J,K),K=1,NGAMS)
   13 FORMAT (F10.0,25X,F20.2)
      RETURN
      END
```

```
$IBFTC .ROTCUR DECK
C    THIS ONE SIMPLY FITS THE ABSORPTION TO A SUM OF GAUSSIANS
C   THEN OUNCHES THEM OUT FOR ROTGND
CCURVE FITTING TO SUM OF GAUSSIANS , FOR THE DIMER ROTATION CALC.
C    THESE GAUSSIANS CAN ALSO BE USED IN THE INDEX OF REFRACTION DECK
C   IT CALLS A SHARE F2 TYPE ROUTINE WHICH WAS MODIFIED FOR F4.    MAT
      DIMENSION A(80,80  ),E( 80),FNUI( 80),THETA( 80),FNUJ( 80),
     1ATRA(  80,80),D(200),B( 80,1),FLAI( 80),FLAJ( 80),E1( 80)
      DIMENSION B1( 80)
      COMMON /IOPOOL/ NI,NO,NK,NP
      CALL IOSET
C    FOR INTERNAL SETUP OF GAUSSIANS, SET FACT =1. PUT IN VALUE OF SP
C   AND WIDTH.  FOR READING IN THE GAUSSIANS, SET FACT =0 AND PUT IN
   10 READ(NI,100)N,START,STOP,DELTA,FACT,SPACE,WIDTH,CMOLS
  100 FORMAT(I5,7F10.0)
      IF(N) 8,8,9
    9 M=(STOP-START)/DELTA+1.
      READ(NI,101)(E1(I),I=1,M)
  101 FORMAT (7F10.4)
      IF (FACT)700,700,701
  700 READ(NI,102) (FNUJ(J),THETA(J),J=1,N)
  102 FORMAT (2F10.0)
      GO TO702
  701 NU=100000./START-WIDTH/200.
      THETA(1)=WIDTH
      FNUJ(1)=100*NU
      N=(10000000./START-10000000./STOP)/SPACE+1.
      DO 703 J=2,N
      FNUJ(J)=FNUJ(J-1)-SPACE
  703 THETA(J)=WIDTH
  702 DO 300 J=1,N
      I=1
      FLAI(I)=START
  400 FNUI(I)=10000000./FLAI(I)
      A(I,J)=EXP(-((FNUI(I)-FNUJ(J))/THETA(J))**2)
      I=I+1
      FLAI(I)=FLAI(I-1)+DELTA
      IF (M-I) 300,400,400
  300 CONTINUE
      DO 303 K=1,N
      DO 302 L=1,N
      ATRA(K,L)=0.
      DO 301 I=1,M
  301 ATRA(K,L)=ATRA(K,L)+A(I,K)*A(I,L)
  302 CONTINUE
  303 CONTINUE
      DO 305 K=1,N
      B(K,1)=0.
      DO 304 I=1,M
      E(I)=E1(I)
  304 B(K,1)=B(K,1)+A(I,K)*E(I)
  305 CONTINUE
      CALL MATINV (ATRA,N,B,1,DET)
      WRITE(NO,199)
  199 FORMAT (14H1CURVE FITTING//)
      WRITE(NO,200)
```

```
  200 FORMAT (50X,22H GAUSSIAN COEFFICIENTS//  3(40H                FRE(
     1Y   COEFF.      WIDTH)//)
      WRITE(NO,201)(FNUJ(J),B(J,1),THETA(J),J=1,N)
  201 FORMAT (3(F20.0,F10.4,F10.0) )
      WRITE(NP,205) (FNUJ(J),B(J,1),THETA(J),J=1,N)
  205 FORMAT (2(F10.0,F10.4,F10.0))
      WRITE(NO,202)
  202 FORMAT(1H0,3(40H          FREQUENCY     OD CALC.      OD EXPL.)   )
      DO 307 I=1,M
      D(I)=0.
      DO 306 J=1,N
  306 D(I)=D(I)+B(J,1)*A(I,J)
  307 CONTINUE
      AVD=0.
      DO 73 I=1,M
   73 AVD = ABS(D(I)-E(I)) +AVD
      AM=M
      AVD=AVD/AM
      WRITE (NO,204) AVD
  204 FORMAT (12H AVG. DEV. =  F10.4)
      WRITE(NO,203)(FNUI(I),D(I),E(I),I=1,M)
  203 FORMAT (3(F16.0,2F12.4) )
C     FIND DEE THE DIPOLE STRENGTH.
      DEE=0.
      DO 751 J=1,N
      B(J,1)=B(J,1)/CMOLS
  751 DEE=DEE + .92*1.772*B(J,1)*THETA(J)/FNUJ(J)
      WRITE (NO,255)                DEE,DD
  255 FORMAT (/3X,24HMONOMER DIPOLE STRENGTH=,F10.5,21HE-38 ESU-CM*
     1 MU=,F8.5,5HDEBYE)
      GO TO 10
    8 CONTINUE
      CALL EXIT
      STOP
      END
```

```
$IBFTC .MATINV DECK
C  THIS IS A F2 SHARE MATINV WHICH WAS RUN THRU SIFT
C  IT IS USED BY THE CRVE FITTING PROGRAM
CMATRIX INVERSION WITH ACCOMPANYING SOLUTION OF LINEAR EQUATIONS
C
      SUBROUTINE MATINV(A,N,B,M,DETERM)
C
      DIMENSION IPIVOT( 80),A(  80,80),B( 80,1),INDEX( 80,2),PIVOT(
C THE FOLLOWING STATEMENT(S) HAVE BEEN MANUFACTURED BY THE TRANSLAT
C   COMPENSATE FOR THE FACT THAT EQUIVALENCE DOES NOT REORDER COMMO
      COMMON  PIVOT  , INDEX  , IPIVOT
C     DIMENSION IPIVOT (100),A(100,100),B(20,1),INDEX(100,2),PIVOT(
C     COMMON PIVOT, INDEX, IPIVOT
      EQUIVALENCE (IROW,JROW), (ICOLUM,JCOLUM), (AMAX, T, SWAP)
C
C     INITIALIZATION
C
   10 DETERM=1.0
   15 DO 20 J=1,N
   20 IPIVOT(J)=0
   30 DO 550 I=1,N
C
C     SEARCH FOR PIVOT ELEMENT
C
   40 AMAX=0.0
   45 DO 105 J=1,N
   50 IF (IPIVOT(J)-1) 60, 105, 60
   60 DO 100 K=1,N
   70 IF (IPIVOT(K)-1) 80, 100, 740
   80 IF (ABS(AMAX)-ABS(A(J,K))) 85, 100, 100
   85 IROW=J
   90 ICOLUM=K
   95 AMAX=A(J,K)
  100 CONTINUE
  105 CONTINUE
  110 IPIVOT(ICOLUM)=IPIVOT(ICOLUM)+1
C
C     INTERCHANGE ROWS TO PUT PIVOT ELEMENT ON DIAGONAL
C
  130 IF (IROW-ICOLUM) 140, 260, 140
  140 DETERM=-DETERM
  150 DO 200 L=1,N
  160 SWAP=A(IROW,L)
  170 A(IROW,L)=A(ICOLUM,L)
  200 A(ICOLUM,L)=SWAP
  205 IF(M) 260, 260, 210
  210 DO 250 L=1, M
  220 SWAP=B(IROW,L)
  230 B(IROW,L)=B(ICOLUM,L)
  250 B(ICOLUM,L)=SWAP
  260 INDEX(I,1)=IROW
  270 INDEX(I,2)=ICOLUM
  310 PIVOT(I)=A(ICOLUM,ICOLUM)
  320 DETERM=DETERM*PIVOT(I)
C
C     DIVIDE PIVOT ROW BY PIVOT ELEMENT
```

```
C
  330 A(ICOLUM,ICOLUM)=1.0
  340 DO 350 L=1,N
  350 A(ICOLUM,L)=A(ICOLUM,L)/PIVOT(I)
  355 IF(M) 380, 380, 360
  360 DO 370 L=1,M
  370 B(ICOLUM,L)=B(ICOLUM,L)/PIVOT(I)
C
C     REDUCE NON-PIVOT ROWS
C
  380 DO 550 L1=1,N
  390 IF(L1-ICOLUM) 400, 550, 400
  400 T=A(L1,ICOLUM)
  420 A(L1,ICOLUM)=0.0
  430 DO 450 L=1,N
  450 A(L1,L)=A(L1,L)-A(ICOLUM,L)*T
  455 IF(M) 550, 550, 460
  460 DO 500 L=1,M
  500 B(L1,L)=B(L1,L)-B(ICOLUM,L)*T
  550 CONTINUE
C
C     INTERCHANGE COLUMNS
C
  600 DO 710 I=1,N
  610 L=N+1-I
  620 IF (INDEX(L,1)-INDEX(L,2)) 630, 710, 630
  630 JROW=INDEX(L,1)
  640 JCOLUM=INDEX(L,2)
  650 DO 705 K=1,N
  660 SWAP=A(K,JROW)
  670 A(K,JROW)=A(K,JCOLUM)
  700 A(K,JCOLUM)=SWAP
  705 CONTINUE
  710 CONTINUE
  740 RETURN
  750 END
```

```
449101DIMEROT                    30                    DIMERO MAIN      05/0
        EXTERNAL FORMULA NUMBER   -   SOURCE STATEMENT    -   INTERNAL F

      COMMON  /IOPOOL/ NI,NO,NK,NP
      CALL IOSET
      CALL ROTS
      REWIND NP
      CALL ROTEM
      REWIND NK
      NP=15
      CALL SELEK
      CALL CCEND
      CALL EXIT
      STOP
      END
BEGIN ASSY. 2055.58
```

```
      SUBROUTINE IOSET
      COMMON /IOPOOL/ NIN,NOUT1,NOUT2,NPUNCH
C  SET FOUR INPUT OUTPUT UNITS FOR IN,TWO OUTPUTS AND PUNCH OUT.
      NIN=2
      NOUT1=3
      NOUT2=35
      NPUNCH=11
      RETURN
      END
BEGIN ASSY. 2223.92
```

```
      SUBROUTINE ROTS
      COMMON /IOPOOL/ NI,NO,NK,NP
C   THIS WAS THE FORM OF ROTSTR USED IN DEC 64 CALCN FOR 30 ANGLES
C  IT CALLS DGNR FOR THE DEGENERATE INTERACTION ROTN TERM
C  AND CALLS NDGNR FOR THE NON DEGENERATE INTERACTION ROTATION TERM
      DIMENSION TITLE(12),FNU(4),DMU(4),GAM(4),V12(4),ROTN(4),FNU1(4)
      NODO=-1
   41 READ(NI,9)                    TITLE
    9 FORMAT (12A6)
      NODO=NODO*(-1)
      READ (NI,10)                Z,RAD1,RAD2,GMINCD,NCASE
   10 FORMAT (4F5.3,I2)
      IF (Z) 27,99,27
C     NCASE  =1 TO 5,FOR CASES OF 1=APA,2=APU,3=APC,4=GPC,5=GPG.
   27 IF (NCASE-5) 20,21,20
   21 NTRANS=4
      GO TO 23
   20 NTRANS=NCASE
   23 READ(NI,11)              (FNU(I),DMU(I),GAM(I),V12(I),I=1,NTRANS)
   11 FORMAT (4F10.0)
  202 WRITE(NO,51)              TITLE,Z,RAD1,RAD2,GMINCD,NCASE,(FNU(I),DMU
     1(I),GAM(I),V12(I), I=1,NTRANS)

   51 FORMAT (12A6/4F10.3,I5/(F10.0,2F10.2,F10.0))
      GMINCR=GMINCD/57.2958
      DO 24 I=1,NTRANS
   24 GAM(I)=GAM(I)/57.2958
      DO 25 I=1,NTRANS
   25 FNU1(I)=FNU(I)
C     RECYCLE POINTFOR NEW ANGLE
   42 DO 26 I=1,NTRANS
   26 FNU(I)=FNU1(I)
      IF (NCASE-2) 301,302,306
  301 CALL DT(Z,RAD1,GMINCR,DMU(1),FNU(1),ROTSTR)
      ROTN(1)=-ROTSTR                          +.001
      ROTN(2)= ROTSTR                          -.001
      FNU(2)=FNU(1)-V12(1)
      FNU(1)=FNU(1)+V12(1)
      NV=1
      NR=2
      GO TO 307
  302 CALL RNDT(Z,RAD1,RAD2,GAM(1),GAM(2),DMU(1),DMU(2),FNU(1),FNU(2),
     1GMINCR,V12(1),ROTSTR)
      ROTN(1)=ROTSTR                           +.001
      ROTN(2)=-ROTSTR                          +.001
      NV=1
      NR=2
      GO TO 307
  306 IF (NCASE-4) 303,304,305
  303 IF (NODO) 60,60,61
   60 CALL RNDT(Z,RAD2,RAD1,GAM(2),GAM(1),DMU(1),DMU(2),FNU(1),FNU(2),
     1GMINCR,V12(1),ROTSTA)
      CALL RNDT(Z,RAD1,RAD2,GAM(2),GAM(3),DMU(2),DMU(3),FNU(2),FNU(3),
     1GMINCR,V12(2),ROTSTC)
      GO TO62
```

```
 61 CALL RNDT(Z,RAD1,RAD2,GAM(1),GAM(2),DMU(2),DMU(1),FNU(1),FNU(2),
   1GMINCR,V12(1),ROTSTA)
    CALL RNDT(Z,RAD1,RAD2,GAM(3),GAM(2),DMU(2),DMU(3),FNU(2),FNU(3),
   1GMINCR,V12(2),ROTSTC)
 62 NR=3
    NV=2
    ROTN(1)=ROTSTA                          +.001
    ROTN(2)=ROTSTC-ROTSTA                   +.001
    ROTN(3)=-ROTSTC                         +.001
    GO TO 307
304 CALL RNDT(Z,RAD1,RAD2,GAM(1),GAM(2),DMU(1),DMU(2),FNU(1),FNU(2),
   1GMINCR,V12(1),ROTSAB)
    CALL RNDT(Z,RAD2,RAD1,GAM(3),GAM(2),DMU(2),DMU(3),FNU(2),FNU(3),
   1GMINCR,V12(2),ROTSBC)
    CALL RNDT(Z,RAD1,RAD2,GAM(3),GAM(4),DMU(3),DMU(4),FNU(3),FNU(4),
   1GMINCR,V12(3),ROTSCD)
    CALL RNDT(Z,RAD1,RAD2,GAM(1),GAM(4),DMU(1),DMU(4),FNU(1),FNU(4),
   1GMINCR,V12(4),ROTSAD)
    NV=4
    NR=4
    ROTN(1)=ROTSAB+ROTSAD                   +.001
    ROTN(2)=ROTSBC-ROTSAB                   +.001
    ROTN(3)=ROTSCD-ROTSBC                   +.001
    ROTN(4)=-ROTSAD-ROTSCD                  +.001
    GO TO 307
305 CALL DT(Z,RAD1,GMINCR,DMU(1),FNU(1),ROTSAA)
    CALL DT(Z,RAD1,GMINCR,DMU(2),FNU(2),ROTSBB)
    CALL RNDT(Z,RAD1,RAD1,GAM(1),GAM(2),DMU(1),DMU(2),FNU(1),FNU(2),
   1GMINCR,V12(1),ROTSAB)
    CALL RNDT(Z,RAD1,RAD1,GAM(2),GAM(1),DMU(1),DMU(2),FNU(1),FNU(2),
   1GMINCR,V12(2),ROTSBA)
    ROTN(1)=-ROTSAA+ROTSAB+ROTSBA           +.001
    ROTN(2)=ROTSAA+ROTSAB+ROTSBA            +.001
    ROTN(3)=-ROTSBB-ROTSBA-ROTSAB           +.001
    ROTN(4)=ROTSBB-ROTSAB-ROTSBA            +.001
    FNU(3)=FNU(2)+V12(4)
    FNU(4)=FNU(2)-V12(4)
    FNU(2)=FNU(1)-V12(3)
    FNU(1)=FNU(1)+V12(3)
    NR=4
    NV=4
307 WRITE(NO,52)
 52 FORMAT (5X,15HFREQUENCY CM-1,5X,22HROTATIONAL STR*10 E 40/)
    WRITE (NO,53)              (FNU(I),ROTN(I),I=1,NR)
 53 FORMAT (2F20.0)
401 WRITE (NP,55) GMINCD,(ROTN(I),FNU(I),I=1,NR)

 55 FORMAT (F10.2/(F10.4,F10.1))
    IF   (GMINCR- .65)313,41,41
313 READ (NI,12)       (V12(I),GMINCD,I=1,NV)
 12 FORMAT (F10.0,25X,F20.0)
    GMINCR=GMINCD/57.2958
    WRITE (NO,54)              GMINCD,(V12(I),I=1,NV)

 54 FORMAT (7H0GAMMA=,F6.2, 7HV12 ARE/(13X,F10.0))
    GO TO 42
```

```
   99 CONTINUE
      RETURN
      END
BEGIN ASSY. 2223.51
```

```
      SUBROUTINE DT (Z,RAD,GAM,FMU,FNU,ROTSTR)
      DIPSTR=FMU**2
      B=2.*RAD*SIN(GAM/2.)
      R12=SQRT (B**2+Z**2)
      B=ABS(B)
      THETA =1.5708 -ATAN(Z/B)
      ROTSTR= 1.5708*FNU*R12*DIPSTR*SIN(GAM)*COS(THETA)/10000.
      RETURN
      END
BEGIN ASSY. 2223.67
```

```
      SUBROUTINE RNDT (Z,RAD1,RAD2,GAM1,GAM2,DMU1,DMU2,FNU1,FNU2,GMINCR,
     1V12,ROTSTR)
      DIPSTR=DMU1*DMU2
      GAM =GAM1-GAM2+GMINCR
      B=2.*RAD2*SIN(GMINCR/2.)
      ALFA= 1.5708 +GMINCR/2.
      C=SQRT (B**2+(RAD1-RAD2)**2 - 2.*B*(RAD1-RAD2)*COS(ALFA))+.000001
      R12= SQRT(C**2+Z**2)
      THETA=1.5708- ATAN(Z/C)
      ROTSTR= 6.2832*V12*FNU1*FNU2/(FNU2**2-FNU1**2)*R12*DIPSTR*SIN(GAM)
     1*COS (THETA)/10000.
      RETURN
      END
BEGIN ASSY. 2223.80
```

```
C     IN THIS DECK NP IS USED FR INPUT OF ROTATIONAL STRENGTHS.
CABSORPTION AND ROTATION OF DIMER.
      SUBROUTINE ROTEM
      COMMON /IOPOOL/NI,NO,NK,NP
      CALL IOSET
      COMMON /XTAB/ X(400)
      CALL XFIL
      DIMENSION E(100,4),THETA(100,4),FNU(100,4),R(100,4),ROTSTR(4),FQ(4
     1),NG(4),CMOLS(4),RATIO(4),DEE(4),DD(4),FLA1(500),COR(4)
     1,CD1(500),ORD1(500),EPT1(500),FNU1(100,4),PEEK(4)
   42 READ        (NI,212) N,START,STOP,DELTA,NB
  212 FORMAT (I5,3F10.0,I5)
      BN=2
      NPTS=(STOP-START)/DELTA+1.
      START1=START
      IF (N) 44,99,44
   44 READ        (NI,231) (NG(J),CMOLS(J),PEEK(J),J=1,NB)
  231 FORMAT(I5,2F10.0)
      KSTART=77777
      WRITE (NK) KSTART
      DO 220 J=1,NB
      NGJ=NG(J)
  220 READ        (NI,214)(FNU1(I,J),E(I,J),THETA(I,J),I=1,NGJ)

  214 FORMAT (6F10.0)
C     FIND D(J) DIPOLE STRENGTH OF JTH BAND AND RATIO(J).
   43 DO 701 J=1,NB
      NGJ=NG(J)
      DEE(J)=0.
      DO 700 I=1,NGJ
      E(I,J)=E(I,J)/CMOLS(J)
  700 DEE(J)= DEE(J)+.92*1.772*E(I,J)*THETA(I,J)/FNU1(I,J)
      DD(J)=SQRT(DEE(J)*.01)
  701 WRITE        (NO,205)DEE(J),DD(J)
  205 FORMAT (/3X,24HMONOMER DIPOLE STRENGTH=,F10.5,21HE-38 ESU-CM**2,OR
     1 MU=,F8.5,5HDEBYE)
   41 READ        (NP,215) GAMMA,(ROTSTR(J),FQ(J),J=1,NB)

  215 FORMAT (F10.0/(2F10.0))
      START=START1
      WRITE (NO,704)          GAMMA,(ROTSTR(J),FQ(J),J=1,NB)

  704 FORMAT (1H1,20X,6HGAMMA=,F6.1,5X,9HFREQUENCY,5X,6HROTSTR/
     1(32X,2F10.0))
      DO 702 J=1,NB
      COR(J)=PEEK(J)-FQ(J)
      RATIO(J)=ROTSTR(J)/DEE(J)*132.6
      NGJ=NG(J)
      DO 703 I=1,NGJ
      FNU(I,J)=FNU1(I,J)-COR(J)
  703 R(I,J)=  E(I,J)*RATIO(J)
   97 WRITE(NO,201)
  201 FORMAT (41HO FREQUENCY   DENSITY  WIDTH     ROTATION//)
  702 WRITE (NO,202)        (FNU(I,J),E(I,J),THETA(I,J),R(I,J),I=1,NGJ)
```

```
  202 FORMAT (F10.0,F10.1,2F10.0)
      NPTN=1
      WRITE (NO,203)
  203 FORMAT (81H0FREQUENCY   DENSITY        CD        ORD  HELIX CD  HEL
     1X ORD TOTAL CD  TOTAL ORD //)
      N200=1
  400 EPT=0.
      RD=0.
      CD=0.
      HRD=0.
      HCD=0.
      DO 301 J=1,NB
      NGJ=NG(J)
      DO 301 I=1,NGJ
      SEX=(EXP(-((START-FNU(I,J))/THETA(I,J))**2))/2.
      EPT=EPT+E(I,J)*SEX
      CD=CD+R(I,J)*SEX
      C=(FNU(I,J)-START)/THETA(I,J)
      IF (ABS (C)-4.) 10,10,11
   11 RINT=1./(2.*C)
      GO TO 12
   10 ICP=100.*C
      IF (ICP) 13,14,15
   13 RINT=-X(ICP)
      GO TO 12
   14 RINT=0.
      GO TO 12
   15 RINT=X(ICP)
   12 RD=RD+R(I,J)*(RINT+THETA(I,J)/(2.*(FNU(I,J)+START))-THETA(I,J)/
     1FNU(I,J))*0.564
  301 CONTINUE
      FLA1(N200)=10000000./START
      IF (NPTN-10) 234,235,235
  235 WRITE(NO,204)    START,EPT,CD,RD,HCD,HRD,TCD,TRD,FLA1(N200)
  204 FORMAT (8F10.0,F10.2)
      NPTN=1
      GO TO 236
  234 NPTN=NPTN+1
  236 ORD1(N200)=RD
      EPT1(N200)=EPT
      CD1(N200)=CD
      N200=N200+1
      START=START+DELTA
      IF (STOP-START) 401,400,400
  401 WRITE(NK)          (FLA1(I),CD1(I),ORD1(I),EPT1(I),I=1,NPTS)
      IF (GAMMA-39.) 41,42,42
   99 KSTART=0
      WRITE (NK)     KSTART
      ENDFILE NK
      REWIND NK
      CALL CHOOSE(NPTS)
      RETURN
      END
BEGIN ASSY. 2224.08
```

```
$IBFTC XFIL.   DECK
      SUBROUTINE XFIL
C  THIS IS SIMPLU A TAPLE OF 400 VALUES OF ERROR FUNCTION
C  IT PLACES THE VALUES IN COMMON FOR INDEX REFRACT AND THE ROTGND
CALCULATIONS OF K-K TRANSFORM
      COMMON /XTAB/ X(400)
      X(  1)=0.00999
      X(  2)=0.01999
      X(  3)=0.02998
      X(  4)=0.03995
      X(  5)=0.04991
      X(  6)=0.05985
      X(  7)=0.06970
      X(  8)=0.07965
      X(  9)=0.08951
      X( 10)=0.09933
      X( 11)=0.10911
      X( 12)=0.11885
      X( 13)=0.12854
      X( 14)=0.13818
```

```
X( 15)=0.14777
X( 16)=0.15729
X( 17)=0.16676
X( 18)=0.17616
X( 19)=0.18549
X( 20)=0.19475
X( 21)=0.20393
X( 22)=0.21303
X( 23)=0.22205
X( 24)=0.23099
X( 25)=0.23983
X( 26)=0.24859
X( 27)=0.25725
X( 28)=0.26581
X( 29)=0.27427
X( 30)=0.28236
X( 31)=0.29088
X( 32)=0.29902
X( 33)=0.30705
X( 34)=0.31496
X( 35)=0.32276
X( 36)=0.33045
X( 37)=0.33801
X( 38)=0.34544
X( 39)=0.35275
X( 40)=0.35994
X( 41)=0.36699
X( 42)=0.37392
X( 43)=0.38071
X( 44)=0.38737
X( 45)=0.39389
X( 46)=0.40028
X( 47)=0.40653
X( 48)=0.41246
X( 49)=0.41860
X( 50)=0.42443
X( 51)=0.43012
X( 52)=0.43566
X( 53)=0.44105
X( 54)=0.44631
X( 55)=0.45141
X( 56)=0.45637
X( 57)=0.46119
X( 58)=0.46586
X( 59)=0.47038
X( 60)=0.47476
X( 61)=0.47899
X( 62)=0.48307
X( 63)=0.48701
X( 64)=0.49080
X( 65)=0.49444
X( 66)=0.49749
X( 67)=0.50130
X( 68)=0.50451
X( 69)=0.50757
X( 70)=0.51050
```

```
X( 71)=0.51328
X( 72)=0.51592
X( 73)=0.51842
X( 74)=0.52078
X( 75)=0.52301
X( 76)=0.52509
X( 77)=0.52705
X( 78)=0.52886
X( 79)=0.53054
X( 80)=0.53210
X( 81)=0.53352
X( 82)=0.53481
X( 83)=0.53598
X( 84)=0.53702
X( 85)=0.53793
X( 86)=0.53873
X( 87)=0.53940
X( 88)=0.53996
X( 89)=0.54040
X( 90)=0.54072
X( 91)=0.54093
X( 92)=0.54103
X( 93)=0.54102
X( 94)=0.54090
X( 95)=0.54068
X( 96)=0.53036
X( 97)=0.53993
X( 98)=0.53941
X( 99)=0.53879
X(100)=0.53807
X(101)=0.53727
X(102)=0.53637
X(103)=0.53538
X(104)=0.53431
X(105)=0.53316
X(106)=0.53192
X(107)=0.53060
X(108)=0.52921
X(109)=0.52774
X(110)=0.52620
X(111)=0.52459
X(112)=0.52291
X(113)=0.52116
X(114)=0.51935
X(115)=0.51748
X(116)=0.51555
X(117)=0.51356
X(118)=0.51152
X(119)=0.50942
X(120)=0.50727
X(121)=0.50507
X(122)=0.50282
X(123)=0.50053
X(124)=0.49820
X(125)=0.49582
X(126)=0.49341
```

X(127)=0.49095
X(128)=0.48847
X(129)=0.48595
X(130)=0.48339
X(131)=0.48081
X(132)=0.47820
X(133)=0.47556
X(134)=0.47290
X(135)=0.47021
X(136)=0.46751
X(137)=0.46478
X(138)=0.46204
X(139)=0.45928
X(140)=0.45650
X(141)=0.45371
X(142)=0.45091
X(143)=0.44810
X(144)=0.44528
X(145)=0.44245
X(146)=0.43962
X(147)=0.43678
X(148)=0.43394
X(149)=0.43109
X(150)=0.42824
X(151)=0.42540
X(152)=0.42255
X(153)=0.41971
X(154)=0.41686
X(155)=0.41403
X(156)=0.41119
X(157)=0.40837
X(158)=0.40555
X(159)=0.40274
X(160)=0.39993
X(161)=0.39714
X(162)=0.39436
X(163)=0.39159
X(164)=0.38883
X(165)=0.38608
X(166)=0.38335
X(167)=0.38063
X(168)=0.37792
X(169)=0.37523
X(170)=0.37255
X(171)=0.36990
X(172)=0.36725
X(173)=0.36463
X(174)=0.36202
X(175)=0.35943
X(176)=0.35686
X(177)=0.35431
X(178)=0.35178
X(179)=0.34926
X(180)=0.34677
X(181)=0.34429
X(182)=0.34184

```
X(183)=0.33941
X(184)=0.33700
X(185)=0.33460
X(186)=0.33223
X(187)=0.32989
X(188)=0.32756
X(189)=0.32525
X(190)=0.32297
X(191)=0.32071
X(192)=0.31847
X(193)=0.31625
X(194)=0.31405
X(195)=0.31188
X(196)=0.30973
X(197)=0.30759
X(198)=0.30549
X(199)=0.30340
X(200)=0.30134
X(201)=0.29929
X(202)=0.29727
X(203)=0.29527
X(204)=0.29330
X(205)=0.29134
X(206)=0.28940
X(207)=0.28749
X(208)=0.28560
X(209)=0.28373
X(210)=0.28188
X(211)=0.28005
X(212)=0.27824
X(213)=0.27646
X(214)=0.27469
X(215)=0.27294
X(216)=0.27122
X(217)=0.26951
X(218)=0.26782
X(219)=0.26615
X(220)=0.26451
X(221)=0.26288
X(222)=0.26127
X(223)=0.25968
X(224)=0.25810
X(225)=0.25655
X(226)=0.25501
X(227)=0.25350
X(228)=0.25200
X(229)=0.25051
X(230)=0.24905
X(231)=0.24760
X(232)=0.24617
X(233)=0.24476
X(234)=0.24336
X(235)=0.24198
X(236)=0.24061
X(237)=0.23926
X(238)=0.23793
```

X(239)=0.23661
X(240)=0.23531
X(241)=0.23402
X(242)=0.23275
X(243)=0.23149
X(244)=0.23025
X(245)=0.22902
X(246)=0.22780
X(247)=0.22660
X(248)=0.22541
X(249)=0.22424
X(250)=0.22308
X(251)=0.22193
X(252)=0.22080
X(253)=0.21967
X(254)=0.21856
X(255)=0.21747
X(256)=0.21638
X(257)=0.21531
X(258)=0.21425
X(259)=0.21320
X(260)=0.21216
X(261)=0.21113
X(262)=0.21012
X(263)=0.20911
X(264)=0.20812
X(265)=0.20713
X(266)=0.20616
X(267)=0.20520
X(268)=0.20425
X(269)=0.20330
X(270)=0.20237
X(271)=0.20145
X(272)=0.20053
X(273)=0.19963
X(274)=0.19873
X(275)=0.19785
X(276)=0.19697
X(277)=0.19610
X(278)=0.19524
X(279)=0.19439
X(280)=0.19355
X(281)=0.19271
X(282)=0.19188
X(283)=0.19107
X(284)=0.19026
X(285)=0.18945
X(286)=0.18866
X(287)=0.18787
X(288)=0.18709
X(289)=0.18632
X(290)=0.18555
X(291)=0.18479
X(292)=0.18404
X(293)=0.18330
X(294)=0.18256
X(295)=0.18183

X(296)=0.18110
X(297)=0.18038
X(298)=0.17967
X(299)=0.17897
X(300)=0.17827
X(301)=0.17758
X(302)=0.17689
X(303)=0.17621
X(304)=0.17553
X(305)=0.17486
X(306)=0.17420
X(307)=0.17354
X(308)=0.17288
X(309)=0.17224
X(310)=0.17160
X(311)=0.17096
X(312)=0.17033
X(313)=0.16970
X(314)=0.16908
X(315)=0.16846
X(316)=0.16785
X(317)=0.16725
X(318)=0.16665
X(319)=0.16605
X(320)=0.16546
X(321)=0.16487
X(322)=0.16429
X(323)=0.16371
X(324)=0.16314
X(325)=0.16257
X(326)=0.16200
X(327)=0.16144
X(328)=0.16088
X(329)=0.16033
X(330)=0.15978
X(331)=0.15924
X(332)=0.15870
X(333)=0.15817
X(334)=0.15763
X(335)=0.15710
X(336)=0.15658
X(337)=0.15606
X(338)=0.15554
X(339)=0.15503
X(340)=0.15452
X(341)=0.15401
X(342)=0.15351
X(343)=0.15301
X(344)=0.15252
X(345)=0.15203
X(346)=0.15154
X(347)=0.15105
X(348)=0.15057
X(349)=0.15009
X(350)=0.14962
X(351)=0.14915
X(352)=0.14868

```
X(353)=0.14821
X(354)=0.14775
X(355)=0.14729
X(356)=0.14683
X(357)=0.14638
X(358)=0.14593
X(359)=0.14548
X(360)=0.14504
X(361)=0.14460
X(362)=0.14416
X(363)=0.14373
X(364)=0.14329
X(365)=0.14286
X(366)=0.14243
X(367)=0.14200
X(368)=0.14158
X(369)=0.14116
X(370)=0.14075
X(371)=0.14033
X(372)=0.13992
X(373)=0.13951
X(374)=0.13910
X(375)=0.13870
X(376)=0.13830
X(377)=0.13790
X(378)=0.13750
X(379)=0.13711
X(380)=0.13672
X(381)=0.13633
X(382)=0.13594
X(383)=0.13555
X(384)=0.13517
X(385)=0.13479
X(386)=0.13441
X(387)=0.13403
X(388)=0.13366
X(389)=0.13329
X(390)=0.13292
X(391)=0.13256
X(392)=0.13219
X(393)=0.13183
X(394)=0.13147
X(395)=0.13111
X(396)=0.13075
X(397)=0.13039
X(398)=0.13004
X(399)=0.12969
X(400)=0.12934
RETURN
END
```

```
$IBFTC SCHOIX LIST,REF,DECK
      SUBROUTINE CHOOSE   (NPTS)
C THIS PICKS OUT MAXIMA AND MINIMA FORM THE ORD COURVES AMD PRINTS THEM
C SINCE THE CURVES AREBE ALWAYS SMOOTHE, IT MAY FINE SPURIOUS
C  MAXIMA AND MINIMA.
       COMMON /IOPOOL/ NI,NO,NK,NP
      DIMENSION FNU(1000),FLA(1000),E(1000),CD(1000),ORD(1000),BLOK(1000)
     1),ORD1(35),ORD2(35),ORD3(35),GAM(35)
   42 GAMMA = -5.7
      NPLO=0
      READ (NK)   KSTART
      IF (KSTART-77777) 99,41,99
   41 READ (NK)  (FLA(I),CD(I),ORD(I),E(I),I=1,NPTS)
      NPLO=NPLO+1
      GAMMA = GAMMA + 5.728
C     TAKE AVERAGES AND DERIVATIVES
      BLOK(1)=ORD(1)+ORD(2)+ORD(3)+ORD(4)
      DO 31 I=5,NPTS,4
      BLOK(I)=ORD(I)+ORD(I+1)+ORD(I+2)+ORD(I+3)
   31 BLOK(I+1)= BLOK(I)-BLOK(I-4)
C     BLOK1,5,9,13 ETC. CONTAIN AVERAGES
C     BLOK 2,6,10,14 ETC. HAVE DIFFERENCES OF BLOK5-2,9-5,13-9, ETC.
C
C     FIND TURNING POINTS
      WRITE (NO,51)  GAMMA,
   51 FORMAT (1H1,5X,6HGAMMA=,F6.1,
     1 ///10X,30HLONG WAVELENGTH TURNING POINT.//)
       WRITE (NO,52)
   52 FORMAT (10X,10HWAVELENGTH,15X,3HORD/)
      DO 32 I=1,NPTS,4
      DERPRD = BLOK(I+1)*BLOK(I+5)
      NPRX=I-4
      NPRW=I+4
      IF (DERPRD) 61,32,32
   32 CONTINUE
      WRITE (NO,54)
   54 FORMAT (14H NO TURN FOUND)
      GO TO 99
   61 WRITE (NO,53) (FLA(I),ORD(I),I=NPRX,NPRW)
   53 FORMAT ( F20.2,F20.0)
      WRITE (NO,55)
   55 FORMAT (1H0,10X,31HMEDIUM WAVELENGTH TURNING POINT/)
C     FIND THE 262 TURNING POINT
      WRITE (NO,52)
      DO 33 I=NPRW,NPTS,4
      DERPRD = BLOK(I+1)*BLOK(I+5)
      NPRX2= I-4
      NPRW2=I+4
      IF (DERPRD) 62,33,33
   33 CONTINUE
      WRITE (NO,54)
      GO TO 99
   62 WRITE (NO,53) (FLA (J),ORD (J),J=NPRX2,NPRW2)
C    FIND SHORT WAVE TURN
      WRITE (NO,56)
   56 FORMAT (1H0,10X,31H SHORT WAVELENGTH TURNING POINT/)
```

```
      WRITE (NO,52)
      DO 34 I=NPRW2,NPTS,4
      DERPRD = BLOK(I+1)*BLOK(I+5)
      NPRX3= I-4
      NPRW3= I+4
      IF (DERPRD) 63,34,34
   34 CONTINUE
      WRITE (NO,54)
   63 WRITE (NO,53) (FLA(J),ORD(J),J=NPRX3,NPRW3)
C     FIND THE CORSSING POINTS
      WRITE (NO,57)
   57 FORMAT (1H0,10X,18HCROSSING POINTS AT)
      WRITE (NO,52)
      NPRA=0
      DO 35 I=2,NPTS
      PROD= ORD(I)*ORD(I-1)
      NPRC=I
      IF (PROD) 64,99,35
   64 IF (NPRA) 99,65,66
   65 NPRA=NPRC
   35 CONTINUE
      WRITE (NO,54)
   66 NPRC1=NPRC-1
      NPRA1= NPRA-1
      WRITE (NO,53) (FLA(I),ORD(I),I=NPRA1,NPRA)
      WRITE (NO,53) (FLA(I),ORD(I),I=NPRC1,NPRC)
C    FIND MAXS AND MINS
      TEX=0.
      TEM=0.
      TES=0
   71 DO 36 I=1,8
      INPRX=I+ NPRX
      INPRX2=I+NPRX2
      INPRX3= I+NPRX3
      TEX=TEX+ORD(INPRX)
      TEM=TEM+ORD(INPRX2)
   36 TES=TES+ORD(INPRX3)
      TEX=TEX/8.
      TEM=TEM/8.
      TES=TES/8.
      WRITE (NO,58) TEX,TEM,TES
   58 FORMAT ( 1H-,10X, 44HAVERAGE VALUES OF ROTATION AT TURNING POINTS/
     11H0,5X, 5HSHORT,10X, 6HMEDIUM,9X, 4HLONG/3F15.0)
      ORD1(NPLO)=TEX
      ORD2(NPLO)=TEM
      ORD3(NPLO)=TES
      GAM(NPLO)=GAMMA
   43 IF (GAMMA-39.0) 41,44,44
   44 CALL PLODO (GAM,ORD1,08,10)
      CALL PLODO (GAM,ORD2,08,10)
      CALL PLODO (GAM,ORD3,08,10)
      GO TO 42
   99 WRITE (NO,153) (FLA(I),ORD(I),CD(I),E(I),BLOK(I),I=1,350)
  153 FORMAT (2F15.8,10X,2F15.8,10X,F15.8)
      RETURN
      END
```

```
$IBFTC .PLODO  LIST,REF,DECK
      SUBROUTINE PLODO  (X,Y,NPTS,LENGTH)
C  THESE TWO PLOT ROUTINES ARE CALLED OFTEN.  ONE PLODI READS IN
C    THE ABSCISSA VALUES FORM LARGEST TO SMALLEST WHILE PLODO READS IN F
C  SMALLEST TO LARGEST
C    THEY PLOT ONLY ONE CURVE TO A FRAME
C NPTS IS THE NUMBER OF POINTS TO BE PLOTTED( THE X TO BE READ IN FROM
C SMALLEST TO LARGEST,THE ASSOCIATED Y HAVING THE SAME INDEX.
C  ONE TITLE CARD IS READ. LENGTH IS IN INCHES
      COMMON /CCPOOL/XMIN,XMAX,YMIN,YMAX,CCXMIN,CCXMAX,CCYMIN,CCYMAX
C     CALL CCBGN              USED TO BE IN.   OUT  JAN  10
      COMMON /IOPOOL/ NI,NO,NK,NP
      DIMENSIONTITLE(12),X(1000),Y(1000),FMT(2)
      READ (NI,11)TITLE
   11 FORMAT(13A6)
      XMIN = X(1)
      XMAX= X(NPTS)
      IF (NI+1) 121,122,121
  121 RCOR=1024.
      NRCOR=1024
      GO TO 123
  122 RCOR=1.
      NRCOR=1
  123 CCXMIN=100./RCOR
      CCYMIN=200./RCOR
      CCYMAX=900./RCOR
      CCXMAX=(100+LENGTH*100)/NRCOR
C  FIND YMAX AND YMIN FOR SCALING PURPOSES
      YMAX=Y(1)
      DO 21 I=2,NPTS
      YDIF=YMAX-Y(I)
      IF (YDIF)22,21,21
   22 YMAX=Y(I)
   21 CONTINUE
      YMIN=Y(1)
      DO 23 I=2,NPTS
      YDIFM=YMIN-Y(I)
      IF (YDIFM) 23,24,24
   24 YMIN=Y(I)
   23 CONTINUE
      CALL CCGRID (LENGTH,2,5,6HLABELS,7,2,5)
      CALL CCLTR(.048828,.097656,0,2,TITLE,78)
      CALL CCPLOT (X,Y,NPTS,4HJOIN)
      WRITE (NO,12)TITLE
   12 FORMAT (1H0,13A6)
      CALL CCNEXT
      RETURN
      END
```

```
      SUBROUTINE SELEK
C  THE ROTGND WRITE OUT BINSRY TAPES OF ROTN ETC VS WAVELENGTH
C  THE CHOOSE AND SELECT DECK ARE TO GET CERTAIN FEATURES OUT OF THE
C  BINARY TAPES
C  SELECT PICK OUT CERTAIN SELECTED VALUES OF GAMMA AND PLOTS THE
C  ROTATION VS WAVELENGTH AND OUTPUTS IT TOO FOR LATER PLOTTING ETC.
C  NP (THE NPUNCH UNIT) IS USED FOR OUTPUT TO CULPRIT IF KPUO=1.
      DIMENSION N(30,16),FLA(0500),ORD(0500),E(0500),CD(0500)
      COMMON /IOPOOL/ NI,NO,NK,NP
      READ (NI,21) JMAX,KPUO
   21 FORMAT (2I5)
      DO 31 J=1,JMAX
   31 READ   (NI,22) (N(I,J),I=1,30)

   22 FORMAT (30I2)
      DO 32 J=1,JMAX
      IG=0
      I=1
      READ (NK) KSTART
      IF (KSTART-77777) 99,41,99
   41 IG=IG+1
      MAXGAM=09
      NPSA=334
      IF (IG-MAXGAM) 46,32,32
   46 READ (NK) (FLA(IR),CD(IR),ORD(IR),E(IR),IR=1,NPSA)
      NSEL=N(I,J)
      IF (NSEL-IG)  41,42,41
   42 I=I+1
      CALL PLODIV (FLA,ORD,334,10)
      WRITE (NO,23)     (FLA(IZ),ORD(IZ),CD(IZ),E(IZ),IZ=1,NPSA)
   23 FORMAT (43H WAVELENGTH     ORD     CD          ABSORPTION/      (4F10.
     10))
      IF (KPUO.NE.1) GO TO 41
      WRITE (NP,24) (FLA(IS),ORD(IS),IS=1,NPSA)
      WRITE (NP,24) (FLA(IS),CD (IS),IS=1,NPSA)
   24 FORMAT (4(F10.1,F10.0))
      GO TO 41
   32 CONTINUE
   99 RETURN
      END
```

```
DIMERO .PLODI                                                          05
        EXTERNAL FORMULA NUMBER   -   SOURCE STATEMENT   -   INTERNAL

      SUBROUTINE PLODIV (X,Y,NPTS,LENGTH)
C NPTS IS THE NUMBER OF POINTS TO BE PLOTTED( THE X TO BE READ IN FROM
C LARGEST TO SMALLEST,THE ASSOCIATED Y HAVING THE SAME INDEX.
C  ONE TITLE CARD IS READ. LENGTH IS IN INCHES
C     CALL CCBGN                          OUT JAN 10
      COMMON /CCPOOL/XMIN,XMAX,YMIN,YMAX,CCXMIN,CCXMAX,CCYMIN,CCYMAX
      COMMON /IOPOOL/ NI,NO,NK,NP
      DIMENSIONTITLE(12),X(0500),Y(0500),FMT(2)
      READ (NI,11)TITLE
   11 FORMAT(13A6)
      XMIN=X(NPTS)
      XMAX=X(1)
      IF (NI+1) 121,122,121
  121 RCOR=1024.
      NRCOR=1024
      GO TO123
  122 RCOR=1.
      NRCOR=1
  123 CONTINUE
      CCXMIN=100./RCOR
      CCYMIN=200./RCOR
      CCYMAX=900./RCOR
      CCXMAX=(100+LENGTH*100)/NRCOR
C  FIND YMAX AND YMIN FOR SCALING PURPOSES
      YMAX=Y(1)
      DO 21 I=2,NPTS
      YDIF=YMAX-Y(I)
      IF (YDIF)22,21,21
   22 YMAX=Y(I)
   21 CONTINUE
      YMIN=Y(1)
      DO 23 I=2,NPTS
      YDIFM=YMIN-Y(I)
      IF (YDIFM) 23,24,24
   24 YMIN=Y(I)
   23 CONTINUE
      CALL CCGRID (LENGTH,2,5,6HLABELS,7,2,5)
      CALL CCLTR(.048828,.097656,0,2,TITLE,78)
      CALL CCPLOT (X,Y,NPTS,4HJOIN)
      WRITE (NO,12)TITLE
   12 FORMAT (1H0,13A6)
      CALL CCNEXT
      RETURN
      END
```

APPENDIX B

Circular Dichroism Curves

In this section we present the computed circular dichroism curves for all 16 dimers. Only one of these (ApA) was discussed in the text since there have been no published measurements of the others. We also include the ORD curve of ApA unscaled.

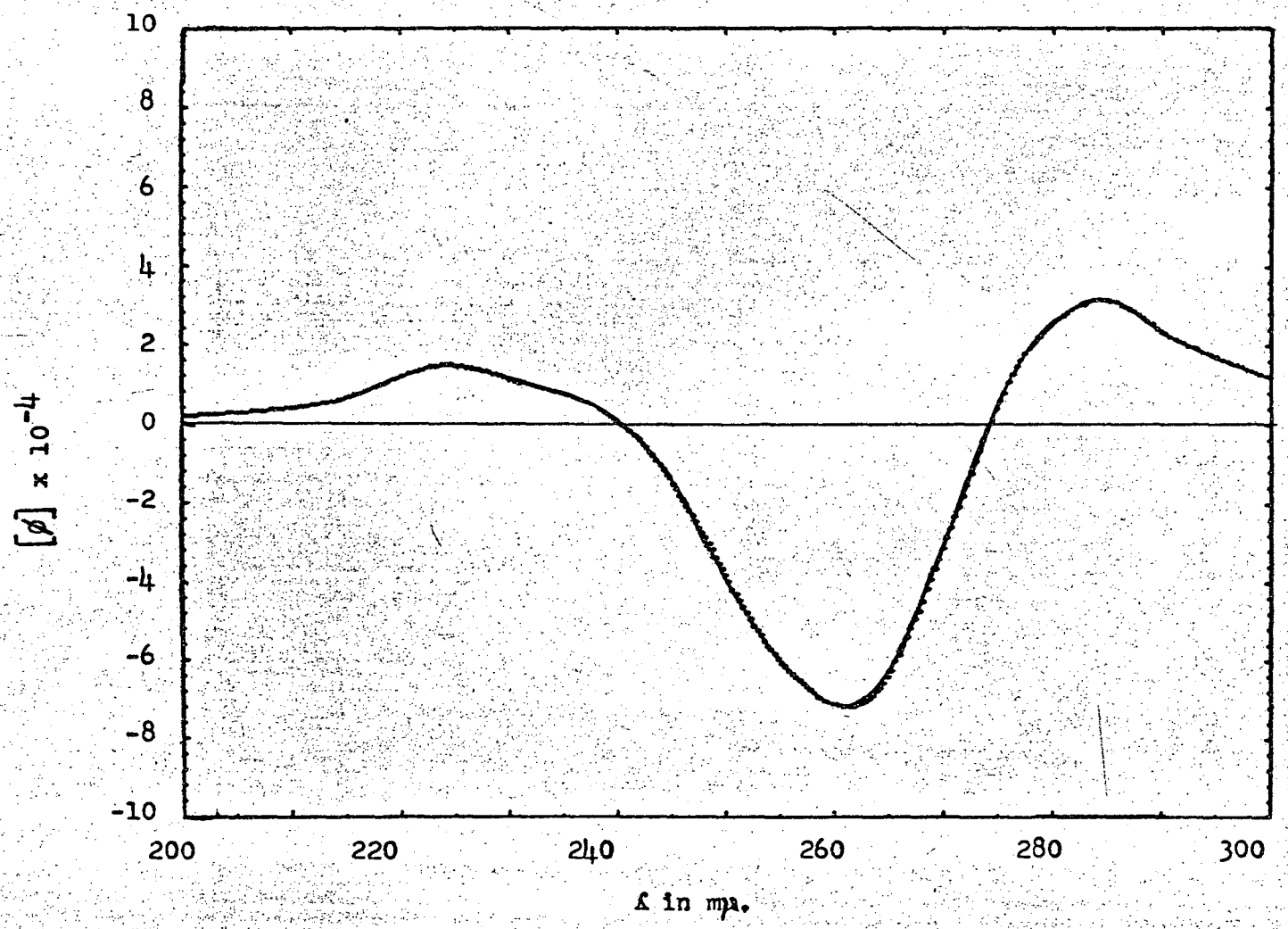

APA ROTATION VS. WAVELENGTH

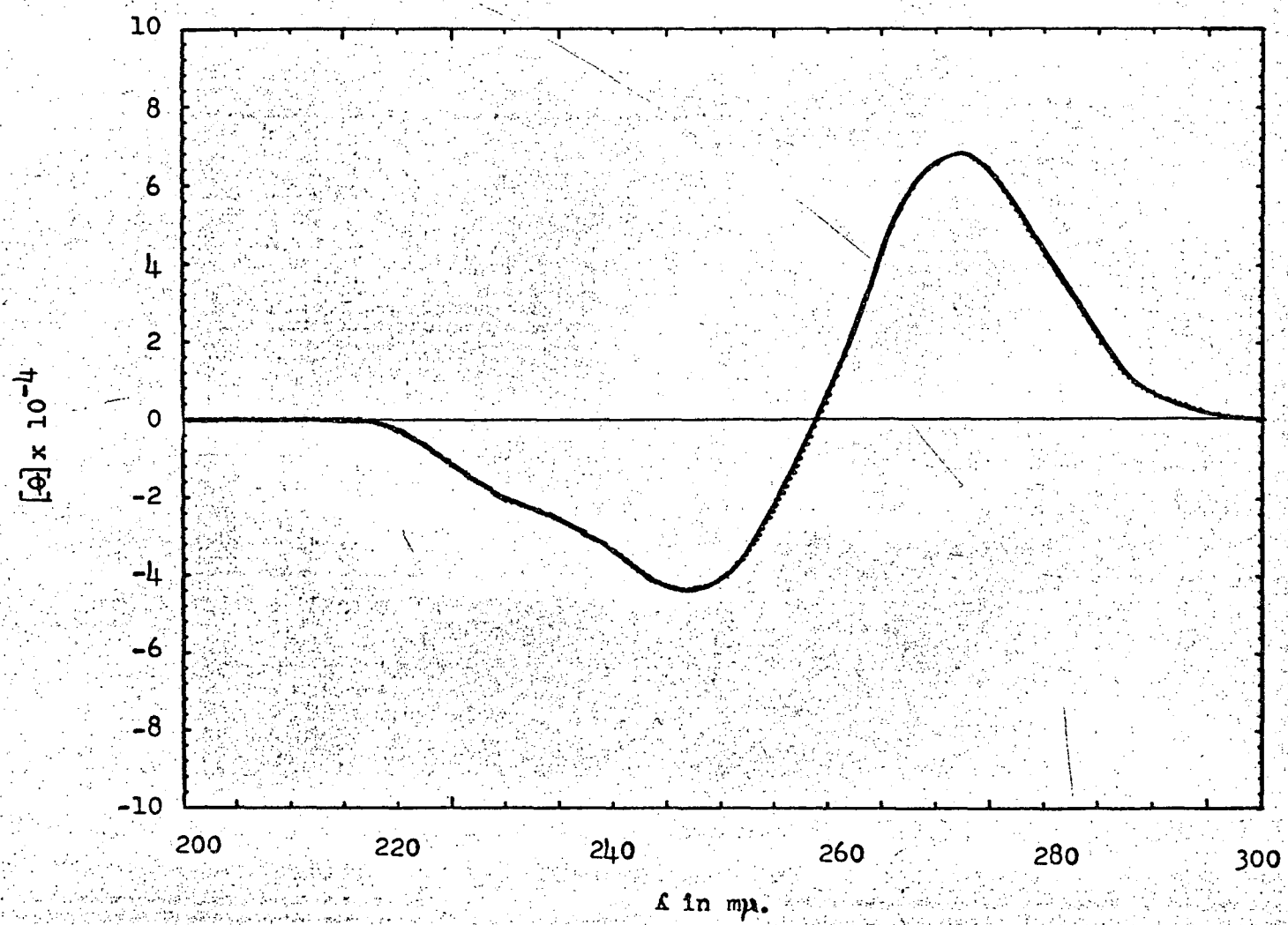

APA CIRCULAR DICHROISM VS. WAVELENGTH

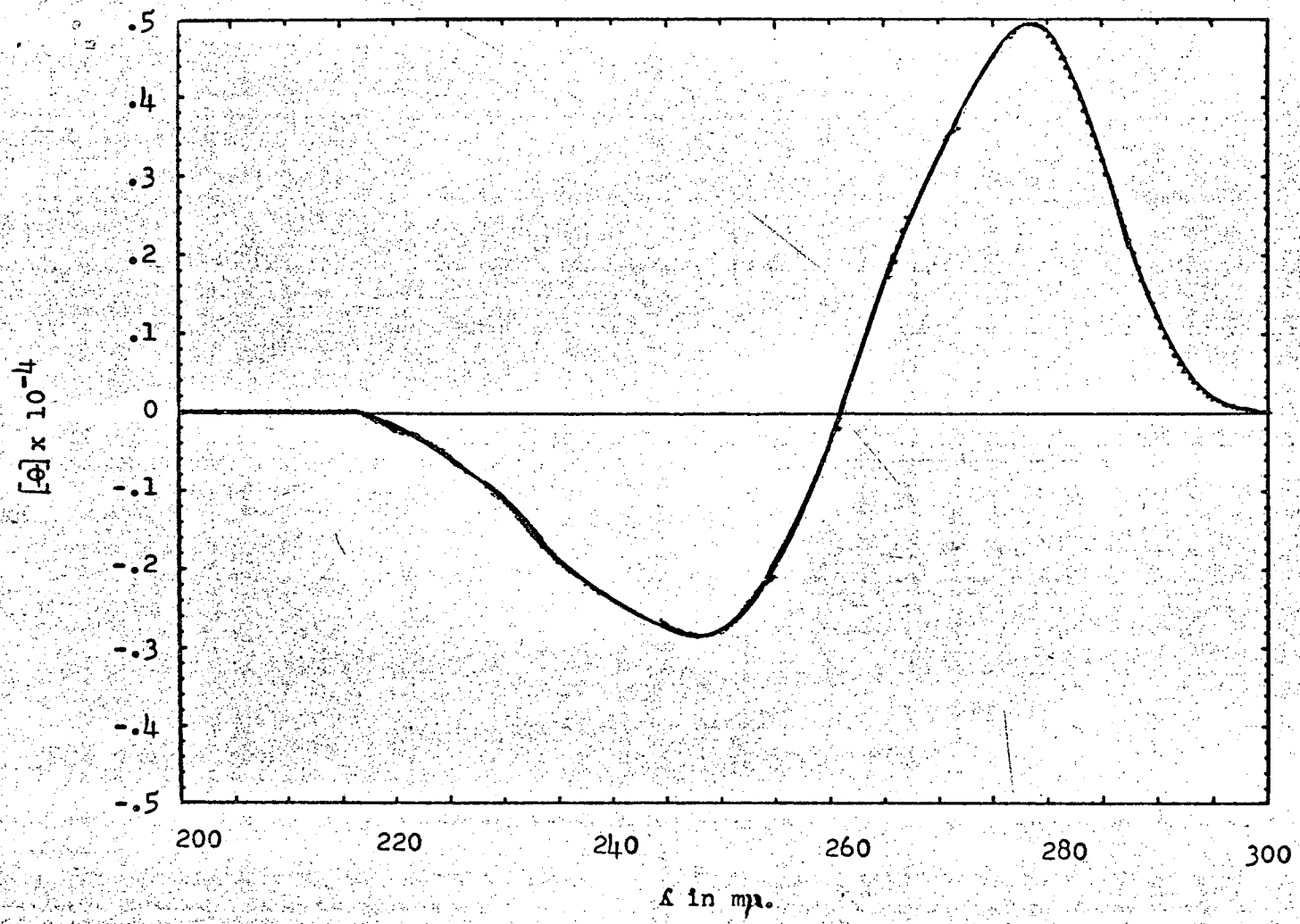

UPU CIRCULAR DICHROISM VS. WAVELENGTH

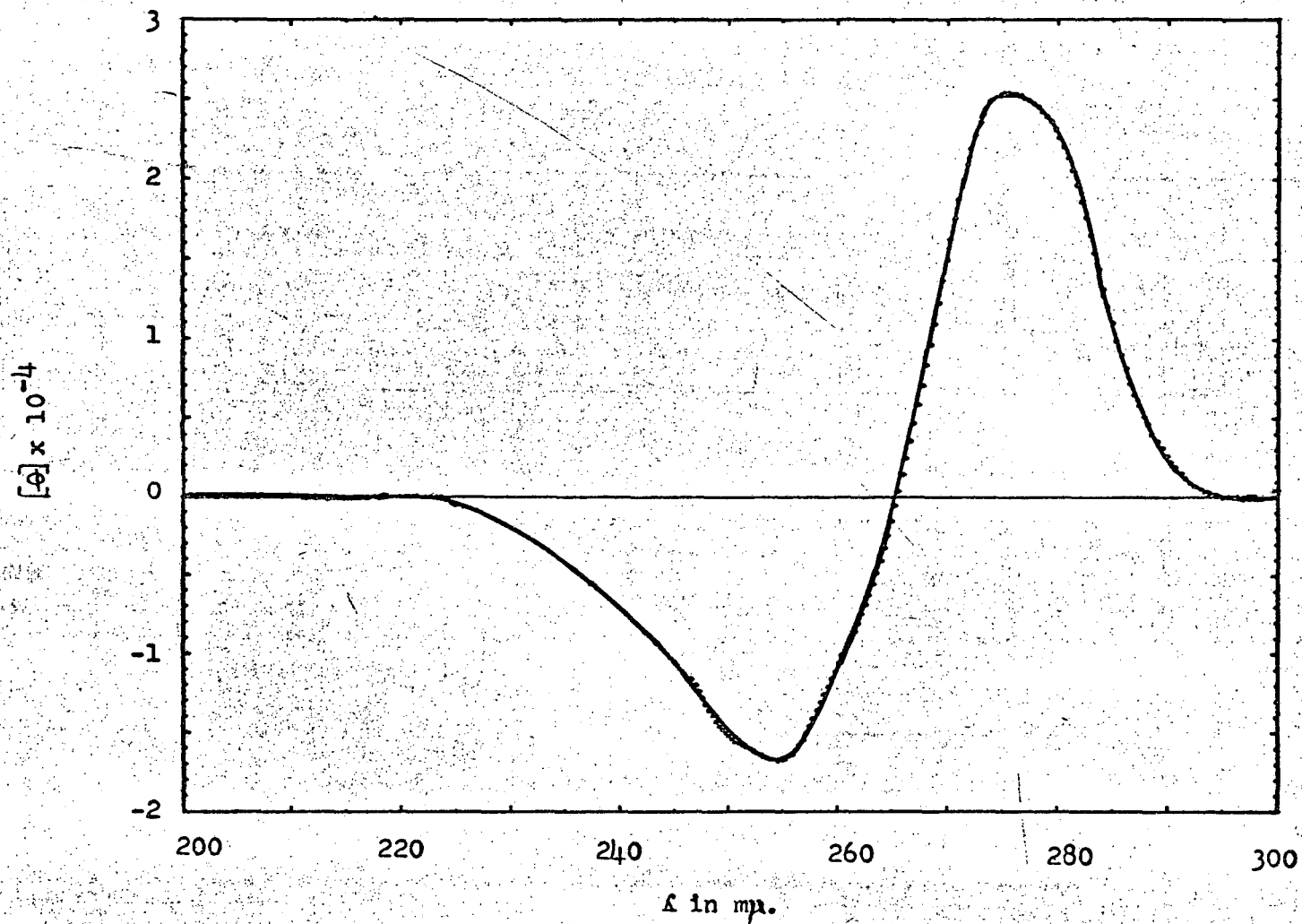

APU CIRCULAR DICHROISM VS. WAVELENGTH

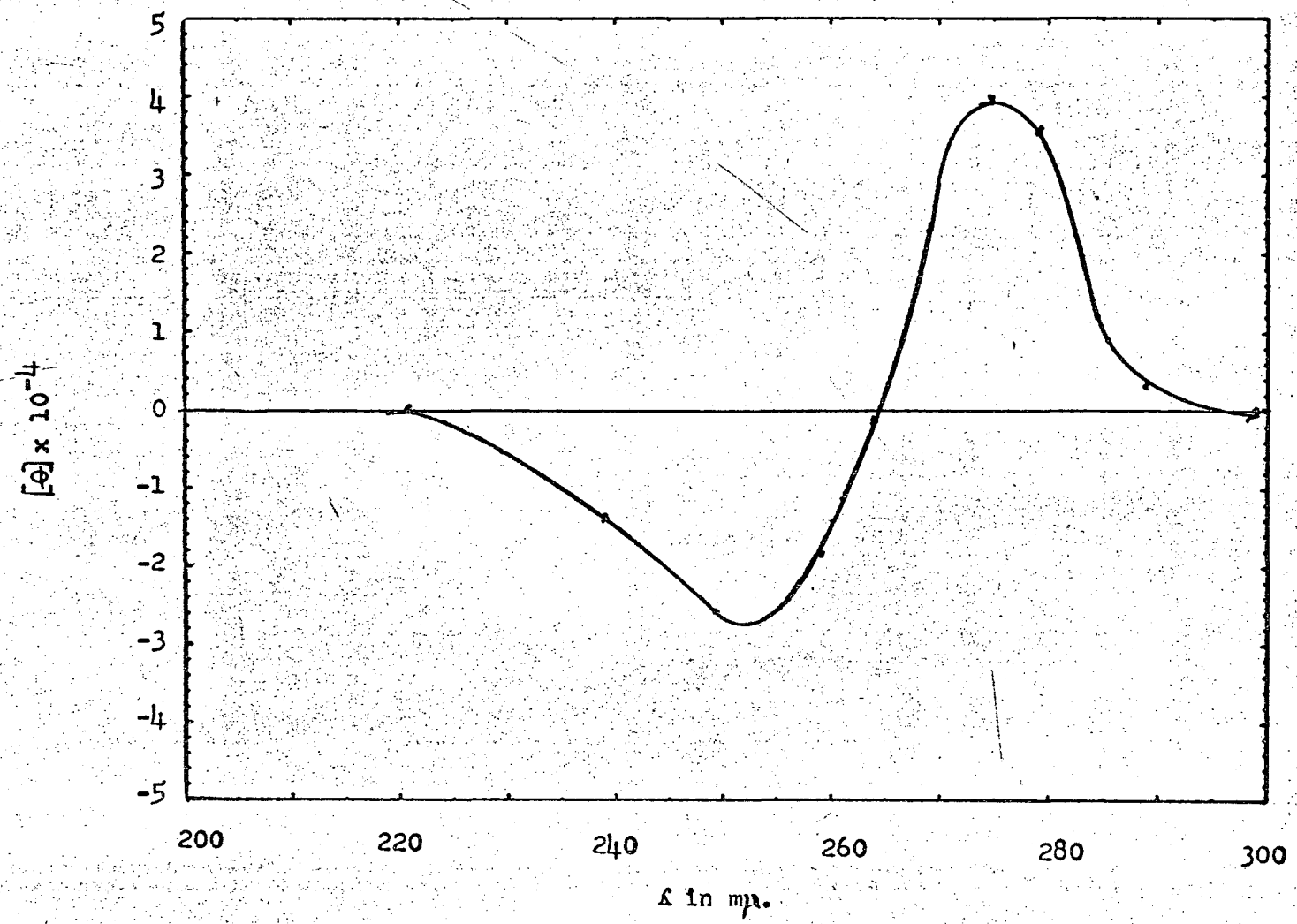

UPA CIRCULAR DICHROISM VS. WAVELENGTH

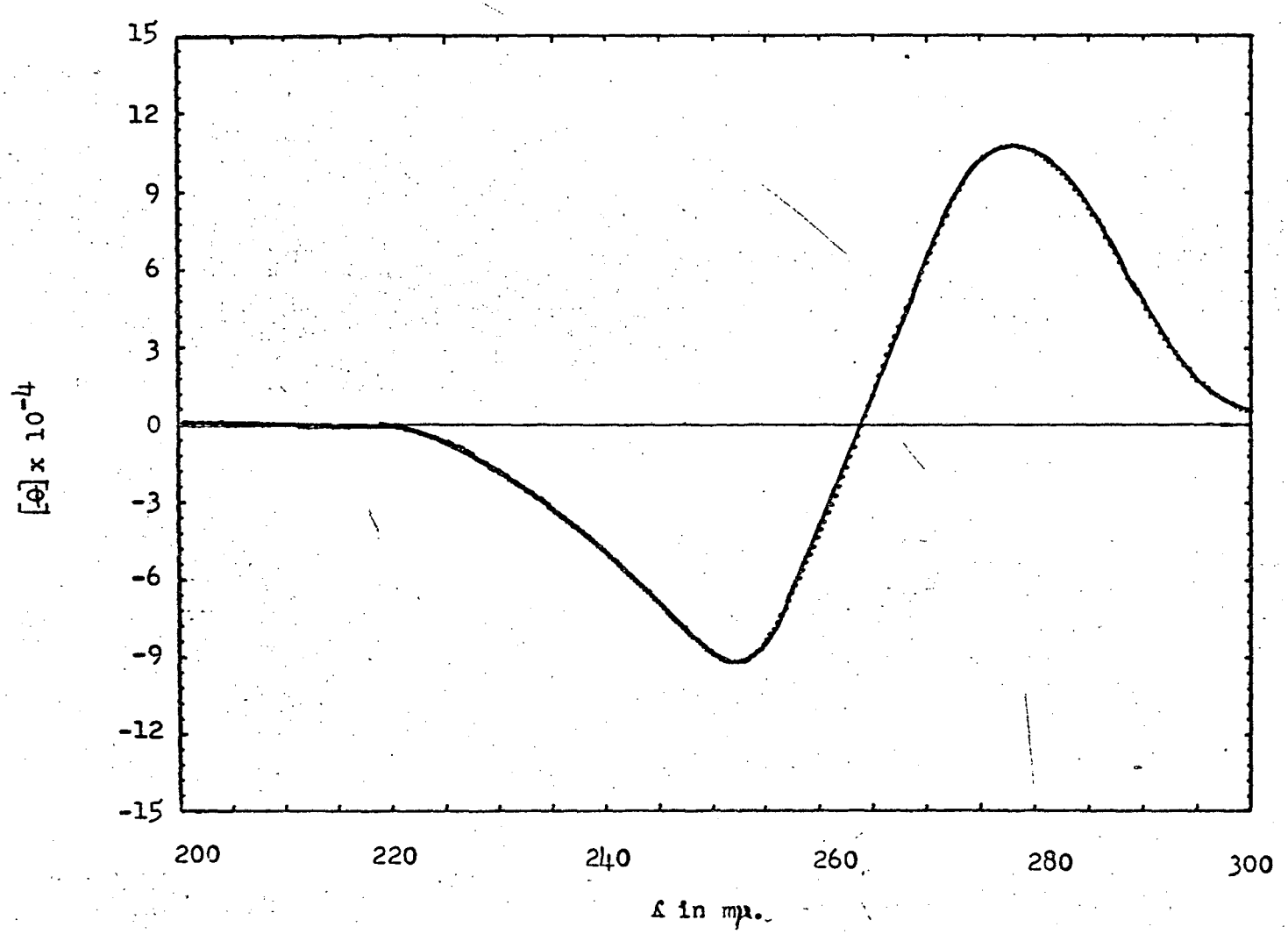

APG CIRCULAR DICHROISM VS. WAVELENGTH

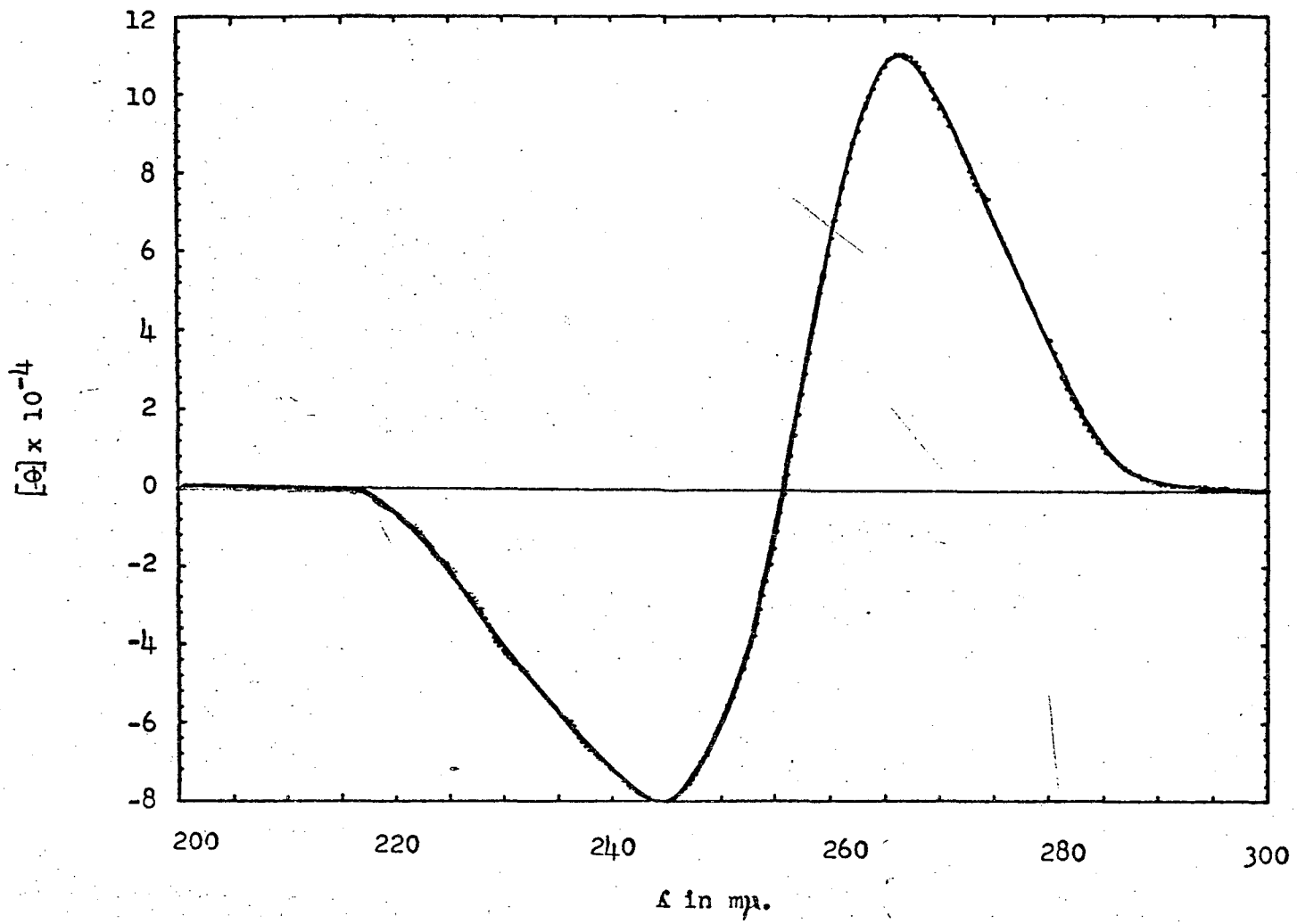

GPA CIRCULAR DICHROISM VS. WAVELENGTH

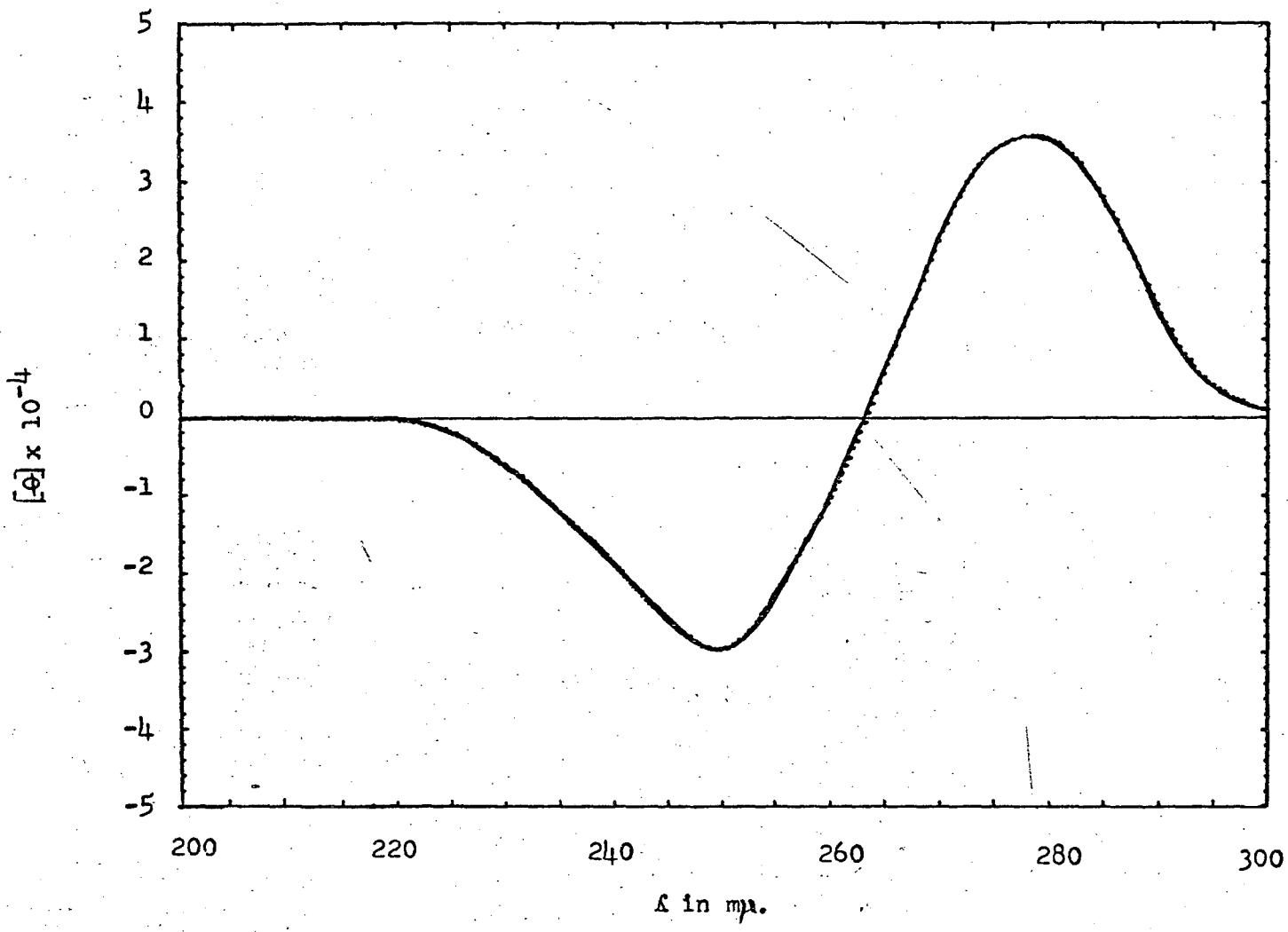

APC CIRCULAR DICHROISM VS. WAVELENGTH

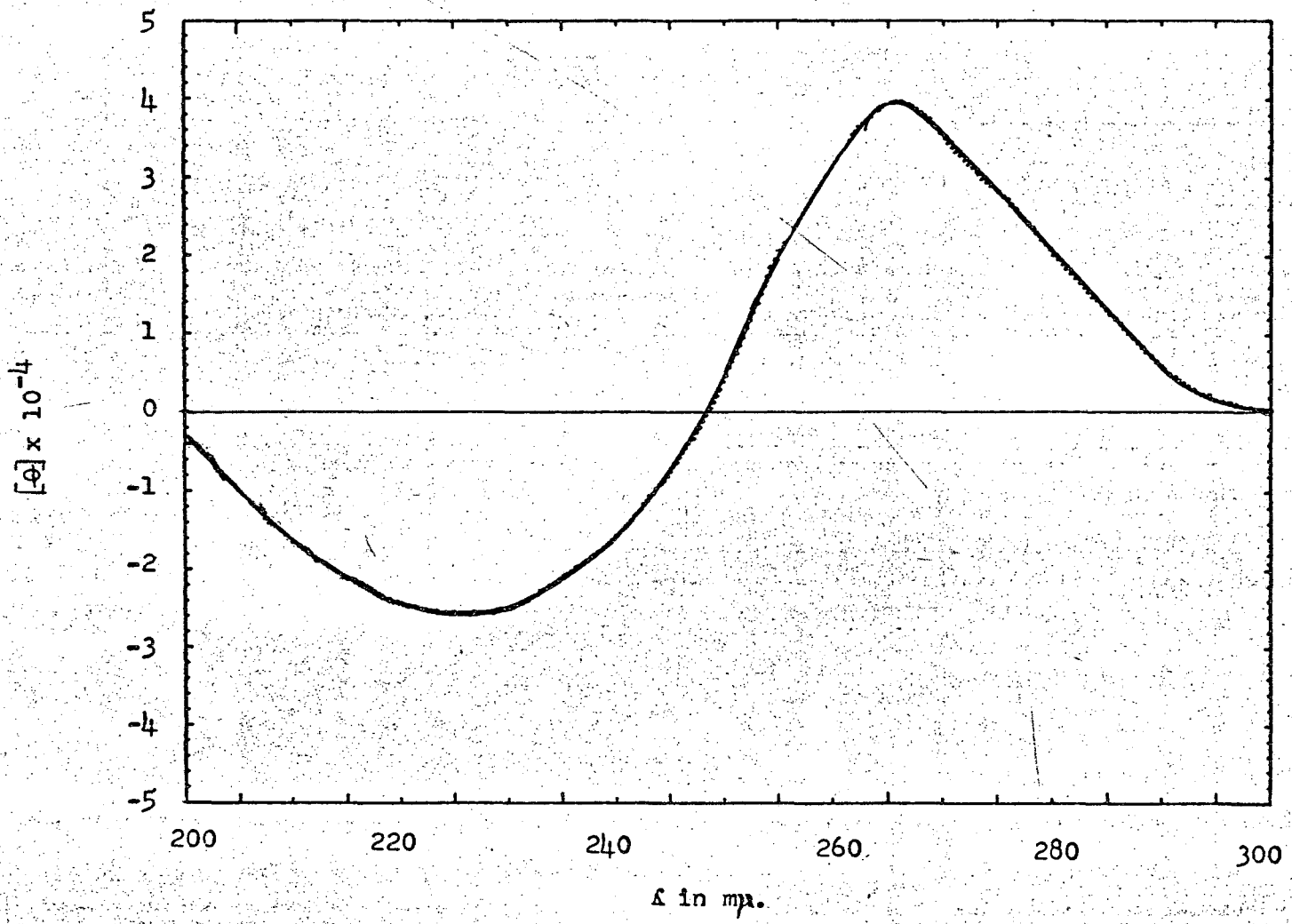

CPA CIRCULAR DICHROISM VS. WAVELENGTH

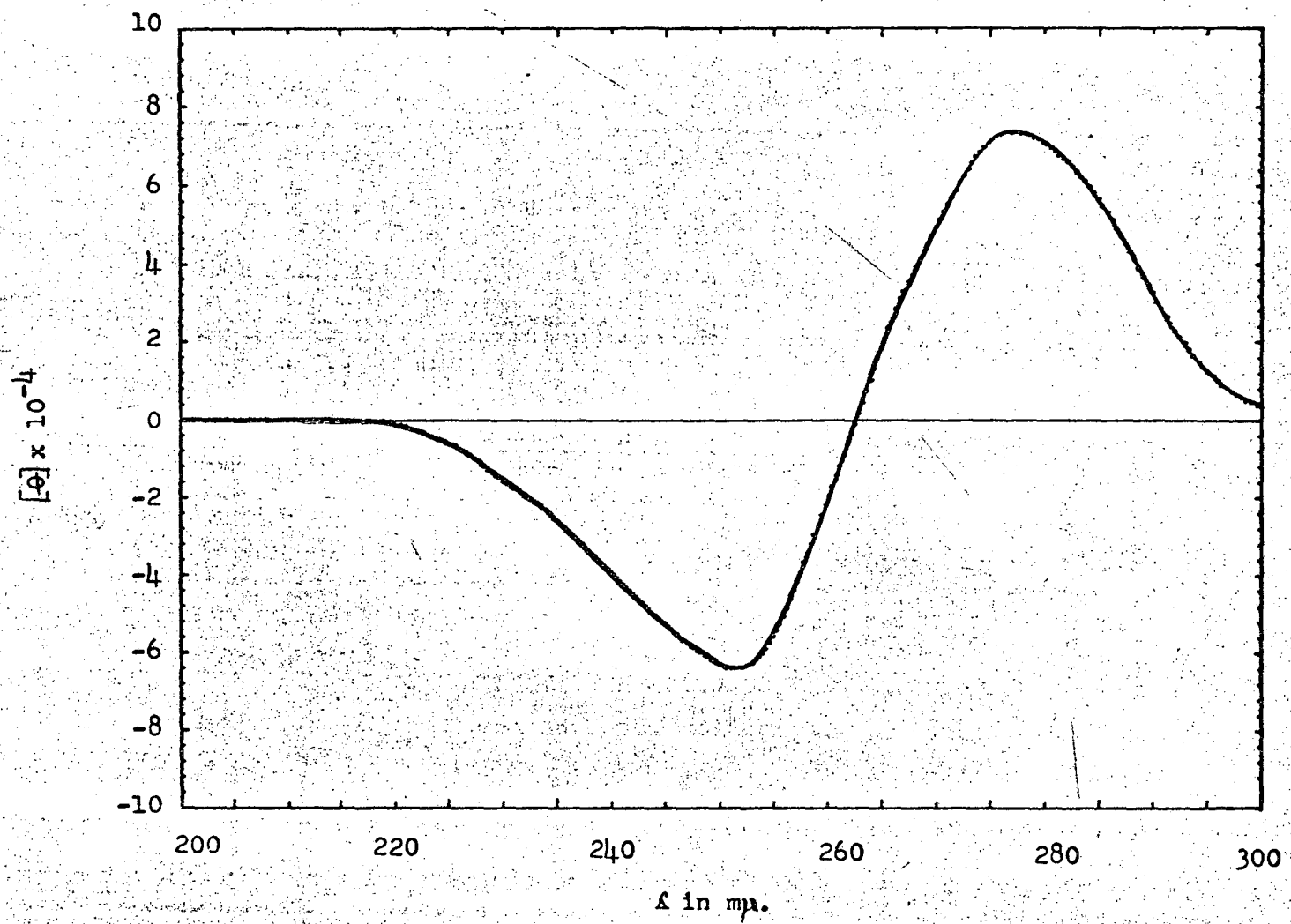

UPG CIRCULAR DICHROISM VS. WAVELENGTH

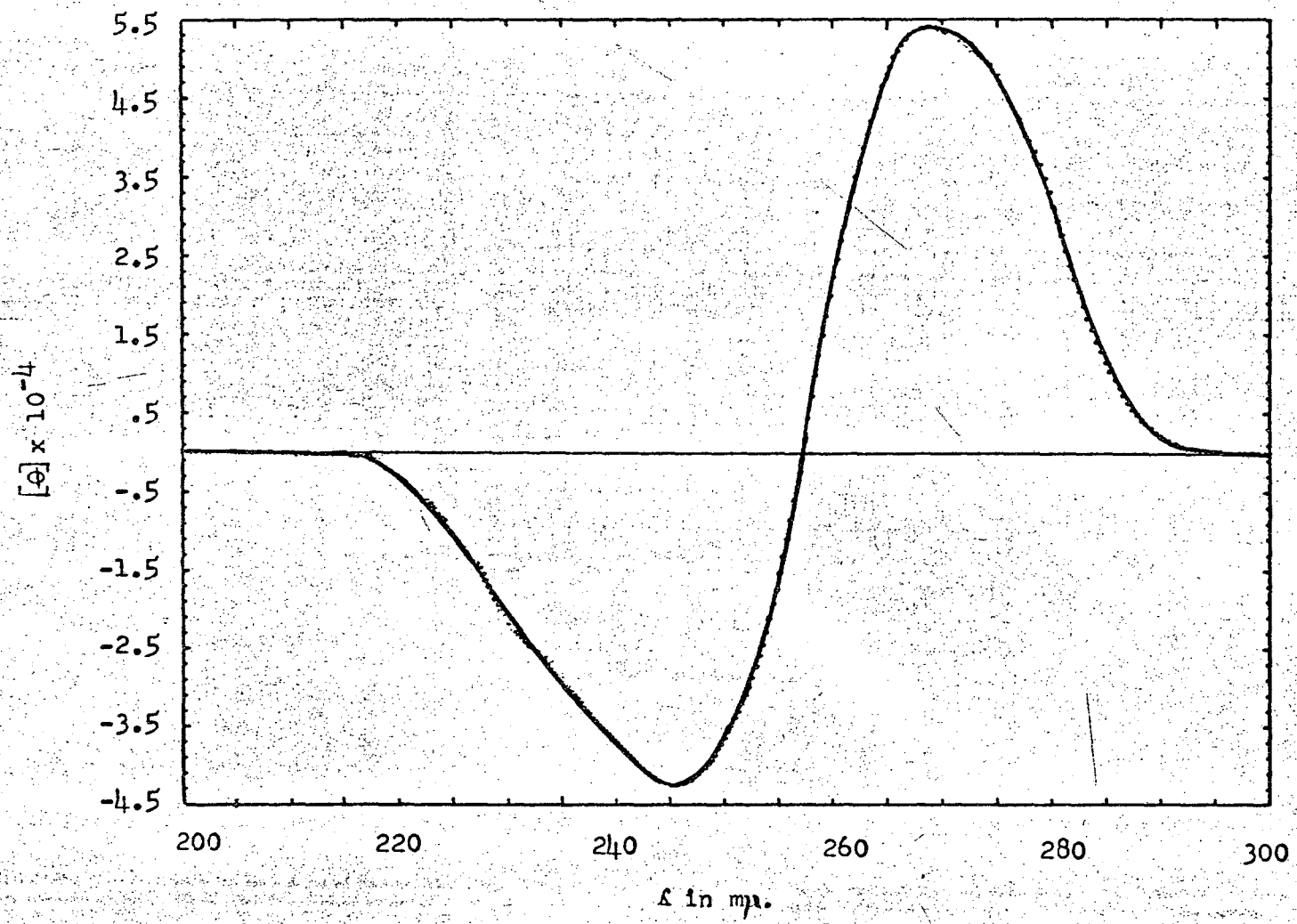

GPU CIRCULAR DICHROISM VS. WAVELENGTH

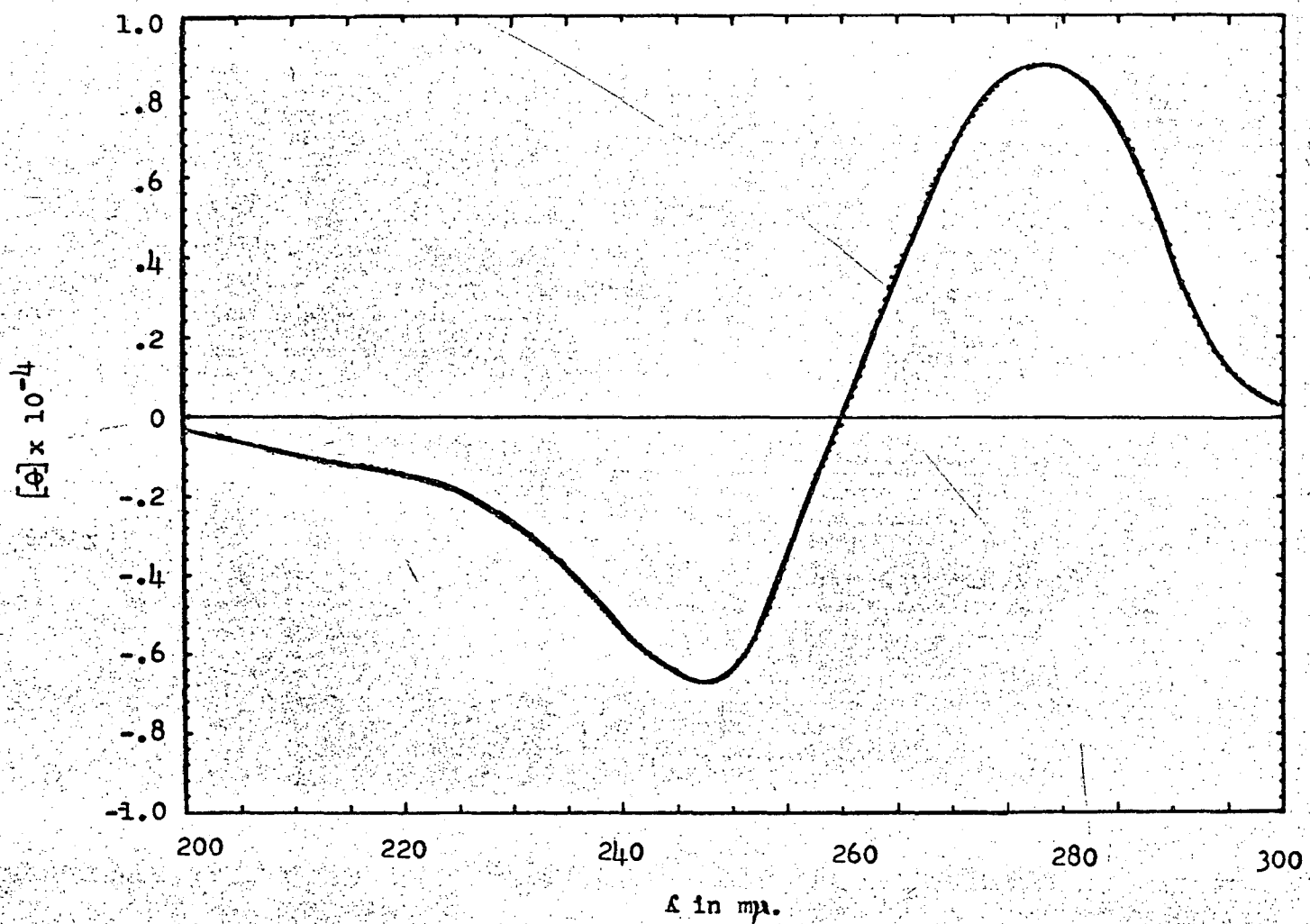

UPC CIRCULAR DICHROISM VS. WAVELENGTH

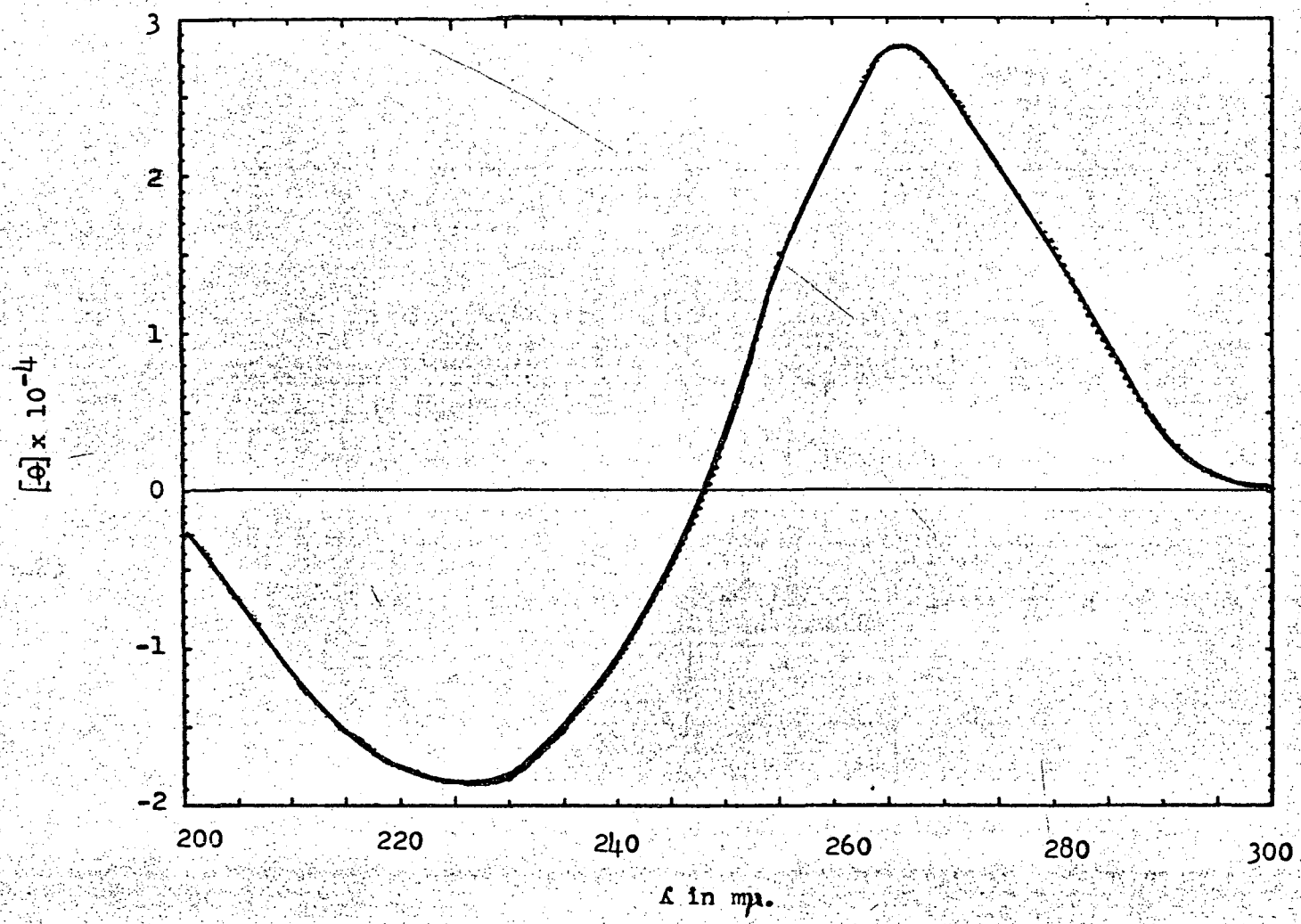

CPU CIRCULAR DICHROISM VS. WAVELENGTH

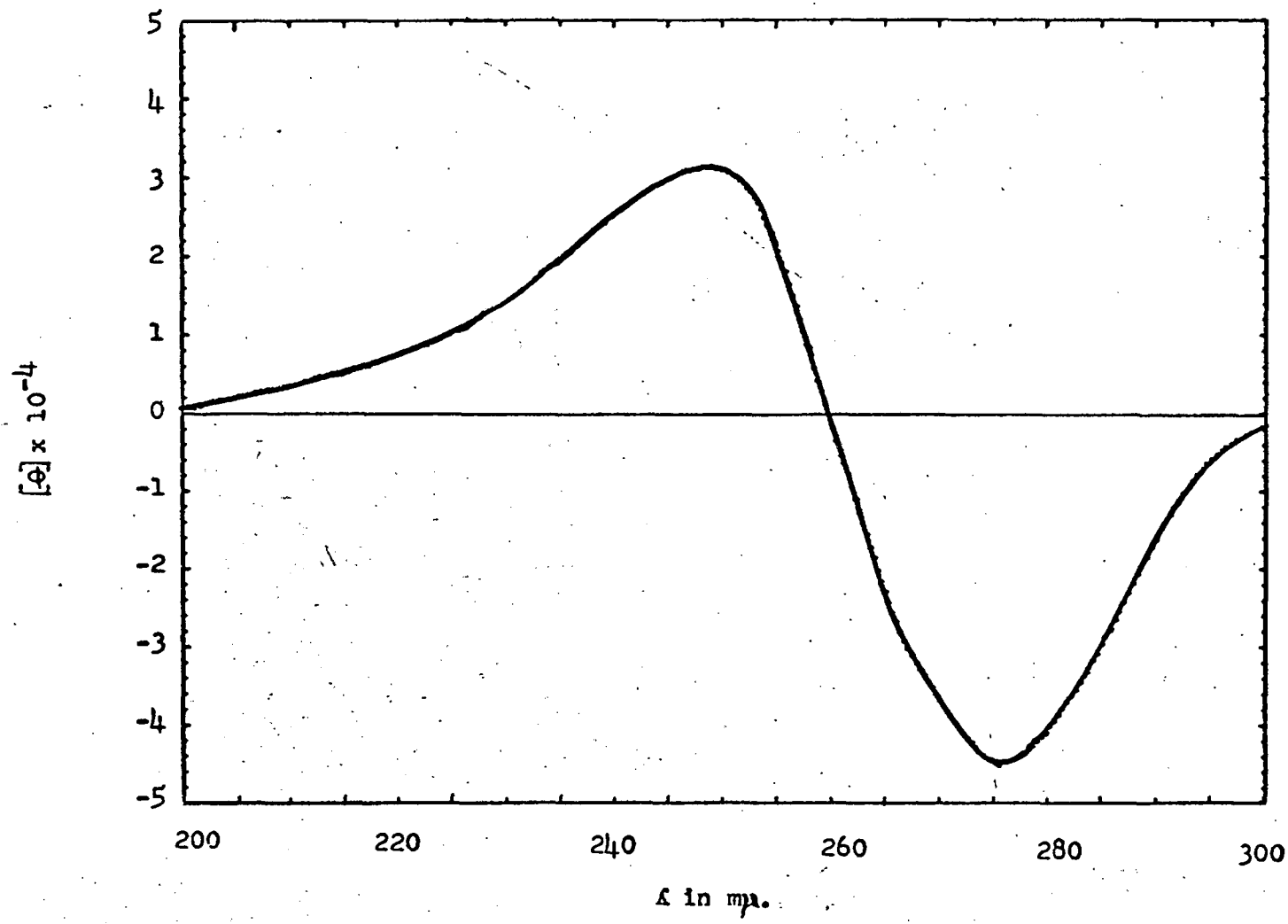

GPC CIRCULAR DICHROISM VS. WAVELENGTH,

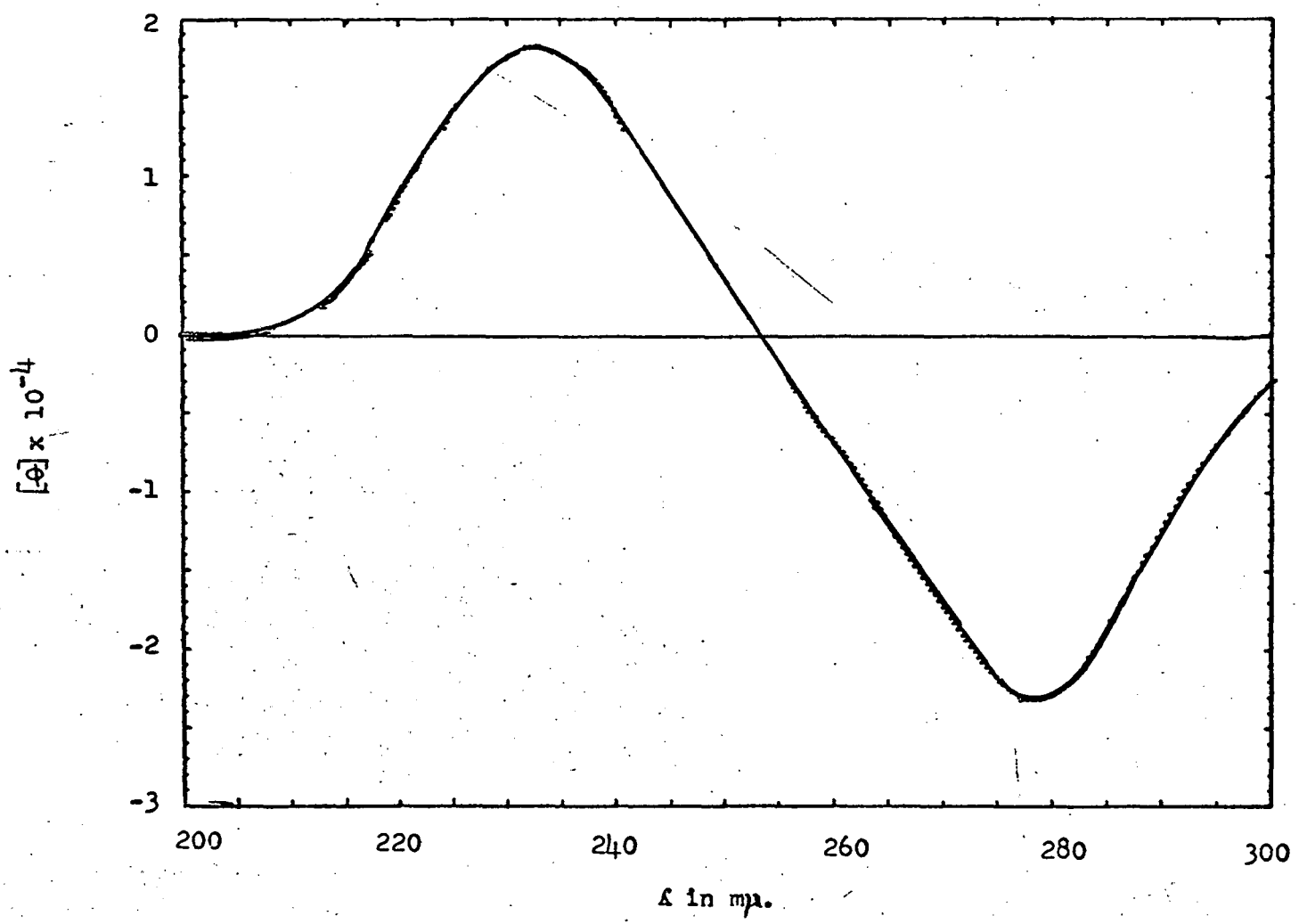

CPG CIRCULAR DICHROISM VS. WAVELENGTH

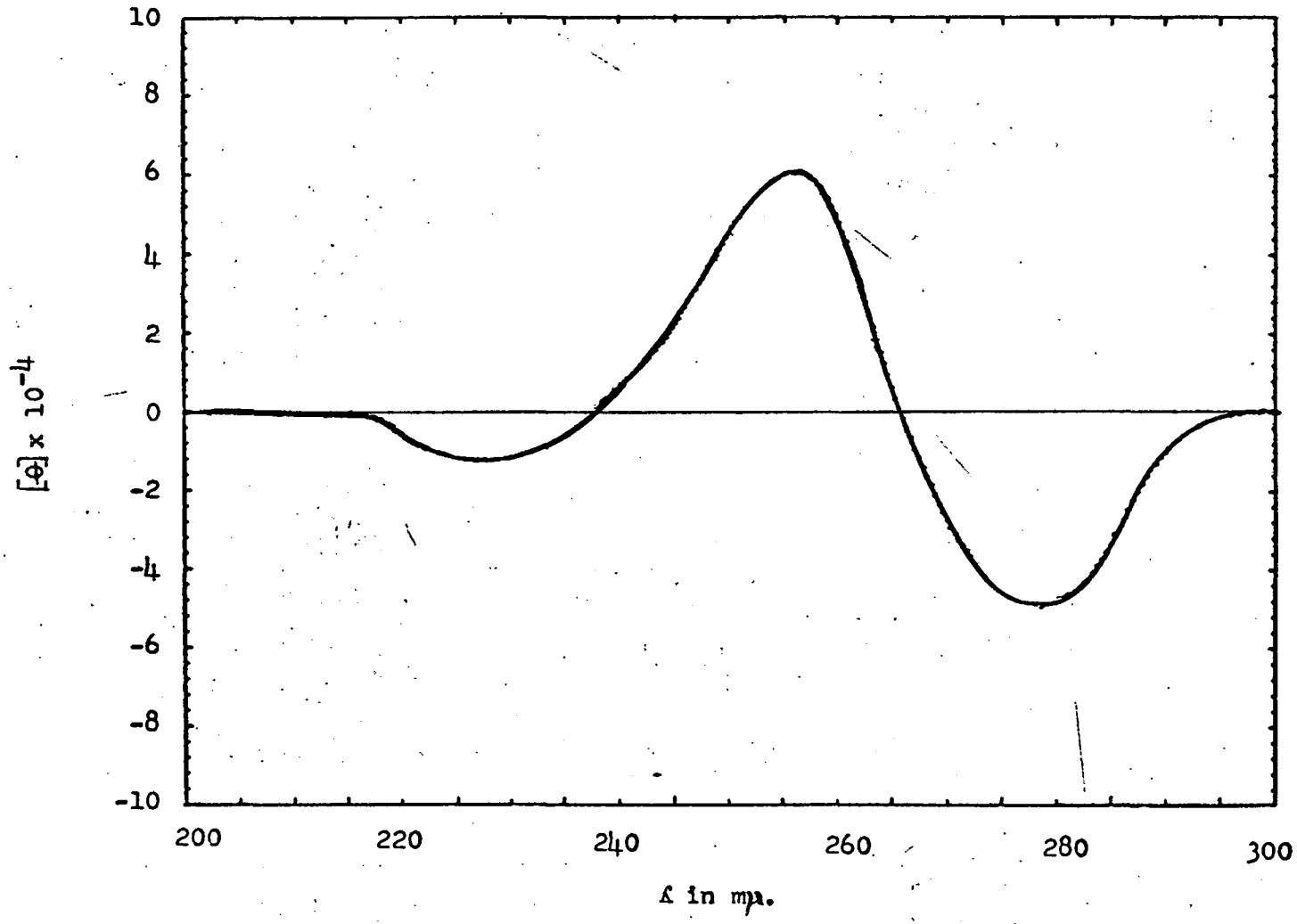

GPG CIRCULAR DICHROISM VS. WAVELENGTH

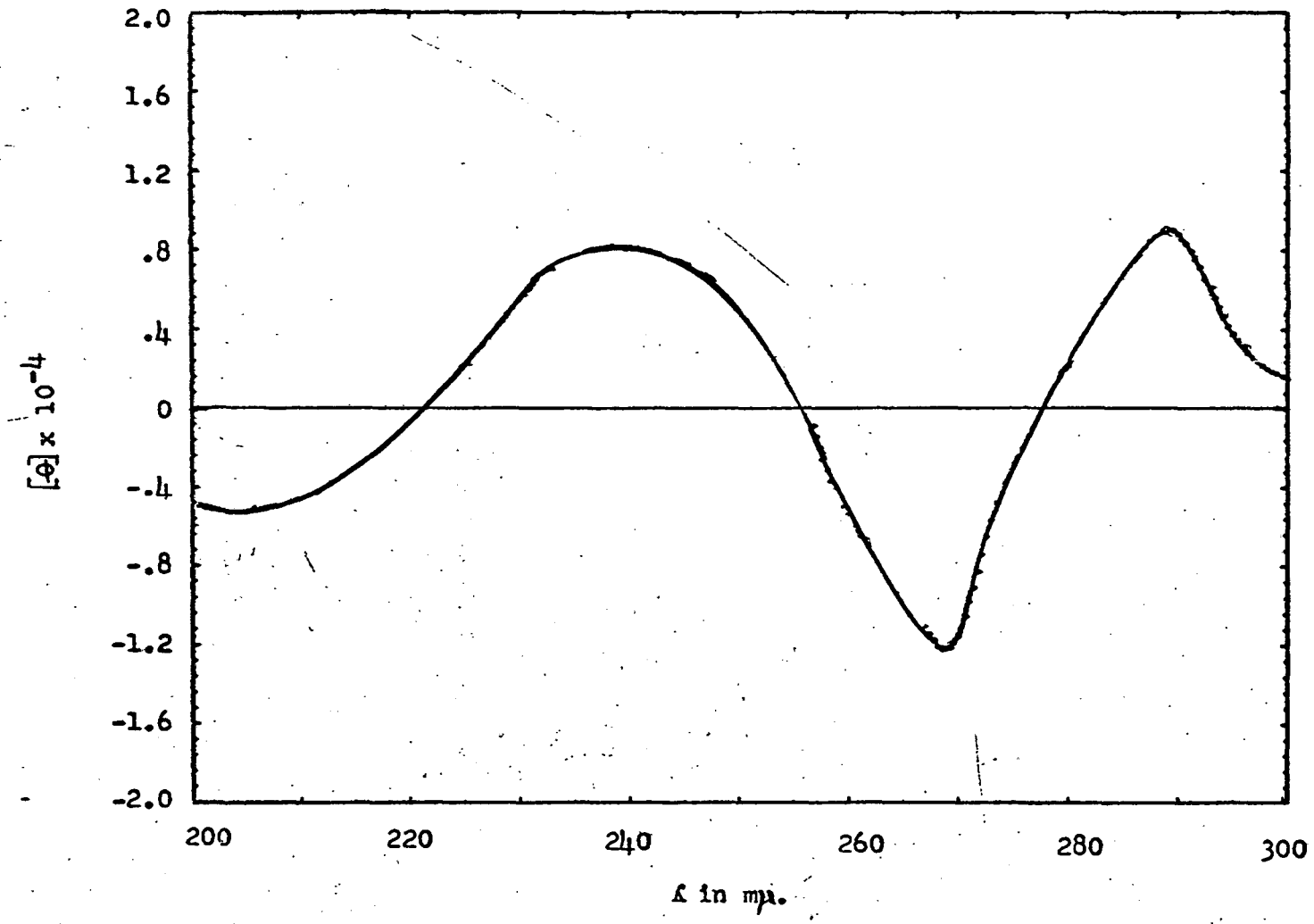

CPC CIRCULAR DICHROISM VS. WAVELENGTH

This report was prepared as an account of Government sponsored work. Neither the United States, nor the Commission, nor any person acting on behalf of the Commission:

A. Makes any warranty or representation, expressed or implied, with respect to the accuracy, completeness, or usefulness of the information contained in this report, or that the use of any information, apparatus, method, or process disclosed in this report may not infringe privately owned rights; or

B. Assumes any liabilities with respect to the use of, or for damages resulting from the use of any information, apparatus, method, or process disclosed in this report.

As used in the above, "person acting on behalf of the Commission" includes any employee or contractor of the Commission, or employee of such contractor, to the extent that such employee or contractor of the Commission, or employee of such contractor prepares, disseminates, or provides access to, any information pursuant to his employment or contract with the Commission, or his employment with such contractor.